



**HAL**  
open science

# Space-Time Discretization of Elasto-Acoustic Wave Equation in Polynomial Trefftz-DG Bases

Elvira Shishenina

► **To cite this version:**

Elvira Shishenina. Space-Time Discretization of Elasto-Acoustic Wave Equation in Polynomial Trefftz-DG Bases. Numerical Analysis [math.NA]. Université de Pau et des Pays l'Adour, 2018. English. NNT: . tel-01953740

**HAL Id: tel-01953740**

**<https://inria.hal.science/tel-01953740>**

Submitted on 13 Dec 2018

**HAL** is a multi-disciplinary open access archive for the deposit and dissemination of scientific research documents, whether they are published or not. The documents may come from teaching and research institutions in France or abroad, or from public or private research centers.

L'archive ouverte pluridisciplinaire **HAL**, est destinée au dépôt et à la diffusion de documents scientifiques de niveau recherche, publiés ou non, émanant des établissements d'enseignement et de recherche français ou étrangers, des laboratoires publics ou privés.



Depth Imaging Partnership



UNIVERSITÉ DE PAU ET DES PAYS DE L'ADOUR  
INSTITUT NATIONAL DE RECHERCHE EN INFORMATIQUE ET EN AUTOMATIQUE  
TOTAL S.A.

Elvira Shishenina

---

## Space-Time Discretization of Elasto-Acoustic Wave Equation in Polynomial Trefftz-DG Bases

---

### Scientific directors

Mme Hélène Barucq, Mr Henri Calandra & Mr Julien Diaz

### Thesis committee

Mme Hélène Barucq	Director of Research, Inria	Advisor
Mr Abderrahmane Bendali	Professor, INSA Toulouse	Examiner
Mr Henri Calandra	Expert in Numerical Methods, Total S.A.	Advisor
Mr José M. Carcione	Professor, INOGS Trieste	Examiner
Mr Bruno Després	Professor, Université Paris VI	Reviewer
Mr Julien Diaz	Director of Research, Inria	Advisor
Mr Peter Monk	Professor, University of Delaware	Reviewer

A thesis submitted in partial fulfilment of the requirements for the degree of  
**Doctor of Philosophy in Mathematics**

December 2018





Depth Imaging Partnership



UNIVERSITÉ DE PAU ET DES PAYS DE L'ADOUR  
INSTITUT NATIONAL DE RECHERCHE EN INFORMATIQUE ET EN AUTOMATIQUE  
TOTAL S.A.

Elvira Shishenina

---

**Discrétisation Espace-Temps d'Équations d'Ondes  
Élasto-Acoustiques dans des Bases Trefftz-DG Polynomiales**

---

**Directeurs scientifiques**

Mme Hélène Barucq, Mr Henri Calandra & Mr Julien Diaz

**Jury de thèse**

Mme Hélène Barucq	Directrice de Recherche, Inria	Advisor
Mr Abderrahmane Bendali	Professeur, INSA Toulouse	Examiner
Mr Henri Calandra	Expert Méthodes Numériques, Total S.A.	Advisor
Mr José M. Carcione	Professeur, INOGS Trieste	Examiner
Mr Bruno Després	Professeur, Université Paris VI	Reviewer
Mr Julien Diaz	Directeur de Recherche, Inria	Advisor
Mr Peter Monk	Professeur, University of Delaware	Reviewer

Thèse pour l'obtention du grade de  
**Docteur en Mathématiques**

Decembre 2018



*As Henri Poincaré once remarked, "solution of a mathematical problem" is a phrase of indefinite meaning. Pure mathematicians sometimes are satisfied with showing that the non-existence of a solution implies a logical contradiction, while engineers might consider a numerical result as the only reasonable goal. Such one sided views seem to reflect human limitations rather than objective values. In itself mathematics is an indivisible organism uniting theoretical contemplation and active application. This address will deal with a topic in which such a synthesis of theoretical and applied mathematics has become particularly convincing.*

R. Courant, 1943



# Abstract

## Space-Time Discretization of Elasto-Acoustic Wave Equations in Polynomial Trefftz-DG Bases

by Elvira Shishenina

Discontinuous Finite Element Methods (DG FEM) have proven flexibility and accuracy for solving wave problems in complex media. However, they require a large number of degrees of freedom, which increases the corresponding computational cost compared with that of continuous finite element methods.

Among the different variational approaches to solve boundary value problems, there exists a particular family of methods, based on the use of trial functions in the form of exact local solutions of the governing equations. The idea was first proposed by Trefftz in 1926 [103], and since then it has been further developed and generalized. A Trefftz-DG variational formulation applied to wave problems reduces to surface integrals that should contribute to decreasing the computational costs.

Trefftz-type approaches have been widely used for time-harmonic problems, while their implementation for time-dependent simulations is still limited. The feature of Trefftz-DG methods applied to time-dependent problems is in the use of space-time meshes. Indeed, standard DG methods lead to the construction of a semi-discrete system of ordinary differential equations in time which are integrated by using an appropriate scheme. But Trefftz-DG methods applied to wave problems lead to a global matrix including time and space discretizations which is huge and sparse. This significantly hampers the deployment of this technology for solving industrial problems.

In this work, we develop a Trefftz-DG framework for solving mechanical wave problems including elasto-acoustic equations. We prove that the corresponding formulations are well-posed and we address the issue of solving the global matrix by constructing an approximate inverse obtained from the decomposition of the global matrix into a block-diagonal one. The inversion is then justified under a CFL-type condition. This idea allows for reducing the computational costs but its accuracy is limited to small computational domains.

According to the limitations of the method, we have investigated the potential of Tent Pitcher algorithms following the recent works of Gopalakrishnan et al. in [51, 52]. It

consists in constructing a space-time mesh made of patches that can be solved independently under a causality constraint. We have obtained very promising numerical results illustrating the potential of Tent Pitcher in particular when coupled with a Trefftz-DG method involving only surface terms. In this way, the space-time mesh is composed of elements which are 3D objects at most. It is also worth noting that this framework naturally allows for local time-stepping which is a plus to increase the accuracy while decreasing the computational burden.

# Abstract

## **Discrétisation Espace-Temps d'Équations d'Ondes Élasto-Acoustiques Formulées dans des Bases Trefftz-DG Polynomiales**

par Elvira Shishenina

Les méthodes d'éléments finis de type Galerkin discontinu (DG FEM) ont démontré précision et efficacité pour résoudre des problèmes d'ondes dans des milieux complexes. Cependant, elles nécessitent un très grand nombre de degrés de liberté, ce qui augmente leur coût de calcul en comparaison du coût des méthodes d'éléments finis continus.

Parmi les différentes approches variationnelles pour résoudre les problèmes aux limites, se distingue une famille particulière, basée sur l'utilisation de fonctions tests qui sont des solutions locales exactes des équations à résoudre. L'idée vient de E. Trefftz en 1926 [103] et a depuis été largement développée et généralisée. Les méthodes variationnelles de type Trefftz-DG appliquées aux problèmes d'ondes se réduisent à des intégrales de surface, ce qui devrait contribuer à réduire les coûts de calcul.

Les approches de type Trefftz ont été largement développées pour les problèmes harmoniques, mais leur utilisation pour des simulations en domaine transitoire est encore limitée. Quand elles sont appliquées dans le domaine temporel, les méthodes de Trefftz utilisent des maillages qui recouvrent le domaine espace-temps. C'est une des particularités de ces méthodes. En effet, les méthodes DG standards conduisent à la construction d'un système semi-discret d'équations différentielles ordinaires en temps qu'on intègre avec un schéma en temps explicite. Mais les méthodes de Trefftz-DG appliquées aux problèmes d'ondes conduisent à résoudre une matrice globale, contenant la discrétisation en espace et en temps, qui est de grande taille et creuse. Cette particularité gêne considérablement le déploiement de cette technologie pour résoudre des problèmes industriels.

Dans ce travail, nous développons un environnement Trefftz-DG pour résoudre des problèmes d'ondes mécaniques, y compris les équations couplées de l'élasto-acoustique. Nous prouvons que les formulations obtenues sont bien posées et nous considérons la difficulté d'inverser la matrice globale en construisant un inverse approché obtenu à partir de la décomposition de la matrice globale en une matrice diagonale par blocs. Cette idée permet de réduire les coûts de calcul mais sa précision est limitée à de petits domaines de calcul. Etant données les limitations de la méthode, nous nous sommes intéressés au potentiel du "Tent Pitcher", en suivant les travaux récents de Gopalakrishnan et al. dans

[51, 52]. Il s'agit de construire un maillage espace-temps composé de macro-éléments qui peuvent être traités indépendamment en faisant une hypothèse de causalité. Nous avons obtenu des résultats préliminaires très encourageants qui illustrent bien l'intérêt du Tent Pitcher, en particulier quand il est couplé à une méthode de Trefftz-DG formulée à partir d'intégrales de surface seulement. Dans ce cas, le maillage espace-temps est composé d'éléments qui sont au plus de dimension 3. Il est aussi important de noter que ce cadre se prête à l'utilisation de pas de temps locaux ce qui est un plus pour gagner en précision avec des coûts de calcul réduits.

# Acknowledgements

I express my deepest gratitude to Prof. Abderrahmane Bendali for accepting to chair my defense committee, as well as to Prof. José M. Carcione who considered my work from the geophysical perspective.

I am grateful to the reviewers Prof. Bruno Després and Prof. Peter Monk for their detailed analysis of my thesis and their contribution to its clarity and accuracy.

Special thanks go to Henri Calandra for his confidence in me and my work and his continuous support of the project in spite of the ambiguous predictions made by the scientific community on its feasibility.

I would like to thank Julien Diaz, who became for me an example of scientific professionalism, and whose contribution to my project can hardly be overestimated.

I thank H el ene Barucq, who besides being an excellent manager of our group, have always found time to attentively supervise and support my work. Putting her soul in everything she does, she not only encourages collaboration between the team members but also creates a family atmosphere in the group.

I have to admit, that there is no way to bake enough cakes to thank my colleagues who are always there to guide and support me. Algiane, Aurelien, Florian, Ha, Juliette, Justine, Lionel, Mamadou, Marie, Marc, Nathan, Pierre, Rose, Sebastien, Sylvie, Simon, Victor, Yder - it has been a great pleasure to share these three years with such passionate and bright researchers.

Last, but not the least, I would like to thank my family, Mariya and Volodymyr for supporting me all these years and giving me the motivation and the energy to take on such challenges. I would have never found the courage to go through these three years if I had not known that I could rely on you.



# Conferences

- |                               |  |
|-------------------------------|--|
| <b>2016. Houston, USA</b>     | Depth Imaging Partnership Annual Workshop  |
| <b>2017. Minneapolis, USA</b> | 13 <sup>th</sup> International Conference on Mathematical and Numerical Aspects of Wave Propagation WAVES'17 |
| <b>2017. Voss, Norway</b>     | European Conference on Numerical Mathematics and Advanced Applications ENUMATH'17                            |
| <b>2017. Paris, France</b>    | Computational Science Engineering and Data Science by TOTAL MATHIAS'17                                       |
| <b>2018. London, England</b>  | International Conference on Spectral and High-Order Methods ICOSAHOM'18                                      |
| <b>2018. New York, USA</b>    | 13 <sup>th</sup> World Congress on Computational Mechanics WCCM'18   |
| <b>2018. Paris, France</b>    | Computational Science Engineering and Data Science by TOTAL MATHIAS'18                                       |



# Publications

H. Barucq, H. Calandra, J. Diaz & E. Shishenina. Space-time Trefftz-DG approximation for elasto-acoustics. *Applicable Analysis Journal*. 2018

H. Barucq, H. Calandra, J. Diaz & E. Shishenina. Trefftz - Discontinuous Galerkin Approach for Solving Elastodynamic Problem. *Accepted for publication Proceedings for European Conference on Numerical Mathematics and Advanced Applications ENUMATH'17*. 2018

H. Barucq, H. Calandra, J. Diaz & E. Shishenina. Space-Time Trefftz - Discontinuous Galerkin Approximation For Elasto-Acoustics. *Research Report (RR-9104) Inria Bordeaux-Sud-Ouest, LMAP-CNRS, Total S.A.* 2017



# Contents

<b>Abstract</b>	<b>viii</b>
<b>Acknowledgements</b>	<b>x</b>
<b>Conferences</b>	<b>xii</b>
<b>Publications</b>	<b>xiv</b>
<b>List of Figures</b>	<b>xxii</b>
<b>List of Tables</b>	<b>xxvi</b>
<b>Abbreviations</b>	<b>xxviii</b>
<b>Physical Constants</b>	<b>xxx</b>
<b>Symbols</b>	<b>xxxii</b>
<b>1 Introduction</b>	<b>1</b>
1.1 Seismic survey . . . . .	1
1.1.1 Seismic wave classification . . . . .	2
1.1.2 Basic numerical methods . . . . .	3
1.2 Plan of the thesis . . . . .	7

---

<b>2</b>	<b>Overview of Trefftz-DG methods</b>	<b>9</b>
2.1	Rayleigh - Ritz method: the origin of finite elements . . . . .	13
2.2	The dawn of variational methods: the impact of Timoshenko, Bubnov and Galerkin . . . . .	13
2.2.1	Stephen Timoshenko . . . . .	14
2.2.2	Ivan Bubnov . . . . .	14
2.2.3	Boris Galerkin . . . . .	15
2.3	Trefftz approach . . . . .	15
2.4	Discontinuous Galerkin method . . . . .	16
2.5	Trefftz - Discontinuous Galerkin (Trefftz-DG) method: recent developments	17
2.6	Conclusion . . . . .	18
<b>3</b>	<b>Trefftz method: theory and application to elasto-acoustics</b>	<b>19</b>
3.1	Application to acoustics . . . . .	23
3.1.1	First order formulation of the acoustic system . . . . .	23
3.1.2	Space-time DG formulation for the acoustic system . . . . .	23
3.1.3	Trefftz-DG formulation for the acoustic system . . . . .	27
3.1.4	Well-posedness of the Trefftz-DG formulation for the acoustic system	28
3.2	Application to elastodynamics . . . . .	34
3.2.1	First order formulation of the elastodynamic system . . . . .	34
3.2.2	Space-time DG formulation for the elastodynamic system . . . . .	35
3.2.3	Trefftz-DG formulation for the elastodynamic system . . . . .	38
3.2.4	Well-posedness of the Trefftz-DG formulation for the elastodynamic system . . . . .	39
3.3	Application to elasto-acoustics . . . . .	43
3.3.1	Transmission conditions for the coupled elasto-acoustic system. . .	43
3.3.2	Space-time DG formulation for the elasto-acoustic system . . . . .	44

---

3.3.3	Trefftz-DG formulation for the elasto-acoustic system . . . . .	46
3.3.4	Well-posedness of Trefftz-DG formulation for the elasto-acoustic system . . . . .	48
3.4	Conclusion . . . . .	50
<b>4</b>	<b>Implementation of the Trefftz-DG method</b>	<b>51</b>
4.1	Numerical algorithm . . . . .	55
4.2	Polynomial basis . . . . .	57
4.3	Computation of the global matrix $M$ . . . . .	59
4.3.1	The reference element . . . . .	60
4.3.2	The "local-to-reference" approach. . . . .	63
4.3.3	The "reference-to-local" approach. . . . .	64
4.4	Inversion of the global matrix . . . . .	65
4.5	Change-over between the time slabs . . . . .	69
4.6	Conclusion . . . . .	71
<b>5</b>	<b>Numerical results</b>	<b>73</b>
5.1	1D Acoustic simulations . . . . .	77
5.1.1	Homogeneous medium with periodical boundary conditions . . . . .	77
5.1.2	Heterogeneous medium with "free-surface" boundary conditions . . . . .	80
5.2	2D Simulations . . . . .	80
5.2.1	2D Acoustics . . . . .	81
5.2.1.1	Homogeneous acoustic medium. Initial conditions . . . . .	81
5.2.1.2	Homogeneous acoustic medium. Source term . . . . .	83
5.2.2	2D Elastodynamics . . . . .	84
5.2.2.1	Homogeneous elastic medium. Initial conditions . . . . .	85
5.2.2.2	Homogeneous elastic medium. Source term . . . . .	88



---

<b>A</b>	<b>Some useful identities for the standard DG terms</b>	<b>137</b>
A.1	Jump and average identities . . . . .	139
A.2	Space and time elementwise integration by parts . . . . .	140
<b>B</b>	<b>Trefftz-DG polynomial basis</b>	<b>141</b>
B.1	2D Acoustic system . . . . .	143
B.2	2D Elastodynamic system . . . . .	144
<b>C</b>	<b>Gaussian quadrature</b>	<b>147</b>
C.1	Integration over the unit segment and square . . . . .	149
C.2	Integration over the unit triangle . . . . .	150
	<b>Bibliography</b>	<b>153</b>



# List of Figures

1.1	Ocean Bottom Seismic Data Acquisition (OBSDA). . . . .	1
1.2	Two different types of body waves: $P$ - and $S$ -waves. . . . .	2
1.3	Two different types of surface waves: Love and Rayleigh waves. . . . .	3
3.1	Example of 1D+time mesh $\mathcal{T}_{Fh}$ on $Q_F$ . . . . .	24
3.2	Example of 1D+time mesh $\mathcal{T}_{Sh}$ on $Q_S$ . . . . .	36
3.3	Example of 1D+time mesh $\mathcal{T}_h \equiv \mathcal{T}_{Fh} \cup \mathcal{T}_{Sh}$ on $Q \equiv [\Omega_F \cup \Omega_S] \times I$ . . . . .	44
4.1	Uniform rectangular mesh $\mathcal{T}_{Fh}$ on $Q_F$ . Element numbering. . . . .	55
4.2	Uniform rectangular mesh $\mathcal{T}_{Fh}$ on $Q_F$ . Decomposing into layers. . . . .	56
4.3	Global algebraic linear system with block-tridiagonal matrix. . . . .	56
4.4	1D+time reference element . . . . .	60
4.5	2D+time reference element . . . . .	60
4.6	3D+time reference element (in section $t = 0$ ) . . . . .	61
4.7	Affine map $F_K$ . Element transformation examples . . . . .	61
5.1	Propagation of the exact and numerical velocities $v_F(x, t)$ in a homogeneous 1D fluid domain ( $\alpha_1 = \beta_1 = 0$ ). . . . .	77
5.2	Propagation of the exact and numerical velocities $v_F(x, t)$ in a homogeneous 1D fluid domain ( $\alpha_1 = \beta_1 = 0$ ). . . . .	78
5.3	Propagation of the exact and numerical velocities $\mathbf{v}_F(x, t)$ in a homogeneous 1D fluid domain ( $\alpha_1 = \beta_1 = 0.5$ ). . . . .	78
5.4	Numerical accuracy as a function of $\Delta t/\Delta x$ in a homogeneous 1D fluid domain. . . . .	79
5.5	Convergence of numerical velocity $v_F$ as a function of cell size $\Delta x = \Delta t$ in a homogeneous 1D fluid domain. . . . .	79
5.6	Propagation of the numerical velocity $v_F(x, t)$ in a heterogeneous 1D fluid domain ( $\alpha_1 = \beta_1 = 0.5$ ). . . . .	80
5.7	Propagation of the numerical velocity $\mathbf{v}_F \equiv (v_F^x, v_F^y)$ and pressure $p$ in a homogeneous 2D fluid domain at time $t = 0.3, 0.4, 0.5$ . . . . .	81
5.8	The exact and numerical velocities $\mathbf{v}_F \equiv (v_F^x, v_F^y)$ and pressure $p$ in a homogeneous 2D fluid domain. . . . .	82
5.9	Propagation of the numerical velocity $\mathbf{v}_F \equiv (v_F^x, v_F^y)$ and pressure $p$ in a homogeneous 2D fluid domain at time $t = 0.3, 0.4, 0.5$ . . . . .	83
5.10	The seismograms for exact and numerical velocities $\mathbf{v}_F \equiv (v_F^x, v_F^y)$ in a homogeneous 2D fluid domain. . . . .	84
5.11	Convergence of the numerical velocity $\mathbf{v}_F$ as a function of cell size $\Delta x = \Delta y = \Delta t$ . . . . .	84

5.12	Propagation of the components $v_S^y$ of velocity and $\sigma^{xx}, \sigma^{yy}$ of stress tensor in a homogeneous 2D solid domain at time $t = 0.3, 0.4, 0.5$ . . . . .	85
5.13	The exact and numerical components $v_S^y$ of velocity and $\sigma^{xx}, \sigma^{yy}$ of stress tensor in a homogeneous 2D solid domain. . . . .	86
5.14	Propagation of the components $v_S^x$ of velocity and $\sigma^{xy}$ of stress tensor in a homogeneous 2D solid domain at time $t = 0.3, 0.4, 0.5$ . . . . .	87
5.15	The exact and numerical components $v_S^x$ of velocity and $\sigma^{xy}$ of stress tensor in a homogeneous 2D solid domain. . . . .	88
5.16	Propagation of the components $v_S^x, v_S^y$ of velocity in a homogeneous 2D solid domain at time $t = 0.3, 0.4, 0.5$ . . . . .	89
5.17	The seismograms for exact and numerical velocities $\mathbf{v}_S \equiv (v_S^x, v_S^y)$ in a homogeneous 2D solid domain. . . . .	89
5.18	Propagation of the components $v_S^x, v_S^y$ of velocity and $\sigma^{xx}, \sigma^{yy}, \sigma^{xy}$ of stress tensor in a homogeneous 2D solid domain at time $t = 0.3, 0.4, 0.5$ . . . . .	90
5.19	Convergence of the numerical velocity $\mathbf{v}_S$ as a function of cell size $\Delta x = \Delta y = \Delta t$ . . . . .	90
5.20	Propagation of numerical velocity $\mathbf{v} = (v^x, v^y)$ in a 2D fluid-solid domain at time $t = 0.5, 0.6, , 0.7$ . . . . .	91
5.21	The seismograms for exact and numerical velocities $\mathbf{v} \equiv (v^x, v^y)$ in a 2D fluid-solid domain. . . . .	92
5.22	Propagation of the components $v_F^x, v_F^y$ of numerical velocity and pressure $p$ in a homogeneous 2D fluid domain. . . . .	93
6.1	General construction of a tent-pitching mesh in 1D. . . . .	102
6.2	Determination of the solvability of the wave equation at point $(x_0, t_0)$ when the solution is known on the green line . . . . .	103
6.3	self-contained cells and optimal cells . . . . .	104
6.4	The case of the time slab . . . . .	105
6.5	1D+time tent-pitching mesh examples . . . . .	106
6.6	Three types of space-time tents. . . . .	107
6.7	Fourth type of space-time tents (heterogeneous fluid-solid macro-cell). . . . .	118
6.8	Space-time tent meshes for 1D+time homogeneous medium. . . . .	122
6.9	Space-time tent meshes for 1D+time heterogeneous medium (refinement $\Delta x/2$ in the right zone) . . . . .	122
6.10	Space-time uniform tent meshes for 2D+time homogeneous medium. . . . .	122
6.11	Propagation of the numerical velocity $v_F(x, t)$ in a homogeneous 1D fluid domain. . . . .	123
6.12	Convergence of the numerical velocity $v_F$ as a function of cell size $\Delta x = 2c_F\Delta t$ . . . . .	124
6.13	Propagation of the numerical velocity $v_F(x, t)$ in a heterogeneous 1D fluid domain. . . . .	124
6.14	Propagation of the numerical velocity $\mathbf{v}_F \equiv (v_F^x, v_F^y)$ and the pressure $p$ in a homogeneous 2D fluid domain at time $t = 0.3, 0.4, 0.5$ . . . . .	125
6.15	The seismograms for the exact and numerical velocities $\mathbf{v}_F \equiv (v_F^x, v_F^y)$ in a homogeneous 2D fluid domain. . . . .	126
6.16	Convergence of the numerical velocity $\mathbf{v}_F$ as a function of cell size $\Delta x = \Delta y = \sqrt{2}c_F\Delta t$ . . . . .	126

---

6.17	Propagation of the numerical velocity $\mathbf{v}_S \equiv (v_S^x, v_S^y)$ in a homogeneous 2D solid domain at time $t = 0.6, 0.7, 0.9$ . . . . .	127
6.18	Propagation of the numerical stress tensor in a homogeneous 2D solid domain. . . . .	128
6.19	The seismograms for the exact and numerical velocities $\mathbf{v}_S \equiv (v_S^x, v_S^y)$ in a homogeneous 2D solid domain at time $t = 0.3, 0.4, 0.5$ . . . . .	128
6.20	Convergence of the numerical velocity $\mathbf{v}_S$ as a function of cell size $\Delta x = \Delta y = \sqrt{2}V_P\Delta t$ . . . . .	129
6.21	Propagation of the numerical velocity $\mathbf{v} \equiv (v^x, v^y)$ in a 2D fluid-solid domain at time $t = 0.3, 0.4, 0.6$ . . . . .	129
6.22	The seismograms for the exact and numerical velocities $\mathbf{v} \equiv (v^x, v^y)$ in a 2D fluid-solid domain. . . . .	130
6.23	Speedup of using three algorithms for different model sizes . . . . .	131



# List of Tables

1.1	Basis and test function choice in widely-used numerical methods [112]. . . . .	5
1.2	Generic properties of the most widely used numerical methods [58]. . . . .	6
4.1	Numerical accuracy regarding the inversion process. . . . .	69
B.1	Trefftz-DG polynomial basis for velocity $v_F = (v_F^x(x, y, t); v_F^y(x, y, t))^T$ and pressure $p = p(x, y, t)$ fields (degree $p=0,1,2,3$ ). . . . .	143
B.2	Trefftz-DG polynomial basis for velocity $v_S = (v_S^x(x, y, t); v_S^y(x, y, t))^T$ and stress $\sigma = (\sigma_{xx}(x, y, t), \sigma_{yy}(x, y, t), \sigma_{xy}(x, y, t))$ fields (degree $p=0,1$ ). . . . .	144
B.3	Trefftz-DG polynomial basis for velocity $v_S = (v_S^x(x, y, t); v_S^y(x, y, t))^T$ and stress $\sigma = (\sigma_{xx}(x, y, t), \sigma_{yy}(x, y, t), \sigma_{xy}(x, y, t))$ fields (degree $p=2$ ). . . . .	145
B.4	Trefftz-DG polynomial basis for velocity $v_S = (v_S^x(x, y, t); v_S^y(x, y, t))^T$ and stress $\sigma = (\sigma_{xx}(x, y, t), \sigma_{yy}(x, y, t), \sigma_{xy}(x, y, t))$ fields (degree $p=3$ ). . . . .	146
C.1	Computed weights $w^G$ and corresponding Gauss points $x^G$ for 15 point integration over the unit segment. . . . .	149
C.2	Computed weights $w^G$ and corresponding Gauss points $(x^G, y^G)$ for $n \times n$ point GQUTS ( $n = 2, 3$ ) [63]. . . . .	150
C.3	Computed weights $w^G$ and corresponding Gauss points $(x^G, y^G)$ for $n \times n$ point GQUTS ( $n = 7$ ) [63]. . . . .	151



# Abbreviations

<b>AS</b>	Acoustic System
<b>BEM</b>	Boundary Element Method
<b>DG</b>	Discontinuous Galerkin
<b>DIP</b>	Depth Imaging Partnership
<b>DPG</b>	Discontinuous Petrov-Galerkin
<b>EAS</b>	Elasto-Acoustic System
<b>ES</b>	Elastodynamic System
<b>FDM</b>	Finite Difference Method
<b>FEM</b>	Finite Element Method
<b>FVM</b>	Finite Volume Method
<b>HDG</b>	Hybridizable Discontinuous Galerkin
<b>IBVP</b>	Initial Boundary Value Problem
<b>OBSDA</b>	Ocean Bottom Seismic Data Acquisition
<b>PDE</b>	Partial Differential Equation
<b>SM</b>	Spectral Method
<b>TC</b>	Transmission Conditions
<b>Trefftz-DG</b>	Trefftz - Discontinuous Galerkin
<b>VEM</b>	Virtual Element Method



# Physical Constants

Bulk modulus	$\kappa = \lambda + \frac{2}{3}\mu$	<i>Pa</i>
Poisson's ratio	$\nu = \frac{\lambda}{2\lambda + \mu}$	1
Young's modulus	$E = \frac{\mu(3\lambda + 2\mu)}{\lambda + \mu}$	<i>Pa</i>
<i>P</i> -wave velocity	$V_P = \left(\frac{\lambda + 2\mu}{\rho}\right)^{1/2}$	<i>m · s<sup>-1</sup></i>
<i>S</i> -wave velocity	$V_S = \left(\frac{\mu}{\rho}\right)^{1/2}$	<i>m · s<sup>-1</sup></i>



# Symbols

$\cdot_F$	"Fluid", acoustic medium index	$\cdot$
$\cdot_S$	"Solid", elastic medium index	$\cdot$
$\Omega_F$	physical space (fluid case)	$m^d$
$\Omega_S$	physical space (solid case)	$m^d$
$\Gamma_{FS} \equiv \Omega_F \cap \Omega_S$	fluid-solid interface	$m^{d-1}$
$\Omega \equiv \Omega_F \cup \Omega_S$	physical space (fluid-solid case)	$m^d$
$d$	physical space dimension	1
$N_{dof}$	number of degrees of freedom	1
$I \equiv [0, T]$	time domain	$s$
$Q_F \equiv \Omega_F \times I$	global space (fluid case)	$m^d \cdot t$
$Q_S \equiv \Omega_S \times I$	global space (solid case)	$m^d \cdot t$
$Q \equiv Q_F \cup Q_S$	global space (fluid-solid case)	$m^d \cdot t$
$\rho_F$	fluid density	$kg \cdot m^{-d}$
$\rho_S$	solid density	$kg \cdot m^{-d}$
$c_F$	acoustic wave velocity	$m \cdot s^{-1}$
$\underline{\underline{C}}$	elastic tensor	$Pa$
$\underline{\underline{A}} \equiv \underline{\underline{C}}^{-1}$	inverse of elastic tensor	$Pa^{-1}$
$ \underline{\underline{A}} $	$ \underline{\underline{A}}  = \sup\{\ \underline{\underline{A}}\phi\ /\ \phi\ , \phi \in \mathbb{R}^{(d+1)d/2}, \phi \neq 0\}$	$\cdot$
$\underline{\underline{\epsilon}}$	strain tensor	$s^{-1}$
$\mathbf{v}_F$	velocity (fluid case)	$m \cdot s^{-1}$
$\omega_F$	test function for velocity (fluid case)	$m \cdot s^{-1}$
$\mathbf{v}_S$	velocity (solid case)	$m \cdot s^{-1}$
$\omega_S$	test function for velocity (solid case)	$m \cdot s^{-1}$
$p$	pressure	$Pa$
$q$	test function for pressure	$Pa$
$\underline{\underline{\sigma}}$	stress tensor	$Pa$
$\underline{\underline{\xi}}$	test function for stress tensor	$Pa$
$\hat{\mathbf{v}}_{Fh}$	numerical flux for $\mathbf{v}_F$	$m \cdot s^{-1}$
$\hat{\mathbf{v}}_{Sh}$	numerical flux for $\mathbf{v}_S$	$m \cdot s^{-1}$

$\hat{p}_h$	numerical flux for $p$	$Pa$
$\hat{\underline{\sigma}}_h$	numerical flux for $\underline{\sigma}$	$Pa$
$\check{\mathbf{v}}_{Fh}$	numerical flux for $\mathbf{v}_F$	$m \cdot s^{-1}$
$\check{\mathbf{v}}_{Sh}$	numerical flux for $\mathbf{v}_S$	$m \cdot s^{-1}$
$\check{p}_h$	numerical flux for $p$	$Pa$
$\check{\underline{\sigma}}_h$	numerical flux for $\underline{\sigma}$	$Pa$
$q$	test function for pressure	$Pa$
$\underline{\xi}$	test function for stress tensor	$Pa$
$p$	approximation degree	$\cdot$
$\phi_v$	basis function for velocity	$m \cdot s^{-1}$
$\phi_p$	basis function for pressure	$Pa$
$\phi_\sigma$	basis function for stress	$Pa$
$f$	source function	$s^{-1}$
$g_{DF}$	boundary condition function (fluid case)	$m \cdot s^{-1}$
$g_{DS}$	boundary condition function (solid case)	$Pa$
$K_F$	element (fluid case)	$\cdot$
$K_S$	element (fluid case)	$\cdot$
$\mathbf{n}_{K_F} \equiv (\mathbf{n}_{K_F}^x, n_{K_F}^t)$	outward pointed unit normal vector to $\partial K_F$	1
$\mathbf{n}_{K_S} \equiv (\mathbf{n}_{K_S}^x, n_{K_S}^t)$	outward pointed unit normal vector to $\partial K_S$	1
$\mathcal{T}_{Fh}$	mesh on $Q_F$	$\cdot$
$\mathcal{T}_{Sh}$	mesh on $Q_S$	$\cdot$
$\mathcal{T}_h$	mesh on $Q$	$\cdot$
$\mathcal{T}_{Fh}^{tp}$	mesh on $Q_F$ (tent-pitching)	$\cdot$
$\mathcal{T}_{Sh}^{tp}$	mesh on $Q_S$ (tent-pitching)	$\cdot$
$\mathcal{T}_h^{tp}$	mesh on $Q$ (tent-pitching)	$\cdot$
$\mathcal{F}_{Fh} \equiv \cup_{K_F \in \mathcal{T}_{Fh}} \partial K_F$	mesh skeleton	$\cdot$
$\mathcal{F}_{Sh} \equiv \cup_{K_S \in \mathcal{T}_{Sh}} \partial K_S$	mesh skeleton	$\cdot$
$\mathcal{F}_h \equiv \mathcal{F}_{Fh} \cup \mathcal{F}_{Sh}$	mesh skeleton	$\cdot$
$\mathcal{F}_h^{QF}$	internal faces (fluid case)	$\cdot$
$\mathcal{F}_h^{QS}$	internal faces (solid case)	$\cdot$
$\mathcal{F}_h^{\Omega F}$	internal $\Omega$ -like faces (fluid case)	$\cdot$
$\mathcal{F}_h^{\Omega S}$	internal $\Omega$ -like faces (solid case)	$\cdot$
$\mathcal{F}_h^{IF}$	internal $I$ -like faces (fluid case)	$\cdot$
$\mathcal{F}_h^{IS}$	internal $I$ -like faces (solid case)	$\cdot$
$\mathcal{F}_h^{DF}$	Dirichlet boundary faces (fluid case)	$\cdot$
$\mathcal{F}_h^{DS}$	Dirichlet boundary faces (solid case)	$\cdot$
$\mathcal{F}_h^{0F}$	initial time faces (fluid case)	$\cdot$
$\mathcal{F}_h^{0S}$	initial time faces (solid case)	$\cdot$
$\mathcal{F}_h^{TF}$	final time faces (fluid case)	$\cdot$

$\mathcal{F}_h^{Ts}$	final time faces (solid case)	·
$\mathcal{F}_h^{FS}$	internal $I$ -like faces (fluid-solid interface)	·
$\mathcal{F}_h^{In}$	inflow faces	·
$\mathcal{F}_h^{Out}$	outflow faces	·
$\mathcal{F}_h^{Vert}$	vertical faces (fluid case)	·
$\mathcal{F}_h^{Int}$	internal vertical faces	·
$\mathcal{F}_h^{QF}$	external vertical faces	·
$T_F$	local Trefftz space (fluid case)	·
$T_S$	local Trefftz space (solid case)	·
$T$	local Trefftz space (fluid-solid case)	·
$\mathbf{T}_F$	Trefftz space (fluid case)	·
$\mathbf{T}_S$	Trefftz space (solid case)	·
$\mathbf{T} \equiv \mathbf{T}_F \times \mathbf{T}_S$	Trefftz space (fluid-solid case)	·
$\mathcal{A}_{TDGF}$	bilinear form (fluid case)	·
$\mathcal{A}_{TDGS}$	bilinear form (solid case)	·
$\mathcal{A}_{TDG}$	bilinear form (fluid-solid case)	·
$\ell_{TDGF}$	linear form (fluid case)	·
$\ell_{TDGS}$	linear form (fluid case)	·
$\ell_{TDG}$	linear form (fluid-solid case)	·
$a_{K_F}^{tp}$	local tent-pitching bilinear form (fluid case)	·
$a_{K_S}^{tp}$	local tent-pitching bilinear form (solid case)	·
$a_K^{tp}$	local tent-pitching bilinear form (fluid-solid case)	·
$l_{K_F}^{tp}$	local tent-pitching linear form (fluid case)	·
$l_{K_S}^{tp}$	local tent-pitching linear form (fluid case)	·
$l_K^{tp}$	local tent-pitching linear form (fluid-solid case)	·
$\mathcal{A}_{TDGF}^{tp}$	global tent-pitching bilinear form (fluid case)	·
$\mathcal{A}_{TDGS}^{tp}$	global tent-pitching bilinear form (solid case)	·
$\mathcal{A}_{TDG}^{tp}$	global tent-pitching bilinear form (fluid-solid case)	·
$\ell_{TDGF}^{tp}$	global tent-pitching linear form (fluid case)	·
$\ell_{TDGS}^{tp}$	global tent-pitching linear form (fluid case)	·
$\ell_{TDG}^{tp}$	global tent-pitching linear form (fluid-solid case)	·
$\alpha, \beta, \delta, \gamma$	penalty parameters	1
$N_t \equiv T/\Delta t$	number of time steps	1
$\hat{K}_\Omega^\pm$	reference "space" face	·
$\hat{K}_I$	reference "time" face	·
$F_K$	"reference to local" affine mapping	·
$F_{K_\Omega^\pm}$	"reference to local" affine mapping for $\hat{K}_\Omega^\pm$ faces	·
$F_{K_I}$	"reference to local" affine mapping for $\hat{K}_I$ faces	·

---

$A_K$	matrix of the transformation $F_K$	·
$J_{F_K}$	Jacobian of the transformation $F_K$	·
$(\hat{\mathbf{x}}, \hat{t})_l^G$	Gaussian nodes inside the reference element	$(m^d, s)$
$w_l^G$	Gaussian weights	1
$N_G$	number of points in Gaussian quadrature	1
$M$	global matrix of Trefftz-DG linear system	·
$M_\Omega$	"space" component of $M$	·
$M_I$	"time" component of $M$	·
$\Delta_\Omega$	surface of local "space" face $K_\Omega$	$m^d$
$\Delta_I$	surface of local "time" face $K_I$	$m^{d-1} \cdot s$
$\kappa \equiv \frac{\Delta_I}{\Delta_\Omega}$	ratio between $\Delta_I$ and $\Delta_\Omega$	1
$I$	identity matrix	·
$n$	number of terms in Taylor expansion for approximate matrix inversion	1
$N_K$	number of elements $K$	
$N_{KL}$	number of elements $L$ - neighbors to $K$	
$M_\Omega^K$	diagonal block of $M_\Omega$ corresponding to element $K$	·
$M_I^K$	diagonal block of $M_I$ corresponding to element $K$	·
$M_I^{KL}$	extra-diagonal block of $M_I$ corresponding to element $L$ - neighbor of $K$	·

# Chapter 1

## Introduction

The systematic collection and analysis of geophysical data is called geophysical survey. Geophysical signals transmitted into the Earth interior are the main tool used by geophysicists. Detection and analysis of these signals are the core parts of geophysical signal processing. In industrial applications they permit a fine mapping of the Earth's structure and serve as a workhorse of the search for natural resources, such as oil, gas, or minerals.

### 1.1 Seismic survey

The main form of geophysical survey is the seismic survey. This method is in fact very close to the ultrasound techniques used in medicine and in a number of other applications.

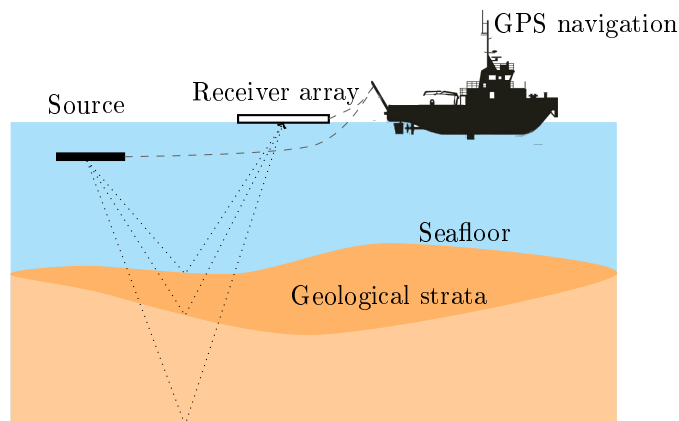


FIGURE 1.1: Ocean Bottom Seismic Data Acquisition (OBSDA).

The sources of pressure waves can be different, depending on the surrounding media: for example, compressed air in fluid, and a vibrator, or explosive in solid media. Waves

created by those techniques are reflected at the interfaces between media layers with different geological properties and recorded by a grid of on-surface detectors: the receiver array (figure 1.1). The acquired data is subjected to numerical analysis, that converts it into a seismic image. This image can be two, three, or four dimensional (in the later case the fourth dimension traces fluid distribution as a function of survey data) [6]. Both the processing and analysis require not only big computational power, but also very sophisticated software that brings together knowledge in mathematics, physics and numerical methods

### 1.1.1 Seismic wave classification

Depending on the propagation type, the seismic waves are grouped into the direct, reflected, refracted and surface waves. The first three types form body waves, which propagate through the entire body, while the surface waves travel only along the surface of the medium. According to the relative direction of local disturbance, the body waves can be of  $P$  - or  $S$  - type (figure 1.2).

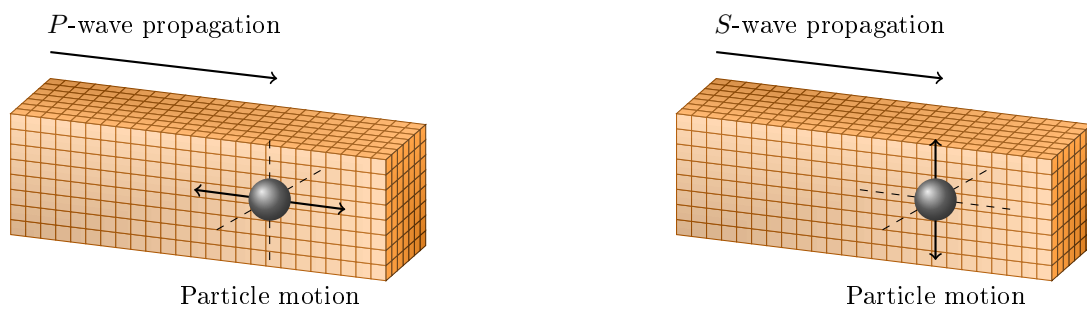


FIGURE 1.2: Two different types of body waves:  $P$ - and  $S$ -waves.

$P$  - motion corresponds to compression and dilation which are directed in the same direction as the wave propagation (along the raypath). This special type of elastic waves is called also an acoustic or pressure wave [6, 25]. It travels faster in materials, so the  $P$  - wave is the first-arriving energy on a seismogram. The  $P$  - wave is generally of higher frequency than  $S$  - and surface waves.

$S$  - motion corresponds to a transverse motion (perpendicular to the direction of propagation, and the raypath).  $S$  - waves do not travel through fluids, so do not exist in air or water.

The velocities of  $P$  - and  $S$  - waves ( $V_P$  and  $V_S$  respectively) are determined by the material properties called elastic constants (or modulus) [25].

The surface waves also include several different types including Love and Rayleigh waves (figure 1.3).

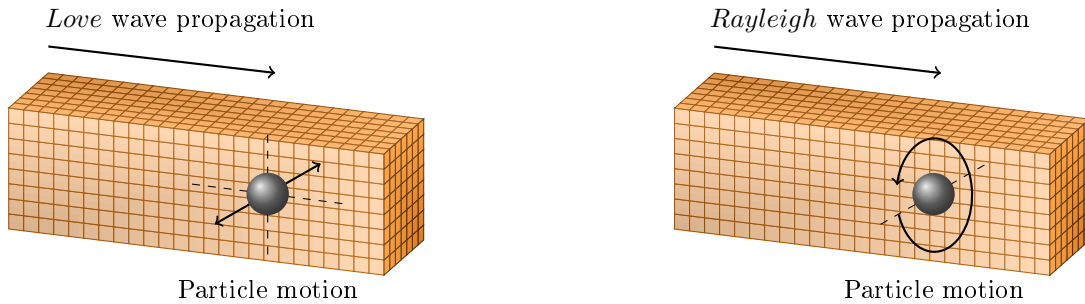


FIGURE 1.3: Two different types of surface waves: Love and Rayleigh waves.

Love waves are characterized by a transverse horizontal motion, perpendicular to the direction of propagation and, generally, parallel to the Earth's surface. Their amplitude is maximum at the surface and decreases as a function of depth. Love waves are dispersive, that is, the wave velocity is dependent on frequency, with low frequencies normally propagating at higher velocity. The depth of penetration of Love waves is also dependent on frequency: lower frequencies correspond to greater depths [25].

Rayleigh motion goes in both directions: direction of propagation and perpendicular to it (in a vertical plane). Rayleigh waves are also dispersive and the amplitudes generally decrease with depth in the Earth [25].

### 1.1.2 Basic numerical methods

Seismic imaging is a classical example of an inverse problem in mathematics. It is called an inverse problem because it starts with the results (receiver data) and then calculates the causes (medium parameters). Mathematically, the inverse problems are usually ill-posed, and their solution is based on iterative reconstruction, with multiple solutions of the corresponding forward problem at each iteration. Thus the performance of inverse problem solvers depend significantly on the efficiency of the solver used for the corresponding forward problem.

Modern computing efficiency has increased to a state where we can compute wave field simulations for realistic 3D models described by parameters of interest provided by seismologists and engineers. Nevertheless, at this stage it is still important to have a good mathematical interpretation of the physical mechanism. A proper method will not only improve the modelling accuracy, but also would give a better mastery of the characterization of the mechanism itself.

Currently, the most popular numerical methods are the grid-based techniques, which interpolate the wave field on a grid of 3D points, for example: Finite Difference Method (FDM), Finite Volume Method (FVM), Finite Element Method (FEM), Spectral Method

(SM) and others. In general, the main differences between the methods lay in the way they represent the exact solution by an approximate one, and in the way this approximate solution satisfies the Partial Differential Equation (PDE). The most widely known FDM, FEM and FVM are all techniques used to derive discrete representation of the spatial derivative operators. Moreover, when adding a time variable, we can address a wide variety of methods for integrating the ordinary differential equations [58].

For a more general description and a better understanding of the construction of a method we provide below some common steps of a standard approximation procedure.

We consider an Initial Boundary Value Problem (IBVP) in a bounded Lipschitz domain  $Q$  as follows:

$$\begin{cases} Lv = f & \text{in } Q, \\ Dv = g & \text{on } \partial Q, \end{cases} \quad (1.1)$$

where the linear operator  $L$  can be decomposed into a product of matrices  $L \equiv S^T O S$ , and  $O$  is a symmetric, positively defined matrix.

We suppose the solution  $v$  of the problem (1.1) can be approximated by the linear combination of basis functions  $\phi_{i,i=1,n}$  in  $Q$  as  $v_h = \sum_{i=1}^n a_i \phi_i$ . The coefficients  $a_{i,i=1,n}$  remain unknown, and computing them requires building a special weighted residual form for the initial problem. Thanks to this form, all the unknown parameters can be obtained by solving a system of algebraic equations [112].

Replacing  $v$  in the (1.1) by its approximate expression, we obtain volume and boundary integrals - residuals, which can be written using the weighting or "test" functions  $\omega_{i,i=1,n}$  in  $Q$  and  $\bar{\omega}_{i,i=1,n}$  at the boundaries  $\partial Q$  in the following form:

$$\int_Q W^T (L(a\Phi) - f) dQ + \int_{\partial Q} \bar{W}^T (D(a\Phi) - g) d\partial Q = 0, \quad (1.2)$$

or after regrouping:

$$\Lambda a = b. \quad (1.3)$$

Here  $\Lambda = \sum_K \Lambda_K$  possesses the finite element properties ( $K$  represents the domain discretization).

Thus, considering a different choice of the trial basis  $\Phi \equiv \phi_{i,i=1,n}$  and test basis  $W \equiv \omega_{i,i=1,n}$  functions provides the multiple approximation procedures [7, 112].

Table 1.1 represents the choice of basis and test functions for some widely-known numerical methods.

Numerical method	Basis function $\Phi \equiv \phi_{i,i=1,n}$	Test function $W \equiv \omega_{i,i=1,n}$
FEM	$W = \Phi = -\overline{W}$ (Galerkin)	defined on a local basis (small support); symmetric $\Lambda$ is obtained by integration by parts, thus, continuity requirements for self-adjoint problem are reduced
SM	as in FEM	defined by series of trigonometric functions or hierarchical polynomials, etc.
FDM	$\phi_i = \delta_i(a_i), i = 1, n$ $\delta$ - is Dirac function	often discontinuous and needs high-order differentiability; collocation process
FVM	as in FDM	$\omega_i = 1$ in $Q_i$ ; $\omega_i = 0$ elsewhere ( $i = 1, n$ ); subdomain collocation
Trefftz-DG	$L\Phi = 0$ - satisfy the governing equation in homogeneous sense; variational formulation remain on boundary	variational formulation: $\int_{\partial I} W^T(t - \bar{t})d\partial I + \int_{\partial\Omega} W^T(v - \bar{v})d\partial\Omega = 0$ , $\bar{v}$ and $\bar{t}$ are prescribed on $\partial\Omega$ and $\partial I$ , where $\partial\Omega \cup \partial I = \partial Q$ ; flexible choice for $W \equiv \omega_{i,i=1,n}$ can be used in applications with: (a) collocation point or subdomain (non-symmetric $\Lambda$ ); (b) least squares (symmetric $\Lambda$ ); (c) Galerkin (symmetric $\Lambda$ )

TABLE 1.1: Basis and test function choice in widely-used numerical methods [112].

We can see from the table 1.1 that Trefftz methods result in a reduction of the number of integration terms in a variational formulation as they must be computed only at the boundaries. However, the global matrices are full, since the functions  $\Phi$  need to be defined over the whole domain. We will return in details to the definition and application of the Trefftz type approximations in chapter 3.

Table 1.2 summarizes general properties of these methods underlining their advantages and drawbacks. Here, "+" represents success, "-" indicates a weakness in the method, and "(+)" reflects that the method with modifications is capable of solving such problems but remains a less natural choice [19].

In the context of the collaborative research program Depth Imaging Partnership (DIP) between Inria and Total, the team-project Magique-3D and the Prospective Lab of Houston develop high-order numerical schemes based mostly on discontinuous finite element

Numerical method	Complex geometries	High-order accuracy and <i>hp</i> -adaptivity	Explicit semi-discrete form	Conservation laws	Elliptic problems
FDM	-	+	+	+	+
FVM	+	-	+	+	(+)
FEM	+	+	-	(+)	+
DG FEM	+	+	+	+	(+)

TABLE 1.2: Generic properties of the most widely used numerical methods [58].

approximation of wave fields. The Discontinuous Galerkin (DG) technique is preferred because it can take into account geometrical and physical features of the environment, and it is well-adapted for parallel computation [11, 58] (see table 1.2). Recently it has been implemented for coupled elasto-acoustic problems, which led to the development of new propagators in time and frequency domains [14, 108].

As was previously mentioned, when compared to the conventional methods based on conforming approximation, the number of degrees of freedom required for achieving a given level of accuracy is higher for DG methods than for conforming ones.

To reduce the cost gap between continuous and discontinuous methods, Hybridizable Discontinuous Galerkin (HDG) methods have been developed and their integration into DIP is under way for both acoustic and elastic domains, with the possibility of numerical coupling (see [70] and references therein).

Another idea to explore consists in using Trefftz approximation space, whose elements are themselves discrete local solutions of the Acoustic System (AS) and Elastodynamic System (ES) [57, 103].

By its construction, the Trefftz method reduces degrees of freedom, since it requires computing only surface integrals to build a variational formulation. We may consider the following advantages of Trefftz method compared to the standard ones: better order of convergence, flexibility in the choice of basis functions, low dispersion, adaptivity and local space-time mesh refinement [57, 103].

It is worth mentioning that most of the studies involving Trefftz approximations consider stationary problems. Time-dependent equations raise a additional difficulty related to the time integration. The use of space-time meshes is then required, easing the implementation of Trefftz approximation in the time-domain.

## 1.2 Plan of the thesis

This work contains four main parts.

Chapter 2 deals with the history of the development of numerical methods for physical systems, addressing the ideas and techniques in the context of increasing computer performance since the Rayleigh-Ritz variational technique, the Trefftz approach and the rise of discontinuous finite element methods.

Chapter 3 is devoted to the development and theoretical analysis of Trefftz-DG method applied to the acoustic, elastodynamic and elasto-acoustic wave propagation systems. A priori error estimates in mesh-dependent norms proves the well-posedness of the acoustic, elastodynamic and elasto-acoustic variational problems, confirming, thus, the existence and uniqueness of the numerical solution. In this chapter we also provide the details of numerical implementation of the algorithm, discuss the choice of basis functions and the optimization techniques corresponding to the global sparse matrix inversion.

The results of numerical tests are presented in chapter 5. We validate the numerical method thanks to some comparisons with analytical solutions obtained with the *Gar6more2D* code [1].

In chapter 6 we investigate the implementation of the variational formulation in tent-pitching meshes following the approach proposed by Gopalakrishnan et al. in [51, 52].

In conclusion we review our results and discuss the possible perspectives of this work.



## Chapter 2

# Overview of Trefftz-DG methods

The last twenty years have seen tremendous progresses in scientific computing which has certainly boosted the development of advanced numerical methods for solving PDEs. Regarding the solution of wave problems set in real domains, the use of high-order methods allows accurate wavefields to be obtained. In the framework of this thesis, we focus on numerical methods based on discontinuous finite element formulations set in Trefftz approximation spaces. The objective is to develop software for solving elasto-acoustic wave problems with the same accuracy as when using standard DG methods but involving less computational burden.

Modern numerical analysis, as well as the practical use of the variational techniques for realistic models, can be credibly said to have been stimulated by the increasing performance of computers. Moreover these methods have a much longer and richer history.

In this chapter we provide a historical account of the development of what we call a Trefftz-DG method and its application to the different classes of problems of numerical analysis.

It is worth noting that this chapter is inspired by the work of Martin J. Gander et al. [48] and Bernardo Cockburn [28] in which we have found very interesting information on Trefftz methods. In the following, we present Trefftz approximation methodology in the framework of DG finite elements. Moreover, as a preamble, we summarize the main achievements leading to the finite element methodology that is widely employed by engineers for solving real problems.



# Contents

2.1	Rayleigh - Ritz method: the origin of finite elements . . . . .	13
2.2	The dawn of variational methods: the impact of Timoshenko, Bubnov and Galerkin . . . . .	13
2.2.1	Stephen Timoshenko . . . . .	14
2.2.2	Ivan Bubnov . . . . .	14
2.2.3	Boris Galerkin . . . . .	15
2.3	Trefftz approach . . . . .	15
2.4	Discontinuous Galerkin method . . . . .	16
2.5	Trefftz-DG method: recent developments . . . . .	17
2.6	Conclusion . . . . .	18



## 2.1 Rayleigh - Ritz method: the origin of finite elements

Lord Rayleigh and Walter Ritz, who independently presented the early results on what will be later known as the finite element method, are nowadays considered as the founders of the subject. In the "Theory of sound" [91], Lord Rayleigh formulated the premises of the finite element method including its implementation. This work was followed by two publications of Walter Ritz [95, 96] in 1908 - 1909, where the method was applied to the calculation of nodal lines of a vibrating plate. These works have a clear practical interest and are based on theoretical works formerly carried out by Gauss and Thompson who highlighted the fundamental link between the variational calculus and the solution of a boundary value problem governed by PDEs.

The first half of the 20<sup>th</sup> century saw the rapid development of the finite element method which was triggered by breakthrough methodologies of Ritz in [94] and [48] meant for solving the longstanding engineering problem of calculating Balmer series.

The only comment that probably has to be added on this first stage of the history of FEM evolution is the story of the founders themselves, in particular of Walter Ritz. It is difficult not to notice that till the recent times there was a huge imbalance between his contribution and the appearance of his name in citations of the main scientific publications of the area. Moreover, the name of the method, "Rayleigh-Ritz", dates back only to the 2000's, while the earlier articles cite it as the "Rayleigh" method.

This evident silencing of Ritz's name is easy to understand by recalling the non-scientific part of the history that went in parallel with the evolution of FEM: since the first publications, he was accused by Rayleigh of plagiarism [92] and these accusations were widely supported by the scientific community. Only in 2005, Leissa showed in his study [74] that Walter Ritz carried out his studies independently and the huge mistake was corrected. From that time, even though the first article was that of Rayleigh, the method is named after both scientists so as to honor the author who dedicated his life to the subject but found very little recognition during his life [48].

## 2.2 The dawn of variational methods: the impact of Timoshenko, Bubnov and Galerkin

As the theory introduced and developed by Rayleigh and Ritz had direct applications, it has attracted the interest not only of pure academics, but even at a bigger scale that of engineers, who were looking for more convenient mathematical tools for solving practical problems that had arisen in the beginning of the 20<sup>th</sup> century. The implementation of

FEM has made huge progress thanks to the works of engineers during the pre-revolution Russian Empire.

### 2.2.1 Stephen Timoshenko

Stephen Timoshenko, a professor of Kyiv Politechnic Institut, was probably the first to realize the importance of the Rayleigh-Ritz method. While giving courses in the institute, he actively explored the Rayleigh-Ritz approach, and applied it later to the buckling problem in his famous textbook "Strength of materials" [102].

It is interesting to note that, while he was inspired initially by Rayleigh's "Theory of sound" [91], he was however one of few researchers who gave credit to Walter Ritz citing him in [101] as a reference for the mathematical description of the method.

Later on, Timoshenko was fired from the institute by the minister of education because of his political activity. Then he moved to Saint-Petersburg where he continued his work on the buckling problem and he developed the theory of elasticity and the theory of beam deflection. In Saint-Petersburg he met other colleagues-engineers: Bubnov, Galerkin, Krylov and Kuteinikov. During these years, in his publications which addressed common engineering problems, he continued to exploit and develop the Rayleigh-Ritz method thus promoting it even further as a powerful tool for engineering calculations.

### 2.2.2 Ivan Bubnov

The works of Timoshenko had inspired a lot of engineers to implement the Rayleigh-Ritz method in their domains of application. One of them, Ivan Bubnov, a naval engineer who earlier participated in the construction of the first Russian submarine, decided to apply the method to ship building.

In 1908, after achieving the position of head of the Institute of Marine Research in Saint-Petersburg, he started to work on the design of the military ships. In 1911, in his work "Structural mechanics applied to ships" [24], he applied for the first time the modified Rayleigh-Ritz approach to considerably simplify the calculation procedure: he directly substituted the expansion for the solution into the differential equation, then multiplied the obtained expression by  $\phi_i dx$  and then integrated over the domain [23, 48]. While he proposed to use a set of orthogonal trigonometric functions  $\phi_i$ , still it was a great step forward in the development of the FEM.

### 2.2.3 Boris Galerkin

Boris Galerkin, an experienced railway engineer, has followed an industrial career path from an engineer on a plant in Kharkov to a position of a steam machine plant director. However, his political activities, notably the labor rights movement, resulted in an arrest in 1906, which has completely changed his life. While in prison, Galerkin decided to abandon his political activities and to dedicate his life to the research. At that time the legal system favored such decisions and during the sentence Galerkin managed to continue the work as an engineer and even to publish his scientific works.

After his imprisonment, Galerkin went on to explore the ongoing research in Europe, in particular visiting Switzerland where he probably met Walter Ritz, as later he cited his publications and even preferred to refer to the Rayleigh-Ritz method as the "Ritz method" [48].

In his famous publication of 1915 [46], that is now cited every time when referring to the Galerkin or Ritz-Galerkin method, he used a similar approach as Bubnov, and he introduced the notion of a mass matrix showing that the chosen set of basis functions do not have to be orthogonal and mentioning that the minimization principle applied by Bubnov can be omitted.

Gathering each of the contributions of Raileigh, Ritz, Timoshenko, Bubnov and Galerkin leads to the statement of the Galerkin method. According to the large number of contributors, it is quite surprising that only the name of Galerkin has been kept. It is very likely that the method has been baptized Galerkin after it had been disseminated in the engineering community by Galerkin who delivered a document, including a simplified setting, on the methodology illustrated by numerous application showcases.

## 2.3 Trefftz approach

The Trefftz approach provides an alternative to the variational approach proposed by Rayleigh and Ritz. The original idea was published in 1926 [103] by Erich Trefftz, a German mathematician and a professor in engineering mechanics of TH Dresden. In his article, the author proposed to use a basis composed of continuous functions which satisfy the homogeneous PDE of interest. Later, this formulation was modified as to search the solution in the form of a boundary integral with the use of the Green functions of the corresponding partial differential equation. The later formulation leads to the solution of a singular-kernel integral [112], that is, as it was pointed out in [113], very similar to the Boundary Element Method (BEM).

The Trefftz method consists in using a basis of Green functions which is very convenient as it easily overcomes the difficulties that may arise for other similar techniques, notably the need to deal with complex operations and non-symmetric linear systems [113]. Moreover, as the trial functions do not need to satisfy the boundary conditions, there is naturally more freedom in their choice.

The further achievements that linked the Trefftz method with the conventional finite element schemes were introduced by Quinlan [89, 90] and Jirousek [64–66]. The resulting approach initially called the "hybrid Trefftz method", nowadays appears under the name of the "Trefftz method" and becoming a promising branch of modern numerical methods [112].

Many authors have worked on the Trefftz approach and on the choice of the corresponding basis functions (see [56, 57] and references therein). The most recent developments were concentrated mainly on the practical aspects of its coupling with the FEM [112].

## 2.4 Discontinuous Galerkin method

The Discontinuous Galerkin Method, or simply DG method, is a technique that was developed in the 1970s in the global context of ensuring energy and moment conservation for the Galerkin approach. For hyperbolic equations, the DG method was applied first in 1973 by Reed and Hill in [93], while for elliptic problems, it was introduced step by step in the works of Babuška, Lions, Zlámal [9] and others. The global idea of the DG method lies in the transformation of the original description of the problem into a set of coupled sub-problems. The DG formulation is obtained after summing up each local formulation set on a single element. The sub-problems are connected by the numerical fluxes which obey certain rules so as for instance to assure conservation laws. During this procedure, the physical characteristics inside each element are considered as constant.

While the DG method had been already well known in other application domains, it has been recently applied to numerous problems of wave dynamics: Maxwell equations [30, 32, 53, 58], vibroacoustic systems, shallow water equations [33, 41, 50], compressible and incompressible Navier-Stokes equations [17, 31, 97], plasma physics [75, 76], and, of course, complex elastic problems [67]. Regarding elastic wave problems, a special extension of the DG method was developed in several papers and among them, important contributions have been carried out by Käser et al. [67, 69], Dumbser et al. [37, 38], and de la Puente et al. [34]. In all these publications, the time dependency of the equations was treated with a global time integration approach, while [38] specifically addressed the local time stepping strategy. In particular, the authors discussed the main issues

of elastic wave problems such as the viscoelastic attenuation, the propagation in the anisotropic media. The arbitrary high-order derivative scheme was also extended to the coupled problem of elasto-acoustics (see [36, 68] and references therein).

Nowadays, the DG method is considered as the cutting-edge method for industrial codes in many application domains. The advantageous position of the DG method is based on multiple factors:

- its overall high-order accuracy for the space discretization along with its ability to account for complicated geometries [28, 58];
- the absence of the continuity restrictions that simplifies the implementation of adaptive mesh strategies [28];
- the degree of the approximating polynomials becomes a local parameter and can be handled easily to take into account the problem features [58];
- the resulting mass matrix has a block-diagonal form and can be inverted block by block allowing the use of highly parallelizable time-domain algorithms [58].

## 2.5 Trefftz-DG method: recent developments

As discussed in the previous section, DG methods are preferred among the scientific community, because they can take into account not only geological and geometrical features of the environment, but also they are well-adapted for parallel computing. Even though DG methods have proven numerical accuracy and flexibility, they are still criticized for requiring a higher number of degrees of freedom compared to the standard methods providing conforming approximations, mostly because they require twice as many more degrees of freedom at element interfaces. The idea to explore the DG type discretization while operating the Trefftz approach seems to be a solution to overcome this computational difficulty [57].

Recently, Trefftz type methods have been widely used with time-harmonic formulations by Farhat, Tezaur, Harari, Hetmaniuk (2003 - 2006) [43, 98], Gabard (2007) [45], Badics (2014) [10], Hiptmair, Moiola, Perugia (2011 - 2016) [59–61, 83], Barucq, Bendali, Diaz, Tordeux, Fares, Mattesi (2017) [15], [13], and others, while studies are still limited for computing transient phenomena. Only few papers are interested in Maxwell equations in time [39, 71, 72, 88], but they are mostly devoted to a theoretical analysis of the method, showing the convergence and stability, and numerical tests with plane waves approximation are restricted to 1D+time dimensional cases. Space-time Trefftz approximation by Lagrange multipliers for the second order formulation of the transient wave equation

was explored in [12, 107]. Recently, Moiola and Perugia (2017) [82] have proposed a Trefftz-DG formulation of the first-order transient acoustic wave equation extending the one-dimensional scheme of Kretzschmar et al. [72] to arbitrary space dimension. In particular, the authors propose a complete a priori error analysis in both mesh-dependent and mesh-independent norms.

## 2.6 Conclusion

This PhD thesis falls under the research program DIP between Inria and Total for the development of advanced numerical methods in geophysical exploration. The background technology is the DG methodology which has a record of accurately approximating wave problems in heterogeneous domains in high-performing computing environment. In this work, we investigate the interest of using DG technology in a Trefftz framework which provides a way to limit the computations on the interfaces of the elements. By this way, we should decrease the computational burden of standard DG approximations. The next chapter deals with the coupling of Trefftz approximations with DG finite elements for solving the first order acoustic, elastodynamic and coupled elasto-acoustic systems.

## Chapter 3

# Trefftz method: theory and application to elasto-acoustics

In this chapter, we apply the Trefftz-DG method for solving first-order acoustic and elastodynamic systems. Then, we couple numerically the two formulations through fluid-solid transmission conditions. We study the well-posedness of the acoustic, elastodynamic and elasto-acoustic Trefftz-DG problems based on mesh-dependent error estimates.

Here and later in this thesis, the subscript  $F$  corresponds to "Fluid" - acoustic medium indicator and  $S$  corresponds to "Solid" - elastic medium indicator.



# Contents

3.1	Application to acoustics . . . . .	23
3.1.1	First order formulation of the acoustic system . . . . .	23
3.1.2	Space-time DG formulation for the acoustic system . . . . .	23
3.1.3	Trefftz-DG formulation for the acoustic system . . . . .	27
3.1.4	Well-posedness of the Trefftz-DG formulation for the acoustic system	28
3.2	Application to elastodynamics . . . . .	34
3.2.1	First order formulation of the elastodynamic system . . . . .	34
3.2.2	Space-time DG formulation for the elastodynamic system . . . . .	35
3.2.3	Trefftz-DG formulation for the elastodynamic system . . . . .	38
3.2.4	Well-posedness of the Trefftz-DG formulation for the elastody- namic system . . . . .	39
3.3	Application to elasto-acoustics . . . . .	43
3.3.1	Transmission conditions for the coupled elasto-acoustic system. . .	43
3.3.2	Space-time DG formulation for the elasto-acoustic system . . . . .	44
3.3.3	Trefftz-DG formulation for the elasto-acoustic system . . . . .	46
3.3.4	Well-posedness of Trefftz-DG formulation for the elasto-acoustic system . . . . .	48
3.4	Conclusion . . . . .	50



### 3.1 Application to acoustics

In physics, the acoustic wave equation defines the propagation of acoustic waves through a fluid medium. It is usually formulated as a second order equation representing the evolution of the pressure field, or in this work we deal with the first order system which describes the evolution of the acoustic pressure  $p$  and the particle velocity  $v$  as functions of coordinates in physical space  $\mathbf{x}$  and time  $t$ . The latter choice is conditioned by the motivation of further numerical coupling of the acoustic formulation with the elastodynamic one, employing the transmission conditions written in terms of velocity and stress.

In the following, we introduce the first order Acoustic System (AS) and build a discrete DG formulation. We describe the associated Trefftz space and derive a Trefftz-DG formulation for the acoustic problem. The analysis of well-posedness of the final Trefftz-DG formulation, based on the coercivity and continuity estimates in mesh-dependent norms, is then presented at the end of this section.

#### 3.1.1 First order formulation of the acoustic system

We introduce a global space-time domain  $Q_F \equiv \Omega_F \times I$ , where  $\Omega_F \subset \mathbb{R}^d$  is a bounded Lipschitz space domain of dimension  $d$  and  $I \equiv [0, T]$  is a time interval. The fluid parameters  $c_F \equiv c_F(\mathbf{x})$  and  $\rho_F \equiv \rho_F(\mathbf{x})$ , standing for the acoustic wave propagation velocity and fluid density respectively, are assumed to be piecewise constant and positive.

We consider the first order acoustic system in terms of velocity  $\mathbf{v}_F \equiv \mathbf{v}_F(\mathbf{x}, t)$  and pressure  $p \equiv p(\mathbf{x}, t)$  fields:

$$\begin{cases} \frac{1}{c_F^2 \rho_F} \frac{\partial p}{\partial t} + \operatorname{div} \mathbf{v}_F = f & \text{in } Q_F, \\ \rho_F \frac{\partial \mathbf{v}_F}{\partial t} + \nabla p = 0 & \text{in } Q_F, \\ \mathbf{v}_F(\cdot, 0) = \mathbf{v}_{F0}, p(\cdot, 0) = p_0 & \text{in } \Omega_F, \\ \mathbf{v}_F \cdot \mathbf{n}_{K_F}^x = g_{D_F} & \text{in } \partial\Omega_F \times I, \end{cases} \quad (3.1)$$

The source term  $f \equiv f(\mathbf{x}, t)$ , the Dirichlet boundary data  $g_{D_F}$ , and the velocity  $\mathbf{v}_{F0}$  and the pressure  $p_0$  are given data.

#### 3.1.2 Space-time DG formulation for the acoustic system

We introduce a non-overlapping space-time mesh  $\mathcal{T}_{Fh}$  composed of Lipschitz smooth elements  $K_F \subset Q_F$ . One additional remark is that, compared to the classical DG

method, where the mesh consists of space elements only, the Trefftz-DG approach requires a space-time mesh on  $Q_F$  composed of space-time elements  $K_F \subset \Omega_F \times I$ . Let  $\mathbf{n}_{K_F} \equiv (\mathbf{n}_{K_F}^x, n_{K_F}^t)$  be the outward pointed unit normal vector on  $\partial K_F$ . We assume that all media parameters are constant in  $K_F$ .

We introduce the space  $V^h(\mathcal{T}_{Fh})$  as a subspace of  $L^2(Q_F)$  defined by  $V^h(\mathcal{T}_{Fh}) = \{\phi \in L^2(Q_F), \phi|_{K_F} \in H^1(K_F)\}$ . The discrete unknowns  $\mathbf{v}_F$  and  $p$  are supposed to be in  $V^h(\mathcal{T}_{Fh})^d$  and  $V^h(\mathcal{T}_{Fh})$  respectively.

Multiplying both equations of (3.1) by the test functions  $q \in V^h(\mathcal{T}_{Fh})$  and  $\boldsymbol{\omega}_F \in V^h(\mathcal{T}_h)^d$  respectively, and integrating by part in time and space, we obtain:

$$\begin{aligned} & - \int_{K_F} \left[ p \left( \frac{1}{c_F^2 \rho_F} \frac{\partial q}{\partial t} + \operatorname{div} \boldsymbol{\omega}_F \right) + \mathbf{v}_F \cdot \left( \rho_F \frac{\partial \boldsymbol{\omega}_F}{\partial t} + \nabla q \right) \right] dv \\ & + \int_{\partial K_F} \left[ \frac{1}{c_F^2 \rho_F} p q n_{K_F}^t + q \mathbf{v}_F \cdot \mathbf{n}_{K_F}^x + \rho_F \mathbf{v}_F \cdot \boldsymbol{\omega}_F n_{K_F}^t + p \boldsymbol{\omega}_F \cdot \mathbf{n}_{K_F}^x \right] ds = \int_{K_F} f q dv. \end{aligned} \quad (3.2)$$

Now that the space-time mesh has been introduced, the mesh skeleton  $\mathcal{F}_{Fh} = \cup_{K_F \in \mathcal{T}_{Fh}} \partial K_F$  can be decomposed into several families of element faces as follows (see figure 3.1):

...	$\mathcal{F}_h^{Q_F}$	internal element faces	
-	$\mathcal{F}_h^{D_F}$	boundary element faces	$(\partial \Omega_F \times [0, T])$
=	$\mathcal{F}_h^{0_F}$	initial time element faces	$(\Omega_F \times \{0\})$
--	$\mathcal{F}_h^{T_F}$	final time element faces	$(\Omega_F \times \{T\})$

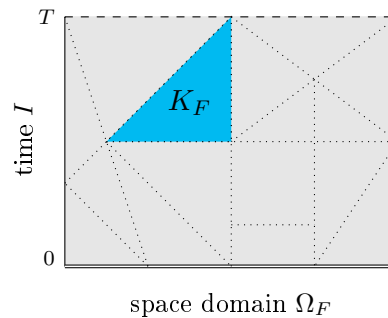


FIGURE 3.1: Example of 1D+time mesh  $\mathcal{T}_{Fh}$  on  $Q_F$ .

The local space-time DG formulation of (3.1) consists in finding  $(\mathbf{v}_{Fh}, p_h) \in V^h(\mathcal{T}_{Fh})^d \times V^h(\mathcal{T}_{Fh})$  such that, for all  $(\boldsymbol{\omega}_F, q) \in V^h(\mathcal{T}_{Fh})^d \times V^h(\mathcal{T}_{Fh})$  and for all  $K_F \in \mathcal{T}_{Fh}$  it holds true:

$$\begin{aligned}
& - \int_{K_F} \left[ p_h \left( \frac{1}{c_F^2 \rho_F} \frac{\partial q}{\partial t} + \operatorname{div} \boldsymbol{\omega}_F \right) + \mathbf{v}_{Fh} \cdot \left( \rho_F \frac{\partial \boldsymbol{\omega}_F}{\partial t} + \nabla q \right) \right] dv \\
& + \int_{\partial K_F} \left[ \frac{1}{c_F^2 \rho_F} \check{p}_h q n_{K_F}^t + q \hat{\mathbf{v}}_{Fh} \cdot \mathbf{n}_{K_F}^x + \rho_F \check{\mathbf{v}}_{Fh} \cdot \boldsymbol{\omega}_F n_{K_F}^t + \hat{p}_h \boldsymbol{\omega}_F \cdot \mathbf{n}_{K_F}^x \right] ds = \int_{K_F} f q dv.
\end{aligned} \tag{3.3}$$

To specify the numerical fluxes  $\hat{\mathbf{v}}_{Fh}$ ,  $\check{\mathbf{v}}_{Fh}$ ,  $\hat{p}_h$  and  $\check{p}_h$ , we introduce notation mimicking the standard DG fluxes. We define the average  $\{\cdot\}$ , the space normal jump  $[\![\cdot]\!]_x$  and the time jump  $[\![\cdot]\!]_t$  between two elements for piecewise-continuous scalar  $p$  and vector  $\mathbf{v}_F$  fields. The indexes " $|K_F^-$ " and " $|K_F^+$ " refer respectively to the interior and the exterior traces for a given element  $K_F$ :

$$\begin{aligned}
\{p\} &\equiv \frac{1}{2}(p|_{K_F^-} + p|_{K_F^+}) && \text{on } \partial K_F^- \cap \partial K_F^+ \in \mathcal{F}_h^{Q_F}, \\
[[p]]_x &\equiv p|_{K_F^-} \mathbf{n}_{K_F^-}^x + p|_{K_F^+} \mathbf{n}_{K_F^+}^x && \text{on } \partial K_F^- \cap \partial K_F^+ \in \mathcal{F}_h^{Q_F}, \\
[[p]]_t &\equiv p|_{K_F^-} n_{K_F^-}^t + p|_{K_F^+} n_{K_F^+}^t && \text{on } \partial K_F^- \cap \partial K_F^+ \in \mathcal{F}_h^{Q_F}, \\
\{\mathbf{v}_F\} &\equiv \frac{1}{2}(\mathbf{v}_F|_{K_F^-} + \mathbf{v}_F|_{K_F^+}) && \text{on } \partial K_F^- \cap \partial K_F^+ \in \mathcal{F}_h^{Q_F}, \\
[[\mathbf{v}_F]]_x &\equiv \mathbf{v}_F|_{K_F^-} \cdot \mathbf{n}_{K_F^-}^x + \mathbf{v}_F|_{K_F^+} \cdot \mathbf{n}_{K_F^+}^x && \text{on } \partial K_F^- \cap \partial K_F^+ \in \mathcal{F}_h^{Q_F}, \\
[[\mathbf{v}_F]]_t &\equiv \mathbf{v}_F|_{K_F^-} n_{K_F^-}^t + \mathbf{v}_F|_{K_F^+} n_{K_F^+}^t && \text{on } \partial K_F^- \cap \partial K_F^+ \in \mathcal{F}_h^{Q_F}.
\end{aligned}$$

The numerical fluxes  $\hat{\mathbf{v}}_{Fh}$ ,  $\check{\mathbf{v}}_{Fh}$ ,  $\hat{p}_h$  and  $\check{p}_h$  on the mesh skeleton  $\mathcal{F}_{Fh} = \bigcup_{K_F \in \mathcal{T}_{Fh}} \partial K_F$  are defined as follows:

$$\begin{aligned}
\begin{pmatrix} \hat{\mathbf{v}}_{Fh} \\ \hat{p}_h \end{pmatrix} &\equiv \begin{pmatrix} \{\mathbf{v}_{Fh}\} + \beta_1 [[p_h]]_x \\ \{p_h\} + \alpha_1 [[\mathbf{v}_{Fh}]]_x \end{pmatrix} && \text{on } \mathcal{F}_h^{Q_F}, \\
\begin{pmatrix} \check{\mathbf{v}}_{Fh} \\ \check{p}_h \end{pmatrix} &\equiv \begin{pmatrix} \{\mathbf{v}_{Fh}\} + \alpha_2 [[\mathbf{v}_{Fh}]]_t \\ \{p_h\} + \beta_2 [[p_h]]_t \end{pmatrix} && \text{on } \mathcal{F}_h^{Q_F}, \\
\begin{pmatrix} \hat{\mathbf{v}}_{Fh} \cdot \mathbf{n}_{K_F}^x \\ \hat{p}_h \end{pmatrix} &\equiv \begin{pmatrix} g_{D_F} \\ p_h + \alpha_1 (\mathbf{v}_{Fh} \cdot \mathbf{n}_{K_F}^x - g_{D_F}) \end{pmatrix} && \text{on } \mathcal{F}_h^{D_F}, \\
\begin{pmatrix} \check{\mathbf{v}}_{Fh} \\ \check{p}_h \end{pmatrix} &\equiv \begin{pmatrix} \mathbf{v}_{Fh} \\ p_h \end{pmatrix} && \text{on } \mathcal{F}_h^{T_F}, \\
\begin{pmatrix} \check{\mathbf{v}}_{Fh} \\ \check{p}_h \end{pmatrix} &\equiv \begin{pmatrix} \left( \frac{1}{2} - \alpha_2 \right) \mathbf{v}_{Fh} + \left( \frac{1}{2} + \alpha_2 \right) \mathbf{v}_{F0} \\ \left( \frac{1}{2} - \beta_2 \right) p_h + \left( \frac{1}{2} + \beta_2 \right) p_0 \end{pmatrix} && \text{on } \mathcal{F}_h^{0_F}.
\end{aligned}$$

Here,  $\alpha_1$ ,  $\alpha_2$ ,  $\beta_1$  and  $\beta_2$  are positive penalty parameters. The additional terms  $\alpha_1 \llbracket \mathbf{v}_{Fh} \rrbracket_x$ ,  $\alpha_2 \llbracket \mathbf{v}_{Fh} \rrbracket_t$ , and  $\beta_1 \llbracket p_h \rrbracket_x$ ,  $\beta_2 \llbracket p_h \rrbracket_t$  called penalty functions, consist of a penalty parameter multiplied by a measure of violation of the constraints. Regarding standard DG methods, they have been shown to be necessary for numerical stability of the scheme [17, 18]. Actually, it will be shown in section 3.1.4 that the choice of non-zero penalty terms will improve the accuracy and convergence results (see chapter 5). Alternative choices of penalty terms are discussed in [9, 17, 18, 22] for standard DG approximations. Herein, because of a lack of literature in Trefftz-DG, we use the most common for standard DG methods penalty terms [30, 84]. It is worth noting that if  $(\mathbf{v}_F, p)$  is solution of (3.1), all the jump terms in definitions of  $\hat{\mathbf{v}}_F$ ,  $\hat{p}$ ,  $\check{\mathbf{v}}_F$ ,  $\check{p}$  vanish, and  $\hat{\mathbf{v}}_F = \check{\mathbf{v}}_F = \mathbf{v}_F$  and  $\hat{p} = \check{p} = p$ , showing the consistency of the numerical fluxes.

Summing the contribution (3.3) of all elements  $K_F \in \mathcal{T}_{Fh}$ , we obtain the DG formulation for (3.1):

Seek  $(\mathbf{v}_{Fh}, p_h) \in V^h(\mathcal{T}_{Fh})^d \times V^h(\mathcal{T}_{Fh})$  such that, for all  $(\boldsymbol{\omega}_F, q) \in V^h(\mathcal{T}_{Fh})^d \times V^h(\mathcal{T}_{Fh})$ , it holds true:

$$\begin{aligned}
& - \sum_{K_F \in \mathcal{T}_{Fh}} \int_{K_F} \left[ p_h \left( \frac{1}{c_F^2 \rho_F} \frac{\partial q}{\partial t} + \operatorname{div} \boldsymbol{\omega}_F \right) + \mathbf{v}_{Fh} \cdot \left( \rho_F \frac{\partial \boldsymbol{\omega}_F}{\partial t} + \nabla q \right) \right] dv \quad (3.4) \\
& + \int_{\mathcal{F}_h^{QF}} \left[ \frac{1}{c_F^2 \rho_F} \{p_h\} \llbracket q \rrbracket_t + \rho_F \{ \mathbf{v}_{Fh} \} \cdot \llbracket \boldsymbol{\omega}_F \rrbracket_t + \{p_h\} \llbracket \boldsymbol{\omega}_F \rrbracket_x + \{ \mathbf{v}_{Fh} \} \cdot \llbracket q \rrbracket_x \right] ds \\
& + \int_{\mathcal{F}_h^{QF}} \left[ \alpha_1 \llbracket \mathbf{v}_{Fh} \rrbracket_x \llbracket \boldsymbol{\omega}_F \rrbracket_x + \beta_1 \llbracket p_h \rrbracket_x \cdot \llbracket q \rrbracket_x + \alpha_2 \rho_F \llbracket \mathbf{v}_{Fh} \rrbracket_t \cdot \llbracket \boldsymbol{\omega}_F \rrbracket_t + \frac{\beta_2}{c_F^2 \rho_F} \llbracket p_h \rrbracket_t \llbracket q \rrbracket_t \right] ds \\
& + \int_{\mathcal{F}_h^{TF}} \left[ \frac{1}{c_F^2 \rho_F} p_h q + \rho_F \mathbf{v}_{Fh} \cdot \boldsymbol{\omega}_F \right] ds - \left( \frac{1}{2} - \beta_2 \right) \int_{\mathcal{F}_h^{0F}} \frac{1}{c_F^2 \rho_F} p_h q ds - \left( \frac{1}{2} - \alpha_2 \right) \int_{\mathcal{F}_h^{0F}} \rho_F \mathbf{v}_{Fh} \cdot \boldsymbol{\omega}_F ds \\
& + \int_{\mathcal{F}_h^{DF}} \left[ p_h \boldsymbol{\omega}_F \cdot \mathbf{n}_{K_F}^x + \alpha_1 (\mathbf{v}_{Fh} \cdot \mathbf{n}_{K_F}^x) (\boldsymbol{\omega}_F \cdot \mathbf{n}_{K_F}^x) \right] ds = \int_{\mathcal{F}_h^{DF}} \left[ \alpha_1 g_{DF} \boldsymbol{\omega}_F \cdot \mathbf{n}_{K_F}^x - q g_{DF} \right] ds \\
& + \left( \frac{1}{2} + \beta_2 \right) \int_{\mathcal{F}_h^{0F}} \frac{1}{c_F^2 \rho_F} p_0 q ds + \left( \frac{1}{2} + \alpha_2 \right) \int_{\mathcal{F}_h^{0F}} \rho_F \mathbf{v}_{F0} \cdot \boldsymbol{\omega}_F ds + \sum_{K_F \in \mathcal{T}_{Fh}} \int_{K_F} f q dv.
\end{aligned}$$

In the following, we restrict the problem to the homogeneous system of equations with a zero source term  $f \equiv 0$  and "free-surface" boundary condition  $g_{DF} \equiv 0$ , in order to simplify the presentation. We do not lose the generality of approach in this case, because both terms appear only in the right-hand side of formulation, and can always be bounded above, provided they are regular enough. However, the numerical applications will involve non-zero source term, periodical and "free-surface" boundaries (see chapter 5).

### 3.1.3 Trefftz-DG formulation for the acoustic system

We introduce a Trefftz space defined by:

$$\mathbf{T}_F(\mathcal{T}_{Fh}) \equiv \left\{ (\boldsymbol{\omega}_F, q) \in V^h(\mathcal{T}_{Fh})^d \times V^h(\mathcal{T}_{Fh}) \text{ such that, } \rho_F \frac{\partial \boldsymbol{\omega}_F}{\partial t} + \nabla q = 0 \text{ and } \frac{1}{c_F^2 \rho_F} \frac{\partial q}{\partial t} + \operatorname{div} \boldsymbol{\omega}_F = 0 \text{ in all } K_F \in \mathcal{T}_{Fh} \right\}.$$

This space is of Trefftz type since it is a subspace of the regular space  $V^h(\mathcal{T}_{Fh})^d \times V^h(\mathcal{T}_{Fh})$  composed of local solutions of the governing equations in the volume under study set in each element  $K_F$ . We consider a discrete Trefftz space  $\mathbf{T}_F^p(\mathcal{T}_{Fh})$  defined by:

$$\mathbf{T}_F^p(\mathcal{T}_{Fh}) \equiv \left\{ (\boldsymbol{\omega}_F, q) \in \mathbf{T}_F(\mathcal{T}_{Fh}), (\boldsymbol{\omega}_F, q) |_{K_F} \in \mathbb{P}^p(K_F)^d \times \mathbb{P}^p(K_F), \text{ for all } K_F \in \mathcal{T}_{Fh} \right\}.$$

According to (3.4), this choice of basis functions leads to remove all volume integral terms in the DG formulation. The corresponding Trefftz-DG formulation for acoustic system reduces then to:

Seek  $(\mathbf{v}_{Fh}, p_h) \in \mathbf{T}_F^p(\mathcal{T}_{Fh})$  such that, for all  $(\boldsymbol{\omega}_F, q) \in \mathbf{T}_F^p(\mathcal{T}_{Fh})$ , it holds true:

$$\begin{aligned} & \int_{\mathcal{F}_h^{QF}} \left[ \frac{1}{c_F^2 \rho_F} \{p_h\} \{q\}_t + \rho_F \{\mathbf{v}_{Fh}\} \cdot \{\boldsymbol{\omega}_F\}_t + \{p_h\} \{\boldsymbol{\omega}_F\}_x + \{\mathbf{v}_{Fh}\} \cdot \{q\}_x \right] ds \\ & + \int_{\mathcal{F}_h^{QF}} \left[ \alpha_1 \{\mathbf{v}_{Fh}\}_x \{\boldsymbol{\omega}_F\}_x + \beta_1 \{p_h\}_x \cdot \{q\}_x + \alpha_2 \rho_F \{\mathbf{v}_{Fh}\}_t \cdot \{\boldsymbol{\omega}_F\}_t + \frac{\beta_2}{c_F^2 \rho_F} \{p_h\}_t \{q\} \right] ds \\ & + \int_{\mathcal{F}_h^{TF}} \left[ \frac{1}{c_F^2 \rho_F} p_h q + \rho_F \mathbf{v}_{Fh} \cdot \boldsymbol{\omega}_F \right] ds - \left( \frac{1}{2} - \beta_2 \right) \int_{\mathcal{F}_h^{0F}} \frac{1}{c_F^2 \rho_F} p_h q \, ds - \left( \frac{1}{2} - \alpha_2 \right) \int_{\mathcal{F}_h^{0F}} \rho_F \mathbf{v}_{Fh} \cdot \boldsymbol{\omega}_F \, ds \\ & + \int_{\mathcal{F}_h^{DF}} \left[ p_h \boldsymbol{\omega}_F \cdot \mathbf{n}_{K_F}^x + \alpha_1 (\mathbf{v}_{Fh} \cdot \mathbf{n}_{K_F}^x) (\boldsymbol{\omega}_F \cdot \mathbf{n}_{K_F}^x) \right] ds = \int_{\mathcal{F}_h^{DF}} \left[ \alpha_1 g_{DF} \boldsymbol{\omega}_F \cdot \mathbf{n}_{K_F}^x - q g_{DF} \right] ds \\ & + \left( \frac{1}{2} + \beta_2 \right) \int_{\mathcal{F}_h^{0F}} \frac{1}{c_F^2 \rho_F} p_0 q \, ds + \left( \frac{1}{2} + \alpha_2 \right) \int_{\mathcal{F}_h^{0F}} \rho_F \mathbf{v}_{F0} \cdot \boldsymbol{\omega}_F \, ds. \end{aligned}$$

Compared to the Trefftz-DG formulation developed by Kretzschmar et al. for Maxwell's equation in [72], we can use arbitrary convex elements, we do not have to discriminate "time" and "space" faces, and we obtain the coercivity more straightforwardly as shown in section 3.1.4. It is also worth mentioning that, compared to the classical space DG formulation (3.4), Trefftz-DG formulation (3.5) does not contain any differential operator (except for a specific choice of boundary conditions, such as higher-order absorbing boundaries).

We introduce the bilinear form  $\mathcal{A}_{TDG_F}(\cdot; \cdot)$  defined by:

$$\begin{aligned}
\mathcal{A}_{TDG_F}((\mathbf{v}_{Fh}, p_h); (\boldsymbol{\omega}_F, q)) \equiv & \quad (3.5) \\
& \int_{\mathcal{F}_h^{Q_F}} \left[ \frac{1}{c_F^2 \rho_F} \{p_h\} [q]_t + \rho_F \{\mathbf{v}_{Fh}\} \cdot [\boldsymbol{\omega}_F]_t + \{p_h\} [\boldsymbol{\omega}_F]_x + \{\mathbf{v}_{Fh}\} \cdot [q]_x \right] ds \\
& + \int_{\mathcal{F}_h^{Q_F}} \left[ \alpha_1 [\mathbf{v}_{Fh}]_x [\boldsymbol{\omega}_F]_x + \beta_1 [p_h]_x \cdot [q]_x + \alpha_2 \rho_F [\mathbf{v}_{Fh}]_t \cdot [\boldsymbol{\omega}_F]_t + \frac{\beta_2}{c_F^2 \rho_F} [p_h]_t [q] \right] ds \\
& + \int_{\mathcal{F}_h^{D_F}} \left[ p_h \boldsymbol{\omega}_F \cdot \mathbf{n}_{K_F}^x + \alpha_1 (\mathbf{v}_{Fh} \cdot \mathbf{n}_{K_F}^x) (\boldsymbol{\omega}_F \cdot \mathbf{n}_{K_F}^x) \right] ds + \int_{\mathcal{F}_h^{T_F}} \left[ \frac{1}{c_F^2 \rho_F} p_h q + \rho_F \mathbf{v}_{Fh} \cdot \boldsymbol{\omega}_F \right] ds \\
& - \left( \frac{1}{2} - \beta_2 \right) \int_{\mathcal{F}_h^{0_F}} \frac{1}{c_F^2 \rho_F} p_h q ds - \left( \frac{1}{2} - \alpha_2 \right) \int_{\mathcal{F}_h^{0_F}} \rho_F \mathbf{v}_{Fh} \cdot \boldsymbol{\omega}_F ds,
\end{aligned}$$

and the linear form  $\ell_{TDG_F}(\cdot)$  defined by:

$$\ell_{TDG_F}(\boldsymbol{\omega}_F, q) \equiv \left( \frac{1}{2} + \beta_2 \right) \int_{\mathcal{F}_h^{0_F}} \frac{1}{c_F^2 \rho_F} p_0 q ds + \left( \frac{1}{2} + \alpha_2 \right) \int_{\mathcal{F}_h^{0_F}} \rho_F \mathbf{v}_{F0} \cdot \boldsymbol{\omega}_F ds. \quad (3.6)$$

It is worth noting that, if  $(\mathbf{v}_F, p)$  is solution of (3.1), then  $\mathcal{A}_{TDG_F}((\mathbf{v}_F, p); (\boldsymbol{\omega}_F, q)) = \mathcal{A}_{TDG_F}((\mathbf{v}_{Fh}, p_h); (\boldsymbol{\omega}_F, q))$  thanks to the consistency of the numerical fluxes. Regarding the above notations, the Trefftz-DG formulation (3.5) can be rewritten as follows:

Seek  $(\mathbf{v}_{Fh}, p_h) \in \mathbf{T}_F^p(\mathcal{T}_{Fh})$  such that, for all  $(\boldsymbol{\omega}_F, q) \in \mathbf{T}_F^p(\mathcal{T}_{Fh})$ , it holds true:

$$\mathcal{A}_{TDG_F}((\mathbf{v}_{Fh}, p_h); (\boldsymbol{\omega}_F, q)) = \ell_{TDG_F}(\boldsymbol{\omega}_F, q). \quad (3.7)$$

If we replace the unknown functions by their decomposition onto the Trefftz basis, the variational problem (3.7) can be solved as a global algebraic linear system whose unknown is the set of coefficients of the Trefftz expansion. This will be done in chapter 4).

In the next section, we analyze the well-posedness of problem (3.7) using estimates in mesh-dependent  $L^2$ -norms.

### 3.1.4 Well-posedness of the Trefftz-DG formulation for the acoustic system

The analysis of well-posedness of the Trefftz-DG problem (3.7) is based on coercivity and continuity estimates. This study is carried out in the framework developed in [72] for the time-dependent Maxwell's problem.

We set  $p_h = q$  and  $\mathbf{v}_{Fh} = \boldsymbol{\omega}_F$ , so that the bilinear form  $\mathcal{A}_{TDG_F}(\cdot; \cdot)$  reads as:

$$\begin{aligned}
& \mathcal{A}_{TDG_F}((\boldsymbol{\omega}_F, q); (\boldsymbol{\omega}_F, q)) \equiv \\
& \int_{\mathcal{F}_h^{QF}} \left[ \frac{1}{c_F^2 \rho_F} \{q\} [q]_t + \rho_F \{\boldsymbol{\omega}_F\} \cdot [\boldsymbol{\omega}_F]_t + \{q\} [\boldsymbol{\omega}_F]_x + \{\boldsymbol{\omega}_F\} \cdot [q]_x \right] ds \\
& + \int_{\mathcal{F}_h^{QF}} \left[ \alpha_1 [\boldsymbol{\omega}_F]_x [\boldsymbol{\omega}_F]_x + \beta_1 [q]_x \cdot [q]_x + \alpha_2 \rho_F [\boldsymbol{\omega}_F]_t \cdot [\boldsymbol{\omega}_F]_t + \frac{\beta_2}{c_F^2 \rho_F} [q]_t [q]_t \right] ds \\
& + \int_{\mathcal{F}_h^{DF}} \left[ p_h \boldsymbol{\omega}_F \cdot \mathbf{n}_{K_F}^x + \alpha_1 (\boldsymbol{\omega}_F \cdot \mathbf{n}_{K_F}^x) (\boldsymbol{\omega}_F \cdot \mathbf{n}_{K_F}^x) \right] ds + \int_{\mathcal{F}_h^{TF}} \left[ \frac{1}{c_F^2 \rho_F} q^2 + \rho_F \boldsymbol{\omega}_F \cdot \boldsymbol{\omega}_F \right] ds \\
& - \left( \frac{1}{2} - \beta_2 \right) \int_{\mathcal{F}_h^{0F}} \frac{1}{c_F^2 \rho_F} q^2 ds - \left( \frac{1}{2} - \alpha_2 \right) \int_{\mathcal{F}_h^{0F}} \rho_F \boldsymbol{\omega}_F \cdot \boldsymbol{\omega}_F ds = \\
& \underbrace{\int_{\mathcal{F}_h^{QF}} \left[ \frac{1}{c_F^2 \rho_F} \{q\} [q]_t + \rho_F \{\boldsymbol{\omega}_F\} \cdot [\boldsymbol{\omega}_F]_t \right] ds}_{[5]} + \underbrace{\beta_2 \int_{\mathcal{F}_h^{0F}} \frac{1}{c_F^2 \rho_F} q^2 ds + \alpha_2 \int_{\mathcal{F}_h^{0F}} \rho_F \boldsymbol{\omega}_F \cdot \boldsymbol{\omega}_F ds}_{[3]} \\
& + \underbrace{\int_{\mathcal{F}_h^{QF}} \left[ \{q\} [\boldsymbol{\omega}_F]_x + \{\boldsymbol{\omega}_F\} \cdot [q]_x \right] ds}_{[6]} + \int_{\mathcal{F}_h^{DF}} q \boldsymbol{\omega}_F \cdot \mathbf{n}_{K_F}^x ds \\
& + \underbrace{\int_{\mathcal{F}_h^{QF}} \left[ \alpha_1 [\boldsymbol{\omega}_F]_x [\boldsymbol{\omega}_F]_x + \beta_1 [q]_x \cdot [q]_x + \alpha_2 \rho_F [\boldsymbol{\omega}_F]_t \cdot [\boldsymbol{\omega}_F]_t + \frac{\beta_2}{c_F^2 \rho_F} [q]_t [q]_t \right] ds}_{[1]} \\
& + \underbrace{\frac{1}{2} \int_{\mathcal{F}_h^{TF}} \left[ \frac{1}{c_F^2 \rho_F} q^2 + \rho_F \boldsymbol{\omega}_F \cdot \boldsymbol{\omega}_F \right] ds}_{[7]} - \underbrace{\frac{1}{2} \int_{\mathcal{F}_h^0} \left[ \frac{1}{c_F^2 \rho_F} q^2 + \rho_F \boldsymbol{\omega}_F \cdot \boldsymbol{\omega}_F \right] ds}_{[7]} \\
& + \underbrace{\frac{1}{2} \int_{\mathcal{F}_h^{TF}} \left[ \frac{1}{c_F^2 \rho_F} q^2 + \rho_F \boldsymbol{\omega}_F \cdot \boldsymbol{\omega}_F \right] ds}_{[2]} + \underbrace{\int_{\mathcal{F}_h^{DF}} \alpha_1 (\boldsymbol{\omega}_F \cdot \mathbf{n}_{K_F}^x) (\boldsymbol{\omega}_F \cdot \mathbf{n}_{K_F}^x) ds}_{[4]}.
\end{aligned}$$

We estimate each term on the right-hand side in mesh-dependent  $L^2$ -norms as follows:

$$\begin{aligned}
[1] & \equiv \int_{\mathcal{F}_h^{QF}} \left[ \alpha_1 [\boldsymbol{\omega}_F]_x [\boldsymbol{\omega}_F]_x + \beta_1 [q]_x \cdot [q]_x + \alpha_2 \rho_F [\boldsymbol{\omega}_F]_t \cdot [\boldsymbol{\omega}_F]_t + \frac{\beta_2}{c_F^2 \rho_F} [q]_t [q]_t \right] ds = \\
& \left\| \alpha_1^{1/2} [\boldsymbol{\omega}_F]_x \right\|_{L^2(\mathcal{F}_h^{QF})}^2 + \left\| \beta_1^{1/2} [q]_x \right\|_{L^2(\mathcal{F}_h^{QF})}^2 + \left\| \alpha_2^{1/2} \rho_F^{1/2} [\boldsymbol{\omega}_F]_t \right\|_{L^2(\mathcal{F}_h^{QF})}^2 \\
& + \left\| \beta_2^{1/2} \left( \frac{1}{c_F^2 \rho_F} \right)^{1/2} [q]_t \right\|_{L^2(\mathcal{F}_h^{QF})}^2;
\end{aligned}$$

$$[2] \equiv \frac{1}{2} \int_{\mathcal{F}_h^{TF}} \left[ \frac{1}{c_F^2 \rho_F} q^2 + \rho_F \boldsymbol{\omega}_F \cdot \boldsymbol{\omega}_F \right] ds = \frac{1}{2} \left\| \left( \frac{1}{c_F^2 \rho_F} \right)^{1/2} q \right\|_{L^2(\mathcal{F}_h^{TF})}^2 + \frac{1}{2} \left\| \rho_F^{1/2} \boldsymbol{\omega}_F \right\|_{L^2(\mathcal{F}_h^{TF})}^2;$$

$$[3] \equiv \beta_2 \int_{\mathcal{F}_h^{0F}} \frac{1}{c_F^2 \rho_F} q^2 ds + \alpha_2 \int_{\mathcal{F}_h^{0F}} \rho_F \boldsymbol{\omega}_F \cdot \boldsymbol{\omega}_F ds = \left\| \beta_2^{1/2} \left( \frac{1}{c_F^2 \rho_F} \right)^{1/2} q \right\|_{L^2(\mathcal{F}_h^{0F})}^2 \\ + \left\| \alpha_2^{1/2} \rho_F^{1/2} \boldsymbol{\omega}_F \right\|_{L^2(\mathcal{F}_h^{0F})}^2;$$

$$[4] \equiv \int_{\mathcal{F}_h^{DF}} \alpha_1 (\boldsymbol{\omega}_F \cdot \mathbf{n}_{K_F}^x) (\boldsymbol{\omega}_F \cdot \mathbf{n}_{K_F}^x) ds = \left\| \alpha_1^{1/2} (\boldsymbol{\omega}_F \cdot \mathbf{n}_{K_F}^x) \right\|_{L^2(\mathcal{F}_h^{DF})}^2;$$

$$[5] \equiv \int_{\mathcal{F}_h^{QF}} \left[ \frac{1}{c_F^2 \rho_F} \{q\} [q]_t + \rho_F \{\boldsymbol{\omega}_F\} \cdot [\boldsymbol{\omega}_F]_t \right] ds \stackrel{(A.1),(A.2)}{=} \frac{1}{2} \int_{\mathcal{F}_h^{QF}} \frac{1}{c_F^2 \rho_F} [q^2]_t ds \\ + \frac{1}{2} \int_{\mathcal{F}_h^{QF}} \rho_F [\boldsymbol{\omega}_F \cdot \boldsymbol{\omega}_F]_t ds;$$

$$[6] \equiv \int_{\mathcal{F}_h^{QF}} \left[ \{q\} [\boldsymbol{\omega}_F]_x + \{\boldsymbol{\omega}_F\} \cdot [q]_x \right] ds + \int_{\mathcal{F}_h^{DF}} q \boldsymbol{\omega}_F \cdot \mathbf{n}_{K_F}^x ds \stackrel{(A.4)}{=} \\ \int_{\mathcal{F}_h^{QF}} [q \boldsymbol{\omega}_F]_x ds + \int_{\mathcal{F}_h^{DF}} q \boldsymbol{\omega}_F \cdot \mathbf{n}_{K_F}^x ds \stackrel{(A.9)}{=} \sum_{K_F \in \mathcal{T}_h K_F} \int (\boldsymbol{\omega}_F \cdot \nabla q + q \operatorname{div} \boldsymbol{\omega}_F) dv;$$

$$[7]+[5] \equiv \frac{1}{2} \int_{\mathcal{F}_h^{TF}} \left[ \frac{1}{c_F^2 \rho_F} q^2 + \rho_F \boldsymbol{\omega}_F \cdot \boldsymbol{\omega}_F \right] ds - \frac{1}{2} \int_{\mathcal{F}_h^{0F}} \left[ \frac{1}{c_F^2 \rho_F} q^2 + \rho_F \boldsymbol{\omega}_F \cdot \boldsymbol{\omega}_F \right] ds \\ + \frac{1}{2} \int_{\mathcal{F}_h^{QF}} \left[ \frac{1}{c_F^2 \rho_F} [q^2]_t + \rho_F [\boldsymbol{\omega}_F \cdot \boldsymbol{\omega}_F]_t \right] ds \stackrel{(A.6),(A.7)}{=} \sum_{K_F \in \mathcal{T}_h K_F} \int \frac{1}{c_F^2 \rho_F} q \frac{\partial q}{\partial t} dv \\ + \sum_{K_F \in \mathcal{T}_h K_F} \int \rho_F \boldsymbol{\omega}_F \cdot \frac{\partial \boldsymbol{\omega}_F}{\partial t} dv;$$

$$[6]+[7] + [5] \equiv \sum_{K_F \in \mathcal{T}_h K_F} \int \frac{1}{c_F^2 \rho_F} q \frac{\partial q}{\partial t} dv + \sum_{K_F \in \mathcal{T}_h K_F} \int \rho_F \boldsymbol{\omega}_F \cdot \frac{\partial \boldsymbol{\omega}_F}{\partial t} dv \\ + \sum_{K_F \in \mathcal{T}_h K_F} \int (\boldsymbol{\omega}_F \cdot \nabla q + q \operatorname{div} \boldsymbol{\omega}_F) dv = \\ \sum_{K_F \in \mathcal{T}_h} \left[ \int_{K_F} \overbrace{q \left( \frac{1}{c_F^2 \rho_F} \frac{\partial q}{\partial t} + \operatorname{div} \boldsymbol{\omega}_F \right)}^{=0 \text{ in } \mathbf{T}_F(\mathcal{T}_h)} dv + \int_{K_F} \overbrace{\boldsymbol{\omega}_F \cdot \left( \rho_F \frac{\partial \boldsymbol{\omega}_F}{\partial t} + \nabla q \right)}^{=0 \text{ in } \mathbf{T}_F(\mathcal{T}_h)} dv \right].$$

Thus, for the bilinear form  $\mathcal{A}_{TDG_F}(\cdot; \cdot)$  we obtain:

$$\begin{aligned} \mathcal{A}_{TDG_F}((\boldsymbol{\omega}_F, q); (\boldsymbol{\omega}_F, q)) &\equiv \left\| \alpha_1^{1/2} \llbracket \boldsymbol{\omega}_F \rrbracket_x \right\|_{L^2(\mathcal{F}_h^{Q_F})}^2 + \left\| \beta_1^{1/2} \llbracket q \rrbracket_x \right\|_{L^2(\mathcal{F}_h^{Q_F})}^2 \\ &+ \left\| \alpha_2^{1/2} \rho_F^{1/2} \llbracket \boldsymbol{\omega}_F \rrbracket_t \right\|_{L^2(\mathcal{F}_h^{Q_F})}^2 + \left\| \beta_2^{1/2} \left( \frac{1}{c_F^2 \rho_F} \right)^{1/2} \llbracket q \rrbracket_t \right\|_{L^2(\mathcal{F}_h^{Q_F})}^2 + \frac{1}{2} \left\| \left( \frac{1}{c_F^2 \rho_F} \right)^{1/2} q \right\|_{L^2(\mathcal{F}_h^{T_F})}^2 \\ &+ \frac{1}{2} \left\| \rho_F^{1/2} \boldsymbol{\omega}_F \right\|_{L^2(\mathcal{F}_h^{T_F})}^2 + \left\| \beta_2^{1/2} \left( \frac{1}{c_F^2 \rho_F} \right)^{1/2} q \right\|_{L^2(\mathcal{F}_h^{0_F})}^2 + \left\| \alpha_2^{1/2} \rho_F^{1/2} \boldsymbol{\omega}_F \right\|_{L^2(\mathcal{F}_h^{0_F})}^2 \\ &+ \left\| \alpha_1^{1/2} (\boldsymbol{\omega}_F \cdot \mathbf{n}_{K_F}^x) \right\|_{L^2(\mathcal{F}_h^{D_F})}^2. \end{aligned}$$

We can see that  $\mathcal{A}_{TDG_F}((\boldsymbol{\omega}_F, q); (\boldsymbol{\omega}_F, q))$  is positive, which leads us to introduce the semi-norm  $||| \cdot |||_{TDG_F}$  given by:

$$|||(\boldsymbol{\omega}_F, q)|||_{TDG_F} \equiv \mathcal{A}_{TDG_F}^{1/2}((\boldsymbol{\omega}_F, q); (\boldsymbol{\omega}_F, q)) \quad (3.8)$$

and defined as follows:

$$\begin{aligned} |||(\boldsymbol{\omega}_F, q)|||_{TDG_F}^2 &\equiv \left\| \alpha_1^{1/2} \llbracket \boldsymbol{\omega}_F \rrbracket_x \right\|_{L^2(\mathcal{F}_h^{Q_F})}^2 + \left\| \beta_1^{1/2} \llbracket q \rrbracket_x \right\|_{L^2(\mathcal{F}_h^{Q_F})}^2 + \left\| \alpha_2^{1/2} \rho_F^{1/2} \llbracket \boldsymbol{\omega}_F \rrbracket_t \right\|_{L^2(\mathcal{F}_h^{Q_F})}^2 \\ &+ \left\| \beta_2^{1/2} \left( \frac{1}{c_F^2 \rho_F} \right)^{1/2} \llbracket q \rrbracket_t \right\|_{L^2(\mathcal{F}_h^{Q_F})}^2 + \left\| \alpha_1^{1/2} (\boldsymbol{\omega}_F \cdot \mathbf{n}_{K_F}^x) \right\|_{L^2(\mathcal{F}_h^{D_F})}^2 \\ &+ \frac{1}{2} \left\| \left( \frac{1}{c_F^2 \rho_F} \right)^{1/2} q \right\|_{L^2(\mathcal{F}_h^{T_F})}^2 + \frac{1}{2} \left\| \rho_F^{1/2} \boldsymbol{\omega}_F \right\|_{L^2(\mathcal{F}_h^{T_F})}^2 + \left\| \beta_2^{1/2} \left( \frac{1}{c_F^2 \rho_F} \right)^{1/2} q \right\|_{L^2(\mathcal{F}_h^{0_F})}^2 \\ &+ \left\| \alpha_2^{1/2} \rho_F^{1/2} \boldsymbol{\omega}_F \right\|_{L^2(\mathcal{F}_h^{0_F})}^2. \end{aligned}$$

We have:

**Theorem 3.1.** *The semi-norm  $||| \cdot |||_{TDG_F}$  is a norm in the Trefftz space  $\mathbf{T}_F(\mathcal{T}_{Fh})$ .*

*Proof.* When  $|||(\boldsymbol{\omega}_F, q)|||_{TDG_F} = 0$ , it automatically implies that  $\boldsymbol{\omega}_F$  and  $q$  satisfy the initial acoustic equations (3.1) with zero initial  $\mathbf{v}_{F0} = p_0 = 0$  and boundary conditions  $g_{D_F} = 0$ , and also with  $f = 0$ , which follows from the fact that  $\boldsymbol{\omega}_F$  and  $p$  are in  $\mathbf{T}_F(\mathcal{T}_{Fh})$ . By the existence and uniqueness theorem for the Cauchy problem (3.1), it admits a unique solution in  $Q_F$ , which is  $\boldsymbol{\omega}_F = 0, q = 0$ .  $\square$

From the theorem 3.1, we straightforwardly get that  $\mathcal{A}_{TDG_F}(\cdot; \cdot)$  is coercive in  $\mathbf{T}_F(\mathcal{T}_{Fh})$  equipped with the norm  $||| \cdot |||_{TDG_F}$ .

Next, we address the continuity property of both  $\mathcal{A}_{TDG_F}(\cdot; \cdot)$  and  $\ell_{TDG_F}(\cdot)$ . For that purpose, it is convenient to introduce the semi-norm  $||| \cdot |||_{TDG_F^*}$  defined by:

$$\begin{aligned} |||(\boldsymbol{\omega}_F, q)|||_{TDG_F^*}^2 &\equiv |||(\boldsymbol{\omega}_F, q)|||_{TDG_F}^2 \\ &+ \left\| \alpha_1^{-1/2} \{q\} \right\|_{L^2(\mathcal{F}_h^{Q_F})}^2 + \left\| \beta_1^{-1/2} \{\boldsymbol{\omega}_F\} \right\|_{L^2(\mathcal{F}_h^{Q_F})}^2 + \left\| \alpha_1^{-1/2} q \right\|_{L^2(\mathcal{F}_h^{D_F})}^2 \\ &+ \left\| \alpha_2^{-1/2} \{\boldsymbol{\omega}_F\} \right\|_{L^2(\mathcal{F}_h^{Q_F})}^2 + \left\| \beta_2^{-1/2} \{q\} \right\|_{L^2(\mathcal{F}_h^{Q_F})}^2 \\ &+ \left\| \left( \frac{1}{2\beta_2} + 1 \right)^{1/2} \left( \frac{1}{c_F^2 \rho_F} \right)^{1/2} q \right\|_{L^2(\mathcal{F}_h^{0_F})}^2 + \left\| \left( \frac{1}{2\alpha_2} + 1 \right)^{1/2} \rho_F^{1/2} \boldsymbol{\omega}_F \right\|_{L^2(\mathcal{F}_h^{0_F})}^2. \end{aligned}$$

Regarding the definition of the semi-norm  $||| \cdot |||_{TDG_F^*}$  we have the following theorem:

**Theorem 3.2.** *The semi-norm  $||| \cdot |||_{TDG_F^*}$  is a norm in  $\mathbf{T}_F$ .*

*Proof.* Indeed, by definition of  $||| \cdot |||_{TDG_F^*}$ , the fact that  $|||(\boldsymbol{\omega}_F, q)|||_{TDG_F^*} = 0$  straightforwardly implies  $|||(\boldsymbol{\omega}_F, q)|||_{TDG_F} = 0$ , that is a norm in  $\mathbf{T}_F(\mathcal{T}_{Fh})$ .  $\square$

Thanks to the norms  $||| \cdot |||_{TDG_F}$  and  $||| \cdot |||_{TDG_F^*}$ , and by using the weighted Cauchy-Schwartz inequality [7], we obtain the continuity estimate for the bilinear form  $\mathcal{A}_{TDG_F}(\cdot; \cdot)$ :

$$|\mathcal{A}_{TDG_F}((\mathbf{v}_F, p); (\boldsymbol{\omega}_F, q))| \leq C_1 |||(\mathbf{v}_F, p)|||_{TDG_F^*} |||(\boldsymbol{\omega}_F, q)|||_{TDG_F}. \quad (3.9)$$

Indeed, if we consider independently each integral term of  $\mathcal{A}_{TDG_F}((\mathbf{v}_F, p); (\boldsymbol{\omega}_F, q))$ , starting from the first one  $\int_{\mathcal{F}_h^{Q_F}} \frac{1}{c_F^2 \rho_F} \{p\} [q]_t ds$ , we can easily verify that:

$$\begin{aligned} \int_{\mathcal{F}_h^{Q_F}} \frac{1}{c_F^2 \rho_F} \{p\} [q]_t ds &\leq \left( \int_{\mathcal{F}_h^{Q_F}} (\beta_2^{-1/2} \{p\})^2 ds \right)^{1/2} \left( \int_{\mathcal{F}_h^{Q_F}} (\beta_2^{1/2} \left( \frac{1}{c_F^2 \rho_F} \right)^{1/2} [q]_t)^2 ds \right)^{1/2} = \\ &\left\| \beta_2^{-1/2} \{p\} \right\|_{L^2(\mathcal{F}_h^{Q_F})} \left\| \beta_2^{1/2} \left( \frac{1}{c_F^2 \rho_F} \right)^{1/2} [q]_t \right\|_{L^2(\mathcal{F}_h^{Q_F})} \\ &\leq |||(\mathbf{v}_F, p)|||_{TDG_F^*} |||(\boldsymbol{\omega}_F, q)|||_{TDG_F}. \end{aligned}$$

We proceed similarly for all the integrals of the bilinear form. By summing the contributions of all the integrals, the inequality (3.9) can be straightforwardly deduced. Using the same approach we can build a bound for linear form  $\ell_{TDG_F}(\cdot)$ , confirming thus its continuity with respect to the  $||| \cdot |||_{TDG_F^*}$  norm:

$$\begin{aligned} |\ell_{TDG_F}(\boldsymbol{\omega}_F, q)| &\leq \\ &\left[ \left\| \left( \frac{1}{2\alpha_2} + 1 \right)^{1/2} \rho_F^{1/2} \mathbf{v}_{F0} \right\|_{L^2(\mathcal{F}_h^{0_F})}^2 + \left\| \left( \frac{1}{2\beta_2} + 1 \right)^{1/2} \left( \frac{1}{c_F^2 \rho_F} \right)^{1/2} p_0 \right\|_{L^2(\mathcal{F}_h^{0_F})}^2 \right]^{1/2} |||(\boldsymbol{\omega}_F, q)|||_{TDG_F}. \end{aligned}$$

**Theorem 3.3.** *The Trefftz-DG variational problem (3.7) admits a unique weak solution  $(\mathbf{v}_{Fh}, p_h) \in \mathbf{T}_F^p(\mathcal{T}_{Fh})$ . Moreover, the following estimate holds true:*

$$\|(\mathbf{v}_F - \mathbf{v}_{Fh}, p - p_h)\|_{TDG_F} \leq (1 + C_1) \inf_{(\boldsymbol{\omega}_F, q) \in \mathbf{T}_F^p(\mathcal{T}_{Fh})} \|(\mathbf{v}_F - \boldsymbol{\omega}_F, p - q)\|_{TDG_F^*}.$$

*Proof.* Supposing the zero initial and boundary conditions in (3.7), the coercivity of the bilinear form  $\mathcal{A}_{TDG_F}(\cdot; \cdot)$  implies straightforwardly  $\mathbf{v}_{Fh} = 0$  and  $p_h = 0$ , proving, thus, the uniqueness of solution of (3.7). Regarding the fact that the space  $\mathbf{T}_F^p(\mathcal{T}_{Fh})$  is finite dimensional, existence of the solution follows from the uniqueness.

Applying the triangle inequality to  $\|(\mathbf{v}_F - \mathbf{v}_{Fh}, p - p_h)\|_{TDG_F}$ , and by definition of the norm  $\|\cdot\|_{TDG_F^*}$ , for all  $(\boldsymbol{\omega}_F, q) \in \mathbf{T}_F^p(\mathcal{T}_{Fh})$  we have:

$$\begin{aligned} \|(\mathbf{v}_F - \mathbf{v}_{Fh}, p - p_h)\|_{TDG_F} &= \|(\mathbf{v}_F - \boldsymbol{\omega}_F + \boldsymbol{\omega}_F - \mathbf{v}_{Fh}, p - q + q - p_h)\|_{TDG_F} \\ &\leq \|(\mathbf{v}_{Fh} - \boldsymbol{\omega}_F, p_h - q)\|_{TDG_F} + \|(\mathbf{v}_F - \boldsymbol{\omega}_F, p - q)\|_{TDG_F} \\ &\leq \|(\mathbf{v}_{Fh} - \boldsymbol{\omega}_F, p_h - q)\|_{TDG_F} + \|(\mathbf{v}_F - \boldsymbol{\omega}_F, p - q)\|_{TDG_F^*}. \end{aligned}$$

Taking into account the consistency of the bilinear form  $\mathcal{A}_{TDG_F}(\cdot; \cdot)$  (3.5) due to the consistency of the numerical fluxes, for all test functions  $(\boldsymbol{\omega}_F, q)$  in continuous Trefftz space  $\mathbf{T}_F(\mathcal{T}_{Fh})$  we deduce:

$$\mathcal{A}_{TDG_F}((\mathbf{v}_{Fh} - \mathbf{v}_F, p_h - p); (\boldsymbol{\omega}_F, q)) = 0.$$

Thus,

$$\mathcal{A}_{TDG_F}((\mathbf{v}_{Fh} - \mathbf{v}_F, p_h - p); (\mathbf{v}_{Fh} - \boldsymbol{\omega}_F, p_h - q)) = 0$$

and

$$\begin{aligned} \mathcal{A}_{TDG_F}((\mathbf{v}_{Fh} - \boldsymbol{\omega}_F, p_h - q); (\mathbf{v}_{Fh} - \boldsymbol{\omega}_F, p_h - q)) &= \\ \mathcal{A}_{TDG_F}((\mathbf{v}_{Fh} - \mathbf{v}_F + \mathbf{v}_F - \boldsymbol{\omega}_F, p_h - p + p - q); (\mathbf{v}_{Fh} - \boldsymbol{\omega}_F, p_h - q)) &= \\ \mathcal{A}_{TDG_F}((\mathbf{v}_F - \boldsymbol{\omega}_F, p - q); (\mathbf{v}_{Fh} - \boldsymbol{\omega}_F, p_h - q)). \end{aligned}$$

Applying the coercivity (3.8) and continuity (3.9) estimates to the latter equality, we obtain:

$$\begin{aligned} \mathcal{A}_{TDG_F}((\mathbf{v}_F - \boldsymbol{\omega}_F, p - q); (\mathbf{v}_{Fh} - \boldsymbol{\omega}_F, p_h - q)) &= \|(\mathbf{v}_{Fh} - \boldsymbol{\omega}_F, p_h - q)\|_{TDG_F}^2, \\ |\mathcal{A}_{TDG_F}((\mathbf{v}_F - \boldsymbol{\omega}_F, p - q); (\mathbf{v}_{Fh} - \boldsymbol{\omega}_F, p_h - q))| & \\ &\leq C_1 \|(\mathbf{v}_F - \boldsymbol{\omega}_F, p - q)\|_{TDG_F^*} \|(\mathbf{v}_{Fh} - \boldsymbol{\omega}_F, p_h - q)\|_{TDG_F}. \end{aligned}$$

It gives:

$$\begin{aligned} & \|\!(\mathbf{v}_{Fh} - \boldsymbol{\omega}_F, p_h - q)\|\|_{TDG_F} + \|\!(\mathbf{v}_F - \boldsymbol{\omega}_F, p - q)\|\|_{TDG_F^*} = \\ & \quad \mathcal{A}_{TDG_F}((\mathbf{v}_F - \boldsymbol{\omega}_F, p - q); (\mathbf{v}_{Fh} - \boldsymbol{\omega}_F, p_h - q)) / \|\!(\mathbf{v}_{Fh} - \boldsymbol{\omega}_F, p_h - q)\|\|_{TDG_F} \\ & \quad + \|\!(\mathbf{v}_F - \boldsymbol{\omega}_F, p - q)\|\|_{TDG_F^*} \leq (1 + C_1) \|\!(\mathbf{v}_F - \boldsymbol{\omega}_F, p - q)\|\|_{TDG_F^*}, \end{aligned}$$

thus,

$$\|\!(\mathbf{v}_F - \mathbf{v}_{Fh}, p - p_h)\|\|_{TDG_F} \leq (1 + C_1) \inf_{(\boldsymbol{\omega}_F, q) \in \mathbf{T}_F^p(\mathcal{T}_{Fh})} \|\!(\mathbf{v}_F - \boldsymbol{\omega}_F, p - q)\|\|_{TDG_F^*}.$$

□

It is worth noting that, since we are working with mesh-dependent norms, we cannot exhibit the order of convergence of the method. To obtain mesh-independent norms, we could investigate how to extend the strategy proposed in [82] to our formulation. The numerical results in chapters 5 and 6 will illustrate the fact that the method converges at least as fast as classical DG methods.

## 3.2 Application to elastodynamics

In this part, we consider the first order elastodynamic system. We introduce the corresponding Trefftz approximation space and we develop a discrete Trefftz-DG formulation for the elastodynamic problem.

The analysis of well-posedness of the final Trefftz-DG formulation is still based on the coercivity and continuity estimates in mesh-dependent  $L^2$ -norms, and it is presented in the end of this section.

### 3.2.1 First order formulation of the elastodynamic system

The elastodynamic system is based on the three fundamental laws of continuum mechanics: motion equation, constitutive equation (Hooke's law), and geometric equation (infinitesimal strain tensor definition) [73].

As in the acoustic case, we introduce a global space-time domain  $Q_S \equiv \Omega_S \times I$ , which is the Cartesian product of a bounded Lipschitz space domain  $\Omega_S \subset \mathbb{R}^d$  of dimension  $d$  and a time interval  $I \equiv [0, T]$ . The Lamé coefficients  $\lambda \equiv \lambda(\mathbf{x})$ ,  $\mu \equiv \mu(\mathbf{x})$  and the solid density  $\rho_S \equiv \rho_S(\mathbf{x})$  are the parameters representing the solid medium, assumed to be piecewise constant and positive.

We then consider the first order formulation of the elastodynamic system in terms of velocity  $\mathbf{v}_S \equiv \mathbf{v}_S(\mathbf{x}, t)$  and stress  $\underline{\boldsymbol{\sigma}} \equiv \underline{\boldsymbol{\sigma}}(\mathbf{x}, t)$  fields:

$$\begin{cases} \frac{\partial \underline{\boldsymbol{\sigma}}}{\partial t} - \underline{\mathbf{C}} \underline{\boldsymbol{\varepsilon}}(\mathbf{v}_S) = 0 & \text{in } Q_S, \\ \rho_S \frac{\partial \mathbf{v}_S}{\partial t} - \mathbf{div} \underline{\boldsymbol{\sigma}} = 0 & \text{in } Q_S, \\ \mathbf{v}_S(\cdot, 0) = \mathbf{v}_{S0}, \underline{\boldsymbol{\sigma}}(\cdot, 0) = \underline{\boldsymbol{\sigma}}_0 & \text{in } \Omega_S, \\ \underline{\boldsymbol{\sigma}} \mathbf{n}_S = \mathbf{g}_{D_S} & \text{in } \partial\Omega_S \times I. \end{cases} \quad (3.10)$$

Here,  $\underline{\mathbf{C}}$  is the elastic tensor (symmetric and positive),  $\underline{\boldsymbol{\varepsilon}}(\mathbf{v}_S) = \frac{1}{2}(\nabla \mathbf{v}_S + \nabla \mathbf{v}_S^T)$  is the infinitesimal strain tensor,  $\mathbf{n}_S \equiv (\mathbf{n}_{S_x}^x, \mathbf{n}_{S_t}^t)$  is the outward pointed unit normal vector on  $\partial\Omega_S \times I$ . The boundary conditions are given by  $\mathbf{g}_{D_S} \equiv \mathbf{g}_{D_S}(\mathbf{x}, t)$ , and the initial data by specifying the velocity  $\mathbf{v}_{S0}$  and the stress  $\underline{\boldsymbol{\sigma}}_0$ .

By the symmetry and positiveness of the tensor  $\underline{\mathbf{C}}$ , the application  $\underline{\boldsymbol{\varepsilon}} \mapsto \underline{\mathbf{C}} \underline{\boldsymbol{\varepsilon}}$  is an isomorphism in the symmetrical tensor space [73]. Thus, we may consider the corresponding inverse application  $\underline{\mathbf{A}}$ , verifying the same properties of symmetry and positiveness. Using this notation, the elastodynamic system (3.10) can be rewritten in an equivalent way as follows:

$$\begin{cases} \underline{\mathbf{A}} \frac{\partial \underline{\boldsymbol{\sigma}}}{\partial t} - \underline{\boldsymbol{\varepsilon}}(\mathbf{v}_S) = 0 & \text{in } Q_S, \\ \rho_S \frac{\partial \mathbf{v}_S}{\partial t} - \mathbf{div} \underline{\boldsymbol{\sigma}} = 0 & \text{in } Q_S, \\ \mathbf{v}_S(\cdot, 0) = \mathbf{v}_{S0}, \underline{\boldsymbol{\sigma}}(\cdot, 0) = \underline{\boldsymbol{\sigma}}_0 & \text{in } \Omega_S, \\ \underline{\boldsymbol{\sigma}} \mathbf{n}_S = \mathbf{g}_{D_S} & \text{in } \partial\Omega_S \times I. \end{cases} \quad (3.11)$$

### 3.2.2 Space-time DG formulation for the elastodynamic system

We introduce a non-overlapping space-time mesh  $\mathcal{T}_{Sh}$  on  $Q_S$  composed of space-time Lipschitz elements  $K_S \subset \Omega_S \times I$ . Let  $\mathbf{n}_{K_S} \equiv (\mathbf{n}_{K_S}^x, \mathbf{n}_{K_S}^t)$  the outward pointed unit normal vector on  $\partial K_S$ . The elastic medium parameters are assumed to be constant in  $K_S$ . The discrete unknowns  $\mathbf{v}_S$  and  $\underline{\boldsymbol{\sigma}}$  are supposed to be in  $V^h(\mathcal{T}_{Sh})^d$  and  $V^h(\mathcal{T}_{Sh})^{d^2}$  respectively. Here again  $V^h(\mathcal{T}_{Sh})$  is the subspace of functions of  $L^2(Q_S)$ , whose restriction on  $K_S$  belongs to the Sobolev space  $H^1(K_S)$ .

Multiplying both equations of (3.11) by the test functions  $\underline{\boldsymbol{\xi}} \in V^h(\mathcal{T}_{Sh})^{d^2}$  and  $\boldsymbol{\omega}_S \in V^h(\mathcal{T}_{Sh})^d$  respectively, and using Green's identities [7], we obtain:

$$\begin{aligned}
& - \int_{K_S} \left[ \underline{\boldsymbol{\sigma}} : \left( \underline{\mathbf{A}} \frac{\partial \underline{\boldsymbol{\xi}}}{\partial t} - \underline{\boldsymbol{\varepsilon}}(\boldsymbol{\omega}_S) \right) + \mathbf{v}_S \cdot \left( \rho_S \frac{\partial \boldsymbol{\omega}_S}{\partial t} - \mathbf{div} \underline{\boldsymbol{\xi}} \right) \right] dv \\
& + \int_{\partial K_S} \left[ \underline{\mathbf{A}} \underline{\boldsymbol{\sigma}} : \underline{\boldsymbol{\xi}} n_{K_S}^t - \underline{\boldsymbol{\xi}} \mathbf{v}_S \cdot \mathbf{n}_{K_S}^x + \rho_S \mathbf{v}_S \cdot \boldsymbol{\omega}_S n_{K_S}^t - \underline{\boldsymbol{\sigma}} : (\boldsymbol{\omega}_S \otimes \mathbf{n}_{K_S}^x) \right] ds = 0.
\end{aligned} \tag{3.12}$$

The mesh skeleton  $\mathcal{F}_{Sh} = \cup_{K_S \in \mathcal{T}_{Sh}} \partial K_S$  can be decomposed into several families of element faces as follows (see figure 3.2):

...	$\mathcal{F}_h^{Q_S}$	internal element faces	
-	$\mathcal{F}_h^{D_S}$	boundary element faces	$(\partial \Omega_S \times [0, T])$
=	$\mathcal{F}_h^{0_S}$	initial time element faces	$(\Omega_S \times \{0\})$
--	$\mathcal{F}_h^{T_S}$	final time element faces	$(\Omega_S \times \{T\})$

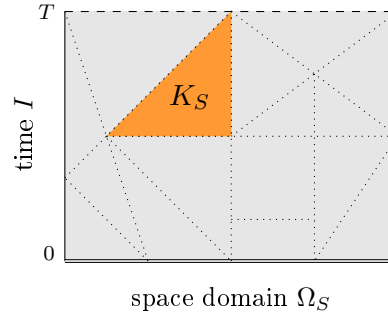


FIGURE 3.2: Example of 1D+time mesh  $\mathcal{T}_{Sh}$  on  $Q_S$ .

The local space-time DG formulation of (3.11) consists in finding  $(\mathbf{v}_{Sh}, \underline{\boldsymbol{\sigma}}_h) \in V^h(\mathcal{T}_{Sh})^d \times V^h(\mathcal{T}_{Sh})^{d^2}$  such that, for all  $(\boldsymbol{\omega}_S, \underline{\boldsymbol{\xi}}) \in V^h(\mathcal{T}_{Sh})^d \times V^h(\mathcal{T}_{Sh})^{d^2}$  and for all  $K_S \in \mathcal{T}_{Sh}$ , it holds true:

$$\begin{aligned}
& - \int_{K_S} \left[ \underline{\boldsymbol{\sigma}}_h : \left( \underline{\mathbf{A}} \frac{\partial \underline{\boldsymbol{\xi}}}{\partial t} - \underline{\boldsymbol{\varepsilon}}(\boldsymbol{\omega}_S) \right) + \mathbf{v}_{Sh} \cdot \left( \rho_S \frac{\partial \boldsymbol{\omega}_S}{\partial t} - \mathbf{div} \underline{\boldsymbol{\xi}} \right) \right] dv \\
& + \int_{\partial K_S} \left[ \underline{\mathbf{A}} \underline{\boldsymbol{\sigma}}_h : \underline{\boldsymbol{\xi}} n_{K_S}^t - \underline{\boldsymbol{\xi}} \hat{\mathbf{v}}_{Sh} \cdot \mathbf{n}_{K_S}^x + \rho_S \check{\mathbf{v}}_{Sh} \cdot \boldsymbol{\omega}_S n_{K_S}^t - \hat{\underline{\boldsymbol{\sigma}}}_h : (\boldsymbol{\omega}_S \otimes \mathbf{n}_{K_S}^x) \right] ds = 0.
\end{aligned} \tag{3.13}$$

To specify the numerical fluxes  $\hat{\mathbf{v}}_{Sh}$ ,  $\check{\mathbf{v}}_{Sh}$ ,  $\hat{\underline{\boldsymbol{\sigma}}}_h$  and  $\check{\underline{\boldsymbol{\sigma}}}_h$ , we introduce the definitions of the average  $\{\cdot\}$ , space normal jumps  $\llbracket \cdot \rrbracket_x$ ,  $\llbracket \cdot \rrbracket_x$  and time jump  $\llbracket \cdot \rrbracket_t$  between two elements for

piecewise-continuous vector  $\mathbf{v}_S$  and tensor  $\underline{\boldsymbol{\sigma}}$  fields as follows:

$$\begin{aligned}
\{\mathbf{v}_S\} &\equiv \frac{1}{2}(\mathbf{v}|_{K_S^-} + \mathbf{v}|_{K_S^+}) && \text{on } \partial K_F^- \cap \partial K_S^+ \in \mathcal{F}_h^{Q_S}, \\
\llbracket \mathbf{v}_S \rrbracket_x &\equiv \mathbf{v}|_{K_S^-} \otimes \mathbf{n}_{K_S^-}^x + \mathbf{v}|_{K_S^+} \otimes \mathbf{n}_{K_S^+}^x && \text{on } \partial K_S^- \cap \partial K_S^+ \in \mathcal{F}_h^{Q_S}, \\
\llbracket \mathbf{v}_S \rrbracket_t &\equiv \mathbf{v}|_{K_S^-} n_{K_S^-}^t + \mathbf{v}|_{K_S^+} n_{K_S^+}^t && \text{on } \partial K_S^- \cap \partial K_S^+ \in \mathcal{F}_h^{Q_S}, \\
\{\underline{\boldsymbol{\sigma}}\} &\equiv \frac{1}{2}(\underline{\boldsymbol{\sigma}}|_{K_S^-} + \underline{\boldsymbol{\sigma}}|_{K_S^+}) && \text{on } \partial K_F^- \cap \partial K_S^+ \in \mathcal{F}_h^{Q_S}, \\
\llbracket \underline{\boldsymbol{\sigma}} \rrbracket_x &\equiv \underline{\boldsymbol{\sigma}}|_{K_S^-} \mathbf{n}_{K_S^-}^x + \underline{\boldsymbol{\sigma}}|_{K_S^+} \mathbf{n}_{K_S^+}^x && \text{on } \partial K_S^- \cap \partial K_S^+ \in \mathcal{F}_h^{Q_S}, \\
\llbracket \underline{\boldsymbol{\sigma}} \rrbracket_t &\equiv \underline{\boldsymbol{\sigma}}|_{K_S^-} n_{K_S^-}^t + \underline{\boldsymbol{\sigma}}|_{K_S^+} n_{K_S^+}^t && \text{on } \partial K_S^- \cap \partial K_S^+ \in \mathcal{F}_h^{Q_S}.
\end{aligned}$$

Here the symbol  $\otimes$  represents the outer product  $\mathbf{v}_S \otimes \mathbf{n}_{K_S}^x$  which is equivalent to a matrix multiplication of  $\mathbf{v}_S (\mathbf{n}_{K_S}^x)^\top$ , provided that  $\mathbf{v}_S$  and  $\mathbf{n}_{K_S}^x$  are represented as a  $d \times 1$  column vectors (which makes  $(\mathbf{n}_{K_S}^x)^\top$  a row vector).

The numerical fluxes  $\hat{\mathbf{v}}_{Sh}$ ,  $\check{\mathbf{v}}_{Sh}$ ,  $\hat{\underline{\boldsymbol{\sigma}}}_h$  and  $\check{\underline{\boldsymbol{\sigma}}}_h$  are defined on the mesh skeleton  $\mathcal{F}_{Sh} =$

$\bigcup_{K_S \in \mathcal{T}_{Sh}} \partial K_S$  as follows:

$$\begin{aligned}
\begin{pmatrix} \hat{\mathbf{v}}_{Sh} \\ \hat{\underline{\boldsymbol{\sigma}}}_h \end{pmatrix} &\equiv \begin{pmatrix} \{\mathbf{v}_{Sh}\} - \delta_1 \llbracket \underline{\boldsymbol{\sigma}}_h \rrbracket_x \\ \{\underline{\boldsymbol{\sigma}}_h\} - \gamma_1 \llbracket \mathbf{v}_{Sh} \rrbracket_x \end{pmatrix} && \text{on } \mathcal{F}_h^{Q_S}, \\
\begin{pmatrix} \check{\mathbf{v}}_{Sh} \\ \check{\underline{\boldsymbol{\sigma}}}_h \end{pmatrix} &\equiv \begin{pmatrix} \{\mathbf{v}_{Sh}\} + \gamma_2 \llbracket \mathbf{v}_{Sh} \rrbracket_t \\ \{\underline{\boldsymbol{\sigma}}_h\} + \delta_2 \llbracket \underline{\boldsymbol{\sigma}}_h \rrbracket_t \end{pmatrix} && \text{on } \mathcal{F}_h^{Q_S}, \\
\begin{pmatrix} \hat{\mathbf{v}}_{Sh} \\ \hat{\underline{\boldsymbol{\sigma}}}_h \mathbf{n}_{K_S}^x \end{pmatrix} &\equiv \begin{pmatrix} \mathbf{v}_{Sh} - \delta_1 (\underline{\boldsymbol{\sigma}}_h \mathbf{n}_{K_S}^x - \mathbf{g}_{D_S}) \\ \mathbf{g}_{D_S} \end{pmatrix} && \text{on } \mathcal{F}_h^{D_S}, \\
\begin{pmatrix} \check{\mathbf{v}}_{Sh} \\ \check{\underline{\boldsymbol{\sigma}}}_h \end{pmatrix} &\equiv \begin{pmatrix} \mathbf{v}_{Sh} \\ \underline{\boldsymbol{\sigma}}_h \end{pmatrix} && \text{on } \mathcal{F}_h^{T_S}, \\
\begin{pmatrix} \check{\mathbf{v}}_{Sh} \\ \check{\underline{\boldsymbol{\sigma}}}_h \end{pmatrix} &\equiv \begin{pmatrix} (\frac{1}{2} - \gamma_2) \mathbf{v}_{Sh} + (\frac{1}{2} + \gamma_2) \mathbf{v}_{S_0} \\ (\frac{1}{2} - \delta_2) \underline{\boldsymbol{\sigma}}_h + (\frac{1}{2} + \delta_2) \underline{\boldsymbol{\sigma}}_0 \end{pmatrix} && \text{on } \mathcal{F}_h^{0_S},
\end{aligned}$$

where  $\delta_1$ ,  $\delta_2$ , and  $\gamma_1$ ,  $\gamma_2$  are positive penalty parameters. For simplicity, herein, we use the most common for standard DG methods penalty terms [30, 84]. We will show in section 3.2.4 that a good choice of penalty parameters can improve accuracy and convergence results (see chapter 5). Alternative choices of penalty terms are discussed in [9, 17, 18, 22] for standard DG approximations. It is worth noting that if  $(\mathbf{v}_S, \underline{\boldsymbol{\sigma}})$  is solution of (3.11), all the jump terms in definitions of  $\hat{\mathbf{v}}_S$ ,  $\hat{\underline{\boldsymbol{\sigma}}}_h$ ,  $\check{\mathbf{v}}_S$ ,  $\check{\underline{\boldsymbol{\sigma}}}_h$  vanish, and  $\hat{\mathbf{v}}_S = \check{\mathbf{v}}_S = \mathbf{v}_S$  and  $\hat{\underline{\boldsymbol{\sigma}}}_h = \check{\underline{\boldsymbol{\sigma}}}_h = \underline{\boldsymbol{\sigma}}$  showing the consistency of the numerical fluxes.

Summing up the contributions of all elements  $K_S \in \mathcal{T}_{Sh}$ , we obtain a DG formulation for (3.11):

Seek  $(\mathbf{v}_{Sh}, \underline{\boldsymbol{\sigma}}_h) \in V^h(\mathcal{T}_{Sh})^d \times V^h(\mathcal{T}_{Sh})^{d^2}$  such that, for all  $(\boldsymbol{\omega}_S, \underline{\boldsymbol{\xi}}) \in V^h(\mathcal{T}_{Sh})^d \times V^h(\mathcal{T}_{Sh})^{d^2}$ , it holds true:

$$\begin{aligned}
& - \sum_{K_S \in \mathcal{T}_h} \int_{K_S} \left[ \underline{\boldsymbol{\sigma}}_h : \left( \underline{\mathbf{A}} \frac{\partial \underline{\boldsymbol{\xi}}}{\partial t} - \underline{\boldsymbol{\varepsilon}}(\boldsymbol{\omega}_S) \right) + \mathbf{v}_{Sh} \cdot \left( \rho_S \frac{\partial \boldsymbol{\omega}_S}{\partial t} - \mathbf{div} \underline{\boldsymbol{\xi}} \right) \right] dv \\
& + \int_{\mathcal{F}_h^{QS}} \left[ \underline{\mathbf{A}} \{ \underline{\boldsymbol{\sigma}}_h \} : \{ \underline{\boldsymbol{\xi}} \}_t + \rho_S \{ \mathbf{v}_{Sh} \} \cdot \{ \boldsymbol{\omega}_S \}_t - \{ \underline{\boldsymbol{\sigma}}_h \} : \{ \boldsymbol{\omega}_S \}_x - \{ \mathbf{v}_{Sh} \} \cdot \{ \underline{\boldsymbol{\xi}} \}_x \right] ds \\
& + \int_{\mathcal{F}_h^{QS}} \left[ \gamma_1 \llbracket \mathbf{v}_{Sh} \rrbracket_x : \llbracket \boldsymbol{\omega}_S \rrbracket_x + \delta_1 \llbracket \underline{\boldsymbol{\sigma}}_h \rrbracket_x \cdot \llbracket \underline{\boldsymbol{\xi}} \rrbracket_x + \gamma_2 \rho_S \llbracket \mathbf{v}_{Sh} \rrbracket_t \cdot \llbracket \boldsymbol{\omega}_S \rrbracket_t + \delta_2 \underline{\mathbf{A}} \llbracket \underline{\boldsymbol{\sigma}}_h \rrbracket_t : \llbracket \underline{\boldsymbol{\xi}} \rrbracket_t \right] ds \\
& - \int_{\mathcal{F}_h^{DS}} \left[ \underline{\boldsymbol{\xi}} \mathbf{v}_{Sh} \cdot \mathbf{n}_{K_S}^x - \delta_1 (\underline{\boldsymbol{\sigma}}_h \mathbf{n}_{K_S}^x) \cdot (\underline{\boldsymbol{\xi}} \mathbf{n}_{K_S}^x) \right] ds + \int_{\mathcal{F}_h^{TS}} \left[ \underline{\mathbf{A}} \underline{\boldsymbol{\sigma}}_h : \underline{\boldsymbol{\xi}} + \rho_S \mathbf{v}_{Sh} \cdot \boldsymbol{\omega}_S \right] ds \\
& - \left( \frac{1}{2} - \delta_2 \right) \int_{\mathcal{F}_h^{0S}} \underline{\mathbf{A}} \underline{\boldsymbol{\sigma}}_h : \underline{\boldsymbol{\xi}} ds - \left( \frac{1}{2} - \gamma_2 \right) \int_{\mathcal{F}_h^{0S}} \rho_S \mathbf{v}_{Sh} \cdot \boldsymbol{\omega}_S ds = \\
& \left( \frac{1}{2} + \delta_2 \right) \int_{\mathcal{F}_h^{0S}} \underline{\mathbf{A}} \underline{\boldsymbol{\sigma}}_0 : \underline{\boldsymbol{\xi}} ds + \left( \frac{1}{2} + \gamma_2 \right) \int_{\mathcal{F}_h^{0S}} \rho_S \mathbf{v}_{S0} \cdot \boldsymbol{\omega}_S ds \\
& + \int_{\mathcal{F}_h^{DS}} \left[ \delta_1 \underline{\boldsymbol{\xi}} \mathbf{g}_{D_S} \cdot \mathbf{n}_{K_S}^x + \mathbf{g}_{D_S} \cdot \boldsymbol{\omega}_S \right] ds.
\end{aligned} \tag{3.14}$$

In the following, we impose a zero source term  $f \equiv 0$  and "free-surface" boundary condition  $\mathbf{g}_{D_S} \equiv 0$ . We do not lose the generality of approach, because both terms appear in the right-hand side of formulation, and can always be bounded above provided they are regular enough. The numerical applications, presented in chapter 5, will involve implementation of zero and non-zero source terms, periodic and "free-surface" boundaries.

### 3.2.3 Trefftz-DG formulation for the elastodynamic system

We define the Trefftz space as follows:

$$\begin{aligned}
\mathbf{T}_S(\mathcal{T}_{Sh}) \equiv \left\{ (\boldsymbol{\omega}_S, \underline{\boldsymbol{\xi}}) \in V^h(\mathcal{T}_{Sh})^d \times V^h(\mathcal{T}_{Sh})^{d^2} \text{ such that, } \underline{\mathbf{A}} \frac{\partial \underline{\boldsymbol{\xi}}}{\partial t} - \underline{\boldsymbol{\varepsilon}}(\boldsymbol{\omega}_S) = 0 \text{ and} \right. \\
\left. \rho_S \frac{\partial \boldsymbol{\omega}_S}{\partial t} - \mathbf{div} \underline{\boldsymbol{\xi}} = 0 \text{ in all } K_S \in \mathcal{T}_{Sh} \right\}.
\end{aligned}$$

This space is of Trefftz type since it is a subspace of the regular space  $V^h(\mathcal{T}_{Sh})^d \times V^h(\mathcal{T}_{Sh})^{d^2}$  composed of local solutions of the volumic equations under study set in each element  $K_S$ . The corresponding discrete Trefftz space  $\mathbf{T}_S^p(\mathcal{T}_{Sh})$  is defined by:

$$\mathbf{T}_S^p(\mathcal{T}_{Sh}) \equiv \left\{ (\boldsymbol{\omega}_F, q) \in \mathbf{T}_S(\mathcal{T}_{Sh}), (\boldsymbol{\omega}_S, \underline{\boldsymbol{\xi}}) |_{K_S} \in \mathbb{P}^p(K_S)^d \times \mathbb{P}^p(K_S)^{d^2}, \text{ for all } K_S \in \mathcal{T}_{Sh} \right\}.$$

According to (3.14), this choice of basis functions leads to the removal of all volume integral terms in the DG formulation.

The corresponding Trefftz-DG formulation for the elastodynamic system reduces to:

Seek  $(\mathbf{v}_{Sh}, \underline{\boldsymbol{\sigma}}_h) \in \mathbf{T}_S^p(\mathcal{T}_{Sh})$  such that, for all  $(\boldsymbol{\omega}_S, \underline{\boldsymbol{\xi}}) \in \mathbf{T}_S^p(\mathcal{T}_{Sh})$ , it holds true:

$$\mathcal{A}_{TDG_S}((\mathbf{v}_{Sh}, \underline{\boldsymbol{\sigma}}_h); (\boldsymbol{\omega}_S, \underline{\boldsymbol{\xi}})) = \ell_{TDG_S}(\boldsymbol{\omega}_S, \underline{\boldsymbol{\xi}}). \quad (3.15)$$

Here the bilinear form  $\mathcal{A}_{TDG_S}(\cdot; \cdot)$  is defined by:

$$\begin{aligned} \mathcal{A}_{TDG_S}((\mathbf{v}_{Sh}, \underline{\boldsymbol{\sigma}}_h); (\boldsymbol{\omega}_S, \underline{\boldsymbol{\xi}})) \equiv & \int_{\mathcal{F}_h^{QS}} \left[ \underline{\mathbf{A}} \{ \underline{\boldsymbol{\sigma}}_h \} : \llbracket \underline{\boldsymbol{\xi}} \rrbracket_t + \rho_S \{ \mathbf{v}_{Sh} \} \cdot \llbracket \boldsymbol{\omega}_S \rrbracket_t \right] - \{ \underline{\boldsymbol{\sigma}}_h \} : \llbracket \boldsymbol{\omega}_S \rrbracket_x - \{ \mathbf{v}_{Sh} \} \cdot \llbracket \underline{\boldsymbol{\xi}} \rrbracket_x \Big] ds \\ & + \int_{\mathcal{F}_h^{QS}} \left[ \gamma_1 \llbracket \mathbf{v}_{Sh} \rrbracket_x : \llbracket \boldsymbol{\omega}_S \rrbracket_x + \delta_1 \llbracket \underline{\boldsymbol{\sigma}}_h \rrbracket_x \cdot \llbracket \underline{\boldsymbol{\xi}} \rrbracket_x + \gamma_2 \rho_S \llbracket \mathbf{v}_{Sh} \rrbracket_t \cdot \llbracket \boldsymbol{\omega}_S \rrbracket_t + \delta_2 \underline{\mathbf{A}} \llbracket \underline{\boldsymbol{\sigma}}_h \rrbracket_t : \llbracket \underline{\boldsymbol{\xi}} \rrbracket_t \right] ds \\ & - \int_{\mathcal{F}_h^{DS}} \left[ \underline{\boldsymbol{\xi}} \mathbf{v}_{Sh} \cdot \mathbf{n}_{K_S}^x - \delta_1 (\underline{\boldsymbol{\sigma}}_h \mathbf{n}_{K_S}^x) \cdot (\underline{\boldsymbol{\xi}} \mathbf{n}_{K_S}^x) \right] ds + \int_{\mathcal{F}_h^{TS}} \left[ \underline{\mathbf{A}} \underline{\boldsymbol{\sigma}}_h : \underline{\boldsymbol{\xi}} + \rho_S \mathbf{v}_{Sh} \cdot \boldsymbol{\omega}_S \right] ds \\ & - \left( \frac{1}{2} - \delta_2 \right) \int_{\mathcal{F}_h^{0S}} \underline{\mathbf{A}} \underline{\boldsymbol{\sigma}}_h : \underline{\boldsymbol{\xi}} ds - \left( \frac{1}{2} - \gamma_2 \right) \int_{\mathcal{F}_h^{0S}} \rho_S \mathbf{v}_{Sh} \cdot \boldsymbol{\omega}_S ds, \end{aligned}$$

and the linear form  $\ell_{TDG_S}(\cdot)$  is defined by:

$$\ell_{TDG_S}(\boldsymbol{\omega}_S, \underline{\boldsymbol{\xi}}) \equiv \left( \frac{1}{2} + \delta_2 \right) \int_{\mathcal{F}_h^{0S}} \underline{\mathbf{A}} \underline{\boldsymbol{\sigma}}_0 : \underline{\boldsymbol{\xi}} ds + \left( \frac{1}{2} + \gamma_2 \right) \int_{\mathcal{F}_h^{0S}} \rho_S \mathbf{v}_{S0} \cdot \boldsymbol{\omega}_S ds.$$

It is worth noting that, if  $(\mathbf{v}_S, \underline{\boldsymbol{\sigma}})$  is solution of (3.11), then  $\mathcal{A}_{TDG_S}((\mathbf{v}_S, \underline{\boldsymbol{\sigma}}); (\boldsymbol{\omega}_S, \underline{\boldsymbol{\xi}})) = \mathcal{A}_{TDG_S}((\mathbf{v}_{Sh}, \underline{\boldsymbol{\sigma}}_h); (\boldsymbol{\omega}_S, \underline{\boldsymbol{\xi}}))$  thanks to the consistency of the numerical fluxes.

### 3.2.4 Well-posedness of the Trefftz-DG formulation for the elastodynamic system

The analysis of well-posedness of the Trefftz-DG formulation (3.15) for the elastodynamic problem is based on coercivity and continuity estimates.

We set  $\underline{\boldsymbol{\sigma}}_h = \underline{\boldsymbol{\xi}}$  and  $\mathbf{v}_{Sh} = \boldsymbol{\omega}_S$ , so that the bilinear form  $\mathcal{A}_{TDG_S}(\cdot; \cdot)$  reads as:

$$\begin{aligned}
\mathcal{A}_{TDG_S}((\boldsymbol{\omega}_S, \underline{\boldsymbol{\xi}}); (\boldsymbol{\omega}_S, \underline{\boldsymbol{\xi}})) &\equiv \\
&\int_{\mathcal{F}_h^{QS}} \left[ \underline{\mathbf{A}}\{\underline{\boldsymbol{\xi}}\} : [\underline{\boldsymbol{\xi}}]_t + \rho_S \{\boldsymbol{\omega}_S\} \cdot [\boldsymbol{\omega}_S]_t \right] - \{\underline{\boldsymbol{\xi}}\} : \llbracket \boldsymbol{\omega}_S \rrbracket_x - \{\boldsymbol{\omega}_S\} \cdot [\underline{\boldsymbol{\xi}}]_x \Big] ds \\
&+ \int_{\mathcal{F}_h^{QS}} \left[ \gamma_1 \llbracket \boldsymbol{\omega}_S \rrbracket_x : \llbracket \boldsymbol{\omega}_S \rrbracket_x + \delta_1 [\underline{\boldsymbol{\xi}}]_x \cdot [\underline{\boldsymbol{\xi}}]_x + \gamma_2 \rho_S [\boldsymbol{\omega}_S]_t \cdot [\boldsymbol{\omega}_S]_t + \delta_2 \underline{\mathbf{A}}[\underline{\boldsymbol{\xi}}]_t : [\underline{\boldsymbol{\xi}}]_t \right] ds \\
&- \int_{\mathcal{F}_h^{DS}} \left[ \underline{\boldsymbol{\xi}} \boldsymbol{\omega}_S \cdot \mathbf{n}_{K_S}^x - \delta_1 (\underline{\boldsymbol{\xi}} \mathbf{n}_{K_S}^x) \cdot (\underline{\boldsymbol{\xi}} \mathbf{n}_{K_S}^x) \right] ds + \int_{\mathcal{F}_h^{TS}} \left[ \underline{\mathbf{A}} \underline{\boldsymbol{\xi}} : \underline{\boldsymbol{\xi}} + \rho_S \boldsymbol{\omega}_S \cdot \boldsymbol{\omega}_S \right] ds \\
&- \left( \frac{1}{2} - \delta_2 \right) \int_{\mathcal{F}_h^{0S}} \underline{\mathbf{A}} \underline{\boldsymbol{\xi}} : \underline{\boldsymbol{\xi}} ds - \left( \frac{1}{2} - \gamma_2 \right) \int_{\mathcal{F}_h^{0S}} \rho_S \boldsymbol{\omega}_S \cdot \boldsymbol{\omega}_S ds = \\
&\underbrace{\int_{\mathcal{F}_h^{QS}} \left[ \underline{\mathbf{A}}\{\underline{\boldsymbol{\xi}}\} : [\underline{\boldsymbol{\xi}}]_t + \rho_S \{\boldsymbol{\omega}_S\} \cdot [\boldsymbol{\omega}_S]_t \right] ds}_{[5']} + \underbrace{\delta_2 \int_{\mathcal{F}_h^{0S}} \underline{\mathbf{A}} \underline{\boldsymbol{\xi}} : \underline{\boldsymbol{\xi}} ds + \gamma_2 \int_{\mathcal{F}_h^{0S}} \rho_S \boldsymbol{\omega}_S \cdot \boldsymbol{\omega}_S ds}_{[3']} \\
&- \underbrace{\int_{\mathcal{F}_h^{QS}} \left[ \{\underline{\boldsymbol{\xi}}\} : \llbracket \boldsymbol{\omega}_S \rrbracket_x + \{\boldsymbol{\omega}_S\} \cdot [\underline{\boldsymbol{\xi}}]_x \right] ds}_{[6']} - \int_{\mathcal{F}_h^{DS}} \underline{\boldsymbol{\xi}} \boldsymbol{\omega}_S \cdot \mathbf{n}_{K_S}^x ds \\
&+ \underbrace{\int_{\mathcal{F}_h^{QS}} \left[ \gamma_1 \llbracket \boldsymbol{\omega}_S \rrbracket_x : \llbracket \boldsymbol{\omega}_S \rrbracket_x + \delta_1 [\underline{\boldsymbol{\xi}}]_x \cdot [\underline{\boldsymbol{\xi}}]_x + \gamma_2 \rho_S [\boldsymbol{\omega}_S]_t \cdot [\boldsymbol{\omega}_S]_t + \delta_2 \underline{\mathbf{A}}[\underline{\boldsymbol{\xi}}]_t : [\underline{\boldsymbol{\xi}}]_t \right] ds}_{[1']} \\
&+ \underbrace{\frac{1}{2} \int_{\mathcal{F}_h^{TS}} \left[ \underline{\mathbf{A}} \underline{\boldsymbol{\xi}} : \underline{\boldsymbol{\xi}} + \rho_S \boldsymbol{\omega}_S \cdot \boldsymbol{\omega}_S \right] ds}_{[7']} - \underbrace{\frac{1}{2} \int_{\mathcal{F}_h^{0S}} \left[ \underline{\mathbf{A}} \underline{\boldsymbol{\xi}} : \underline{\boldsymbol{\xi}} + \rho_S \boldsymbol{\omega}_S \cdot \boldsymbol{\omega}_S \right] ds}_{[7']} \\
&+ \underbrace{\frac{1}{2} \int_{\mathcal{F}_h^{TS}} \left[ \underline{\mathbf{A}} \underline{\boldsymbol{\xi}} : \underline{\boldsymbol{\xi}} + \rho_S \boldsymbol{\omega}_S \cdot \boldsymbol{\omega}_S \right] ds}_{[2']} + \underbrace{\int_{\mathcal{F}_h^{DS}} \delta_1 (\underline{\boldsymbol{\xi}} \mathbf{n}_{K_S}^x) \cdot (\underline{\boldsymbol{\xi}} \mathbf{n}_{K_S}^x) ds}_{[4]}.
\end{aligned}$$

We estimate each term on the right-hand side in mesh-dependent  $L^2$ -norms as follows:

$$\begin{aligned}
[1'] &\equiv \int_{\mathcal{F}_h^{QS}} \left[ \gamma_1 \llbracket \boldsymbol{\omega}_S \rrbracket_x : \llbracket \boldsymbol{\omega}_S \rrbracket_x + \delta_1 [\underline{\boldsymbol{\xi}}]_x \cdot [\underline{\boldsymbol{\xi}}]_x + \gamma_2 \rho_S [\boldsymbol{\omega}_S]_t \cdot [\boldsymbol{\omega}_S]_t + \delta_2 \underline{\mathbf{A}}[\underline{\boldsymbol{\xi}}]_t : [\underline{\boldsymbol{\xi}}]_t \right] ds = \\
&\left\| \delta_1^{1/2} [\underline{\boldsymbol{\xi}}]_x \right\|_{L^2(\mathcal{F}_h^{QS})}^2 + \left\| \gamma_1^{1/2} \llbracket \boldsymbol{\omega}_S \rrbracket_x \right\|_{L^2(\mathcal{F}_h^{QS})}^2 + \left\| \delta_2^{1/2} \underline{\mathbf{A}}[\underline{\boldsymbol{\xi}}]_t \right\|_{L^2(\mathcal{F}_h^{QS})}^2 \\
&+ \left\| \gamma_2^{1/2} \rho_S^{1/2} [\boldsymbol{\omega}_S]_t \right\|_{L^2(\mathcal{F}_h^{QS})}^2;
\end{aligned}$$

$$[2'] \equiv \frac{1}{2} \int_{\mathcal{F}_h^{TS}} [\underline{\underline{\mathbf{A}\xi}} : \underline{\xi} + \rho_S \boldsymbol{\omega}_S \cdot \boldsymbol{\omega}_S] ds = \frac{1}{2} \left\| \underline{\xi} \right\|_{L^2(\mathcal{F}_h^{TS})}^2 + \frac{1}{2} \left\| \rho_S^{1/2} \boldsymbol{\omega}_S \right\|_{L^2(\mathcal{F}_h^{TS})}^2;$$

$$[3'] \equiv \delta_2 \int_{\mathcal{F}_h^{0S}} \underline{\underline{\mathbf{A}\xi}} : \underline{\xi} ds + \gamma_2 \int_{\mathcal{F}_h^{0S}} \rho_S \boldsymbol{\omega}_S \cdot \boldsymbol{\omega}_S ds = \left\| \delta_2^{1/2} \underline{\xi} \right\|_{L^2(\mathcal{F}_h^{0S})}^2 + \left\| \gamma_2^{1/2} \rho_S^{1/2} \boldsymbol{\omega}_S \right\|_{L^2(\mathcal{F}_h^{0S})}^2;$$

$$[4'] \equiv \int_{\mathcal{F}_h^{DS}} \delta_1 (\underline{\xi} \mathbf{n}_{K_S}^x) \cdot (\underline{\xi} \mathbf{n}_{K_S}^x) ds = \left\| \delta_1^{1/2} (\underline{\xi} \mathbf{n}_{K_S}^x) \right\|_{L^2(\mathcal{F}_h^{DS})}^2;$$

$$[5'] \equiv \int_{\mathcal{F}_h^{QS}} [\underline{\underline{\mathbf{A}\xi}} : \underline{\xi}]_t + \rho_S \{\boldsymbol{\omega}_S\} \cdot \{\boldsymbol{\omega}_S\}_t ds \stackrel{(A.2),(A.3)}{=} \frac{1}{2} \int_{\mathcal{F}_h^{QS}} \underline{\underline{\mathbf{A}\xi}} : \underline{\xi}]_t ds \\ + \frac{1}{2} \int_{\mathcal{F}_h^{QS}} \rho_S [\boldsymbol{\omega}_S \cdot \boldsymbol{\omega}_S]_t ds;$$

$$[6'] \equiv - \int_{\mathcal{F}_h^{QS}} [\{\boldsymbol{\omega}_S\} \cdot \underline{\xi}]_x + \{\underline{\xi}\} : \{\boldsymbol{\omega}_S\}_x ds - \int_{\mathcal{F}_h^{DS}} \underline{\xi} \boldsymbol{\omega}_S \cdot \mathbf{n}_{K_S}^x ds \stackrel{(A.5)}{=} - \int_{\mathcal{F}_h^{QS}} \underline{\xi} \boldsymbol{\omega}_S \cdot \mathbf{n}_{K_S}^x ds \\ - \int_{\mathcal{F}_h^{DS}} \underline{\xi} \boldsymbol{\omega}_S \cdot \mathbf{n}_{K_S}^x ds \stackrel{(A.10)}{=} - \sum_{K_S \in \mathcal{T}_{Sh}} \int_{K_S} (\boldsymbol{\omega}_S \cdot \mathbf{div} \underline{\xi} + \underline{\xi} : \underline{\boldsymbol{\varepsilon}}(\boldsymbol{\omega}_S)) dv dv;$$

$$[7'] + [5'] \equiv \frac{1}{2} \int_{\mathcal{F}_h^{TS}} [\underline{\underline{\mathbf{A}\xi}} : \underline{\xi} + \rho_S \boldsymbol{\omega}_S \cdot \boldsymbol{\omega}_S] ds - \frac{1}{2} \int_{\mathcal{F}_h^{0S}} [\underline{\underline{\mathbf{A}\xi}} : \underline{\xi} + \rho_S \boldsymbol{\omega}_S \cdot \boldsymbol{\omega}_S] ds \\ + \frac{1}{2} \int_{\mathcal{F}_h^{QS}} [\underline{\underline{\mathbf{A}\xi}} : \underline{\xi}]_t + \rho_S [\boldsymbol{\omega}_S \cdot \boldsymbol{\omega}_S]_t ds \stackrel{(A.7),(A.8)}{=} \sum_{K_S \in \mathcal{T}_h} \int_{K_S} \underline{\xi} : \frac{\partial \underline{\underline{\mathbf{A}\xi}}}{\partial t} dv \\ + \sum_{K_S \in \mathcal{T}_{Sh}} \int_{K_S} \rho_S \boldsymbol{\omega}_S \cdot \frac{\partial \boldsymbol{\omega}_S}{\partial t} dv;$$

$$[6'] + [7'] + [5'] \equiv - \sum_{K_S \in \mathcal{T}_{Sh}} \int_{K_S} (\boldsymbol{\omega}_S \cdot \mathbf{div} \underline{\xi} + \underline{\xi} : \underline{\boldsymbol{\varepsilon}}(\boldsymbol{\omega}_S)) dv dv \\ + \sum_{K_S \in \mathcal{T}_{Sh}} \int_{K_S} \underline{\xi} : \frac{\partial \underline{\underline{\mathbf{A}\xi}}}{\partial t} dv + \sum_{K_S \in \mathcal{T}_{Sh}} \int_{K_S} \rho_S \boldsymbol{\omega}_S \cdot \frac{\partial \boldsymbol{\omega}_S}{\partial t} dv = \\ \sum_{K_S \in \mathcal{T}_{Sh}} \left[ \int_{K_S} \underline{\xi} : \left( \overbrace{\frac{\partial \underline{\underline{\mathbf{A}\xi}}}{\partial t}}^{=0 \text{ in } \mathbf{T}_S(\mathcal{T}_{Sh})} - \underline{\boldsymbol{\varepsilon}}(\boldsymbol{\omega}_S) \right) dv + \int_{K_S} \boldsymbol{\omega}_S \cdot \left( \overbrace{\rho_S \frac{\partial \boldsymbol{\omega}_S}{\partial t} - \mathbf{div} \underline{\xi}}^{=0 \text{ in } \mathbf{T}_S(\mathcal{T}_{Sh})} \right) dv \right].$$

Similarly to the acoustic case, we introduce two mesh-dependent semi-norms in  $\mathbf{T}_S(\mathcal{T}_{Sh})$ :

$$\begin{aligned} |||(\boldsymbol{\omega}_S, \underline{\boldsymbol{\xi}})|||_{TDG_S}^2 &\equiv \left\| \gamma_1^{1/2} \llbracket \boldsymbol{\omega}_S \rrbracket_x \right\|_{L^2(\mathcal{F}_h^{QS})}^2 + \left\| \delta_1^{1/2} \llbracket \underline{\boldsymbol{\xi}} \rrbracket_x \right\|_{L^2(\mathcal{F}_h^{QS})}^2 + \left\| \gamma_2^{1/2} \rho_S^{1/2} \llbracket \boldsymbol{\omega}_S \rrbracket_t \right\|_{L^2(\mathcal{F}_h^{QS})}^2 \\ &\quad + \left\| \delta_2^{1/2} | \llbracket \underline{\boldsymbol{\xi}} \rrbracket_t | \underline{\mathbf{A}} \right\|_{L^2(\mathcal{F}_h^{QS})}^2 + \left\| \delta_1^{1/2} (\underline{\boldsymbol{\xi}} \mathbf{n}_{K_S}^x) \right\|_{L^2(\mathcal{F}_h^{DS})}^2 + \frac{1}{2} \left\| | \underline{\boldsymbol{\xi}} | \underline{\mathbf{A}} \right\|_{L^2(\mathcal{F}_h^{TS})}^2 \\ &\quad + \frac{1}{2} \left\| \rho_S^{1/2} \boldsymbol{\omega}_S \right\|_{L^2(\mathcal{F}_h^{TS})}^2 + \left\| \delta_2^{1/2} | \underline{\boldsymbol{\xi}} | \underline{\mathbf{A}} \right\|_{L^2(\mathcal{F}_h^{0S})}^2 + \left\| \gamma_2^{1/2} \rho_S^{1/2} \boldsymbol{\omega}_S \right\|_{L^2(\mathcal{F}_h^{0S})}^2, \end{aligned}$$

$$\begin{aligned} |||(\boldsymbol{\omega}_S, \underline{\boldsymbol{\xi}})|||_{TDG_S^*}^2 &\equiv |||(\boldsymbol{\omega}_S, \underline{\boldsymbol{\xi}})|||_{TDG_S}^2 \\ &\quad + \left\| \delta_1^{-1/2} \{ \boldsymbol{\omega}_S \} \right\|_{L^2(\mathcal{F}_h^{QS})}^2 + \left\| \gamma_1^{-1/2} \{ \underline{\boldsymbol{\xi}} \} \right\|_{L^2(\mathcal{F}_h^{QS})}^2 + \left\| \delta_1^{-1/2} \boldsymbol{\omega}_S \right\|_{L^2(\mathcal{F}_h^{DS})}^2 \\ &\quad + \left\| \gamma_2^{-1/2} \{ \boldsymbol{\omega}_S \} \right\|_{L^2(\mathcal{F}_h^{QS})}^2 + \left\| \delta_2^{-1/2} \{ \underline{\boldsymbol{\xi}} \} \right\|_{L^2(\mathcal{F}_h^{QS})}^2 \\ &\quad + \left\| \left( \frac{1}{2\delta_2} + 1 \right)^{1/2} | \underline{\boldsymbol{\xi}} | \underline{\mathbf{A}} \right\|_{L^2(\mathcal{F}_h^{0S})}^2 + \left\| \left( \frac{1}{2\gamma_2} + 1 \right)^{1/2} \rho_S^{1/2} \boldsymbol{\omega}_S \right\|_{L^2(\mathcal{F}_h^{0S})}^2. \end{aligned}$$

**Theorem 3.4.** *The semi-norms  $||| \cdot |||_{TDG_S}$  and  $||| \cdot |||_{TDG_S^*}$  are norms in the Trefftz space  $\mathbf{T}_S(\mathcal{T}_{Sh})$ .*

*Proof.* The proof is similar to those of theorems 3.1 and 3.2.  $\square$

From theorem 3.4, we obtain that  $\mathcal{A}_{TDG_S}(\cdot, \cdot)$  is coercive in  $\mathbf{T}_S(\mathcal{T}_{Sh})$ , equipped with the norm  $||| \cdot |||_{TDG_S}$ .

Furthermore, using a weighted Cauchy-Schwartz inequality, we obtain the following continuity estimates with respect to the chosen norms for the bilinear form:

$$|\mathcal{A}_{TDG_S}((\mathbf{v}_S, \boldsymbol{\sigma}); (\boldsymbol{\omega}_S, \underline{\boldsymbol{\xi}}))| \leq C_2 |||(\mathbf{v}_S, \boldsymbol{\sigma})|||_{TDG_S^*} |||(\boldsymbol{\omega}_S, \underline{\boldsymbol{\xi}})|||_{TDG_S},$$

and for the linear form:

$$\begin{aligned} |\ell_{TDG_S}(\boldsymbol{\omega}_S, \underline{\boldsymbol{\xi}})| &\leq \tag{3.16} \\ &\left[ \left\| \left( \frac{1}{2\gamma_2} + 1 \right)^{1/2} \rho_S^{1/2} \mathbf{v}_{S0} \right\|_{L^2(\mathcal{F}_h^{0S})}^2 + \left\| \left( \frac{1}{2\delta_2} + 1 \right)^{1/2} \underline{\mathbf{A}}^{1/2} \boldsymbol{\sigma}_0 \right\|_{L^2(\mathcal{F}_h^{0S})}^2 \right]^{1/2} |||(\boldsymbol{\omega}_S, \underline{\boldsymbol{\xi}})|||_{TDG_S}. \end{aligned}$$

**Theorem 3.5.** *The Trefftz-DG variational problem (3.15) admits a unique weak solution  $(\mathbf{v}_{Sh}, \boldsymbol{\sigma}_h) \in \mathbf{T}_S^p(\mathcal{T}_{Sh})$ . Moreover, the following estimate holds true:*

$$|||(\mathbf{v}_S - \mathbf{v}_{Sh}, \boldsymbol{\sigma} - \boldsymbol{\sigma}_h)|||_{TDG_S} \leq (1 + C_2) \inf_{(\boldsymbol{\omega}_S, \underline{\boldsymbol{\xi}}) \in \mathbf{T}_S^p(\mathcal{T}_{Sh})} |||(\mathbf{v}_S - \boldsymbol{\omega}_S, \boldsymbol{\sigma} - \underline{\boldsymbol{\xi}})|||_{TDG_S^*}.$$

*Proof.* The proof reproduces the steps in the proof of theorem 3.5 for acoustic problem. It is based on the fact that the space  $\mathbf{T}_S^p(\mathcal{T}_{Sh})$  is finite dimensional, on the consistency of the bilinear form  $\mathcal{A}_{TDG_S}(\cdot; \cdot)$ , and on the above coercivity and continuity estimates.  $\square$

### 3.3 Application to elasto-acoustics

The elasto-acoustic wave propagation could be simply modeled by considering the acoustic media as a limit case of elasto-isotropic media. Indeed, it might be possible to solve the elastodynamic problem with variable coefficients, and then, to treat the acoustic medium as a particular region of the heterogeneous elastic medium with the shear modulus  $\mu \equiv 0$  or even infinitely small. However, from a practical point of view, this approach would require computing the six components of the stress tensor, instead of one actual unknown, which corresponds to the pressure. Moreover, if the numerical code is based on a discretization by  $H^1$  finite elements, the consideration of the limit case  $\mu \equiv 0$  would destroy the coercivity in  $H^1$  norms, while a choice of a very small  $\mu$  would result in numerical artifacts, due to a slow  $S$ -wave appearance. An example of this phenomena has been described by Bossy in [21].

Taking into account the foreseen implementation of the numerical solution in the case of inverse problem, where the goal is to reconstruct media parameters, we consider a transmission problem between the first order elastodynamic and acoustic systems. This choice is indeed seen as more adapted to the imaging conditions applied for inversion, and provides straight-forwardly the quantities of interest for the inverse problem.

In this section, we introduce the elasto-acoustic system based on the numerical coupling of proper acoustic (3.1) and elastodynamic (3.11) systems by transmission conditions. We will use the results and notations introduced previously for the acoustic (section 3.1) and elastic (section 3.2) cases, to apply Trefftz-DG approximation to the coupled Elasto-Acoustic System (EAS) and to establish well-posedness of the problem.

#### 3.3.1 Transmission conditions for the coupled elasto-acoustic system.

Transmission conditions impose the continuity of velocity and normal stress components at the interface  $\Gamma_{FS} \equiv \Omega_F \cap \Omega_S$ . The velocities aligned to the interface and the tangential stress remain unconstrained [73]:

$$\begin{cases} \mathbf{v}_F \cdot \mathbf{n}_{\Gamma_{FS}} = \mathbf{v}_S \cdot \mathbf{n}_{\Gamma_{FS}} & \text{at } \Gamma_{FS}, \\ -p\mathbf{n}_{\Gamma_{FS}} = \underline{\boldsymbol{\sigma}}\mathbf{n}_{\Gamma_{FS}} & \text{at } \Gamma_{FS}. \end{cases} \quad (3.17)$$

Here  $\mathbf{n}_{\Gamma_{FS}}$  is a unit normal vector to  $\Gamma_{FS}$ .

Multiplying (3.17) by the test functions  $q$  and  $\boldsymbol{\omega}_S$  respectively, and integrating by part in time and space, we obtain the following identities:

$$\begin{aligned} \int_{\Gamma_{FS}} (\mathbf{v}_F \cdot \mathbf{n}_{\Gamma_{FS}}) q ds &= \int_{\Gamma_{FS}} (\mathbf{v}_S \cdot \mathbf{n}_{\Gamma_{FS}}) q ds, \\ - \int_{\Gamma_{FS}} (p \mathbf{n}_{\Gamma_{FS}}) \cdot \boldsymbol{\omega}_S ds &= \int_{\Gamma_{FS}} (\underline{\boldsymbol{\sigma}} \mathbf{n}_{\Gamma_{FS}}) \cdot \boldsymbol{\omega}_S ds. \end{aligned} \quad (3.18)$$

We will apply (3.18) to the incoming and outgoing flux terms at  $\Gamma_{FS}$ , to couple the previously obtained formulations for acoustic and elastodynamic systems.

### 3.3.2 Space-time DG formulation for the elasto-acoustic system

The space-time mesh  $\mathcal{T}_h$  on  $Q \equiv Q_F \cup Q_S$  is composed of the meshes  $\mathcal{T}_{Fh}$  and  $\mathcal{T}_{Sh}$  of space-time Lipschitz elements  $K_F \subset \Omega_F \times I$  and  $K_S \subset \Omega_S \times I$  respectively, with the mesh skeleton  $\mathcal{F}_h \equiv [\cup_{K_F \in \mathcal{T}_{Fh}} \partial K_F] \cup [\cup_{K_S \in \mathcal{T}_{Sh}} \partial K_S]$  and its subsets (see figure 3.3):

...	$\mathcal{F}_h^{Q_F}$	internal element faces (acoustics)	
...	$\mathcal{F}_h^{Q_S}$	internal element faces (elastodynamics)	
-	$\mathcal{F}_h^{D_F}$	boundary element faces	$(\partial\Omega_F \times [0, T])$
-	$\mathcal{F}_h^{D_S}$	boundary element faces	$(\partial\Omega_S \times [0, T])$
=	$\mathcal{F}_h^{0_F}$	initial time element faces	$(\Omega_F \times \{0\})$
=	$\mathcal{F}_h^{0_S}$	initial time element faces	$(\Omega_S \times \{0\})$
--	$\mathcal{F}_h^{T_F}$	final time element faces	$(\Omega_F \times \{T\})$
--	$\mathcal{F}_h^{T_S}$	final time element faces	$(\Omega_S \times \{T\})$
...	$\mathcal{F}_h^{FS}$	fluid-solid interface element faces	$(\Gamma_{FS} \times [0, T])$

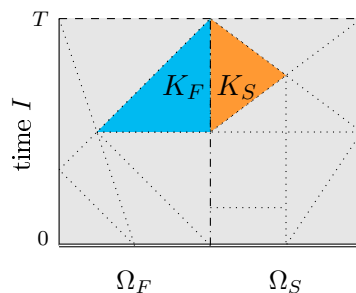


FIGURE 3.3: Example of 1D+time mesh  $\mathcal{T}_h \equiv \mathcal{T}_{Fh} \cup \mathcal{T}_{Sh}$  on  $Q \equiv [\Omega_F \cup \Omega_S] \times I$ .

The space-time DG formulation of the coupled problem consists in finding  $(\mathbf{v}_{Fh}, p_h, \mathbf{v}_{Sh}, \underline{\boldsymbol{\sigma}}_h) \in V^h(\mathcal{T}_{Fh})^d \times V^h(\mathcal{T}_{Fh}) \times V^h(\mathcal{T}_{Sh})^d \times V^h(\mathcal{T}_{Sh})^{d^2}$  such that, for all

$K_F, K_S \in \mathcal{T}_h$  and for all  $(\boldsymbol{\omega}_F, q, \boldsymbol{\omega}_S, \boldsymbol{\xi}) \in V^h(\mathcal{T}_{Fh})^d \times V^h(\mathcal{T}_{Fh}) \times V^h(\mathcal{T}_{Sh})^d \times V^h(\mathcal{T}_{Sh})^{d^2}$  it holds true:

$$\begin{aligned}
& - \int_{K_F} \left[ p_h \left( \frac{1}{c_F^2 \rho_F} \frac{\partial q}{\partial t} + \operatorname{div} \boldsymbol{\omega}_F \right) + \mathbf{v}_{Fh} \cdot \left( \rho_F \frac{\partial \boldsymbol{\omega}_F}{\partial t} + \nabla q \right) \right] dv \\
& + \int_{\partial K_F} \left[ \frac{1}{c_F^2 \rho_F} \check{p}_h q n_{K_F}^t + q \hat{\mathbf{v}}_{Fh} \cdot \mathbf{n}_{K_F}^x + \rho_F \check{\mathbf{v}}_{Fh} \cdot \boldsymbol{\omega}_F n_{K_F}^t + \hat{p}_h \boldsymbol{\omega}_F \cdot \mathbf{n}_{K_F}^x \right] ds = \int_{K_F} f q dv, \\
& - \int_{K_S} \left[ \boldsymbol{\sigma}_h : \left( \underline{\mathbf{A}} \frac{\partial \boldsymbol{\xi}}{\partial t} - \underline{\boldsymbol{\varepsilon}}(\boldsymbol{\omega}_S) \right) + \mathbf{v}_{Sh} \cdot \left( \rho_S \frac{\partial \boldsymbol{\omega}_S}{\partial t} - \operatorname{div} \boldsymbol{\xi} \right) \right] dv \\
& + \int_{\partial K_S} \left[ \underline{\mathbf{A}} \check{\boldsymbol{\sigma}}_h : \boldsymbol{\xi} n_{K_S}^t - \boldsymbol{\xi} \hat{\mathbf{v}}_{Sh} \cdot \mathbf{n}_{K_S}^x + \rho_S \check{\mathbf{v}}_{Sh} \cdot \boldsymbol{\omega}_S n_{K_S}^t - \hat{\boldsymbol{\sigma}}_h : (\boldsymbol{\omega}_S \otimes \mathbf{n}_{K_S}^x) \right] ds = 0.
\end{aligned}$$

We recall the definition of numerical fluxes  $\hat{\mathbf{v}}_{Fh}, \check{\mathbf{v}}_{Fh}, \hat{p}_h, \check{p}_h, \hat{\mathbf{v}}_{Sh}, \check{\mathbf{v}}_{Sh}, \hat{\boldsymbol{\sigma}}_h$  and  $\check{\boldsymbol{\sigma}}_h$  from the previous sections:

$$\begin{aligned}
\begin{pmatrix} \hat{\mathbf{v}}_{Fh} \\ \hat{p}_h \end{pmatrix} & \equiv \begin{pmatrix} \{\mathbf{v}_{Fh}\} + \beta_1 \llbracket p_h \rrbracket_x \\ \{p_h\} + \alpha_1 \llbracket \mathbf{v}_{Fh} \rrbracket_x \end{pmatrix} & \text{on } \mathcal{F}_h^{QF}, \\
\begin{pmatrix} \check{\mathbf{v}}_{Fh} \\ \check{p}_h \end{pmatrix} & \equiv \begin{pmatrix} \{\mathbf{v}_{Fh}\} + \alpha_2 \llbracket \mathbf{v}_{Fh} \rrbracket_t \\ \{p_h\} + \beta_2 \llbracket p_h \rrbracket_t \end{pmatrix} & \text{on } \mathcal{F}_h^{QF}, \\
\begin{pmatrix} \hat{\mathbf{v}}_{Fh} \cdot \mathbf{n}_{K_F}^x \\ \hat{p}_h \end{pmatrix} & \equiv \begin{pmatrix} g_{DF} \\ p_h + \alpha_1 (\mathbf{v}_{Fh} \cdot \mathbf{n}_{K_F}^x - g_{DF}) \end{pmatrix} & \text{on } \mathcal{F}_h^{DF}, \\
\begin{pmatrix} \check{\mathbf{v}}_{Fh} \\ \check{p}_h \end{pmatrix} & \equiv \begin{pmatrix} \mathbf{v}_{Fh} \\ p_h \end{pmatrix} & \text{on } \mathcal{F}_h^{TF}, \\
\begin{pmatrix} \check{\mathbf{v}}_{Fh} \\ \check{p}_h \end{pmatrix} & \equiv \begin{pmatrix} \left( \frac{1}{2} - \alpha_2 \right) \mathbf{v}_{Fh} + \left( \frac{1}{2} + \alpha_2 \right) \mathbf{v}_{F0} \\ \left( \frac{1}{2} - \beta_2 \right) p_h + \left( \frac{1}{2} + \beta_2 \right) p_0 \end{pmatrix} & \text{on } \mathcal{F}_h^{0F}, \\
\begin{pmatrix} \hat{\mathbf{v}}_{Sh} \\ \hat{\boldsymbol{\sigma}}_h \end{pmatrix} & \equiv \begin{pmatrix} \{\mathbf{v}_{Sh}\} - \delta_1 \llbracket \boldsymbol{\sigma}_h \rrbracket_x \\ \{\boldsymbol{\sigma}_h\} - \gamma_1 \llbracket \mathbf{v}_{Sh} \rrbracket_x \end{pmatrix} & \text{on } \mathcal{F}_h^{QS}, \\
\begin{pmatrix} \check{\mathbf{v}}_{Sh} \\ \check{\boldsymbol{\sigma}}_h \end{pmatrix} & \equiv \begin{pmatrix} \{\mathbf{v}_{Sh}\} + \gamma_2 \llbracket \mathbf{v}_{Sh} \rrbracket_t \\ \{\boldsymbol{\sigma}_h\} + \delta_2 \llbracket \boldsymbol{\sigma}_h \rrbracket_t \end{pmatrix} & \text{on } \mathcal{F}_h^{QS}, \\
\begin{pmatrix} \hat{\mathbf{v}}_{Sh} \\ \hat{\boldsymbol{\sigma}}_h \cdot \mathbf{n}_{K_S}^x \end{pmatrix} & \equiv \begin{pmatrix} \mathbf{v}_{Sh} - \delta_1 (\boldsymbol{\sigma}_h \cdot \mathbf{n}_{K_S}^x - g_{DS}) \\ g_{DS} \end{pmatrix} & \text{on } \mathcal{F}_h^{DS}, \\
\begin{pmatrix} \check{\mathbf{v}}_{Sh} \\ \check{\boldsymbol{\sigma}}_h \end{pmatrix} & \equiv \begin{pmatrix} \mathbf{v}_{Sh} \\ \boldsymbol{\sigma}_h \end{pmatrix} & \text{on } \mathcal{F}_h^{TS}, \\
\begin{pmatrix} \check{\mathbf{v}}_{Sh} \\ \check{\boldsymbol{\sigma}}_h \end{pmatrix} & \equiv \begin{pmatrix} \left( \frac{1}{2} - \gamma_2 \right) \mathbf{v}_{Sh} + \left( \frac{1}{2} + \gamma_2 \right) \mathbf{v}_{S0} \\ \left( \frac{1}{2} - \delta_2 \right) \boldsymbol{\sigma}_h + \left( \frac{1}{2} + \delta_2 \right) \boldsymbol{\sigma}_0 \end{pmatrix} & \text{on } \mathcal{F}_h^{0S},
\end{aligned}$$

In addition, we introduce the numerical fluxes through the fluid-solid interface by using the transmission conditions (3.17):

$$\begin{pmatrix} \hat{\mathbf{v}}_{Fh} \cdot \mathbf{n}_{K_F}^x \\ \hat{p}_h \\ \hat{\mathbf{v}}_{Sh} \\ \hat{\underline{\boldsymbol{\sigma}}}_h \mathbf{n}_{K_S}^x \end{pmatrix} \equiv \begin{pmatrix} \mathbf{v}_{Sh} \cdot \mathbf{n}_{K_F}^x + \delta_1 (\underline{\boldsymbol{\sigma}}_h \mathbf{n}_{K_F}^x + p_h \mathbf{n}_{K_F}^x) \cdot \mathbf{n}_{K_F}^x \\ p_h + \alpha_1 (\mathbf{v}_{Fh} \cdot \mathbf{n}_{K_F}^x - \mathbf{v}_{Sh} \cdot \mathbf{n}_{K_F}^x) \\ \mathbf{v}_{Sh} - \delta_1 (\underline{\boldsymbol{\sigma}}_h \mathbf{n}_{K_S}^x + p_h \mathbf{n}_{K_S}^x) \\ -p_h \mathbf{n}_{K_S}^x + \alpha_1 (\mathbf{v}_{Fh} \cdot \mathbf{n}_{K_S}^x - \mathbf{v}_{Sh} \cdot \mathbf{n}_{K_S}^x) \mathbf{n}_{K_S}^x \end{pmatrix} \quad \text{on } \mathcal{F}_h^{FS}.$$

As in the previous sections, without losing generality and in order to simplify the presentation, we restrict the model to the homogeneous system of equations with a trivial source term  $f \equiv 0$  and "free-surface" boundary conditions  $g_{D_F} \equiv 0$ ,  $\mathbf{g}_{D_S} \equiv 0$ .

### 3.3.3 Trefftz-DG formulation for the elasto-acoustic system

We define the Trefftz space for the coupled problem. It is composed of the Trefftz spaces previously defined for acoustic and elastodynamic cases:  $\mathbf{T}(\mathcal{T}_h) \equiv \mathbf{T}_F(\mathcal{T}_{Fh}) \times \mathbf{T}_S(\mathcal{T}_{Sh})$ . Similarly to the continuous Trefftz space, the discrete Trefftz space is defined by:  $\mathbf{T}^p(\mathcal{T}_h) \equiv \mathbf{T}_F^p(\mathcal{T}_{Fh}) \times \mathbf{T}_S^p(\mathcal{T}_{Sh})$ . Thus, the Trefftz-DG formulation for elasto-acoustic system reads as: *Seek  $(\mathbf{v}_{Fh}, p_h, \mathbf{v}_{Sh}, \underline{\boldsymbol{\sigma}}_h) \in \mathbf{T}^p(\mathcal{T}_h)$  such that, for all  $(\boldsymbol{\omega}_F, q, \boldsymbol{\omega}_S, \underline{\boldsymbol{\xi}}) \in \mathbf{T}^p(\mathcal{T}_h)$ , it holds true:*

$$\begin{aligned} & \int_{\mathcal{F}_h^{QF}} \left[ \frac{1}{c_F^2 \rho_F} \{p_h\} \{q\}_t + \rho_F \{\mathbf{v}_{Fh}\} \cdot \{[\boldsymbol{\omega}_F]\}_t + \{p_h\} \{[\boldsymbol{\omega}_F]\}_x + \{\mathbf{v}_{Fh}\} \cdot \{[q]\}_x \right] ds \\ & + \int_{\mathcal{F}_h^{QF}} \left[ \alpha_1 [\mathbf{v}_{Fh}]_x \{[\boldsymbol{\omega}_F]\}_x + \beta_1 [p_h]_x \cdot [q]_x + \alpha_2 \rho_F [\mathbf{v}_{Fh}]_t \cdot \{[\boldsymbol{\omega}_F]\}_t + \frac{\beta_2}{c_F^2 \rho_F} [p_h]_t [q]_t \right] ds \\ & + \int_{\mathcal{F}_h^{TF}} \left[ \frac{1}{c_F^2 \rho_F} p_h q + \rho_F \mathbf{v}_{Fh} \cdot \boldsymbol{\omega}_F \right] ds \\ & - \left( \frac{1}{2} - \beta_2 \right) \int_{\mathcal{F}_h^{0F}} \frac{1}{c_F^2 \rho_F} p_h q \, ds - \left( \frac{1}{2} - \alpha_2 \right) \int_{\mathcal{F}_h^{0F}} \rho_F \mathbf{v}_{Fh} \cdot \boldsymbol{\omega}_F \, ds \\ & + \int_{\mathcal{F}_h^{DF}} \alpha_1 (\mathbf{v}_{Fh} \cdot \mathbf{n}_{K_F}^x) (\boldsymbol{\omega}_F \cdot \mathbf{n}_{K_F}^x) ds + \int_{\mathcal{F}_h^{DF} \cup \mathcal{F}_h^{FS}} p_h \boldsymbol{\omega}_F \cdot \mathbf{n}_{K_F}^x \, ds \\ & + \int_{\mathcal{F}_h^{FS}} \alpha_1 (\mathbf{v}_{Fh} \cdot \mathbf{n}_{K_F}^x - \mathbf{v}_{Sh} \cdot \mathbf{n}_{K_F}^x) (\boldsymbol{\omega}_F \cdot \mathbf{n}_{K_F}^x) ds + \int_{\mathcal{F}_h^{FS}} q \mathbf{v}_{Sh} \cdot \mathbf{n}_{K_F}^x \, ds \\ & + \int_{\mathcal{F}_h^{FS}} \delta (\underline{\boldsymbol{\sigma}}_h \mathbf{n}_{K_F}^x + p \mathbf{n}_{K_F}^x) \cdot (q \mathbf{n}_{K_F}^x) ds = \\ & \left( \frac{1}{2} + \beta_2 \right) \int_{\mathcal{F}_h^{0F}} \frac{1}{c_F^2 \rho_F} p_0 q \, ds + \left( \frac{1}{2} + \alpha_2 \right) \int_{\mathcal{F}_h^{0F}} \rho_F \mathbf{v}_{F0} \cdot \boldsymbol{\omega}_F \, ds. \end{aligned}$$

$$\begin{aligned}
& \int_{\mathcal{F}_h^{QS}} \left[ \underline{\mathbf{A}} \{ \underline{\boldsymbol{\sigma}}_h \} : \underline{\boldsymbol{\xi}}_t + \rho_S \{ \mathbf{v}_{Sh} \} \cdot \underline{\boldsymbol{\omega}}_S \Big|_t \right] - \{ \underline{\boldsymbol{\sigma}}_h \} : \underline{\boldsymbol{\omega}}_S \Big|_x - \{ \mathbf{v}_{Sh} \} \cdot \underline{\boldsymbol{\xi}} \Big|_x \Big] ds \\
& + \int_{\mathcal{F}_h^{QS}} \left[ \gamma_1 \underline{\boldsymbol{\omega}}_S \Big|_x : \underline{\boldsymbol{\omega}}_S \Big|_x + \delta_1 \underline{\boldsymbol{\sigma}}_h \Big|_x \cdot \underline{\boldsymbol{\xi}} \Big|_x + \gamma_2 \rho_S \underline{\boldsymbol{\omega}}_S \Big|_t \cdot \underline{\boldsymbol{\omega}}_S \Big|_t + \delta_2 \underline{\mathbf{A}} \{ \underline{\boldsymbol{\sigma}}_h \} \Big|_t : \underline{\boldsymbol{\xi}} \Big|_t \right] ds \\
& + \int_{\mathcal{F}_h^{TS}} \left[ \underline{\mathbf{A}} \underline{\boldsymbol{\sigma}}_h : \underline{\boldsymbol{\xi}} + \rho_S \mathbf{v}_{Sh} \cdot \underline{\boldsymbol{\omega}}_S \right] ds \\
& - \left( \frac{1}{2} - \delta_2 \right) \int_{\mathcal{F}_h^{0S}} \underline{\mathbf{A}} \underline{\boldsymbol{\sigma}}_h : \underline{\boldsymbol{\xi}} ds - \left( \frac{1}{2} - \gamma_2 \right) \int_{\mathcal{F}_h^{0S}} \rho_S \mathbf{v}_{Sh} \cdot \underline{\boldsymbol{\omega}}_S ds \\
& + \int_{\mathcal{F}_h^{DS}} \delta_1 (\underline{\boldsymbol{\sigma}}_h \mathbf{n}_{K_S}^x) \cdot (\underline{\boldsymbol{\xi}} \mathbf{n}_{K_S}^x) ds - \int_{\mathcal{F}_h^{DS} \cup \mathcal{F}_h^{FS}} \underline{\boldsymbol{\xi}} \mathbf{v}_{Sh} \cdot \mathbf{n}_{K_S}^x ds \\
& + \int_{\mathcal{F}_h^{FS}} \delta_1 (\underline{\boldsymbol{\sigma}}_h \mathbf{n}_{K_S}^x + p_h \mathbf{n}_{K_S}^x) \cdot (\underline{\boldsymbol{\xi}} \mathbf{n}_{K_S}^x) ds + \int_{\mathcal{F}_h^{FS}} p \underline{\boldsymbol{\omega}}_S \cdot \mathbf{n}_{K_S}^x ds \\
& - \int_{\mathcal{F}_h^{FS}} \alpha_1 (\mathbf{v}_{Fh} \cdot \mathbf{n}_{K_S}^x - \mathbf{v}_{Sh} \cdot \mathbf{n}_{K_S}^x) (\underline{\boldsymbol{\omega}}_S \cdot \mathbf{n}_{K_S}^x) \Big] ds = \\
& \left( \frac{1}{2} + \delta_2 \right) \int_{\mathcal{F}_h^{0S}} \underline{\mathbf{A}} \underline{\boldsymbol{\sigma}}_0 : \underline{\boldsymbol{\xi}} ds + \left( \frac{1}{2} + \gamma_2 \right) \int_{\mathcal{F}_h^{0S}} \rho_S \mathbf{v}_{S0} \cdot \underline{\boldsymbol{\omega}}_S ds
\end{aligned}$$

or, by summing the two equations above:

Seek  $(\mathbf{v}_{Fh}, p_h, \mathbf{v}_{Sh}, \underline{\boldsymbol{\sigma}}_h) \in \mathbf{T}^p(\mathcal{T}_h)$  such that, for all  $(\underline{\boldsymbol{\omega}}_F, q, \underline{\boldsymbol{\omega}}_S, \underline{\boldsymbol{\xi}}) \in \mathbf{T}^p(\mathcal{T}_h)$ , it holds true:

$$\mathcal{A}_{TDG}((\mathbf{v}_{Fh}, p_h, \mathbf{v}_{Sh}, \underline{\boldsymbol{\sigma}}_h); (\underline{\boldsymbol{\omega}}_F, q, \underline{\boldsymbol{\omega}}_S, \underline{\boldsymbol{\xi}})) = \ell_{TDG}(\underline{\boldsymbol{\omega}}_F, q, \underline{\boldsymbol{\omega}}_S, \underline{\boldsymbol{\xi}}). \quad (3.19)$$

Here, the bilinear form  $\mathcal{A}_{TDG}(\cdot; \cdot)$  can be rewritten in terms of  $\mathcal{A}_{TDG_F}(\cdot; \cdot)$  and  $\mathcal{A}_{TDG_S}(\cdot; \cdot)$ , formerly defined in the acoustic and elastodynamic cases, as follows:

$$\begin{aligned}
\mathcal{A}_{TDG}((\mathbf{v}_{Fh}, p_h, \mathbf{v}_{Sh}, \underline{\boldsymbol{\sigma}}_h); (\underline{\boldsymbol{\omega}}_F, q, \underline{\boldsymbol{\omega}}_S, \underline{\boldsymbol{\xi}})) = & \\
& \mathcal{A}_{TDG_F}((\mathbf{v}_{Fh}, p_h); (\underline{\boldsymbol{\omega}}_F, q)) + \mathcal{A}_{TDG_S}((\mathbf{v}_{Sh}, \underline{\boldsymbol{\sigma}}_h); (\underline{\boldsymbol{\omega}}_S, \underline{\boldsymbol{\xi}})) \\
& + \int_{\mathcal{F}_h^{FS}} \left[ q \mathbf{v}_{Sh} \cdot \mathbf{n}_{K_F}^x - p \underline{\boldsymbol{\omega}}_S \cdot \mathbf{n}_{K_F}^x \right] ds \\
& + \int_{\mathcal{F}_h^{FS}} \left[ \alpha_1 (\mathbf{v}_{Fh} \cdot \mathbf{n}_{K_F}^x - \mathbf{v}_{Sh} \cdot \mathbf{n}_{K_F}^x) (\underline{\boldsymbol{\omega}}_F \cdot \mathbf{n}_{K_F}^x - \underline{\boldsymbol{\omega}}_S \cdot \mathbf{n}_{K_F}^x) \right] ds \\
& + \int_{\mathcal{F}_h^{FS}} \left[ \delta_1 (\underline{\boldsymbol{\sigma}}_h \mathbf{n}_{K_S}^x + p_h \mathbf{n}_{K_S}^x) \cdot (\underline{\boldsymbol{\xi}} \mathbf{n}_{K_S}^x + q \mathbf{n}_{K_S}^x) \right] ds.
\end{aligned}$$

Furthermore, the linear form  $\ell_{TDG}(\cdot)$  can be also represented in the terms of  $\ell_{TDG_F}(\cdot)$  and  $\ell_{TDG_S}(\cdot)$ :

$$\ell_{TDG}(\boldsymbol{\omega}_F, q, \boldsymbol{\omega}_S, \underline{\boldsymbol{\xi}}) = \ell_{TDG_F}(\boldsymbol{\omega}_F, q) + \ell_{TDG_S}(\boldsymbol{\omega}_S, \underline{\boldsymbol{\xi}}).$$

### 3.3.4 Well-posedness of Trefftz-DG formulation for the elasto-acoustic system

We start by setting  $p_h = q$ ,  $\mathbf{v}_{Fh} = \boldsymbol{\omega}_F$ ,  $\underline{\boldsymbol{\sigma}}_h = \underline{\boldsymbol{\xi}}$  and  $\mathbf{v}_{Sh} = \boldsymbol{\omega}_S$ , so that the form  $\mathcal{A}_{TDG}(\cdot; \cdot)$  reads as:

$$\begin{aligned} \mathcal{A}_{TDG}((\boldsymbol{\omega}_F, q, \boldsymbol{\omega}_S, \underline{\boldsymbol{\xi}}); (\boldsymbol{\omega}_F, q, \boldsymbol{\omega}_S, \underline{\boldsymbol{\xi}})) &= \\ & \mathcal{A}_{TDG_F}((\boldsymbol{\omega}_F, q); (\boldsymbol{\omega}_F, q)) + \mathcal{A}_{TDG_S}((\boldsymbol{\omega}_S, \underline{\boldsymbol{\xi}}); (\boldsymbol{\omega}_S, \underline{\boldsymbol{\xi}})) \\ & + \int_{\mathcal{F}_h^{FS}} \overbrace{\left[ q\boldsymbol{\omega}_S \cdot \mathbf{n}_{K_F}^x - q\boldsymbol{\omega}_S \cdot \mathbf{n}_{K_F}^x \right]}^{=0} ds \\ & + \int_{\mathcal{F}_h^{FS}} \left[ \alpha_1(\boldsymbol{\omega}_F \cdot \mathbf{n}_{K_F}^x - \boldsymbol{\omega}_S \cdot \mathbf{n}_{K_F}^x)(\boldsymbol{\omega}_F \cdot \mathbf{n}_{K_F}^x - \boldsymbol{\omega}_S \cdot \mathbf{n}_{K_F}^x) \right] ds \\ & + \int_{\mathcal{F}_h^{FS}} \left[ \delta_1(\underline{\boldsymbol{\xi}}\mathbf{n}_{K_S}^x + q\mathbf{n}_{K_S}^x) \cdot (\underline{\boldsymbol{\xi}}\mathbf{n}_{K_S}^x + q\mathbf{n}_{K_S}^x) \right] ds. \end{aligned}$$

We restate the previously obtained estimates for  $\mathcal{A}_{TDG_F}((\boldsymbol{\omega}_F, q); (\boldsymbol{\omega}_F, q))$  and  $\mathcal{A}_{TDG_S}((\boldsymbol{\omega}_S, \underline{\boldsymbol{\xi}}); (\boldsymbol{\omega}_S, \underline{\boldsymbol{\xi}}))$ . Thus, for  $\mathcal{A}_{TDG}((\boldsymbol{\omega}_F, q, \boldsymbol{\omega}_S, \underline{\boldsymbol{\xi}}); (\boldsymbol{\omega}_F, q, \boldsymbol{\omega}_S, \underline{\boldsymbol{\xi}}))$  we obtain:

$$\begin{aligned} \mathcal{A}_{TDG}((\boldsymbol{\omega}_F, q, \boldsymbol{\omega}_S, \underline{\boldsymbol{\xi}}); (\boldsymbol{\omega}_F, q, \boldsymbol{\omega}_S, \underline{\boldsymbol{\xi}})) &\equiv |||(\boldsymbol{\omega}_F, q)|||_{TDG_F}^2 + |||(\boldsymbol{\omega}_S, \underline{\boldsymbol{\xi}})|||_{TDG_S}^2 \\ & + \left\| \alpha_1^{1/2}(\boldsymbol{\omega}_F \cdot \mathbf{n}_{K_F}^x - \boldsymbol{\omega}_S \cdot \mathbf{n}_{K_F}^x) \right\|_{L^2(\mathcal{F}_h^{FS})}^2 \\ & + \left\| \delta_1^{1/2}(\underline{\boldsymbol{\xi}}\mathbf{n}_{K_S}^x + q\mathbf{n}_{K_S}^x) \right\|_{L^2(\mathcal{F}_h^{FS})}^2. \end{aligned}$$

Thanks to the positiveness of  $\mathcal{A}_{TDG_S}((\boldsymbol{\omega}_S, \underline{\boldsymbol{\xi}}); (\boldsymbol{\omega}_S, \underline{\boldsymbol{\xi}}))$ , we consider the semi-norm  $||| \cdot |||_{TDG}$  given by  $|||(\boldsymbol{\omega}_F, q, \boldsymbol{\omega}_S, \underline{\boldsymbol{\xi}})|||_{TDG} \equiv \mathcal{A}_{TDG}^{1/2}((\boldsymbol{\omega}_F, q, \boldsymbol{\omega}_S, \underline{\boldsymbol{\xi}}); (\boldsymbol{\omega}_F, q, \boldsymbol{\omega}_S, \underline{\boldsymbol{\xi}}))$ , and defined by:

$$\begin{aligned} |||(\boldsymbol{\omega}_F, q, \boldsymbol{\omega}_S, \underline{\boldsymbol{\xi}})|||_{TDG}^2 &\equiv |||(\boldsymbol{\omega}_F, q)|||_{TDG_F}^2 + |||(\boldsymbol{\omega}_S, \underline{\boldsymbol{\xi}})|||_{TDG_S}^2 \\ & + \left\| \alpha_1^{1/2}(\boldsymbol{\omega}_F \cdot \mathbf{n}_{K_F}^x - \boldsymbol{\omega}_S \cdot \mathbf{n}_{K_F}^x) \right\|_{L^2(\mathcal{F}_h^{FS})}^2 \\ & + \left\| \delta_1^{1/2}(\underline{\boldsymbol{\xi}}\mathbf{n}_{K_S}^x + q\mathbf{n}_{K_S}^x) \right\|_{L^2(\mathcal{F}_h^{FS})}^2. \end{aligned}$$

We have the following theorem:

**Theorem 3.6.** *The semi-norm  $||| \cdot |||_{TDG}$  is a norm in the Trefftz space  $\mathbf{T}(\mathcal{T}_h)$ .*

*Proof.* The proof is based on the approach proposed in the proof of theorem 3.1 for  $||| \cdot |||_{TDG_F}$ .  $\square$

The coercivity of the bilinear form  $\mathcal{A}_{TDG}(\cdot; \cdot)$  with respect to the chosen norm  $||| \cdot |||_{TDG}$  follows straightforwardly from theorem 3.6.

In order to prove the continuity properties of  $\mathcal{A}_{TDG}(\cdot; \cdot)$  and  $\ell_{TDG}(\cdot)$ , we introduce the semi-norm  $||| \cdot |||_{TDG^*}$  defined by:

$$\begin{aligned} |||(\boldsymbol{\omega}_F, q, \boldsymbol{\omega}_S, \underline{\boldsymbol{\xi}})|||_{TDG^*}^2 &\equiv |||(\boldsymbol{\omega}_F, q)|||_{TDG_F^*}^2 + |||(\boldsymbol{\omega}_S, \underline{\boldsymbol{\xi}})|||_{TDG_S^*}^2 \\ &+ \left\| q \right\|_{L^2(\mathcal{F}_h^{FS})}^2 + \left\| \boldsymbol{\omega}_S \right\|_{L^2(\mathcal{F}_h^{FS})}^2. \end{aligned}$$

Arguing similarly as for theorems 3.1 and 3.2, it can be easily shown that:

**Theorem 3.7.** *The semi-norm  $||| \cdot |||_{TDG^*}$  is a norm in the Trefftz space  $\mathbf{T}(\mathcal{T}_h)$ .*

*Proof.* See the proof for theorems 3.1 and 3.2.  $\square$

Using a weighted Cauchy-Schwartz inequality [7], we obtain the following continuity estimates:

$$|\mathcal{A}_{TDG}((\mathbf{v}_F, p, \mathbf{v}_S, \underline{\boldsymbol{\sigma}}); (\boldsymbol{\omega}_F, q, \boldsymbol{\omega}_S, \underline{\boldsymbol{\xi}}))| \leq C_1 + C_2 |||(\mathbf{v}_F, p, \mathbf{v}_S, \underline{\boldsymbol{\sigma}})|||_{TDG^*} |||(\boldsymbol{\omega}_F, q, \boldsymbol{\omega}_S, \underline{\boldsymbol{\xi}})|||_{TDG},$$

$$\begin{aligned} |\ell_{TDG}(\boldsymbol{\omega}_F, q, \boldsymbol{\omega}_S, \underline{\boldsymbol{\xi}})| &\leq \left[ \left\| \left( \frac{1}{2\alpha_2} + 1 \right)^{1/2} \rho_F^{1/2} \mathbf{v}_{F0} \right\|_{L^2(\mathcal{F}_h^{0F})}^2 + \left\| \left( \frac{1}{2\beta_2} + 1 \right)^{1/2} \left( \frac{1}{c_F^2 \rho_F} \right)^{1/2} p_0 \right\|_{L^2(\mathcal{F}_h^{0F})}^2 \right. \\ &\left. + \left\| \left( \frac{1}{2\gamma_2} + 1 \right)^{1/2} \rho_F^{1/2} \mathbf{v}_{S0} \right\|_{L^2(\mathcal{F}_h^{0S})}^2 + \left\| \left( \frac{1}{2\delta_2} + 1 \right)^{1/2} \underline{\mathbf{A}}^{1/2} \underline{\boldsymbol{\sigma}}_0 \right\|_{L^2(\mathcal{F}_h^{0S})}^2 \right]^{1/2} |||(\boldsymbol{\omega}_F, q, \boldsymbol{\omega}_S, \underline{\boldsymbol{\xi}})|||_{TDG}, \end{aligned}$$

and, as a result, the following theorem:

**Theorem 3.8.** *The Trefftz-DG variational problem (3.19) admits a unique weak solution  $(\mathbf{v}_{Fh}, p_h, \mathbf{v}_{Sh}, \underline{\boldsymbol{\sigma}}_h) \in \mathbf{T}^p(\mathcal{T}_h)$ . Moreover, the following estimate holds true:*

$$\begin{aligned} |||(\mathbf{v}_F - \mathbf{v}_{Fh}, p - p_h, \mathbf{v}_S - \mathbf{v}_{Sh}, \underline{\boldsymbol{\sigma}} - \underline{\boldsymbol{\sigma}}_h)|||_{TDG} &\leq \\ (1 + C_1 + C_2) \inf_{(\boldsymbol{\omega}_F, q, \boldsymbol{\omega}_S, \underline{\boldsymbol{\xi}}) \in \mathbf{T}^p(\mathcal{T}_h)} &|||(\mathbf{v}_F - \boldsymbol{\omega}_F, p - q, \mathbf{v}_S - \boldsymbol{\omega}_S, \underline{\boldsymbol{\sigma}} - \underline{\boldsymbol{\xi}})|||_{TDG^*}. \end{aligned}$$

*Proof.* The proof follows from the ones for theorems 3.3 and 3.5.  $\square$

### **3.4 Conclusion**

In this chapter, we have presented the theory of space-time Trefftz-DG method applied to the first-order formulations of the acoustic, elastodynamic and coupled elastic-acoustic systems. We have established well-posedness of each formulation based on the mesh-dependent estimates, which gave us a motivation for further numerical implementation of the method.

In the next chapter we will discuss in details the algorithm of implementation as well as different analytical and numerical approaches for its optimization.

## Chapter 4

# Implementation of the Trefftz-DG method

In this chapter, we consider the example of a one-dimensional homogeneous medium, in order to ease the description of the implementation and to provide a first proof of concept of our algorithm. The Trefftz-DG method allows a variety of choices of mesh element forms, provided they are weakly distorted to form a regular polygon. However, it is important to note that the matrix that represents the global linear system in Trefftz-DG method is only sparse, while it is a block-diagonal for the standard DG method. The implementation is indeed very different, since DG methods only consider the space discretization leading to a semi-discrete system, while Trefftz-DG methods are based on a full integration both in time and space. DG formulation requires then the combination with the time scheme and the block-diagonal structure of the DG mass matrix allows using an explicit scheme. The computational costs are thus optimized, even if the time step must satisfy the CFL condition. In the case of Trefftz-DG formulation, a direct implementation leads to invert a global but sparse matrix which tends to be huge. Hence, to reduce the computational time, we propose to divide the global space-time  $Q$  in thin time slabs, corresponding to the right-prism elements, with horizontal faces ( $\Omega$ - or "space" faces) parallel to the physical space domain  $\Omega$ . This assumption gives us the possibility to resolve the global problem layer by layer, considering final values on the top of the current time slab as the initial data for the next slab. Thus, we naturally decrease the size of matrix to be inverted which contributes to reduce the computational time. This approach is similar to the one, introduced for space-time DG methods in [8, 62].

However, the inversion technique we proposed at first turns out to be limited when considering large problems. That is why we derive another technique which is based on the decomposition of the global matrix into a block-diagonal matrix representing the

integration along the  $\Omega$  - faces only. It amounts to separating the time and the space under a CFL - like condition. This technique actually requires some stability conditions, but significantly accelerates the algorithm execution.

# Contents

4.1	Numerical algorithm . . . . .	55
4.2	Polynomial basis . . . . .	57
4.3	Computation of the global matrix $M$ . . . . .	59
4.3.1	The reference element . . . . .	60
4.3.2	The "local-to-reference" approach. . . . .	63
4.3.3	The "reference-to-local" approach. . . . .	64
4.4	Inversion of the global matrix . . . . .	65
4.5	Change-over between the time slabs . . . . .	69
4.6	Conclusion . . . . .	71



## 4.1 Numerical algorithm

We choose a one-dimensional space domain  $\Omega_F \equiv [x_L, x_R]$ , and a time domain  $I \equiv [0, T]$ , so that  $Q_F \equiv \Omega_F \times I$  represents a rectangle.

In order to simplify the presentation, we start with a uniform mesh  $\mathcal{T}_{Fh}$  on  $Q_F$  which is composed of non-overlapping rectangular elements  $K_F^k$ ,  $k = 1, \dots, N_K$ ,  $N_K = N_x \times N_t$ , with edges parallel to the space and time axes, and equal to  $\Delta x = (x_R - x_L)/N_x$  and  $\Delta t = T/N_t$  respectively (see figure 4.1).

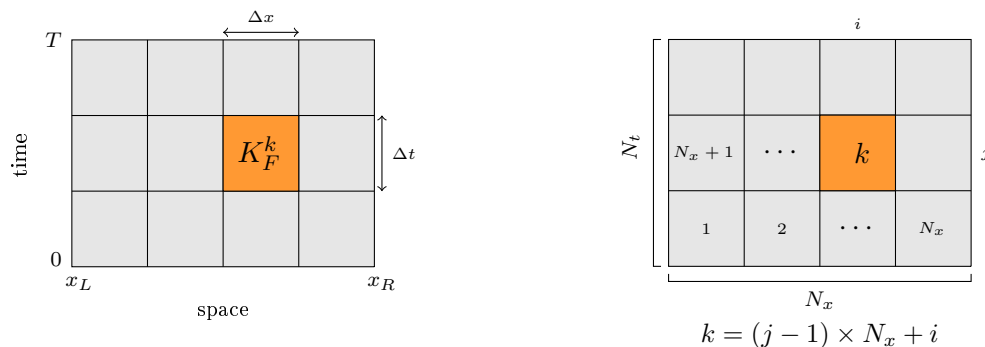


FIGURE 4.1: Uniform rectangular mesh  $\mathcal{T}_{Fh}$  on  $Q_F$ . Element numbering.

Once we have defined the discrete approximation space, we can solve the problem inside each element  $K$ , communicating the corresponding values at the boundaries  $\partial K$  by the incoming and outgoing fluxes. Thus, the variational problem is represented by a global algebraic linear system, with a global sparse matrix  $M$ , of size equals to the total number of elements multiplied by the number of degrees of freedom per element, that is  $(N_t \times N_x \times N_{dof})$ .

Just as was formerly discussed, the space-time formulation leads to the inversion of a sparse but not block-diagonal matrix. The computational costs are thus increased compared to standard DG formulations. In order to optimize the execution of the algorithm, we propose to solve the problem "layer by layer", considering the final results, computed in the current time layer at time  $t$ , as initial values for the next slab at time  $t + \Delta t$  (see figure 4.2). Inside each time slab, we solve the formulation inside each element, taking into account incoming and outgoing fluxes.

In this example of a 1D+time rectangular mesh, each element communicates with its two neighbours (left "L" and right "R" ones). Thus, the global matrix has a block-tridiagonal form, of size  $N_t$  times smaller than the original one (see figure 4.3).

We can also reduce the numerical costs by computing the space and time integrals on faces of one reference element (unit square), and then, by projecting the computed values

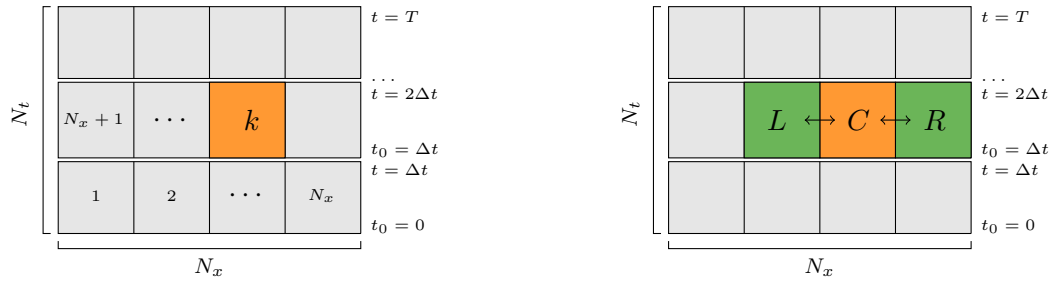
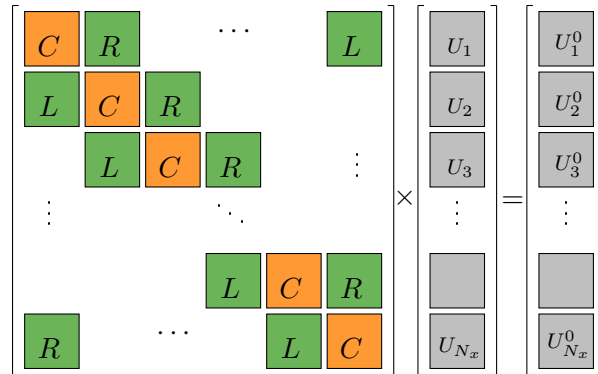

 FIGURE 4.2: Uniform rectangular mesh  $\mathcal{T}_{Fh}$  on  $Q_F$ . Decomposing into layers.


FIGURE 4.3: Global algebraic linear system with block-tridiagonal matrix.

onto all mesh elements (it is simply a multiplication by  $\Delta x$  and  $\Delta t$  for space and time integration respectively in the case of rectangular mesh).

We have written a short pseudo-code, which describes the algorithm of the method implementation. It is important to notice that the main loop, which represents propagation in time, contains three fundamental stages:

- 1) computation of the approximation coefficients  $U$  of the numerical solution in the current time slab  $[t_{j-1}, t_j]$  (step 6);
- 2) computation of the intermediate numerical solutions  $V$  and  $P$  thanks to the approximation coefficients  $U$  at the end of the current time slab  $t_j$ , using the  $t_{snap}$  function, which computes the trace of the numerical solution at time  $t_j$  (steps 7 - 8).
- 3) update of the initial values - computation of  $U_0 = 0.5(V_0 + P_0)$  (the right-hand side) at the beginning  $t_j$  of the next time slab  $[t_j, t_{j+1}]$ , thanks to the intermediate numerical solutions  $V$  and  $P$  from the steps 7 - 8, using the  $L^2$ -projection function  $L^2_{proj}$  (steps 9 - 11).

The idea of removing the last two stages, corresponding to the "projection" of the approximation coefficients onto the numerical solution, is quite attractive, because it will provide a faster implementation of the code: we could re-use directly the vector of approximate coefficients computed in the previous slab. We will explore this possibility in section 4.5.

```

Data:  $V_0, P_0$  % initial velocity and pressure fields
          $c, \rho, \Omega, I$  % domain parameters
          $\Delta x, \Delta t, N_x, N_t, N_{dof}$  % mesh and DG parameters
Result:  $V_T, P_T$  % final velocity and pressure fields
Initiate:
0  $\phi^v, \phi^p$  % initiation of the polynomial basis
Compute:
1  $V_{aux0} = L_{proj}^2(V_0, \phi^v)$  % velocity and pressure linear terms at  $t = 0$ 
2  $P_{aux0} = L_{proj}^2(P_0, \phi^p)$ 
3  $U_0 = 0.5(V_{aux0} + P_{aux0})$  % the initial condition vector (right-hand side)
4  $M$  % computing the global matrix  $M$ 
5  $invM = M^{-1}$  % inversion of the global matrix  $M$ 
for  $j = 1 : N_t$  do
  Compute:
  6  $U = invM U_0$  % vector of the coefficients for approximate
  % solution in the time slab  $[(j-1)\Delta t, j\Delta t]$ 
  7  $V = t_{snap}(U, \phi^v, t_j)$  % intermediate approximate solutions for velocity
  8  $P = t_{snap}(U, \phi^p, t_j)$  % and pressure fields at  $t_j = j\Delta t$ 
  9  $V_{aux0} = L_{proj}^2(V, \phi^v)$  % intermediate velocity and pressure linear
  10  $P_{aux0} = L_{proj}^2(P, \phi^p)$  % terms at  $t_j = j\Delta t$ 
  11  $U_0 = 0.5(V_{aux0} + P_{aux0})$  % update of the right-hand side
end
Compute:
12  $V_T = t_{snap}(U, \phi^v, t_{N_t})$  % final approximate solutions for velocity and
13  $P_T = t_{snap}(U, \phi^p, t_{N_t})$  % pressure fields at  $t_{N_t} = N_t\Delta t$ 

```

In the next sections, we detail the important steps of the algorithm, such as the construction of the Trefftz space-time polynomial basis, the computation of the global matrix  $M$  and its inversion, and also both the update of the initial data and change-over between the time slabs.

## 4.2 Polynomial basis

As discussed in the previous chapter, one of the advantages of Trefftz-type methods is the flexibility in the choice of basis functions. The main constraint is to satisfy the Trefftz property inside each element. Trefftz - or "T"-functions for non-stationary problems were discussed in many papers by Zieliński et al. in [111], Cialkovski et al. in [27], Maciag in [79], Grysa et al. in [54], Kretzchmar et al. in [72], Moiola et al. in [82], Banjai et al. in [12] and their references therein.

To perform the numerical simulations, we have computed a polynomial basis, defined in the reference element, using Taylor expansions of generating exponential functions which are local solutions of the initial system of equations. We have extended the algorithm

for computing wave polynomials, solutions of the second order transient wave equation, proposed by Maciag in [78], to the first order AS and ES of dimension one and higher.

To explain our approach, we consider the example of a 1D acoustic problem:

$$\begin{cases} \frac{\partial p}{\partial t} + c_F^2 \frac{\partial v_F}{\partial x} = 0, \\ \frac{\partial v_F}{\partial t} + \frac{\partial p}{\partial x} = 0. \end{cases}$$

Using Fourier method of separation of variables (see [49]) we obtain two solutions

$$g^v(a, b, x, t) = e^{i(ax+bc_Ft)}, \quad g^p(a, b, x, t) = -c_F e^{i(bx+ac_Ft)},$$

for  $v_F$  and  $p$  respectively, which satisfy the initial acoustic equations if  $a^2 = b^2$  (we consider them as the generating functions of wave polynomials for velocity and pressure).

We decompose both generating functions in Taylor expansions as follows:

$$\begin{aligned} e^{i(ax+bc_Ft)} &= \sum_{n=0}^{\infty} \sum_{k=0}^n S_{n-k,k}^v(x, t) a^{n-k} b^k, \\ -c_F e^{i(bx+ac_Ft)} &= \sum_{n=0}^{\infty} \sum_{k=0}^n S_{n-k,k}^p(x, t) a^{n-k} b^k, \end{aligned}$$

where  $S_{n-k,k}^v(x, t)$  and  $S_{n-k,k}^p(x, t)$  are polynomials of variables  $x, t$  involving the medium parameter  $c_F$ . Replacing  $b^2$  by  $a^2$  in both series we obtain:

$$\begin{aligned} e^{i(ax+bc_Ft)} &= \sum_{n=0}^{\infty} \sum_{k=0, k < 2}^n Q_{n-k,k}^v(x, t) a^{n-k} b^k, \\ -c_F e^{i(bx+ac_Ft)} &= \sum_{n=0}^{\infty} \sum_{k=0, k < 2}^n Q_{n-k,k}^p(x, t) a^{n-k} b^k. \end{aligned}$$

The real ( $R^v$  and  $R^p$ ) and imaginary ( $I^v$  and  $I^p$ ) parts of polynomials  $Q^v$  and  $Q^p$  satisfy the initial acoustic equations:

$$\begin{aligned} R_{n-k,k}^v(x, t) &= \Re(Q_{n-k,k}^v(x, t)), & I_{n-k,k}^v(x, t) &= \Im(Q_{n-k,k}^v(x, t)), \\ R_{n-k,k}^p(x, t) &= \Re(Q_{n-k,k}^p(x, t)), & I_{n-k,k}^p(x, t) &= \Im(Q_{n-k,k}^p(x, t)). \end{aligned}$$

By varying the parameters  $k$  and  $n$  in the above formulation we obtain:

$$\begin{array}{llll}
R_{00}^v = 1 & I_{00}^v = 0 & R_{00}^p = -c_F & I_{00}^p = 0 \\
R_{10}^v = 0 & I_{10}^v = x & R_{10}^p = 0 & I_{10}^p = -c_F^2 t \\
R_{01}^v = 0 & I_{01}^v = c_F t & R_{01}^p = 0 & I_{01}^p = -c_F x \\
R_{20}^v = -\frac{x^2}{2} - \frac{c_F^2 t^2}{2} & I_{20}^v = 0 & R_{20}^p = c_F \left( \frac{x^2}{2} + \frac{c_F^2 t^2}{2} \right) & I_{20}^p = 0 \\
R_{11}^v = -c_F x t & I_{11}^v = 0 & R_{11}^p = c_F^2 x t & I_{11}^p = 0 \\
R_{02}^v = 0 & I_{02}^v = 0 & R_{02}^p = 0 & I_{02}^p = 0 \\
R_{30}^v = 0 & I_{30}^v = -\frac{x^3}{6} - \frac{x c_F^2 t^2}{2} & R_{30}^p = 0 & I_{30}^p = c_F \left( \frac{c_F^3 t^3}{6} + \frac{x^2 c_F t}{2} \right) \\
R_{21}^v = 0 & I_{21}^v = -\frac{c_F^3 t^3}{6} - \frac{x^2 c_F t}{2} & R_{21}^p = 0 & I_{21}^p = c_F \left( \frac{x^3}{6} + \frac{x c_F^2 t^2}{2} \right) \\
R_{12}^v = 0 & I_{12}^v = 0 & R_{12}^p = 0 & I_{12}^p = 0 \\
R_{03}^v = 0 & I_{03}^v = 0 & R_{03}^p = 0 & I_{03}^p = 0
\end{array}$$

Thus, a space-time wave polynomial basis for the first-order acoustic wave equation can be written as follows (approximation degree  $p=3$ ):

$$\begin{array}{llll}
\hat{\phi}_1^v = 0 & \hat{\phi}_2^v = 1 & \hat{\phi}_3^v = x & \hat{\phi}_4^v = c_F t \\
\hat{\phi}_1^p = -c_F & \hat{\phi}_2^p = 0 & \hat{\phi}_3^p = -c_F^2 t & \hat{\phi}_4^p = -c_F x \\
\hat{\phi}_5^v = -\frac{x^2}{2} - \frac{c_F^2 t^2}{2} & \hat{\phi}_6^v = -c_F x t & \hat{\phi}_7^v = -\frac{x^3}{6} - \frac{x c_F^2 t^2}{2} & \hat{\phi}_8^v = -\frac{c_F^3 t^3}{6} - \frac{x^2 c_F t}{2} \\
\hat{\phi}_5^p = c_F^2 x t & \hat{\phi}_6^p = c_F \left( \frac{x^2}{2} + \frac{c_F^2 t^2}{2} \right) & \hat{\phi}_5^p = c_F \left( \frac{c_F^3 t^3}{6} + \frac{x^2 c_F t}{2} \right) & \hat{\phi}_6^p = c_F \left( \frac{x^3}{6} + \frac{x c_F^2 t^2}{2} \right)
\end{array}$$

This basis contains the pairs of polynomial functions  $(\hat{\phi}^v, \hat{\phi}^p)$ , corresponding to the velocity and pressure respectively, which are locally defined on the mesh element and satisfying the Trefftz property inside this element, and of degrees less or equal to  $p$  ( $p = 0, 1, 2, 3$ ), to provide an approximation of order  $p$ .

By their construction, the Trefftz basis functions are not attached to the coordinates of the degrees of freedom inside the element, contrary to the Lagrange polynomials. Even if we compute only surface integrals, we can evaluate the final approximation solution in any point of the whole element refinement. We refer the reader to appendix B for bases we use in 2D acoustics and elastodynamics.

### 4.3 Computation of the global matrix $M$

In this section, we detail the computation of the global matrix  $M$  of the system. We introduce the reference element and the transformation operator between the points of the reference and local mesh element. It is worth noting that we use basis functions that are defined in the whole element even if we only need their trace on the faces of the element. Indeed as we have explained in the previous section the basis functions are constructed as local solutions of the wave equation into an element, while the variational formulation involves only their traces on the faces of the element. We compare two approaches for computing the integral terms that constitute the global matrix  $M$ , with respect to the choice of system of coordinates.

### 4.3.1 The reference element

We consider the reference element  $\hat{K}_F$  with its vertices  $\hat{s}_i(\hat{\mathbf{x}}_i, \hat{t}_i)$ ,  $i = 1, N_{ver}$ .

For a 1D+time model,  $\hat{K}_F$  is a unit square with vertices  $\hat{s}_1(0, 0)$ ,  $\hat{s}_2(1, 0)$ ,  $\hat{s}_3(1, 1)$ ,  $\hat{s}_4(0, 1)$  in the case of rectangular meshes (figure 4.4(a)), and a right unit triangle with vertices  $\hat{s}_1(0, 0)$ ,  $\hat{s}_2(1, 0)$ ,  $\hat{s}_3(0, 1)$  in the case of triangular meshes (figure 4.4(b)).

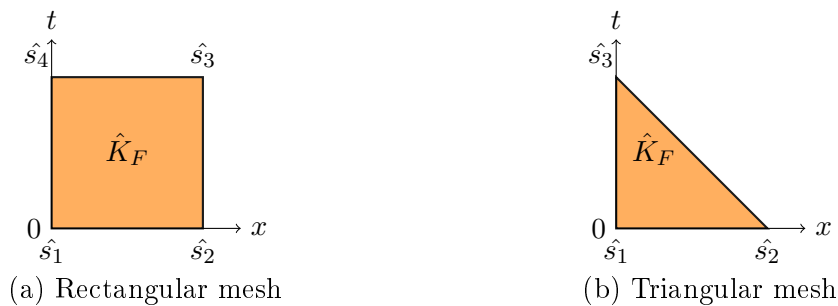


FIGURE 4.4: 1D+time reference element

For a 2D+time model,  $\hat{K}_F$  is a unit cube with vertices  $\hat{s}_1(0, 0, 0)$ ,  $\hat{s}_2(1, 0, 0)$ ,  $\hat{s}_3(1, 1, 0)$ ,  $\hat{s}_4(0, 1, 0)$ ,  $\hat{s}_5(0, 0, 1)$ ,  $\hat{s}_6(1, 0, 1)$ ,  $\hat{s}_7(1, 1, 1)$ ,  $\hat{s}_8(0, 1, 1)$  in the case of rectangular meshes in space (figure 4.5(a)), and a right prism with vertices  $\hat{s}_1(0, 0, 0)$ ,  $\hat{s}_2(1, 0, 0)$ ,  $\hat{s}_3(0, 1, 0)$ ,  $\hat{s}_4(0, 0, 1)$ ,  $\hat{s}_5(1, 0, 1)$ ,  $\hat{s}_6(0, 1, 1)$  in the case of triangular meshes in space (figure 4.5(b)).

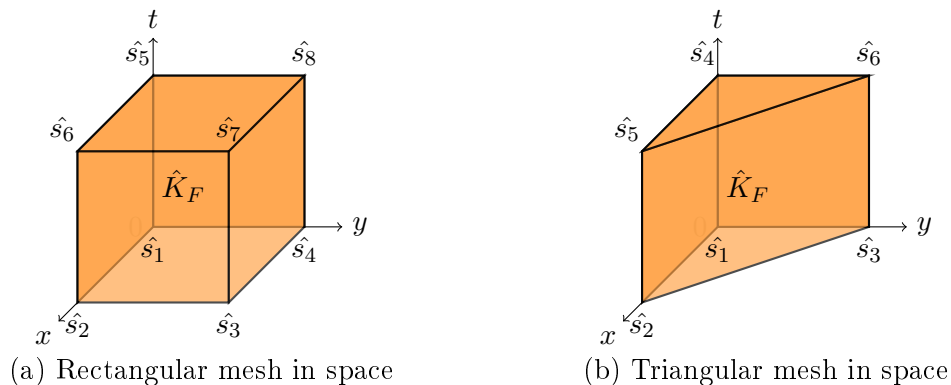
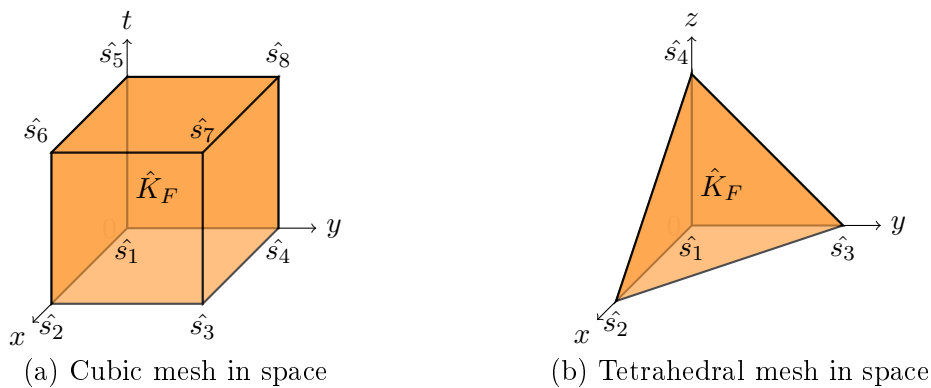
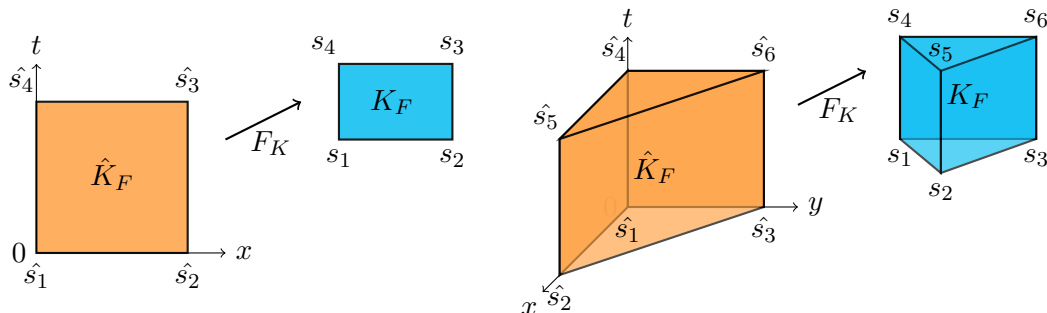


FIGURE 4.5: 2D+time reference element

For a 3D+time model,  $\hat{K}_F$  is a unit 4D cube with vertices  $\hat{s}_1(0, 0, 0, 0)$ ,  $\hat{s}_2(1, 0, 0, 0)$ ,  $\hat{s}_3(1, 1, 0, 0)$ ,  $\hat{s}_4(0, 1, 0, 0)$ ,  $\hat{s}_5(0, 0, 1, 0)$ ,  $\hat{s}_6(1, 0, 1, 0)$ ,  $\hat{s}_7(1, 1, 1, 0)$ ,  $\hat{s}_8(0, 1, 1, 0)$ ,  $\hat{s}_9(0, 0, 0, 1)$ ,  $\hat{s}_{10}(1, 0, 0, 1)$ ,  $\hat{s}_{11}(1, 1, 0, 1)$ ,  $\hat{s}_{12}(0, 1, 0, 1)$ ,  $\hat{s}_{13}(0, 0, 1, 1)$ ,  $\hat{s}_{14}(1, 0, 1, 1)$ ,  $\hat{s}_{15}(1, 1, 1, 1)$ ,  $\hat{s}_{16}(0, 1, 1, 1)$  in the case of cubic meshes in space (figure 4.6(a)), and a 4D right prism with vertices  $\hat{s}_1(0, 0, 0, 0)$ ,  $\hat{s}_2(1, 0, 0, 0)$ ,  $\hat{s}_3(0, 1, 0, 0)$ ,  $\hat{s}_4(0, 0, 1, 0)$ ,  $\hat{s}_5(0, 0, 0, 1)$ ,  $\hat{s}_6(1, 0, 0, 1)$ ,  $\hat{s}_7(0, 1, 0, 1)$ ,  $\hat{s}_8(0, 0, 1, 1)$  in the case of tetrahedral meshes in space (figure 4.6(b)).

FIGURE 4.6: 3D+time reference element (in section  $t = 0$ )

For each local element  $K_F$  of the mesh, it exists a linear transformation  $F_K : (\hat{\mathbf{x}}, \hat{t}) \rightarrow (\mathbf{x}, t)$  which transforms any point  $(\hat{\mathbf{x}}, \hat{t})$  in the element of reference  $\hat{K}_F$  into the point  $(\mathbf{x}, t)$  in the local element  $K_F$  (see figure 4.7).

FIGURE 4.7: Affine map  $F_K$ . Element transformation examples

We define the operator  $F_K(\hat{\mathbf{x}}, \hat{t})$  as follows:

1D+time meshes:

$$F_K(\hat{x}, \hat{t}) = \begin{pmatrix} x_1 \\ t_1 \end{pmatrix} + \begin{pmatrix} x_2 - x_1 & 0 \\ 0 & t_3 - t_1 \end{pmatrix} \begin{pmatrix} \hat{x} \\ \hat{t} \end{pmatrix} \quad (\text{rectangular cells}),$$

$$F_K(\hat{x}, \hat{t}) = \begin{pmatrix} x_1 \\ t_1 \end{pmatrix} + \begin{pmatrix} x_2 - x_1 & x_3 - x_1 \\ t_2 - t_1 & t_3 - t_1 \end{pmatrix} \begin{pmatrix} \hat{x} \\ \hat{t} \end{pmatrix} \quad (\text{triangular cells}),$$

2D+time meshes:

$$F_K(\hat{x}, \hat{y}, \hat{t}) = \begin{pmatrix} x_1 \\ y_1 \\ t_1 \end{pmatrix} + \begin{pmatrix} x_2 - x_1 & 0 & 0 \\ 0 & y_3 - y_1 & 0 \\ 0 & 0 & t_5 - t_1 \end{pmatrix} \begin{pmatrix} \hat{x} \\ \hat{y} \\ \hat{t} \end{pmatrix} \quad (\text{cubic cells}),$$

$$F_K(\hat{x}, \hat{y}, \hat{t}) = \begin{pmatrix} x_1 \\ y_1 \\ t_1 \end{pmatrix} + \begin{pmatrix} x_2 - x_1 & x_3 - x_1 & 0 \\ y_2 - y_1 & y_3 - y_1 & 0 \\ 0 & 0 & t_4 - t_1 \end{pmatrix} \begin{pmatrix} \hat{x} \\ \hat{y} \\ \hat{t} \end{pmatrix} \quad (\text{prism cells}),$$

and 3D+time meshes:

$$F_K(\hat{x}, \hat{y}, \hat{z}, \hat{t}) = \begin{pmatrix} x_1 \\ y_1 \\ z_1 \\ t_1 \end{pmatrix} + \begin{pmatrix} x_2 - x_1 & 0 & 0 & 0 \\ 0 & y_3 - y_1 & 0 & 0 \\ 0 & 0 & z_5 - z_1 & 0 \\ 0 & 0 & 0 & t_9 - t_1 \end{pmatrix} \begin{pmatrix} \hat{x} \\ \hat{y} \\ \hat{z} \\ \hat{t} \end{pmatrix} \quad (\text{4D cubic cells});$$

$$F_K(\hat{x}, \hat{y}, \hat{z}, \hat{t}) = \begin{pmatrix} x_1 \\ y_1 \\ z_1 \\ t_1 \end{pmatrix} + \begin{pmatrix} x_2 - x_1 & x_3 - x_1 & x_4 - x_1 & 0 \\ y_2 - y_1 & y_3 - y_1 & y_4 - y_1 & 0 \\ z_2 - z_1 & z_3 - z_1 & z_4 - z_1 & 0 \\ 0 & 0 & 0 & t_5 - t_1 \end{pmatrix} \begin{pmatrix} \hat{x} \\ \hat{y} \\ \hat{z} \\ \hat{t} \end{pmatrix} \quad (\text{4D prism cells}),$$

or, in vector-matrix form  $F_K(\hat{\mathbf{x}}, \hat{t}) \equiv A_K \begin{pmatrix} \hat{\mathbf{x}} \\ \hat{t} \end{pmatrix} + \mathbf{b}_K$ .

For each reference element  $\hat{K}_F$  we introduce the following notation:

- we denote by  $\hat{K}_\Omega^+$  and  $\hat{K}_\Omega^-$  faces - the reference faces at the top and at the bottom of the time slab, where the time variable  $\hat{t}$  is fixed and equal to 1 and 0 respectively. In particular, we denote by  $\hat{K}_\Omega$  the projection of  $\hat{K}_\Omega^\pm$  on  $\mathbb{R}^d$  such that  $\hat{K}_\Omega = \{\hat{\mathbf{x}} \mid (\hat{\mathbf{x}}, 0) \in \hat{K}_\Omega^-\} = \{\hat{\mathbf{x}} \mid (\hat{\mathbf{x}}, 1) \in \hat{K}_\Omega^+\}$ ;

- we denote by  $\hat{K}_I$  faces - the reference faces in  $\partial\hat{K}_\Omega \times [0, 1]$ .

In figure 4.5 (b)  $\hat{K}_\Omega^+$  and  $\hat{K}_\Omega^-$  are the triangular faces on the top and bottom respectively, while  $\hat{K}_I$  is the set of vertical rectangular faces.

Taking into account the above notation, we introduce the operators  $F_{K_\Omega^\pm}$  and  $F_{K_I}$  that transform any point  $(\hat{\mathbf{x}}, \hat{t})$  of the reference face  $\hat{K}_\Omega^\pm$  and  $\hat{K}_I$  to the point  $(\mathbf{x}, t)$  of the corresponding local element face  $K_\Omega^\pm$  and  $K_I$  respectively. These operators can be written in the terms of a formerly defined operator  $F_K$  as follows:

$$\begin{aligned} F_{K_\Omega^+}(\hat{\mathbf{x}}) &= F_K(\hat{\mathbf{x}}, 1), & \hat{\mathbf{x}} &\in \hat{K}_\Omega, \\ F_{K_\Omega^-}(\hat{\mathbf{x}}) &= F_K(\hat{\mathbf{x}}, 0), & \hat{\mathbf{x}} &\in \hat{K}_\Omega, \\ F_{K_I}(\hat{\mathbf{x}}, \hat{t}) &= F_K(\hat{\mathbf{x}}, \hat{t}), & (\hat{\mathbf{x}}, \hat{t}) &\in \partial\hat{K}_\Omega \times [0, 1]. \end{aligned}$$

The Jacobian  $J_{F_K}$  of the transformation  $F_K$  corresponds to the matrix  $A_K$  where  $|J_{F_K}| = |\det(A_K)|$  is the volume of the local element. The Jacobian  $J_{F_K^{-1}}$  of the inverse transformation  $F_K^{-1}$  satisfies  $|J_{F_K^{-1}}| = |\det(A_K)|^{-1}$ . In particular, for the Jacobian  $J_{F_{K_\Omega^\pm}}$  of

transformation  $F_{K_\Omega^\pm}$  we have:  $|J_{F_{K_\Omega^\pm}}| = \Delta_\Omega \propto (\Delta x)^d$  - surface of the local  $K_\Omega^\pm$  face. For the Jacobian  $J_{F_{K_I}}$  of transformation  $F_{K_I}$  we have:  $|J_{F_{K_I}}| = \Delta_I \propto (\Delta x)^{d-1} \Delta t$  - surface of the local  $K_I$  face

Thanks to this "reference-to-local" transformation and its inverse, we have different possibilities of choice of coordinate system to calculate the global matrix  $M$ . The use of the reference or local basis has its specific advantages, regarding the numerical implementation, and it will be discussed in the next section.

### 4.3.2 The "local-to-reference" approach.

The global matrix  $M$  consists of integrals of basis function products on the local element faces. Generally speaking, it reduces to the computation of the following surface integrals:

$$\begin{aligned}\mathcal{I}_{K_\Omega^\pm}^{i,j} &= \int_{K_\Omega^\pm} \phi_i \phi_j d\mathbf{x}, \quad i, j = 1, N_{dof}, \\ \mathcal{I}_{K_I}^{i,j} &= \int_{K_I} \phi_i \phi_j d(\mathbf{x}, t), \quad i, j = 1, N_{dof}.\end{aligned}$$

In the above formulas, the notation  $d\mathbf{x}$  stands for the elementary measure of the face  $K_\Omega^\pm$  and  $d(\mathbf{x}, t)$  denotes the elementary measure of  $K_I$ .

As we have mentioned previously, there exist the linear transformation  $F_{K_\Omega^\pm}$  and  $F_{K_I}$  that transforms the reference (or global) basis functions into the local ones. Thus, the integrals  $\mathcal{I}_{K_\Omega^\pm}^{i,j}$  and  $\mathcal{I}_{K_I}^{i,j}$  can be written as follows:

$$\begin{aligned}\mathcal{I}_{K_\Omega^\pm}^{i,j} &= \int_{K_\Omega^\pm} \phi_i \phi_j d\mathbf{x} = \int_{\hat{K}_\Omega^\pm} [\hat{\phi}_i \circ F_{K_\Omega^\pm}^{-1}] [\hat{\phi}_j \circ F_{K_\Omega^\pm}^{-1}] d\mathbf{x} = |J_{F_{K_\Omega^\pm}}| \int_{\hat{K}_\Omega^\pm} \hat{\phi}_i \hat{\phi}_j d\hat{\mathbf{x}} = \\ &\quad \Delta_\Omega \int_{\hat{K}_\Omega^\pm} \hat{\phi}_i \hat{\phi}_j d\hat{\mathbf{x}}, \\ \mathcal{I}_{K_I}^{i,j} &= \int_{K_I} \phi_i \phi_j d(\mathbf{x}, t) = \int_{\hat{K}_I} [\hat{\phi}_i \circ F_{K_I}^{-1}] [\hat{\phi}_j \circ F_{K_I}^{-1}] d(\mathbf{x}, t) = |J_{F_{K_I}}| \int_{\hat{K}_I} \hat{\phi}_i \hat{\phi}_j d(\hat{\mathbf{x}}, \hat{t}) = \\ &\quad \Delta_I \int_{\hat{K}_I} \hat{\phi}_i \hat{\phi}_j d(\hat{\mathbf{x}}, \hat{t}).\end{aligned}$$

We then obtain:

$$\mathcal{I}_{K_\Omega^\pm}^{i,j} = \Delta_\Omega \mathcal{I}_{\hat{K}_\Omega^\pm}^{i,j} \quad \text{and} \quad \mathcal{I}_{K_I}^{i,j} = \Delta_I \mathcal{I}_{\hat{K}_I}^{i,j},$$

It means that once we have defined the basis functions in the reference element (unit square, right triangle or right prism etc.), we can compute all the integral terms on the reference faces, and then "re-project" the obtained integral values on the local element multiplying by  $\Delta_\Omega \propto (\Delta x)^d$  or  $\Delta_I \propto (\Delta x)^{d-1} \Delta t$ .

The advantage of this approach is that, in the case of homogeneous medium with regular mesh, instead of computing the integrals  $N_K$  times, we compute them once for all inside the reference element. To turn to the reference element for defining its basis functions allows to compute all the integrals analytically. This technique is commonly used for the classical DG methods. For the Trefftz-DG methods, the basis functions depend on the parameters of the medium, thus the "reference-to-local" approach can be used in the case of homogeneous media only. In heterogeneous medium, since the basis functions have to be recomputed on each element, it is preferable to use the technique described in the next section.

### 4.3.3 The "reference-to-local" approach.

When we consider the Trefftz approximation space, the "local-to-reference" approach becomes less useful, because the Trefftz basis functions inside the local element depends on the medium parameters inside this element (see section 4.2). Thus, the number of different projections of local basis functions to the reference element is the total number of elements, so we can lose the advantage of an analytical integration.

That is why we turn to an approximation procedure, such as a Gaussian quadrature, to compute the surface integrals straightforwardly on each local element face. it is worth noting that this process can be easily parallelized.

Let  $(\hat{\mathbf{x}}, \hat{t})_l^G$  be the Gaussian nodes inside the reference element, and  $w_l^G$  the corresponding weights ( $l = 1, N_G$ ). We obtain the following formulations:

$$\begin{aligned} \mathcal{I}_{K_\Omega^\pm}^{i,j} &= \int_{K_\Omega^\pm} \phi_i \phi_j d\mathbf{x} = \sum_{l=1}^{N_G} [\phi_i \phi_j](\mathbf{x})_l^G w_l^G = |J_{F_{K_\Omega^\pm}}| \sum_{l=1}^{N_G} [[\phi_i \phi_j] \circ F_{K_\Omega^\pm}](F_{K_\Omega^\pm}(\hat{\mathbf{x}}))_l^G w_l^G = \\ &\Delta_\Omega \sum_{l=1}^{N_G} [\phi_i \phi_j](F_{K_\Omega^\pm}(\hat{\mathbf{x}}))_l^G w_l^G, \end{aligned}$$

$$\begin{aligned} \mathcal{I}_{K_I}^{i,j} &= \int_{K_I} \phi_i \phi_j d(\mathbf{x}, t) = \sum_{l=1}^{N_G} [\phi_i \phi_j](\mathbf{x}, t)_l^G w_l^G = |J_{F_{K_I}}| \sum_{l=1}^{N_G} [[\phi_i \phi_j] \circ F_{K_I}](F_{K_I}(\hat{\mathbf{x}}, \hat{t}))_l^G w_l^G = \\ &\Delta_I \sum_{l=1}^{N_G} [\phi_i \phi_j](F_{K_I}(\hat{\mathbf{x}}, \hat{t}))_l^G w_l^G, \end{aligned}$$

and the corresponding algorithm steps:

```

for  $i = 1 : N_{dof}$  do
  for  $j = 1 : N_{dof}$  do
     $I_{K_\Omega}(i, j) = 0$ 
     $I_{K_I}(i, j) = 0$ 
    for  $l = 1 : N_G$  do
      Compute:
       $(\mathbf{x})_l^G = F_{K_\Omega^\pm}(\hat{\mathbf{x}})_l^G$ 
       $(\mathbf{x}, t)_l^G = F_{K_I}(\hat{\mathbf{x}}, \hat{t})_l^G$ 
       $I_{K_\Omega^\pm}(i, j) = I_{K_\Omega^\pm} i, j + [\phi_i \phi_j](\mathbf{x})_l^G w_l^G$ 
       $I_{K_I}(i, j) = I_{K_I} i, j + [\phi_i \phi_j](\mathbf{x}, t)_l^G w_l^G$ 
    end
     $I_{K_\Omega^\pm}(i, j) = \Delta_\Omega I_{K_\Omega^\pm}(i, j)$ 
     $I_{K_I}(i, j) = \Delta_I I_{K_I}(i, j)$ 
  end
end

```

The Gaussian nodes and the corresponding weights for a quadrangle and a triangle are given in appendix C.

To summarize, the "reference-to-local" approach requires computing  $N_x \times N_t$  matrices, while the "local-to-reference" one calls for the computation of a single matrix. We can decrease this number of operations to  $N_x$  by combining both approaches. Indeed, since the physical parameters only depend on the space variables, we can compute the global matrix  $M$  into the interval  $[0, \Delta t]$  and use it for the next time slabs.

## 4.4 Inversion of the global matrix

Once we have computed the global matrix  $M$ , the next step in the algorithm is its inversion. The model described in section 4.1 shows that the method can be efficiently applied to examples of structured meshes of smaller dimensions. However, for higher dimensions, with more general meshes inside each time slab, we are faced with the inversion of a sparse matrix (contrary to the classical DG method where the mass-matrix is block-diagonal), which is really challenging for further applications of the method to real data in industry. Indeed, we could reach the memory limitations of the computers as occurs currently when solving harmonic problems.

We consider the Trefftz-DG formulation of AS previously introduced in section 3.1. We refer to the section 3.1.2 of previous chapter for the notation regarding the mesh skeleton  $\mathcal{F}_{Fh} = \cup_{K_F \in \mathcal{T}_{Fh}} \partial K_F$  and its subsets. In particular we divide the family of internal element faces into two subsets  $\mathcal{F}_h^{QF} \equiv \mathcal{F}_h^{\Omega F} \cup \mathcal{F}_h^{IF}$ , where  $\mathcal{F}_h^{\Omega F}$  corresponds to the "space"

or  $K_\Omega$ -faces (parallel to the physical space domain), and  $\mathcal{F}_h^{I_F}$  corresponds to the "time" or  $K_I$ -faces (parallel to the time axis). The Trefftz-DG formulation reads as:

Seek  $(\mathbf{v}_{Fh}, p_h) \in V^h(\mathcal{T}_{Fh})^d \times V^h(\mathcal{T}_{Fh})$  such that, for all  $(\boldsymbol{\omega}_F, q) \in \mathbf{T}_F(\mathcal{T}_{Fh})$ , it holds true:

$$\mathcal{A}_{TDG_F}((\mathbf{v}_{Fh}, p_h); (\boldsymbol{\omega}_F, q)) = \ell_{TDG_F}(\boldsymbol{\omega}_F, q).$$

Here the bilinear form  $\mathcal{A}_{TDG_F}(\cdot; \cdot)$  is defined by:

$$\begin{aligned} \mathcal{A}_{TDG_F}((\mathbf{v}_{Fh}, p_h); (\boldsymbol{\omega}_F, q)) \equiv & \int_{\mathcal{F}_h^{I_F}} \left[ \{p_h\} [\boldsymbol{\omega}_F]_x + \{\mathbf{v}_{Fh}\} \cdot [q]_x + \alpha_1 [\mathbf{v}_{Fh}]_x [\boldsymbol{\omega}_F]_x + \beta_1 [p_h]_x \cdot [q]_x \right] ds \\ & + \int_{\mathcal{F}_h^{T_F}} \left[ \frac{1}{c_F^2 \rho_F} p_h q + \rho_F \mathbf{v}_{Fh} \cdot \boldsymbol{\omega}_F \right] ds - \frac{1}{2} \int_{\mathcal{F}_h^{0_F}} \left[ \frac{1}{c_F^2 \rho_F} p_h q + \rho_F \mathbf{v}_{Fh} \cdot \boldsymbol{\omega}_F \right] ds \\ & + \int_{\mathcal{F}_h^{D_F}} \left[ p \boldsymbol{\omega}_F \cdot \mathbf{n}_{K_F}^x + \alpha_1 (\mathbf{v}_{Fh} \cdot \mathbf{n}_{K_F}^x) (\boldsymbol{\omega}_F \cdot \mathbf{n}_{K_F}^x) \right] ds, \end{aligned}$$

and the linear form  $\ell_{TDG_F}(\cdot)$  is defined by:

$$\ell_{TDG_F}(\boldsymbol{\omega}_F, q) \equiv \frac{1}{2} \int_{\mathcal{F}_h^{0_F}} \left[ \frac{1}{c_F^2 \rho_F} p_h q + \rho_F \mathbf{v}_{Fh} \cdot \boldsymbol{\omega}_F \right] ds.$$

The bilinear form  $\mathcal{A}_{TDG_F}(\cdot; \cdot)$  consists of two terms  $\mathcal{A}_{TDG_F}^\Omega(\cdot; \cdot)$  and  $\mathcal{A}_{TDG_F}^I(\cdot; \cdot)$  defined as follows:

$$\mathcal{A}_{TDG_F}((\mathbf{v}_{Fh}, p_h); (\boldsymbol{\omega}_f, q)) \equiv \underbrace{\int_{\mathcal{F}_h^{T_F}} + \int_{\mathcal{F}_h^{0_F}}}_{\mathcal{A}_{TDG_F}^\Omega} + \underbrace{\int_{\mathcal{F}_h^{I_F}} + \int_{\mathcal{F}_h^{D_F}}}_{\mathcal{A}_{TDG_F}^I}.$$

The global matrix  $M$ , which corresponds to  $\mathcal{A}_{TDG_F}$ , can be represented by the sum of two matrices  $\Delta_\Omega M_\Omega$  and  $\Delta_I M_I$  corresponding to  $\mathcal{A}_{TDG_F}^\Omega$  and  $\mathcal{A}_{TDG_F}^I$  respectively, as follows:

$$M = \Delta_\Omega M_\Omega + \Delta_I M_I.$$

Here,  $\Delta_\Omega \propto (\Delta x)^d$  and  $\Delta_I \propto (\Delta x)^{d-1} \Delta t$  correspond to the surfaces of the local "space" ( $K_\Omega^{+,-}$ ) and "time" ( $K_I$ ) faces respectively (see section 4.3 for more details). This decomposition is of particular interest since  $M_\Omega$  is block-diagonal. Indeed, we have:

$$\Delta_\Omega M_\Omega + \Delta_I M_I = \left( \Delta_\Omega M_\Omega \right) \left( \mathbf{I} + \frac{\Delta_I}{\Delta_\Omega} M_\Omega^{-1} M_I \right) = \left( \Delta_\Omega M_\Omega \right) \left( \mathbf{I} + \kappa P \right),$$

Here  $\mathbf{I}$  is the identity matrix,  $\kappa \equiv \frac{\Delta_\Omega}{\Delta_I} \propto \frac{\Delta t}{\Delta x}$ , and  $P \equiv M_\Omega^{-1} M_I$ .

If  $\|\kappa P\|$  is sufficiently small, we can apply the Maclaurin formula in order to obtain the polynomial expansion for  $M^{-1}$  as follows:

$$M^{-1} \equiv (\mathbf{I} + \kappa P)^{-1} (\Delta_{\Omega} M_{\Omega})^{-1} = \left( \sum_{n=0}^{\infty} (-1)^n \kappa^n P^n \right) (\Delta_{\Omega} M_{\Omega})^{-1}.$$

This representation reduces the inversion of the sparse matrix  $M$  to the inversion of its block-diagonal component  $M_{\Omega}^{-1}$  and the multiplication of the inverted block-diagonal "space" matrix  $M_{\Omega}$  by the sparse "time" matrix  $M_I$ .

We now detail step by step the algorithm for constructing the approximate inverse of  $M$ . At first, we compute the diagonal blocks  $M_{\Omega}^K$  and  $M_I^K$  of the matrices  $M_{\Omega}$  and  $M_I$  respectively, which corresponds to the local integration at the faces of the element  $K$ , taking into account the outgoing internal numerical fluxes. Then we compute the extra-diagonal blocks  $M_I^{KL}$  of the matrix  $M_I$ , that correspond to the integration at local element faces  $K$ , taking into account the fluxes between the element  $K$  and its  $N_{KL}$  neighbors  $L$ .

```

for  $K = 1 : N_K$  do
  Compute:
  4.1  $M_{\Omega}^K$ 
  4.2  $M_I^K$ 
  for  $L = 1 : N_{KL}$  do
    Compute:
    4.3  $M_I^{KL}$ 
  end
end

```

Then, we proceed to the numerical inversion of  $M_{\Omega}^K$  block by block, and to the computing of the products  $(M_{\Omega}^K)^{-1} M_I^K$  and  $(M_{\Omega}^K)^{-1} M_I^{KL}$ .

```

for  $K = 1 : N_K$  do
  Compute:
  5.1  $invM_{\Omega}^K = (M_{\Omega}^K)^{-1}$ 
  5.2  $invM_{\Omega I}^K = (M_{\Omega}^K)^{-1} M_I^K$ 
  for  $L = 1 : N_{KL}$  do
    Compute:
    5.3  $invM_{\Omega I}^{KL} = (M_{\Omega}^K)^{-1} M_I^{KL}$ 
  end
end

```

Once we have computed all the necessary terms, we can explicitly update block by block the initial solution  $U_0^K$  at time  $t$ . We describe the number of auxiliary intermediate stages, corresponding to the number of the Taylor expansion terms, as follows:

```

% 0 :  $U_{aux0} = M_{\Omega}^{-1} U_0$ 
for  $K = 1 : N_K$  do
  Compute:
  5.4  $U_{aux0}^K = invM_{\Omega}^K U_0^K$ 
end

% 1 :  $U_{aux1} = U_{aux0} - (M_{\Omega}^{-1} M_I) U_{aux0}$ 
for  $K = 1 : N_K$  do
  Compute:
  5.5  $U_{aux1}^K = invM_{\Omega}^K U_{aux0}^K - invM_{\Omega I}^K invM_{\Omega}^K U_{aux0}^K$ 
  for  $L = 1 : N_{KL}$  do
    Compute:
    5.6  $U_{aux1}^K = U_{aux1}^K - invM_{\Omega I}^{KL} U_{aux0}^L$ 
  end
end

% 2 :  $U_{aux2} = U_{aux0} - (M_{\Omega}^{-1} M_I) U_{aux0} + (M_{\Omega}^{-1} M_I)^2 U_{aux0} = U_{aux0} - (M_{\Omega}^{-1} M_I) U_{aux1}$ 
for  $K = 1 : N_K$  do
  Compute:
  5.7  $U_{aux2}^K = invM_{\Omega}^K U_{aux0}^K - invM_{\Omega I}^K U_{aux1}^K$ 
  for  $L = 1 : N_{KL}$  do
    Compute:
    5.8  $U_{aux2}^K = U_{aux2}^K - invM_{\Omega I}^{KL} U_{aux1}^L$ 
  end
end

```

and so on. Furthermore, after the second stage we can reuse the allocated arrays for the auxiliary variables  $U_{aux1}$  and  $U_{aux2}$ , increasing the number of Taylor expansion terms for achieving the necessary accuracy level. The last auxiliary solution is considered as the updated solution at time  $t + \Delta t$

The proposed approach provides an explicit way for solving the initial linear system approximately. Even though it requires a CFL - type condition, justifying the approximate solution of the system, it significantly accelerates the algorithm execution.

In table 4.1 we compare the numerical accuracy of the Trefftz-DG method in a 2D homogeneous acoustic case for both the exact and approximate matrix inversions as a function of the mesh size and of the number  $n$  of terms in the Taylor expansion. We use the space-time polynomial basis of degree  $p=3$  for approximation. We can see that, by choosing  $n = 5$  in the approximate algorithm, we achieve the same accuracy as in the exact inversion case, while the maximal time of run is reduced by a factor 18.

The approximate inversion ( $\kappa = 10^{-2}$ ).

$n$	$\Delta x = 10^{-2}$	$\Delta x = 2 \cdot 10^{-2}$	$\Delta x = 5 \cdot 10^{-2}$	$\Delta x = 10^{-1}$
3	1.4166e-05	4.3741e-05	2.8780e-04	2.5772e-03
4	3.1623e-07	1.2656e-06	5.3868e-05	1.2674e-03
<b>5</b>	<b>2.8903e-07</b>	<b>9.1744e-07</b>	<b>4.1029e-05</b>	<b>1.3010e-03</b>
CPU time	$2.59 \cdot 10^2$	$1.14 \cdot 10^2$	$0.39 \cdot 10^2$	$0.16 \cdot 10^2$

The exact inversion ( $\kappa = 10^{-2}$ ).

$n$	$\Delta x = 10^{-2}$	$\Delta x = 2 \cdot 10^{-2}$	$\Delta x = 5 \cdot 10^{-2}$	$\Delta x = 10^{-1}$
.	<b>2.2540e-07</b>	<b>8.9583e-07</b>	<b>5.5811e-05</b>	<b>1.3004e-03</b>
CPU time	$4.75 \cdot 10^3$	$2.02 \cdot 10^3$	$5.51 \cdot 10^2$	$1.97 \cdot 10^2$

TABLE 4.1: Numerical accuracy regarding the inversion process.

## 4.5 Change-over between the time slabs

As it was discussed in section 4.1, once we have obtained the vector  $U$  of the coefficients of the intermediate numerical solution at time  $t_j = j\Delta t$  of the time slab  $[t_{j-1}, t_j]$  (step 6), we must update the initial data  $U_0$  in order to perform the computation in the next time slab  $[t_j, t_{j+1}]$ . Basically, it consists in building the intermediate numerical solutions  $V$  and  $P$  (steps 7-8) at time  $t_j$  as follows:

$$V = \sum_{i=1}^{N_{dof}} U_i \phi_i^v(\cdot, t_j), \quad P = \sum_{i=1}^{N_{dof}} U_i \phi_i^p(\cdot, t_j),$$

then, in computing the  $L^2$ -projections  $V_{aux0}$  and  $P_{aux0}$  of the intermediate solutions  $V$  and  $P$  respectively (steps 9-10) as follows:

$$V_{aux0} = \int_{\partial K} \sum_{k=1}^{N_{dof}} V \phi_k^v(\cdot, t_j) d\mathbf{x}, \quad P_{aux0} = \int_{\partial K} \sum_{k=1}^{N_{dof}} P \phi_k^p(\cdot, t_j) d\mathbf{x},$$

and then, in updating the right-hand side  $U_0 = 1/2(V_{aux0} + P_{aux0})$  (step 11).

By the linearity of the integrals, we can combine all the above steps into one as follows:

$$\begin{aligned} U_0^K &= \frac{1}{2}(V_{aux0}^K + P_{aux0}^K) = \frac{1}{2} \int_{\partial K} \sum_{k=1}^{N_{dof}} V^K \phi_k^v(\cdot, t_j) d\mathbf{x} + \int_{\partial K} \sum_{k=1}^{N_{dof}} P^K \phi_k^p(\cdot, t_j) d\mathbf{x} = \\ &= \frac{1}{2} \left( \int_{\partial K} \sum_{k=1}^{N_{dof}} \left[ \sum_{i=1}^{N_{dof}} U_i^K \phi_i^v(\cdot, t_j) \right] \phi_k^v(\cdot, t_j) d\mathbf{x} + \int_{\partial K} \sum_{k=1}^{N_{dof}} \left[ \sum_{i=1}^{N_{dof}} U_i^K \phi_i^p(\cdot, t_j) \right] \phi_k^p(\cdot, t_j) d\mathbf{x} \right) = \\ &= \frac{1}{2} \left( \int_{\partial K} \sum_{i,k=1}^{N_{dof}} U_i^K \left( \phi_i^v(\cdot, t_j) \phi_k^v(\cdot, t_j) + \phi_i^p(\cdot, t_j) \phi_k^p(\cdot, t_j) \right) d\mathbf{x} \right) = \frac{1}{2} (U^K)^T M_0^K, \end{aligned}$$

where

$$[M_0^K]_{i,k}(\cdot, t) = \int_{\partial K} \phi_i^v(\cdot, t_j) \phi_k^v(\cdot, t_j) + \phi_i^p(\cdot, t_j) \phi_k^p(\cdot, t_j) d\mathbf{x}. \quad (4.1)$$

It means that the procedures  $t_{snap}$  and  $L_{proj}^2$  (steps 7 - 10 of the initial algorithm) can be replaced by  $M_0 U$ , where  $M_0$  is the block-diagonal matrix whose blocks are defined by (4.1), and  $U$  is the vector of coefficients defining the intermediate numerical solution.

Furthermore, we can include this step into the explicit procedure of matrix inversion as follows:

```

for  $K = 1 : N_K$  do
  Compute:
  4.1  $M_\Omega^K$ 
  4.2  $M_I^K$ 
  4.3  $0.5M_0^K$ 
  4.4  $invM_\Omega^K = (M_\Omega^K)^{-1}$ 
  4.5  $invM_{\Omega I}^K = (M_\Omega^K)^{-1}M_I^K$ 
  4.6  $invM_{\Omega 0}^K = 0.5invM_\Omega^K M_0^K$ 
  for  $L = 1 : N_{KL}$  do
    Compute:
    4.7  $invM_{\Omega I}^{KL} = (M_\Omega^K)^{-1}M_I^{KL}$ 
  end
end

% 0 :  $U_{aux0} = 0.5(M_\Omega^{-1}M_0)U_0$ 

for  $K = 1 : N_K$  do
  Compute:
  5.1  $U_{aux0}^K = invM_{\Omega 0}^K U_0^K$ 
end

% 1 :  $U_{aux1} = U_{aux0} - (M_\Omega^{-1}M_I)U_{aux0}$ 

for  $K = 1 : N_K$  do
  Compute:
  5.2  $U_{aux1}^K = invM_{\Omega 0}^K U_{aux0}^K - invM_{\Omega I}^K U_{aux0}^K$ 
  for  $L = 1 : N_{KL}$  do
    Compute:
    5.3  $U_{aux1}^K = U_{aux1}^K - invM_{\Omega I}^{KL} U_{aux0}^L$ 
  end
end

```

```

% 2 :  $U_{aux2} = U_{aux0} - (M_{\Omega}^{-1}M_I)U_{aux0} + (M_{\Omega}^{-1}M_I)^2 U_{aux0} = U_{aux0} - (M_{\Omega}^{-1}M_I)U_{aux1}$ 
for  $K = 1 : N_K$  do
  Compute:
  5.4  $U_{aux2}^K = invM_{\Omega 0}^K U_{aux0}^K - invM_{\Omega I}^K U_{aux1}^K$ 
  for  $L = 1 : N_{KL}$  do
    Compute:
    5.5  $U_{aux2}^K = U_{aux2}^K - invM_{\Omega I}^{KL} U_{aux1}^L$ 
  end
end
end

```

We introduce also the function  $L_{coeff}^2$ , which computes the coefficients of the decomposition of the initial data  $^{1/2}(V_0 + P_0)$  in the basis  $(\phi^v, \phi^p)$ :

$$L_{coeff}^2(V_0, P_0, \phi^v, \phi^p) = \frac{1}{2} \left( L_{proj}^2(V_0, \phi^v) + L_{proj}^2(P_0, \phi^p) \right) M_0^{-1}. \quad (4.2)$$

Thus, the global algorithm reduces to the following one:

```

Data:  $V_0, P_0$  % initial velocity and pressure fields
          $c, \rho, \Omega, I$  % domain parameters
          $\Delta x, \Delta t, N_x, N_t, N_{dof}$  % mesh and DG parameters
Result:  $V_T, P_T$  % final velocity and pressure fields
Initiate:
0  $\phi^v, \phi^p$  % initiation of the polynomial basis
Compute:
1  $U_0 = L_{coeff}^2(V_0, P_0, \phi^v, \phi^p)$  % the initial condition vector (second member)
4  $M_{\Omega}, M_I, M_0,$  % computing the components of matrix  $M$ 
    $invM_{\Omega}, invM_{\Omega I}, invM_{\Omega 0}$ 
for  $j = 1 : N_t$  do
  Compute:
  5  $U = invM U_0$  % vector of the coefficients for approximate
                    % solution in the time slab  $[(j-1)\Delta t, j\Delta t]$ 
  11  $U_0 = U$  % update of the right-hand side
end
Compute:
12  $V_T = t_{snap}(U, \phi^v, t_{N_t})$  % final approximate solutions for velocity and
13  $P_T = t_{snap}(U, \phi^p, t_{N_t})$  % pressure fields at  $t_{N_t} = N_t \Delta t$ 

```

where  $L_{coeff}^2$  is a function, that computes the coefficients of decomposition of the initial data  $0.5(V_0 + P_0)$  in basis  $(\phi^v, \phi^p)$ .

## 4.6 Conclusion

We have developed an algorithm for solving the Trefftz-DG formulation described in the previous chapter, and we have detailed the most important points for its implementation

on the example of an acoustic model with mesh composed of parallel in time slabs.

We have proposed some analytical approaches for reducing the numerical cost and optimizing the memory resources defined as the optimization of the change-over between the time slabs, and the approximate inversion of the global sparse matrix. The approximative was validated by comparison with exact inversion, showing better numerical performance.

The next step is the development of the code and validation of the algorithm numerically. In chapter 5 we propose some numerical tests for 1D+time and 2D+time acoustic, elastodynamic and elasto-acoustic models. We compare the numerical solutions to analytical ones, and develop a numerical convergence analysis.

## Chapter 5

# Numerical results

This chapter contains numerical results obtained when solving the 1D+time and 2D+time wave equations previously introduced in chapter 3. We have started by developing a prototype *MATLAB*® code using the algorithm based on the exact inversion of the global matrix, to provide some numerical tests quickly and understand how the method could work for larger problems. The validation of the numerical experiments has been done thanks to the code *Gar6more2D* [1] which has been developed by Magique-3D. *Ga6more2D* computes analytical solutions in various bi-layered media including the elasto-acoustic case. It employs the method of Cagniard - de Hoop [36].

In this chapter, we deliver a series of numerical experiments in the case of an elasto-acoustic domain. In each case, we study the impact of the penalty terms on the accuracy of the solution. It turns out that the convergence curves demonstrate a property of superconvergence in 1D+time tests.

We have also implemented the method based on the approximate inversion of the global matrix into the HPC software *Elasticus*. The implementation has been validated with some comparisons with analytical solutions provided by *Gar6more2D*. We illustrate this with the 2D acoustic example at the end of this chapter.



# Contents

5.1	1D Acoustic simulations . . . . .	77
5.1.1	Homogeneous medium with periodical boundary conditions . . . . .	77
5.1.2	Heterogeneous medium with "free-surface" boundary conditions . . . . .	80
5.2	2D Simulations . . . . .	80
5.2.1	2D Acoustics . . . . .	81
5.2.1.1	Homogeneous acoustic medium. Initial conditions . . . . .	81
5.2.1.2	Homogeneous acoustic medium. Source term . . . . .	83
5.2.2	2D Elastodynamics . . . . .	84
5.2.2.1	Homogeneous elastic medium. Initial conditions . . . . .	85
5.2.2.2	Homogeneous elastic medium. Source term . . . . .	88
5.2.3	2D Elasto-acoustics . . . . .	91
5.3	Fortran 2D simulations . . . . .	92
5.3.1	2D Acoustic simulation . . . . .	94
5.4	Conclusion . . . . .	94



## 5.1 1D Acoustic simulations

In this section we provide some numerical tests for 1D+time homogeneous and heterogeneous acoustic modelings with periodic and free-surface boundary conditions, computed with the method based on the exact inversion of the global matrix. We assess the numerical accuracy of the method with respect to the choice of penalty parameters, and we compare convergence curves for different degrees of approximation.

Here and in the remainder of the thesis, all the parameters are dimensionless.

### 5.1.1 Homogeneous medium with periodical boundary conditions

We start with an example of wave propagation, induced by initial velocity and pressure, in the absence of external forces. The global space  $Q_F$  is represented by the acoustic domain  $\Omega_F = [0, 1]$  and the time interval  $I = [0, 1]$ . Periodical boundary conditions are imposed at the boundaries. We consider a uniform rectangular mesh with  $\Delta t = \Delta x = 0.01$ . We set the media parameters  $\rho_F = c_F = 1$ . The space-time approximation degree is  $p=3$ . As initial conditions, we consider two periodic functions: the "sine" function:  $v_{F0} = \sin(2\pi x)$  and  $p_0 = -c_F v_{F0}$ , and the "hat" function:  $v_{F0}(x) = 0$ ,  $x \in [0, 1/3) \cup [2/3, 1]$ ,  $v_{F0}(x) = x - 1/3$ ,  $x \in [1/3, 1/2)$ ,  $v_{F0}(x) = -x + 2/3$ ,  $x \in [1/2, 2/3)$  and  $p_0 = -c_F v_{F0}$ .

Figures 5.1 - 5.3 show the propagation of the velocity  $v_F$  for initial "sine" (figure 5.1) and "hat" (figures 5.2 - 5.3) conditions, with different values of the penalty parameters  $\alpha_1$  and  $\beta_1$ . Figures 5.1 - 5.3 (a) correspond to the propagation in time of the numerical velocity. Figures 5.1 - 5.3 (b) compare the numerical and exact velocities at the final time  $t = 1$ .

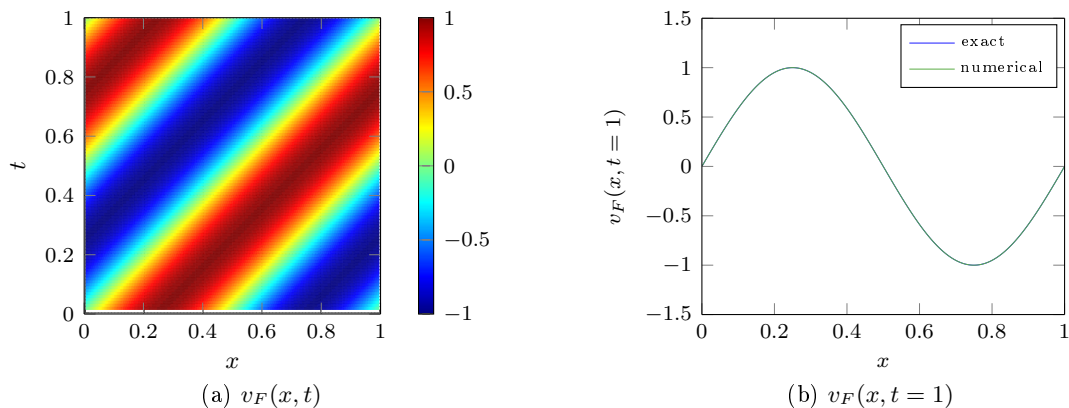


FIGURE 5.1: Propagation of the exact and numerical velocities  $v_F(x, t)$  in a homogeneous 1D fluid domain ( $\alpha_1 = \beta_1 = 0$ ).

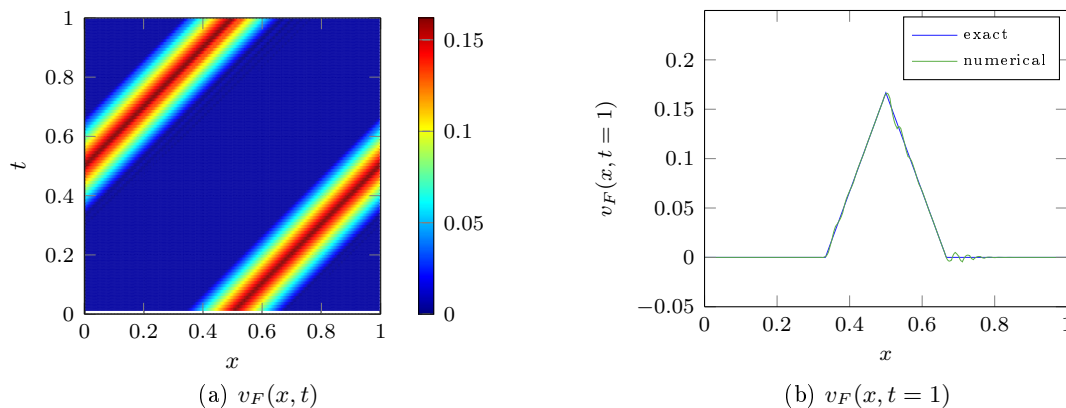


FIGURE 5.2: Propagation of the exact and numerical velocities  $v_F(x, t)$  in a homogeneous 1D fluid domain ( $\alpha_1 = \beta_1 = 0$ ).

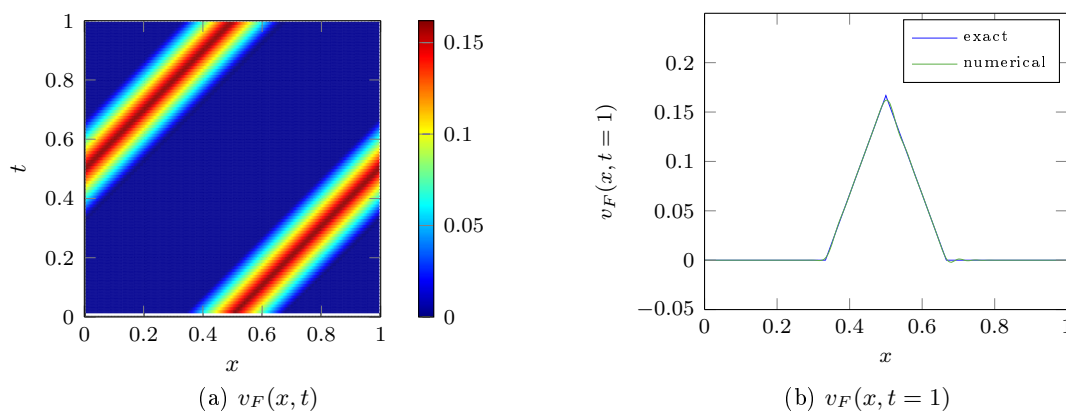


FIGURE 5.3: Propagation of the exact and numerical velocities  $v_F(x, t)$  in a homogeneous 1D fluid domain ( $\alpha_1 = \beta_1 = 0.5$ ).

We can observe that in the "sine" test case, where the initial wave is regular enough, the approximation works well even with zero penalty parameters ( $\alpha_1 = \beta_1 = 0$ ) (figure 5.1).

However, if we choose a less regular initial condition ("hat" case), the numerical solution with zero penalty becomes less stable at the end of propagation (figure 5.2), compared to the case with  $\alpha_1 = \beta_1 = 0.5$  (figure 5.3).

We have studied the dependency of the numerical accuracy on the mesh size and penalty coefficients. For this, we have fixed four different values of  $\Delta x$  from 0.006 to 0.03, and for each  $\Delta x$ , we have varied the value of  $\Delta t$ . In figure 5.4, we represent the numerical accuracy as a function of ratio  $\Delta t/\Delta x$  for four different values of  $\Delta x$ . We can observe that in all the four cases, the minimum of the numerical error for velocity  $v_F$  corresponds to the ratio  $\Delta t/\Delta x = 1/(1 + \alpha_1)$ .

Figure 5.5 shows the results of convergence of the velocity for zero (a) and non-zero (b)

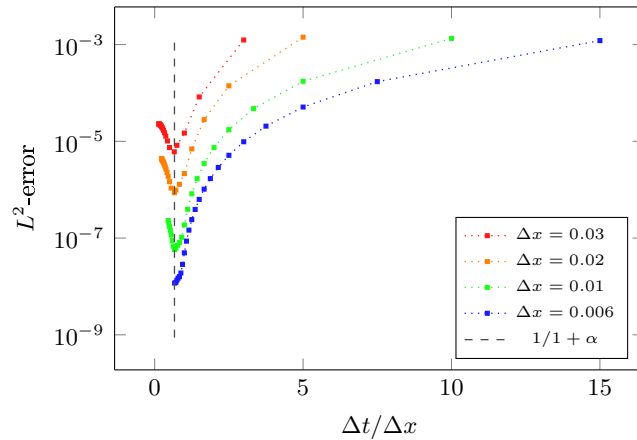


FIGURE 5.4: Numerical accuracy as a function of  $\Delta t/\Delta x$  in a homogeneous 1D fluid domain.

penalty parameters. The convergence curves have been computed for different approximation degrees  $p=0, 1, 2, 3$ , and they depict the  $L^2$ -norm in time and space of numerical error as a function of cell size  $\Delta x = \Delta t$ .

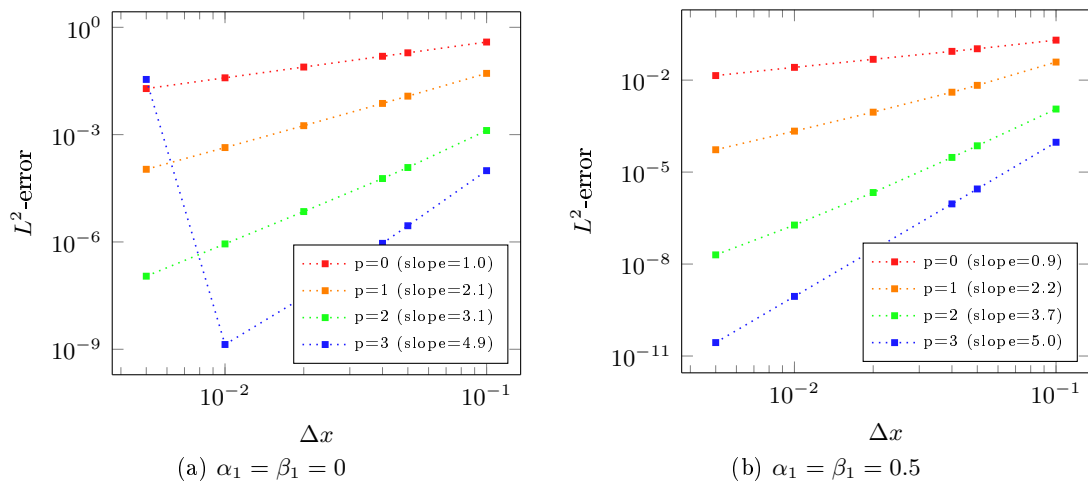


FIGURE 5.5: Convergence of numerical velocity  $v_F$  as a function of cell size  $\Delta x = \Delta t$  in a homogeneous 1D fluid domain.

We can see that the convergence rate is of order  $p+1$  or higher, which is conform to the theoretical estimates of [82]. In figure 5.5 (a), the numerical solution diverges when  $p=3$  and  $\Delta x = \Delta t$  is very small. The convergence can be achieved by adding penalty terms ( $\alpha_1 = \beta_1 = 0.5$ ) into the scheme (see figure 5.5 (b)).

As formerly seen in chapter 3.1.4, the stability of the variational formulation does not depend on the penalty terms from the theoretical point of view. However, the numerical tests show that a non-zero penalization improves the convergence rate. The question of an optimal choice of penalty parameters is still open.

### 5.1.2 Heterogeneous medium with "free-surface" boundary conditions

We consider a bi-layered acoustic domain  $\Omega_F = [0, 0.6) \cup [0.6, 1]$ , and a time interval  $I = [0, 1]$ . We set the following medium and mesh parameters:  $\Delta x_1 = 0.01$ ,  $\Delta t_1 = 0.01$ ,  $c_{F1} = 1$ ,  $\Delta x_2 = 0.02$ ,  $\Delta t_2 = 0.01$ ,  $c_{F2} = 2$ . The space-time approximation degree is  $p=3$ . To generate the propagation phenomenon, we choose a Gaussian function as the initial condition for velocity  $v_{F0}(x) = \exp(-40\pi^2(x - 0.2)^2)$  and pressure  $p_0(x) = -c_F v_{F0}$ . The "free-surface" boundary conditions are imposed in this model.

Figure 5.6 (a) shows the propagation of the numerical velocity in bi-layered medium, while figure 5.6 (b) represents the numerical solution at time  $t = 0.45$ .

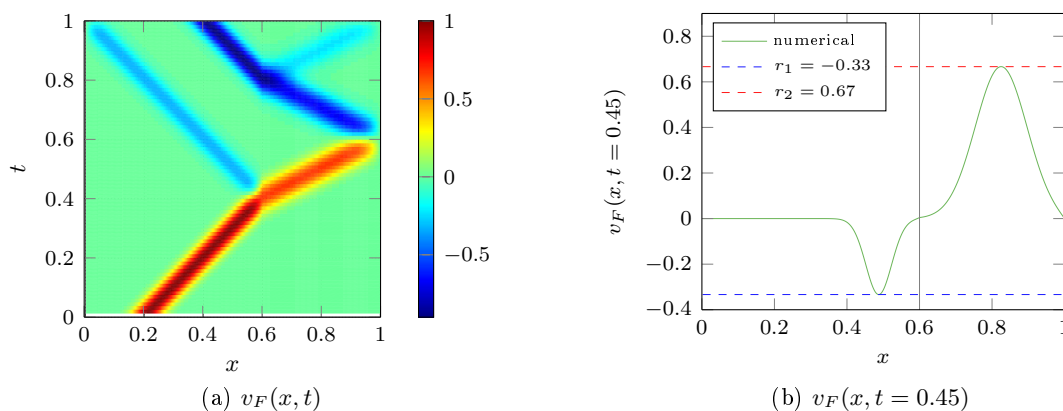


FIGURE 5.6: Propagation of the numerical velocity  $v_F(x, t)$  in a heterogeneous 1D fluid domain ( $\alpha_1 = \beta_1 = 0.5$ ).

The propagation of the numerical solution through the interface between the two layers fits well to the physics of the model, based on the values of the reflection coefficients  $r_1$  and  $r_2$ . They can be analytically computed using the medium parameters as follows:  $r_1 = (c_{F1} - c_{F2})(c_{F1} + c_{F2})^{-1} = -0.33$  and  $r_2 = 2c_{F1}(c_{F1} + c_{F2})^{-1} = 0.67$ . We can observe in figure 5.6 (b) that the amplitude of the incident and reflected waves are bounded by the values of  $r_1$  (blue dashed line) and  $r_2$  (red dashed line) respectively, thus validating the propagation of the numerical solution.

## 5.2 2D Simulations

In this section, we present results obtained when applying the Trefftz-DG algorithm to the 2D acoustic, elastic, and elasto-acoustic problems. The code we use at first is a prototype MATLAB® version. It is based on the exact inversion of the global matrix, thus, technically speaking, it is quite limited. This version has been created in order to investigate the method and its algorithm in general, and to perform some basic numerical tests for its validation.

We choose the penalty parameters  $\alpha_1 = \beta_1 = 0.5$  for 2D acoustic tests, and  $\delta_1 = \gamma_1 = 0.5$  for 2D elastodynamic tests (full upwind fluxes).

### 5.2.1 2D Acoustics

In this section, we test the Trefftz-DG formulation applied to the 2D+time acoustic model. We validate the numerical results by comparison with analytical solutions, and we analyze the convergence of the numerical solution for different degrees of approximation.

#### 5.2.1.1 Homogeneous acoustic medium. Initial conditions

We consider a 2D homogeneous acoustic medium  $\Omega_F \equiv [0, 1] \times [0, 1]$  with periodic boundary conditions and the time interval  $I \equiv [0, 1]$ . We set the medium parameters  $c_F = 1$ ,  $\rho_F = 1$  in  $\Omega_F \times I$ . We consider the uniform rectangular mesh with parameters

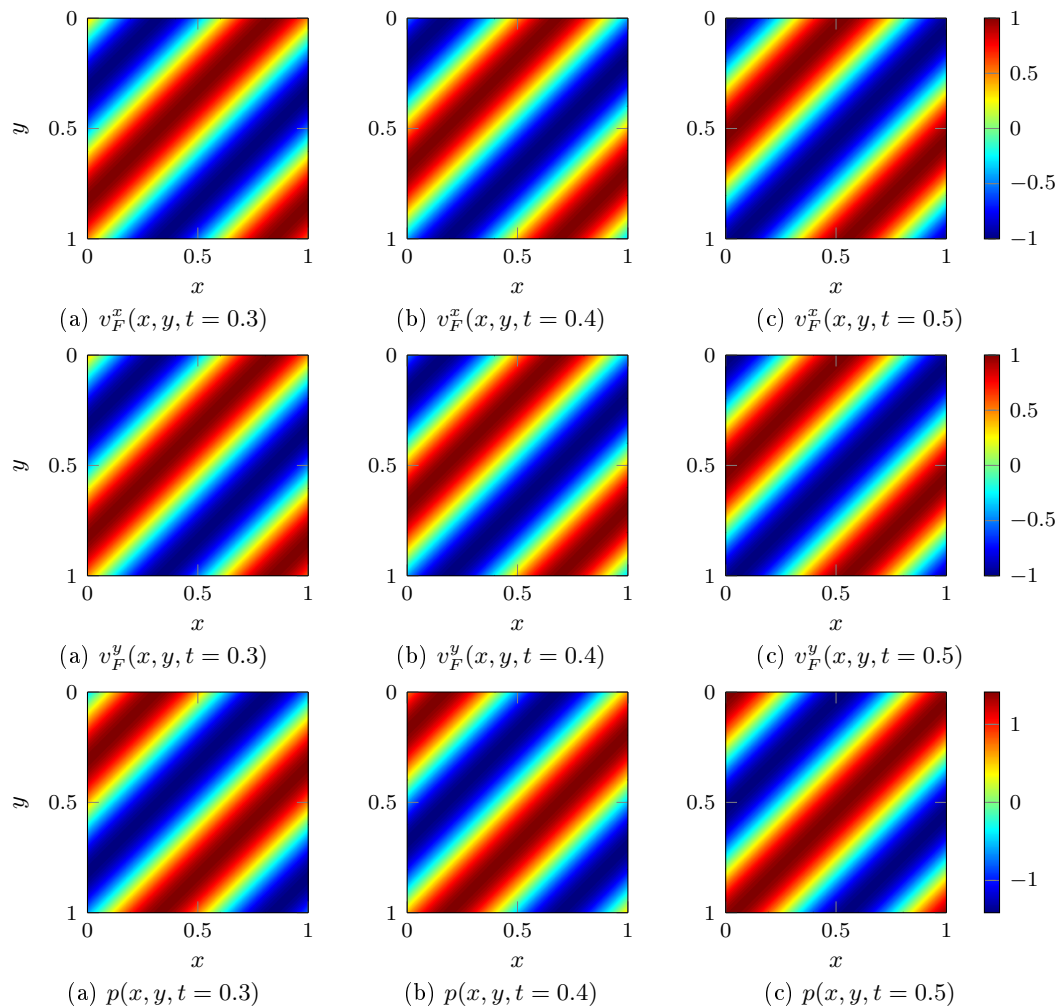


FIGURE 5.7: Propagation of the numerical velocity  $\mathbf{v}_F \equiv (v_F^x, v_F^y)$  and pressure  $p$  in a homogeneous 2D fluid domain at time  $t = 0.3, 0.4, 0.5$ .

$\Delta t = 0.01$ ,  $\Delta x = \Delta y = 0.02$ . The space-time approximation degree is  $p=2$ . We choose  $v_{F0}^x(x, y) = v_{F0}^y(x, y) = \sin(2\pi(x + y))$  and  $p_0(x, y) = -\sqrt{2}c_F \sin(2\pi(x + y))$  as the initial data. Figure 5.7 depicts the propagation of the components  $v_F^x, v_F^y$  of the numerical velocity  $\mathbf{v}_F \equiv (v_F^x, v_F^y)$ , and pressure  $p$ .

We have computed the exact solutions to validate the numerical ones. In figure 5.8 we show the snapshots for the components  $v_F^x, v_F^y$  of the exact and numerical velocities and pressure  $p$  taken at time  $t = 0.3$  (a),  $t = 0.5$  (b) when  $y = 0.5$  is fixed. We can see that the exact solutions are well-approximated by the numerical solutions in all the test examples.

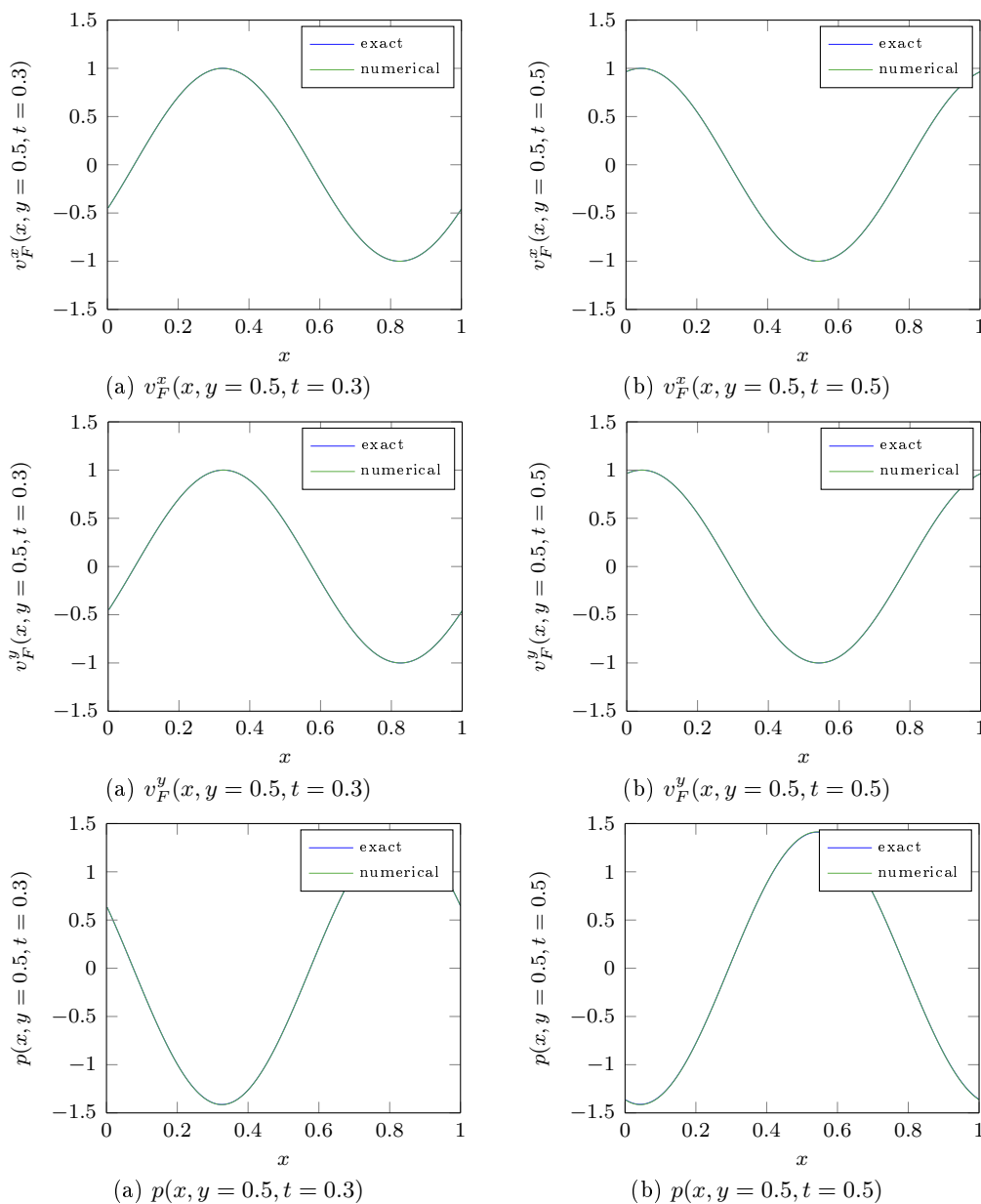


FIGURE 5.8: The exact and numerical velocities  $\mathbf{v}_F \equiv (v_F^x, v_F^y)$  and pressure  $p$  in a homogeneous 2D fluid domain.

### 5.2.1.2 Homogeneous acoustic medium. Source term

We consider a 2D homogeneous acoustic medium  $\Omega_F \equiv [0, 1] \times [0, 1]$  with "free-surface" boundary conditions and a time interval  $I \equiv [0, 1]$ . We retain the medium and mesh parameters from the previous test. The space-time approximation degree is  $p=2$ . The source term at the point  $(0.5, 0.5)$  is represented by the function  $f(t) = -50\pi^2(t - 0.2) \cdot \exp(-25\pi^2(t - 0.2)^2)$ .

Figure 5.9 depicts the propagation of the components  $v_F^x, v_F^y$  of numerical velocity  $\mathbf{v}_F \equiv (v_F^x, v_F^y)$ , and pressure  $p$ .

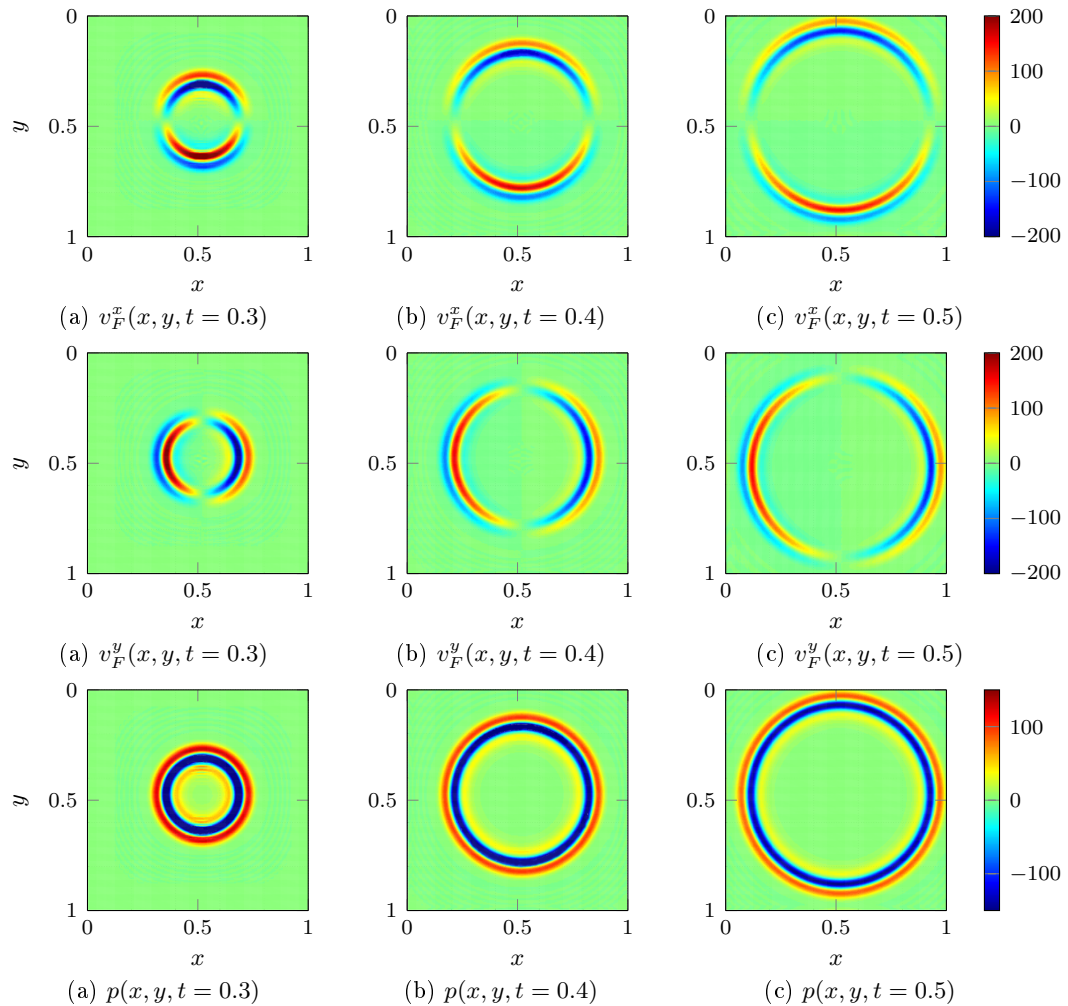


FIGURE 5.9: Propagation of the numerical velocity  $\mathbf{v}_F \equiv (v_F^x, v_F^y)$  and pressure  $p$  in a homogeneous 2D fluid domain at time  $t = 0.3, 0.4, 0.5$ .

The numerical seismograms have been computed at point  $(0.25, 0.25)$ . They have been validated by the analytical solutions, computed with *Gar6more2D* [1] (figure 5.10).

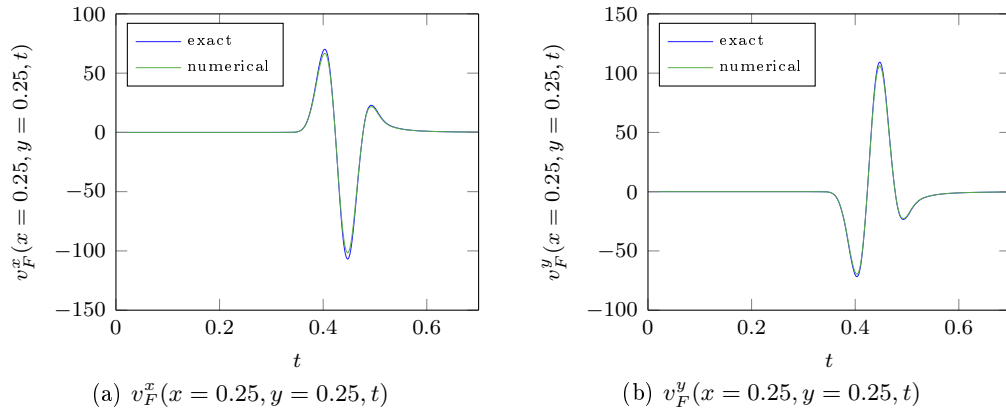


FIGURE 5.10: The seismograms for exact and numerical velocities  $\mathbf{v}_F \equiv (v_F^x, v_F^y)$  in a homogeneous 2D fluid domain.

Figure 5.11 shows the convergence curves computed for different degrees of approximation  $p=0, 1, 2, 3$ . They represent the  $L^2$ -norm in time and space of numerical error as a function of cell size  $\Delta x = \Delta y = \Delta t$ .

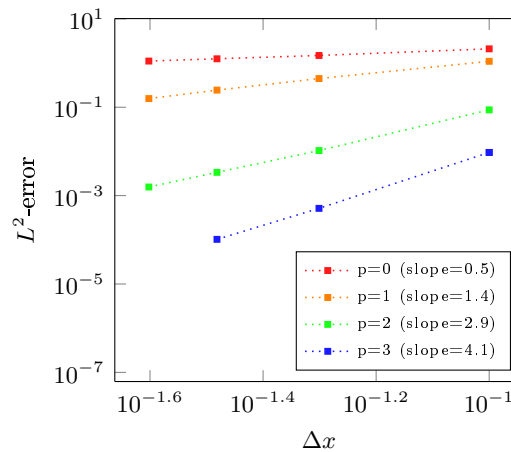


FIGURE 5.11: Convergence of the numerical velocity  $\mathbf{v}_F$  as a function of cell size  $\Delta x = \Delta y = \Delta t$ .

In all the cases, the convergence is at least of order  $p$ , and for  $p = 2, 3$ , we obtain the optimal order of convergence  $p+1$ , as predicted by [82], though we use a source point that does not satisfy all regularity requirements.

### 5.2.2 2D Elastodynamics

In this section, we implement numerically the Trefftz-DG formulation for the 2D elastodynamic problem developed in chapter 3.2. We consider two homogeneous examples of elastic domain with periodic (section 5.2.2.1) and "free-surface" (section 5.2.2.2) boundary conditions. The source term is imposed in the last case. We compare the numerical

and analytical solutions, and we provide convergence results for different degrees of approximation.

### 5.2.2.1 Homogeneous elastic medium. Initial conditions

We consider a 2D homogeneous elastic medium  $\Omega_S \equiv [0, 1] \times [0, 1]$  with periodic boundary conditions and a time interval  $I \equiv [0, 1]$ . The medium parameters  $\mu = 1$ ,  $\lambda = 1$ ,  $\rho_S = 1$ ,  $V_P = \sqrt{\frac{\lambda+2\mu}{\rho_S}} = \sqrt{3}$ ,  $V_S = \sqrt{\frac{\mu}{\rho_S}} = 1$  are set to be constant in  $\Omega_S \times I$ . We consider a uniform rectangular mesh with parameters  $\Delta t = 0.03$ ,  $\Delta x = \Delta y = 0.03$ . The degree of approximation in space and time is  $p=2$ . We perform two numerical simulations in order to test the propagation of  $P$ - and  $S$ -waves separately.

#### $P$ -wave propagation.

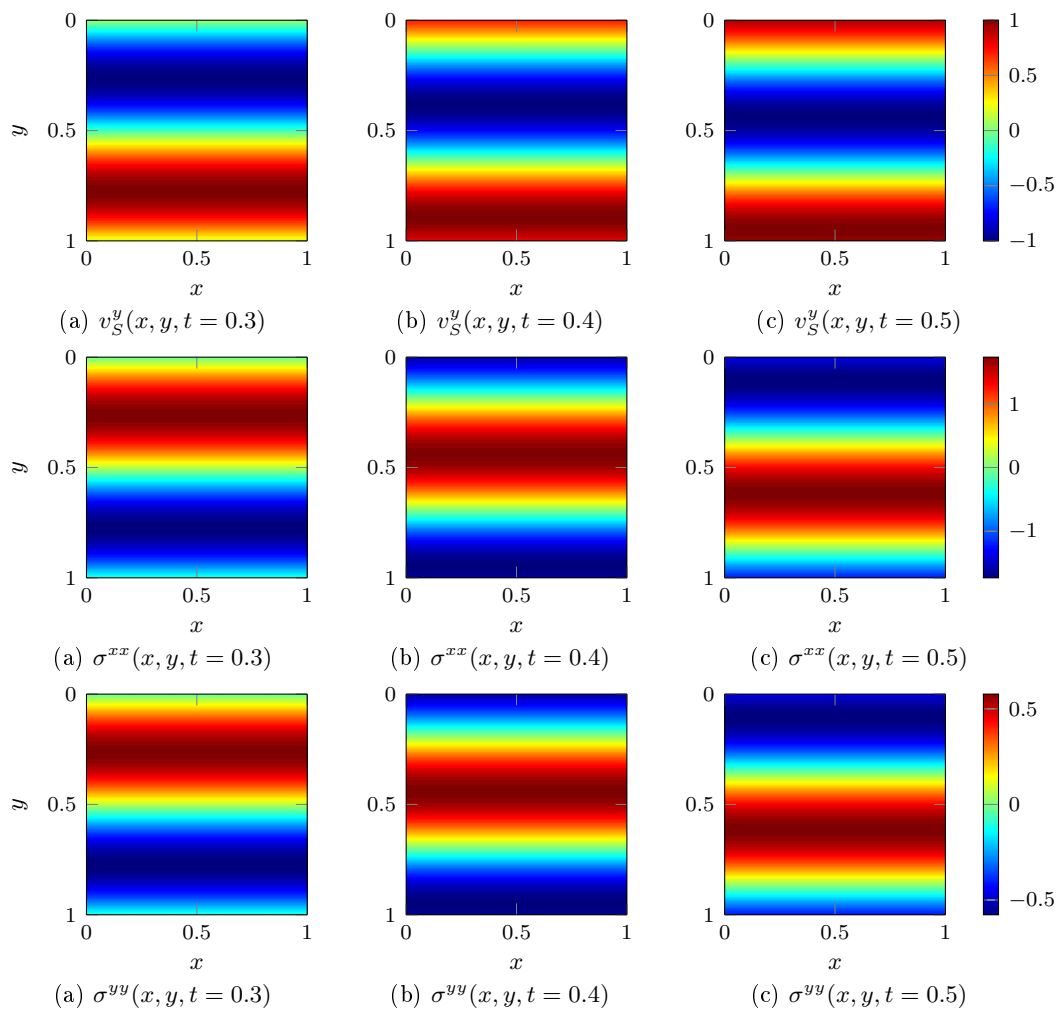


FIGURE 5.12: Propagation of the components  $v_S^y$  of velocity and  $\sigma^{xx}$ ,  $\sigma^{yy}$  of stress tensor in a homogeneous 2D solid domain at time  $t = 0.3, 0.4, 0.5$ .

We choose  $v_{S0}^y(x, y) = \sin(2\pi y)$ ,  $\sigma_0^{xx}(x, y) = -\sqrt{3}\sin(2\pi y)$ ,  $\sigma_0^{yy}(x, y) = -1/\sqrt{3}\sin(2\pi y)$  and  $v_{S0}^x(x, y) = \sigma_0^{xy}(x, y) = 0$  as initial data. In this case, we expect to observe the propagation in the  $y$ -direction of the components  $v_S^y$  and  $\sigma^{xx}$ ,  $\sigma^{yy}$ , with a speed given by  $V_P$ , while  $v_S^x$  and  $\sigma^{xy}$  remain inactive.

Figure 5.12 shows the propagation of the components  $v_S^y(x, y, t)$  of the numerical velocity and  $\sigma^{xx}(x, y, t)$ ,  $\sigma^{yy}(x, y, t)$  of the stress tensor at times  $t = 0.3$ ,  $t = 0.4$ ,  $t = 0.5$ . The pattern of the propagation perfectly corresponds to the physics of the initial model.

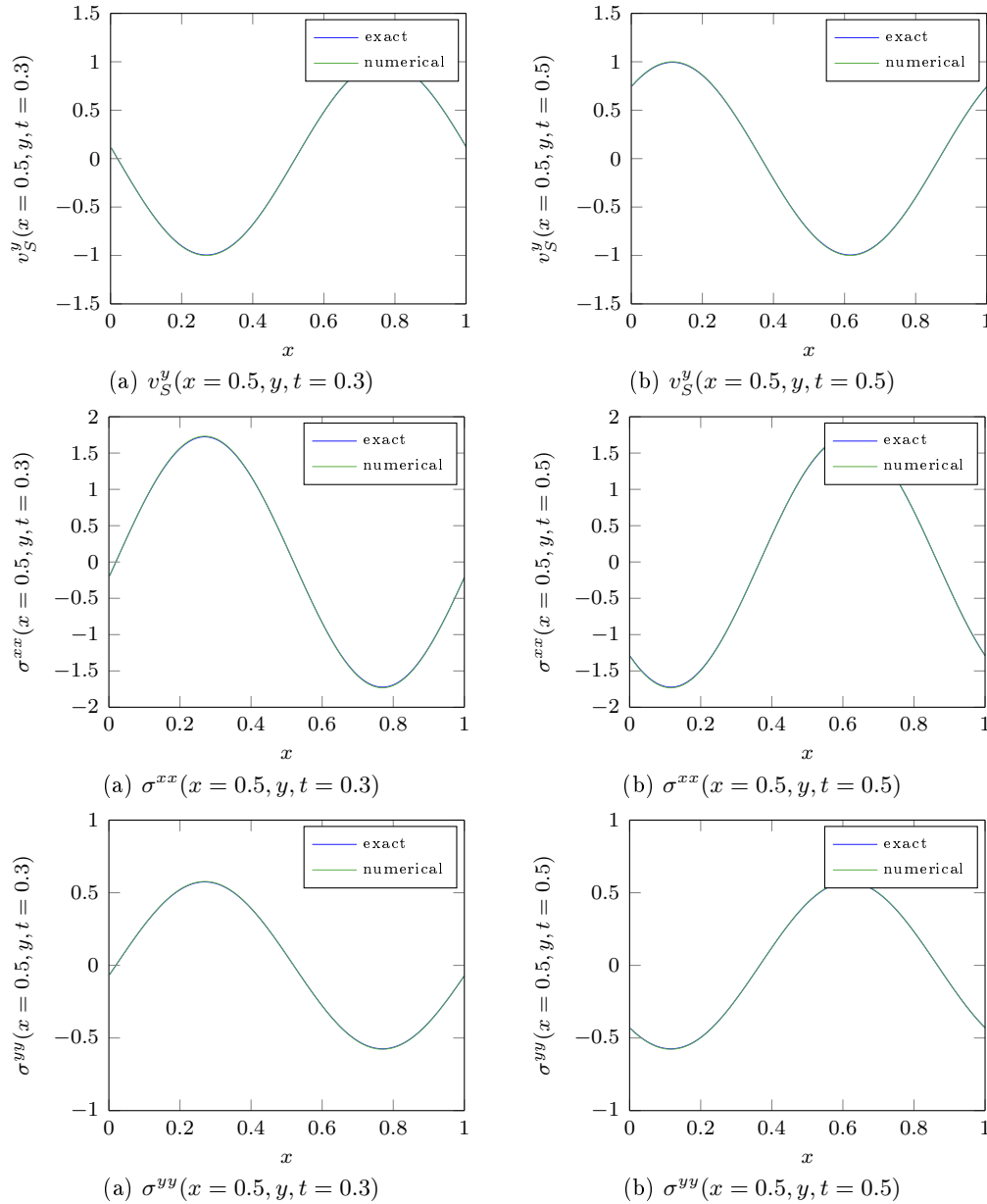


FIGURE 5.13: The exact and numerical components  $v_S^y$  of velocity and  $\sigma^{xx}$ ,  $\sigma^{yy}$  of stress tensor in a homogeneous 2D solid domain.

We have validated the computed numerical solutions by comparison with the exact solutions. Figure 5.13 represents the time snaps for the components  $v_S^y$  of the exact and

numerical velocities and  $\sigma^{xx}$ ,  $\sigma^{yy}$  of the exact and numerical stress tensor taken at time  $t = 0.3$ ,  $t = 0.5$  with a fixed  $x = 0.5$ . We can observe that the exact and approximate solutions match well.

### ***S*-wave propagation.**

To test the *S*-wave propagation, we consider the following initial velocity and stress tensor:  $v_{S0}^x(x, y) = \sin(2\pi y)$ ,  $\sigma_0^{xy}(x, y) = -\sin(2\pi y)$ , and  $v_{S0}^y(x, y) = \sigma_0^{xx}(x, y) = \sigma_0^{yy}(x, y) = 0$ .

The propagation of the components  $v_S^x(x, y, t)$  of the velocity and  $\sigma^{xy}(x, y, t)$  of the stress tensor at times  $t = 0.3$ ,  $t = 0.4$ ,  $t = 0.5$  is represented in figure 5.14. Compared to the previous *P*-wave case, we observe the propagation in the  $y$ -direction of the components  $v_S^x$  and  $\sigma^{xy}$  with the speed equal to  $V_S$ , while the others  $v_S^y$  and  $\sigma^{xx}$ ,  $\sigma^{yy}$  remain inactive.

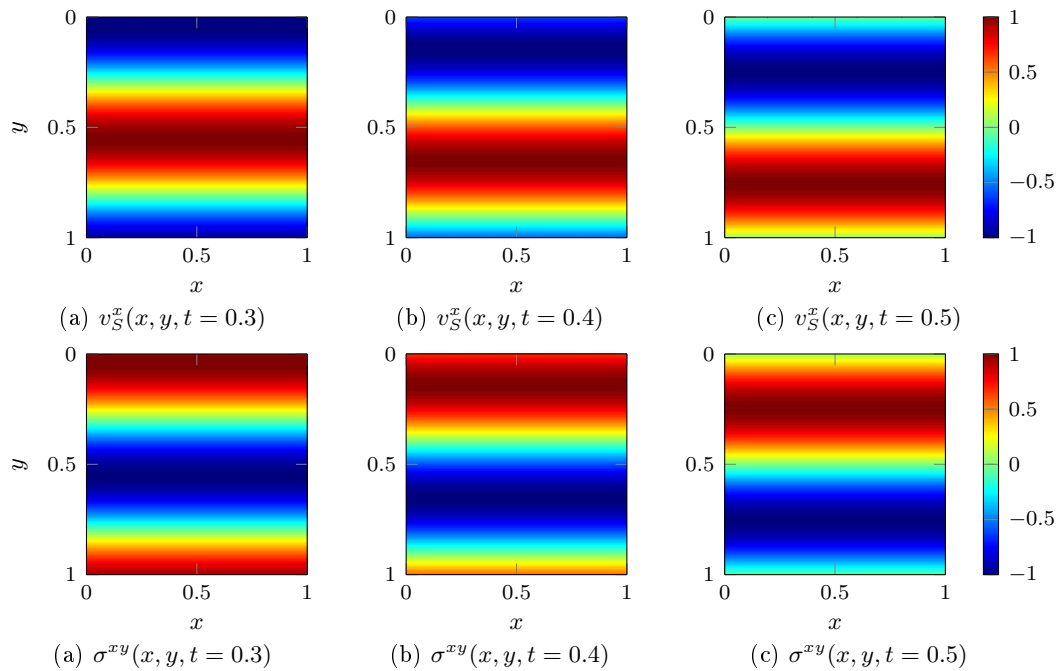


FIGURE 5.14: Propagation of the components  $v_S^x$  of velocity and  $\sigma^{xy}$  of stress tensor in a homogeneous 2D solid domain at time  $t = 0.3, 0.4, 0.5$ .

In figure 5.15, the exact and approximate solutions of the components  $v_S^y$  of the velocity, and  $\sigma^{xy}$  of the stress tensor taken at time  $t = 0.3$ ,  $t = 0.5$  ( $x = 0.5$  is fixed) are compared. Since both solutions match well, the numerical results are thus validated by the exact ones.

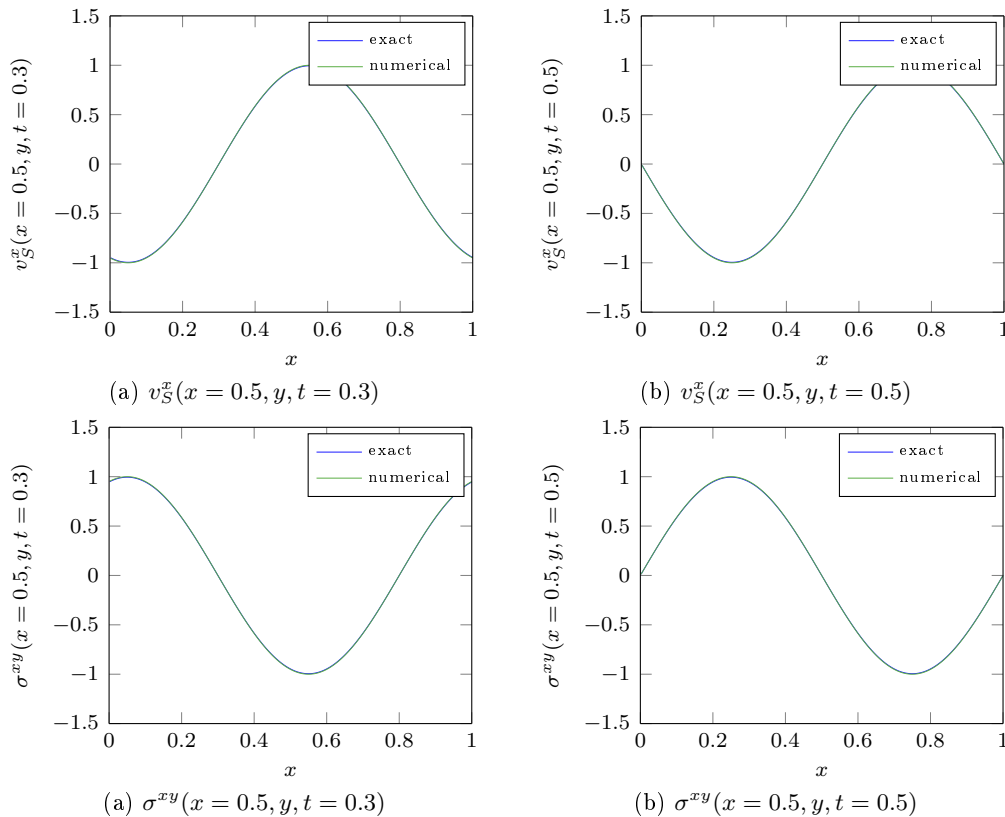


FIGURE 5.15: The exact and numerical components  $v_S^x$  of velocity and  $\sigma^{xy}$  of stress tensor in a homogeneous 2D solid domain.

### 5.2.2.2 Homogeneous elastic medium. Source term

We consider a 2D homogeneous elastic medium  $\Omega_S \equiv [0, 1] \times [0, 1]$  with "free-surface" boundary conditions and a time interval  $I \equiv [0, 1]$ . We set the medium parameters  $\mu = 1$ ,  $\lambda = 1$ ,  $\rho_S = 1$  in  $\Omega_S \times I$ . We consider a uniform rectangular mesh with  $\Delta t = \Delta x = \Delta y = 0.03$ . The space-time approximation degree is  $p=2$ . The source term  $f(t) = -50^2 \pi^2 (t - 0.2) \cdot \exp(-25 \pi^2 (t - 0.2)^2)$  is set at the point  $(0.5, 0.5)$ .

Figure 5.16 shows the propagation of the components  $v_S^x$ ,  $v_S^y$  of the numerical velocity  $\mathbf{v}_S$  in a homogeneous 2D elastic medium. The propagation of the components  $\sigma^{xx}$ ,  $\sigma^{yy}$ ,  $\sigma^{xy}$  of the numerical stress tensor  $\underline{\sigma}$  is represented in figure 5.18. Due to the limits of our prototype code, we were not able to consider a larger domain. In order to avoid the reflections from the "free-surface" boundaries, and to obtain the proper seismograms, the propagation was stopped at an early stage, that is before the  $S$ -wave appears. The numerical artifacts in figure 5.18 are caused by the source point in the elastodynamic domain. Similar effects are also observed while simulating the numerical stress propagation in a solid medium by a standard DG method. This side effect is localized in the zone of the source and does not impact the computed seismograms. However, we have to improve the implementation of the source term in order to get rid of these artifacts. The

numerical solutions are validated by analytical solutions computed with *Gar6more2D* [1]. In figure 5.17, we observe a correct match between the analytical and approximate curves. Furthermore, it gives a clear motivation for developing efficient software, suited to more realistic physical models. The results of convergence of the numerical velocity computed for different approximation degrees  $p=0, 1, 2, 3$  are given in figure 5.19. They represent the  $L^2$ -norm in time and space of numerical error as a function of cell size  $\Delta x = \Delta y = \Delta t$ . The convergence is at least of order  $p$  and for  $p = 3$  we recover the optimal order of convergence of classical DG methods even though we use a source point which does not satisfy the regularity requirements.

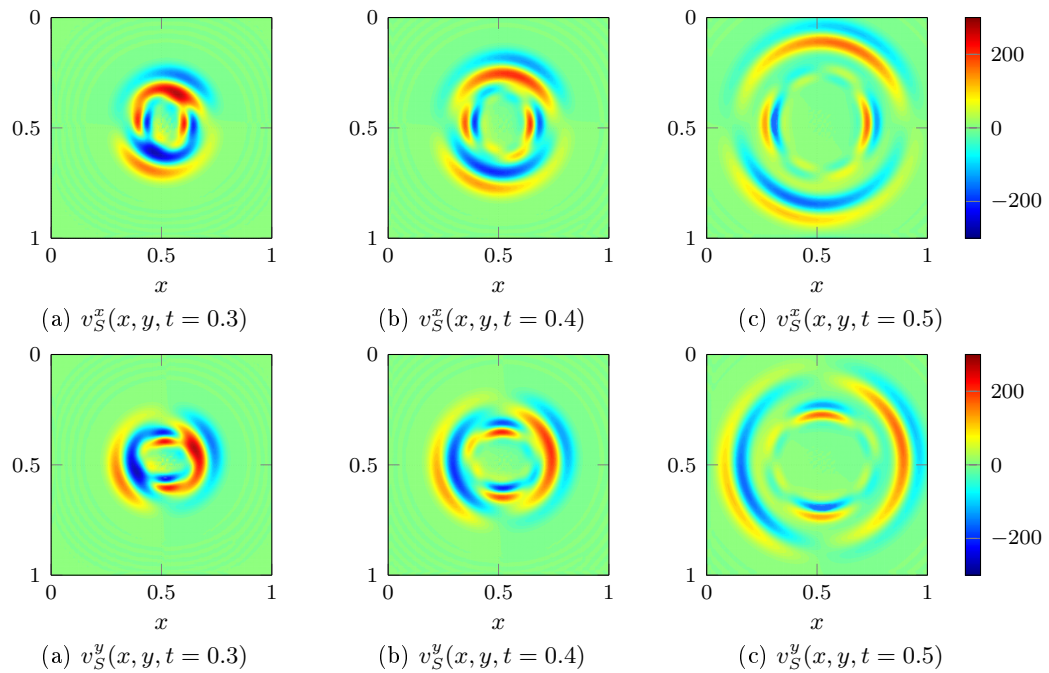


FIGURE 5.16: Propagation of the components  $v_S^x$ ,  $v_S^y$  of velocity in a homogeneous 2D solid domain at time  $t = 0.3, 0.4, 0.5$ .

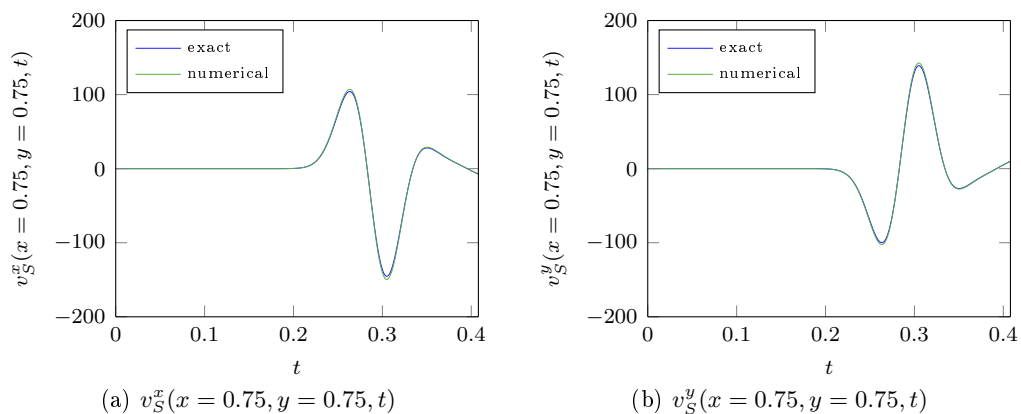


FIGURE 5.17: The seismograms for exact and numerical velocities  $\mathbf{v}_S \equiv (v_S^x, v_S^y)$  in a homogeneous 2D solid domain.

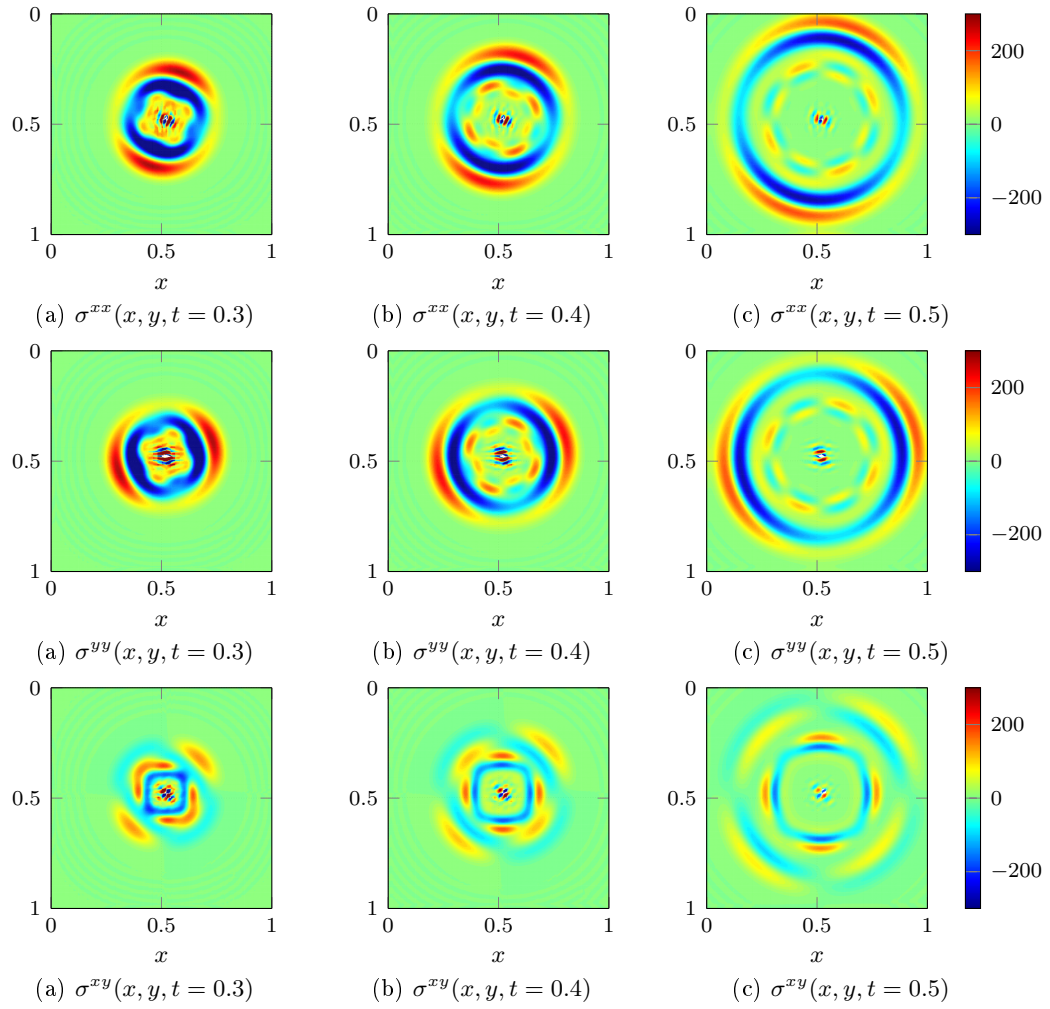


FIGURE 5.18: Propagation of the components  $v_S^x$ ,  $v_S^y$  of velocity and  $\sigma^{xx}$ ,  $\sigma^{yy}$ ,  $\sigma^{xy}$  of stress tensor in a homogeneous 2D solid domain at time  $t = 0.3, 0.4, 0.5$ .

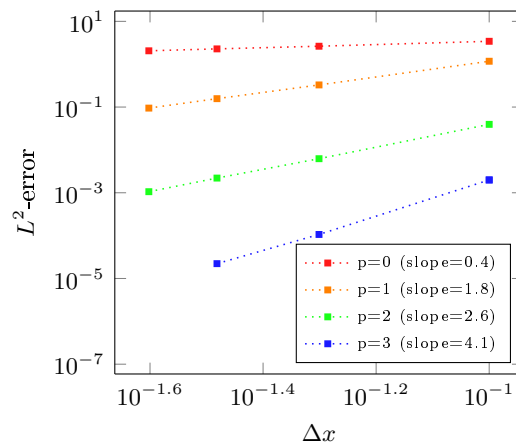


FIGURE 5.19: Convergence of the numerical velocity  $v_S$  as a function of cell size  $\Delta x = \Delta y = \Delta t$ .

### 5.2.3 2D Elasto-acoustics

Once we have developed the acoustic and elastodynamic propagators, we can proceed to their numerical coupling by imposing appropriate numerical fluxes, as was explained in chapter 3.3.

The coupled fluid-solid medium is a unit square, and it contains two identical in form rectangular layers:  $[0, 0.5] \times [0, 1]$  filled by a fluid and  $[0.5, 1] \times [0, 1]$  corresponding to the solid part of the medium. The simulation is performed along the time interval  $I = [0, 1]$ . We consider a uniform rectangular mesh with steps  $\Delta t = \Delta x = \Delta y = 0.03$  over the whole domain. The medium parameters are  $\rho_F = 1.0$ ,  $c_F = 2.0$  in the acoustic medium,  $\rho_S = 1.0$ ,  $\lambda = 1.0$ ,  $\mu = 2.0$  in the elastic medium. The space-time approximation degree is  $p=3$ . We consider zero initial conditions, and introduce a source term in the acoustic layer. The source signal emitted at the point  $(0.5, 0.25)$  is represented by the function  $f(t) = 40\pi^2(t - 0.3) \cdot \exp(-40\pi^2(t - 0.3)^2)$ , so that we have approximately five elements per wavelength.

The snapshots depicting the numerical velocity at time  $t = 0.5, 0.6, 0.7$  are represented in figure 5.20.

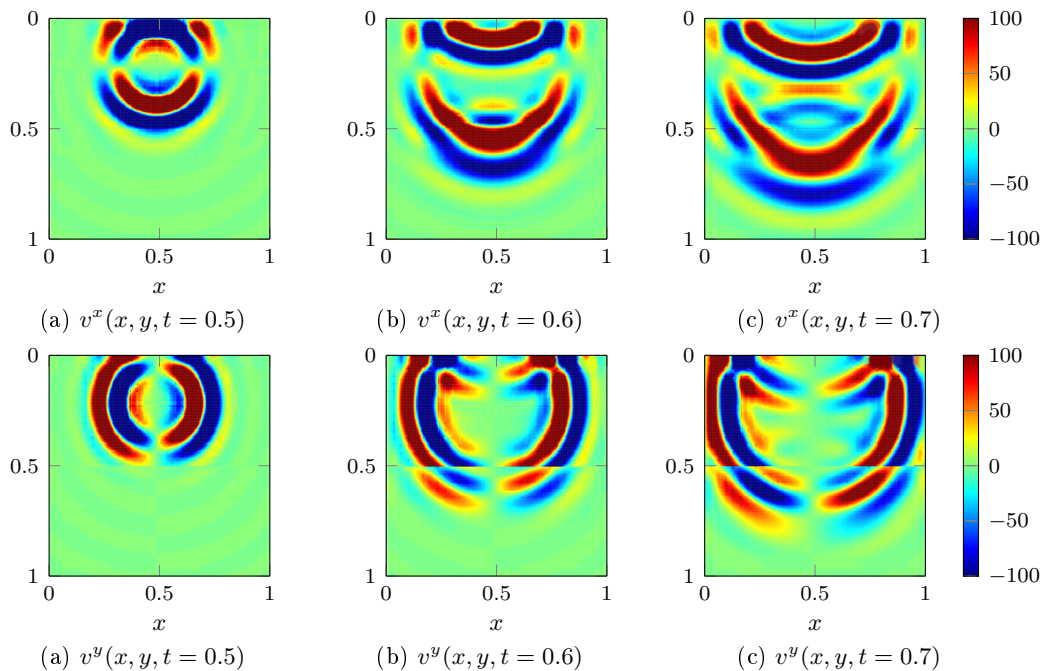


FIGURE 5.20: Propagation of numerical velocity  $\mathbf{v} = (v^x, v^y)$  in a 2D fluid-solid domain at time  $t = 0.5, 0.6, 0.7$ .

The pattern of propagation corresponds perfectly to physical predictions. Even if the model is limited (large mesh of  $30 \times 30$  rectangles in space, Dirichlet boundaries, which

causes many reflections), we can observe all type of waves ( $P$ ,  $S$  - waves, incident, reflected waves and waves of  $P$ ,  $S$  - head waves).

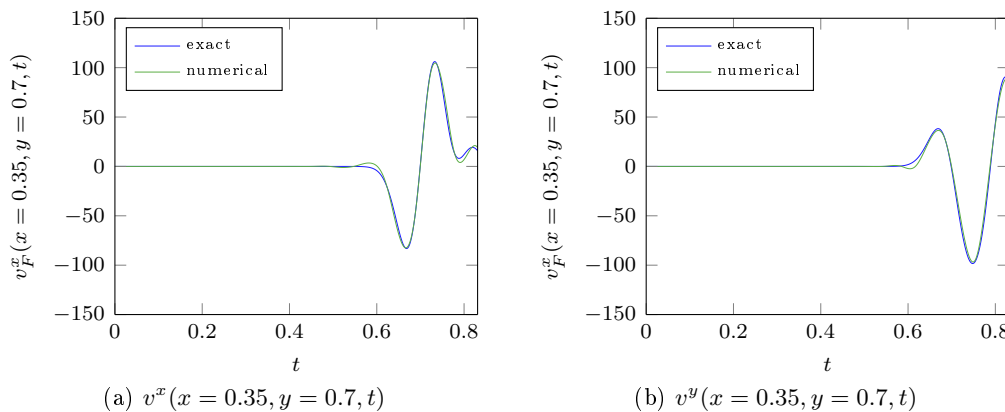


FIGURE 5.21: The seismograms for exact and numerical velocities  $\mathbf{v} \equiv (v^x, v^y)$  in a 2D fluid-solid domain.

In order to validate this test case, we have compared the numerical signals with the analytical ones, computed by using the *Gar6more2D* [1] code. We show an example at the receiver (0.35, 0.70) in figure 5.21. We can observe that the signals match well, regarding both the frequencies and amplitudes. There are still some imperfections, which are caused by the large discretization and the reflections from the "free-surface" boundaries.

### 5.3 Fortran 2D simulations

The prototype *MATLAB*® implementation based on the exact matrix inversion has been developed to perform fast proof of concept of the method. We have obtained convincing preliminary results which led us to consider the implementation of our method into an HPC environment.

*Elasticus* is a Magique-3D in-house platform for solving wave propagation problems in acoustic, elastic and mixed media of spatial dimensions one up to three, which employs the DG and Spectral Method (SM) for space integration, different time-schemes for time integration (Runge-Kutta, Leap-Frog). It allows different types of structured and non-structured meshes (triangles, rectangles, tetrahedrons, cubes). *Elasticus* is written in *Fortran*, and it has a parallel structure.

We have integrated the space-time Trefftz-DG propagators based on the approximate matrix inversion for 1D and 2D acoustic problems in the framework of the *Elasticus* code.

In this section we provide some numerical tests, illustrating this implementation for 2D acoustics with structured and non-structured triangular in space meshes.

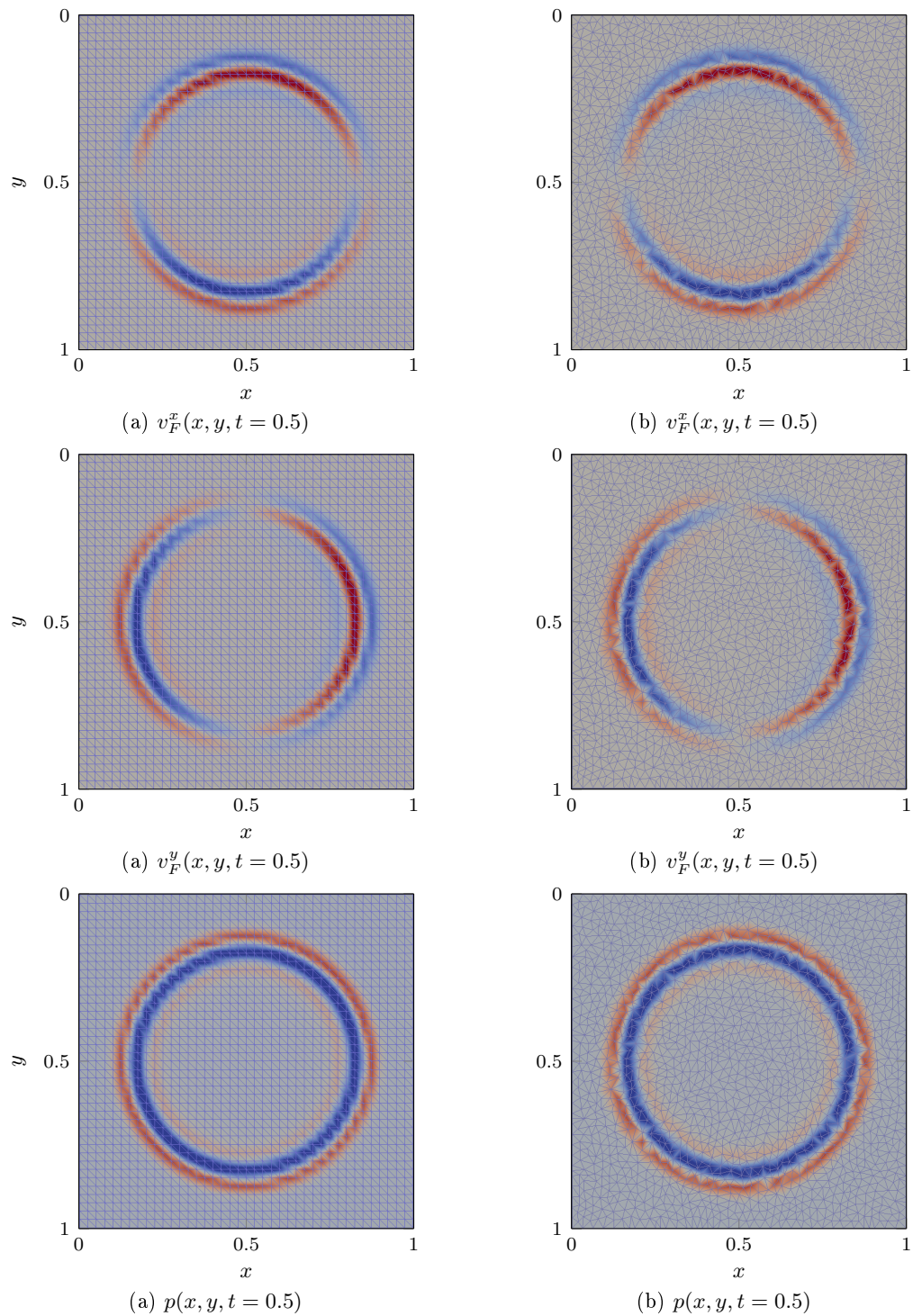


FIGURE 5.22: Propagation of the components  $v_F^x$ ,  $v_F^y$  of numerical velocity and pressure  $p$  in a homogeneous 2D fluid domain.

### 5.3.1 2D Acoustic simulation

The acoustic medium is represented by a unit square  $\Omega_F = [0, 1] \times [0, 1]$ , and the time propagation is  $I = [0, 1]$ . We consider two examples of triangular meshes: a structured mesh with 3200 elements, and an unstructured mesh with 3100 elements. The medium parameters are  $\rho_F = 1.0$ ,  $c_F = 1.0$ . The degree of approximation in space and time is  $p=3$ . The penalty parameters are  $\alpha_1 = \beta_1 = \delta_1 = \gamma_1 = 0.5$ . We consider zero initial conditions, and introduce a source term in the middle of the space domain. The source signal is emitted at the point  $(0.5, 0.5)$  and is defined by  $f(t) = 200\pi^2(t - 0.2) \cdot \exp(-100\pi^2(t - 0.2)^2)$ .

In figure 5.22, we display the components  $v_F^x$ ,  $v_F^y$  of the numerical velocity and the pressure  $p$  at time  $t = 0.5$  in the case of structured (a) and unstructured (b) meshes.

*Elasticus* code includes many routines and functions that we could have reused for the implementation of the Trefftz-DG propagator. However, some specific features of the Trefftz-DG method, in particular the dependency of the basis functions on medium parameters and the space-time integration (see chapter 4 and sections 4.3-4.4), have implied the creation of new *Fortran* modules to construct the global matrix to be solved. Moreover, the change-over algorithm has required the construction from scratch of a specific routine. Some routines have also been developed for delivering the snapshots and the seismograms.

The parallelization of the new Trefftz-DG propagator is still in progress, as well as the analysis of performance involving comparisons with standard DG and SM propagators based on a semi-discrete formulation coupled with the time integration schemes.

## 5.4 Conclusion

We have developed new numerical propagators for the acoustic, elastodynamic and coupled elasto-acoustic problems in one and two dimensions. We have considered different examples of homogeneous and heterogeneous media with periodic and "free-surface" boundary conditions. The numerical results have been validated by analytical solutions computed with the *Gar6more2D* code [1]. The solution methodology has demonstrated some limitations. This arise because it applies a space-time integration leading to the representation of the discrete system by a huge sparse matrix whose straightforward inversion is expensive. We find ourselves in a situation of using an implicit scheme which tends to be unpopular with geophysical exploration engineers who use the solution of wave problems inside an iterative process of inversion for reconstructing very large propagation domains. Thus, the computational costs for solving the forward problems must be

---

as low as possible and the space-time integration that we have proposed at first does not take the main feature of DG formulation that is basically to favor a solution methodology element-by-element. Fortunately, we have observed that it is possible to decompose the global matrix by separating the time variable from the space ones. By this way, we can benefit from the block diagonal structure of the standard DG formulation and we end up with an explicit scheme. We have then performed numerical experiments which clearly illustrate the advantages of the split version of the discrete problem but we acknowledge that our approach still has computational limits as shown by some of the numerical experiments where the accuracy may drop because of computational resource limitation. In the next chapter, we propose to overcome this limitation by coupling the Trefftz-DG approach with the so-called Tent Pitcher algorithm in order to provide a naturally explicit scheme without decomposing the global matrix.



## Chapter 6

# Explicit Trefftz-DG method on tent-pitching meshes

The previous chapters have been devoted to the development of a Trefftz-DG formulation for mechanical wave problems, inspired by theoretical work carried out for acoustic and electromagnetic waves [72, 82]. We have shown that the resulting scheme was implicit and required the inversion of a huge matrix. Using an approximation of the inverse of this matrix, we have been able to derive an explicit scheme, but we still had to face to computational resource limitations.

To reduce the computational cost, we propose now to use the fact that space-time DG formulation can be solved element-by-element, provided the space-time mesh conforms to certain causality constraints [29, 77, 86, 100, 109, 110]. The corresponding algorithm, called the Tent-Pitcher algorithm, was originally proposed by Üngör et al. in 2000 [104, 105] and generalized by Erickson et al. in 2005 [40]. It consists in meshing the space-time domain by using an advancing front method limited in time by the finite speed of propagation principle. In this way, the mesh is composed of patches which are connected by causality only. Each patch contains a certain number of elements and the patches that do not share any causal property are solved independently. The Tent Pitcher is thus well adapted for a parallel implementation [99]. Moreover, it has been shown in [2] that the original Tent Pitcher can be improved as an adaptive algorithm which confers the algorithm interesting features for solving industrial wave problems. The beginning of the 21<sup>th</sup> has seen the publication of a series of very interesting papers addressing the space-time discretization of hyperbolic problems [2–5, 84]. In particular, P. Monk and G. Richter [84] have proposed a semi-explicit scheme for acoustics and electromagnetism that results from the inversion of the matrices obtained from a patch of elements. However it requires the uses of dD+time volumic elements whose implementation is not obvious

and could discourage practitioners. This could explain why this approach has not been followed. However, some papers have recently reconsidered the Tent Pitcher [51, 52, 85].

In this chapter, we propose to follow their ideas by extending the Trefftz-DG formulation to Tent Pitcher. It is worth noting that our formulation avoids  $dD+time$  elements thanks to the Trefftz framework. This is an important feature that deserves to be underlined in the perspective of an industrial porting of our algorithm.

# Contents

6.1	Preliminaries . . . . .	101
6.2	Tent-pitching Trefftz-DG formulation . . . . .	107
6.2.1	Tent-pitching Trefftz-DG formulation for the acoustic system . . .	107
6.2.2	Tent-pitching Trefftz-DG formulation for the elastodynamic system	114
6.2.3	Tent-pitching Trefftz-DG formulation for the elasto-acoustic system	117
6.3	Space-time tent mesh examples . . . . .	121
6.3.1	1D+time homogeneous and heterogeneous tent meshes . . . . .	121
6.3.2	2D+time homogeneous tent mesh . . . . .	121
6.4	Numerical results . . . . .	122
6.4.1	1D Acoustics . . . . .	123
6.4.1.1	Homogeneous acoustic medium with periodical boundary conditions . . . . .	123
6.4.1.2	Heterogeneous acoustic medium with periodic boundary conditions . . . . .	124
6.4.2	Homogeneous 2D acoustics . . . . .	125
6.4.3	Homogeneous 2D elastodynamics . . . . .	127
6.4.4	2D Elasto-acoustics . . . . .	129
6.4.5	Test of performance . . . . .	130
6.5	Conclusion . . . . .	131



## 6.1 Preliminaries

The Tent Pitcher algorithm has been introduced for solving hyperbolic problems in the context of space-time integration. It consists in making use of the finite speed of wave propagation to deploy an element-by-element solution methodology for hyperbolic equations. To explain the implementation of the Tent Pitcher, let us consider the pressure field governed by the 1D acoustic wave equation. We have decided to consider this case to simplify the presentation of the algorithm, but the generalization to higher dimensions and to the first order formulation can be done thanks to representation formulas [42]. Indeed, the key point for the Tent Pitcher implementation is the propagation of the compact support of the data.

Let  $p$  be the solution to the 1D wave equation:

$$\frac{1}{c_F^2} \frac{\partial^2 p}{\partial t^2} - \frac{\partial^2 p}{\partial x^2} = 0,$$

with initial data:

$$p(0, x) = p_0(x), \quad \frac{\partial}{\partial t} p(0, x) = p_1(x).$$

We assume that  $p_0$  and  $p_1$  are given in an interval, that is for instance  $[0, R]$ . Then the pressure field admits the representation:

$$p(t, x) = \frac{1}{2}(p_0(x - c_F t) + p_0(x + c_F t)) + \frac{1}{2c_F} \int_{x - c_F t}^{x + c_F t} p_1(s) ds.$$

Then, we can see that from the knowledge of  $p_0$  and  $p_1$  in  $[0, R]$ , we get the values of  $p$  in the triangle depicted in figure 6.1(a). This triangle is obtained by joining the line of slope  $1/c_F$  from point  $(0, 0)$  to the line of slope  $1/c_F$  from point  $(0, R)$ . This construction can be replicated with any set of data as long as they are compactly supported, which unifies the first stage of the tent pitching mesh construction as a set of triangles (see figure 6.1(b)). We have considered the possibility of having a velocity  $c_F$  that is piecewise constant and a set of initial data defined locally in a set of segments covering the space interval. The shape of the different triangles differs because of different values both of the velocity and the size of the support of the initial data. At this stage, we have the solution defined inside the first layer of the tent pitching mesh. We plot in green the edges where the solution is known, either because it has been computed at previous step, or because the edge is on the boundary, and we plot in blue the edges where the solution is unknown. The next steps consist in continuing the construction of the solution layer by layer with the same principle by using the values of the pressure field on the boundaries

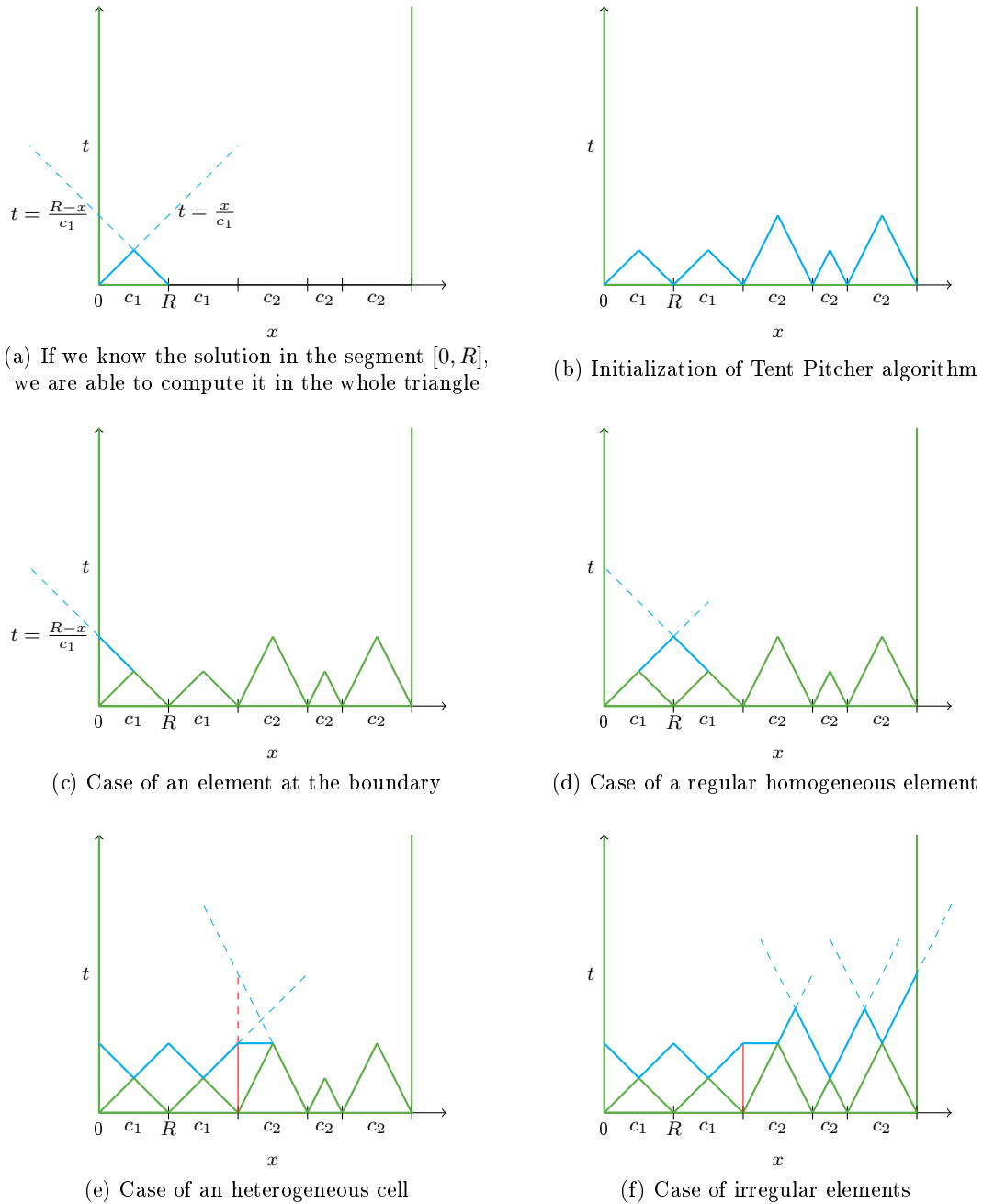


FIGURE 6.1: General construction of a tent-pitching mesh in 1D.

of the elements defining the first level of the mesh. That leads to building the second level of the tent pitching mesh as depicted in figure 6.1(c)-(f).

Figure 6.1(c)-(f) shows that the variety of elements of level 2 is larger. Figure 6.1(c) shows the case of an element on the (left) boundary. In this case, it is obtained by simply connecting the line of slope  $1/c_{F1}$  from the right vertex to the vertical boundary. In figure 6.1(d), we present the case of a regular homogeneous cell, which is obtained by joining the line of slope  $-1/c_{F1}$  from the right vertex to the line of slope  $1/c_{F1}$  from the left vertex. In figure 6.1(e), we present the case of an heterogeneous cell. Here, we

have to account for the fact that we use a Trefftz basis which has been constructed for homogeneous domains. Hence, we have to split the cell into two sub-cells, thanks to the vertical red line which is drawn at the interface between the two media. This line is vertical because we assume that the physical parameters do not vary in time. It is worth noting that the blue line has no common point with the line of slope  $1/c_{F1}$  from the left vertex and the line of slope  $1/c_{F2}$  coming from the right vertex. Thus we use the lowest point of the triangle formed by these three lines to construct the cell of level 2. In figure 6.1(f), we have a non-regular homogeneous elements obtained by joining the line of slope  $1/c_{F2}$  from the right vertex to the line of slope  $1/c_{F2}$  from the left vertex. The only difference with regular element is that the resulting cell is not diamond-shaped.

Now, we address the question of whether or not the solution to the 1D wave equation can be computed at a given point  $(x_0, t_0)$ . In order to simplify the presentation we assume here that the domain is homogeneous. Let  $C_{x_0, t_0}$  be the lower part of the cone defined by the two lines of slope  $1/c_F$  and  $1/c_F$  coming from  $x_0, t_0$ . We say that  $C_{x_0, t_0}$  is the dependence cone. The solution to the 1D wave equation can be computed at point  $(x_0, t_0)$  if and only if there exists a line, or a broken line, that connects the two lines of the cone (see figure 6.2).

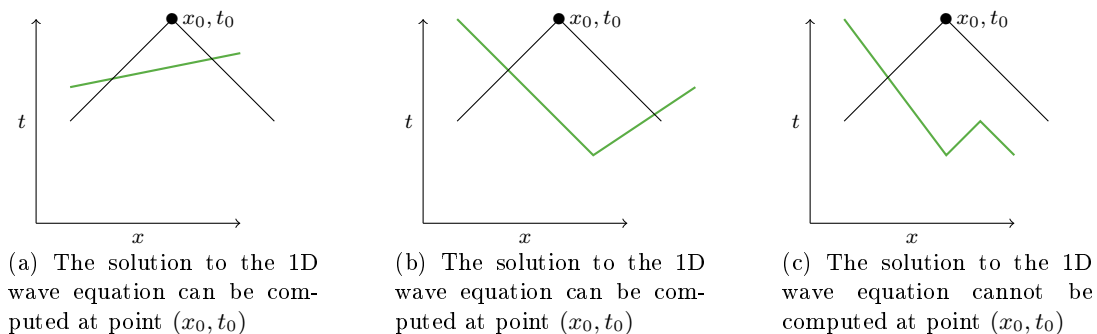


FIGURE 6.2: Determination of the solvability of the wave equation at point  $(x_0, t_0)$  when the solution is known on the green line

Using this characterization, we can now determine whether or not the solution can be computed on a given cell. We consider a convex polygonal cell and we split its edges in three categories: the inflow edges, such that the temporal part of the outwardly directed normal is negative ( $n_t < 0$ ), the outflow edges, such that the temporal part of the outwardly directed normal is positive ( $n_t > 0$ ) and the vertical edges which are parallel to the time axis. We assume that the vertical edges are only edges on the boundary or internal edges that split the cell into two sub-cells (for instance in the case of heterogeneity). We adopt the same terminology as in [84] where the Tent Pitcher is coupled with a standard DG formulation involving both volume and surface integrals.

We say that a cell is self-contained if the solution of the wave equation can be computed at any point of the cell as soon as the solution is known on the inflow boundaries. A

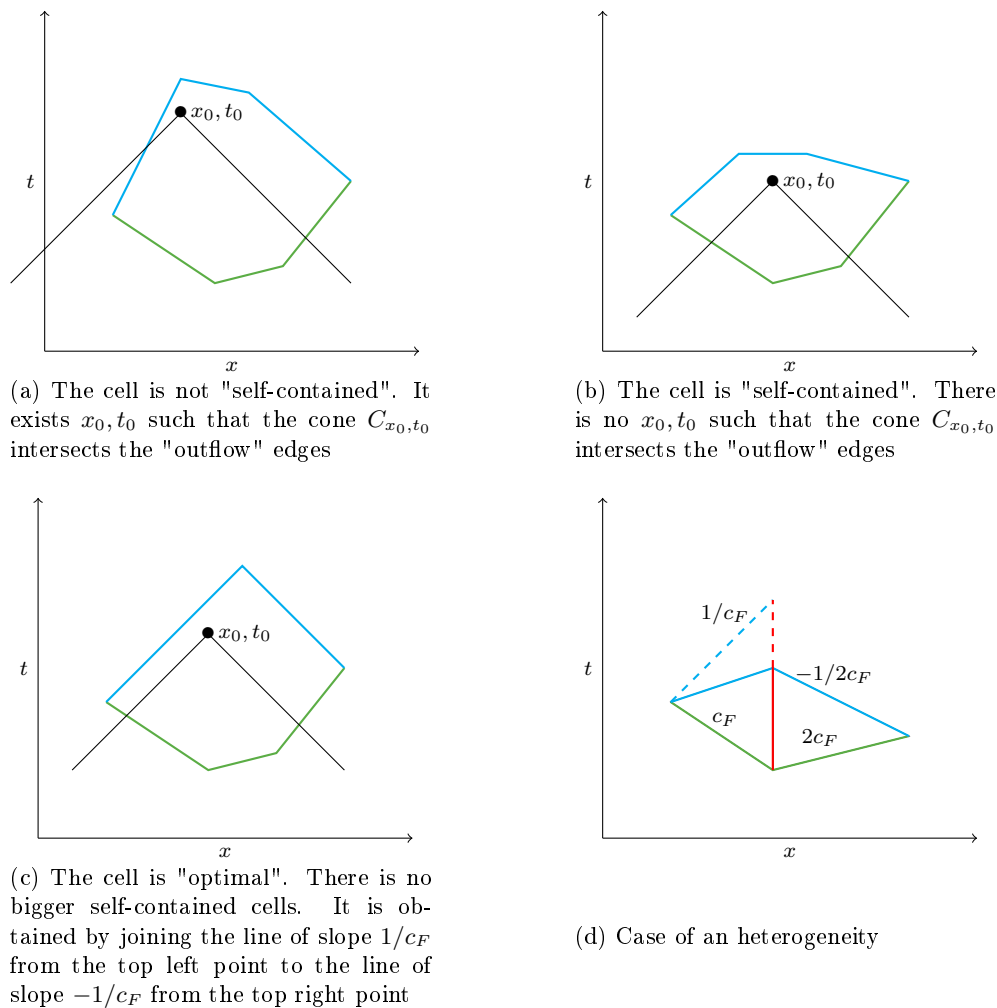


FIGURE 6.3: self-contained cells and optimal cells

cell is self-contained if and only if there is no point  $(x_0, t_0)$  such that the cone  $C_{x_0, t_0}$  intersects the outflow boundary. In figure 6.3(a), the cell is not self-contained since there exists a point where  $C_{x_0, t_0}$  intersects the blue outflow boundary. In figure 6.3(b), the cell is self-contained but its size is not optimal, since there exists points outside the cell where the solution of the wave equation can be computed from the inflow boundary. In figure 6.3(c), the cell is both self-contained and optimal-shaped. We can easily show that a cell is self-contained if and only if the absolute value of the slope of all the segments of the outflow boundary is smaller than  $1/c_F$  (in order to avoid intersection with the dependence cone. In other word, the normal of the outflow boundary should satisfy  $|n_x|/n_t < 1/c_F$  everywhere. The cell is optimal is and only if the outflow boundary is composed of only two edges, one of slope  $1/c_F$ , the other one of slope  $-1/c_F$ .

In the case of a heterogeneous cell, we have to introduce an internal edge at the discontinuity, parallel to the time axis. We assume here that the velocity is  $c_F$  in the left, and  $2c_F$  in the right. To build an optimal cell from the inflow edges, (1) we compute the

intersection of the line of slope  $1/c_F$  starting from the top left point and of the vertical edge; (2) we compute the intersection of the line of slope  $-1/2c_F$  starting from the top right point and of the vertical edge; (3) we keep the lowest point; (4) we join this last point with the top left point and with the top right point (see figure 6.3(d)). The implementation in the elasto-acoustic case is similar, hence we do not detail it.

In the previous chapter, we proposed to mesh the domain with time slabs orthogonal to the time axis and to solve each time slab explicitly. It is actually possible to revisit this strategy in the Tent Pitcher framework. In figure 6.4(a), we consider each cell of the slab independently. In this case, the vertical edges are considered as outflow edges since we do not know the solution on these edges at time step  $n$ . Obviously, these edges do not satisfy the condition  $|n_x|/n_t < 1/c_F$  and the cells are not self-contained. Now, if we consider the macro-element containing all the cells of the time slabs, the vertical edges become internal edges, except the external edges that are part of the inflow set thanks to the boundary condition. Hence, the only outflow edges are the top horizontal ones, which clearly satisfy the condition  $|n_x|/n_t < 1/c_F$ , and the time slab is self-contained.

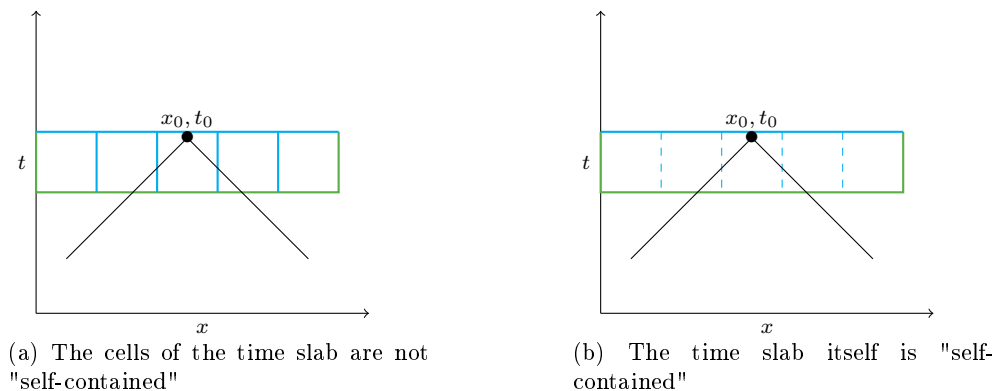


FIGURE 6.4: The case of the time slab

We can now describe typical meshes that could be used to solve wave equation problems. Four of these meshes are depicted in figure 6.5. In each figure, the number inside a given cell corresponds to the stage at which the cell has to be involved. Figure 6.5(a) represents the case of a homogeneous media (with  $c_F = 2$ ) with an initial mesh that is regular. In this case, we begin with computing the solution inside the triangles (1), then we can compute the solution inside the diamond-shaped (2), then (3), and so on. Here, every edge satisfies exactly the condition  $|n_x|/n_t = 1/c_F$ . In figures 6.5(b) and 6.5(c), we assume that two cells of the mesh have been refined by a factor 2. In practice, this could be done for instance to capture strong variations of the initial conditions, or to represent faithfully the geometry of an obstacle or of a topography. In figure 6.5(b), each cell is optimal. In this case, we observe that the refinement propagates with the wave front. This is very useful in order to follow some particular behaviors of the wave, but it is not convenient if the refinement is just to model the geometry of the medium

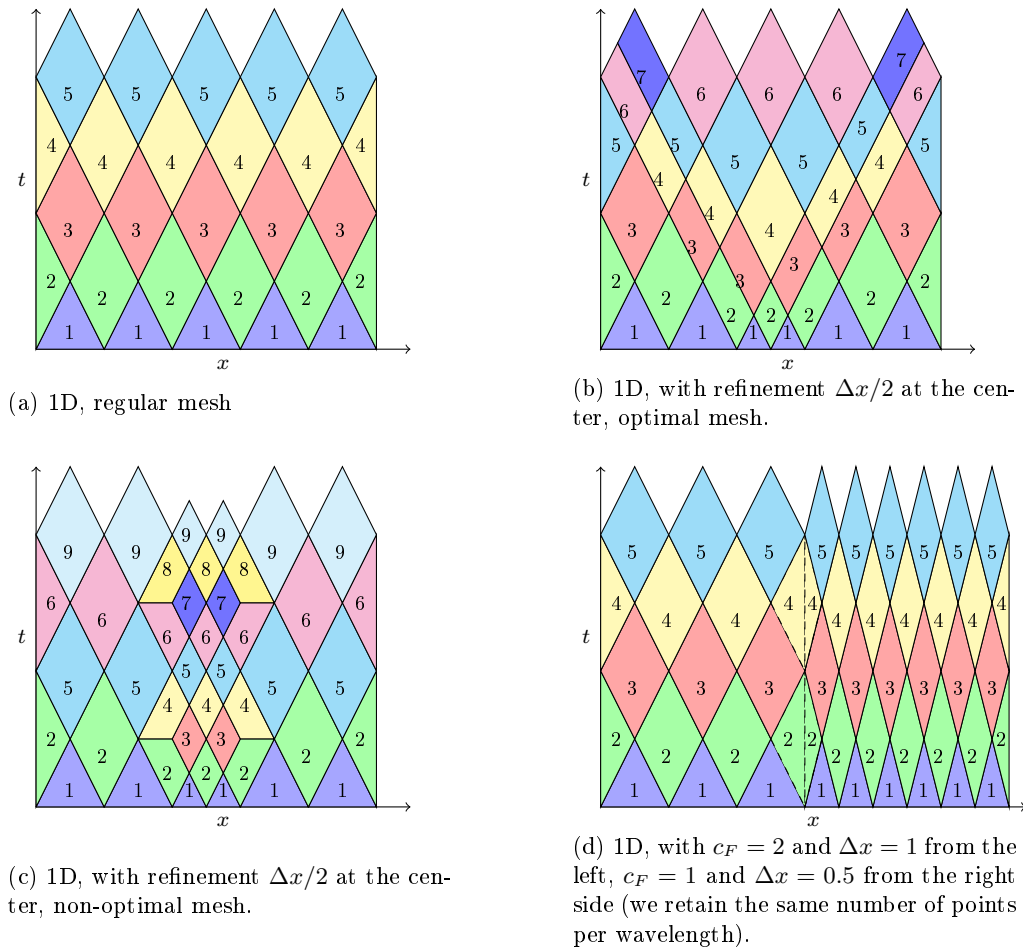


FIGURE 6.5: 1D+time tent-pitching mesh examples

(which is not supposed to move with the wavefront). In this latter configuration, it is possible to prevent the refinement from following the wavefront by adding a constraint on the nodes of the mesh imposing that each node is either aligned with the nodes of the grid defined at  $t = 0$  or aligned with the center of the cells defined at  $t = 0$  (see figure 6.5(c)). Of course, in return, we may use cells whose shape is not optimal. At last, in figure 6.5(d), we consider the case of an heterogeneous medium with  $c_F = 2$  on the left and  $c_F = 1$  on the right. We assume that the size of the cells covering the right part of the mesh is halved in order to keep the same number of points per wavelength everywhere. At the interface between the two media, we glue the right element and the left element thanks to a vertical edge (the dashed line in the picture). Hence, in this case (figure 6.5(d)) the two elements constitute a macro-element, that will give rise to a linear system involving the unknowns of both elements. Although, in the case of higher dimension, we can obtain several sub-cells connecting into one macro-cell through the interface of heterogeneity.

## 6.2 Tent-pitching Trefftz-DG formulation

In this section, we couple a Tent Pitcher algorithm with the Trefftz-DG formulation for acoustic, elastodynamic and elasto-acoustic equations. We study well-posedness of the problem, showing a conditional stability.

### 6.2.1 Tent-pitching Trefftz-DG formulation for the acoustic system

As it was discussed previously, the tent strategy consists in progressively constructing a conforming space-time mesh  $\mathcal{T}_{Fh}^{tp}$  on  $Q_F \equiv \Omega_F \times I$  of arbitrarily shaped non-overlapping space-time elements  $K_F$ , and in solving element-by-element the space-time Trefftz-DG formulation locally on the outflow edges, using as initial data the results on the inflow edges obtained previously for the neighbour tents. Thus, instead of considering a global mesh skeleton  $\mathcal{F}_{Fh} = \cup_{K_F \in \mathcal{T}_{Fh}^{tp}} \partial K_F$  over the whole space-time domain  $Q_F$ , it is preferable to focus locally on each macro-cell  $K_F$  of the tent along with its boundaries.

The cell edges can be categorized with respect to the component  $n_{K_F}^t$  of the outwardly directed unit normal vector  $\mathbf{n}_{K_F} \equiv (\mathbf{n}_{K_F}^x, n_{K_F}^t)$ , as follows:

$$\begin{array}{lll} \mathcal{F}_h^{In}(K_F) & \text{inflow boundaries of } K_F & (n_{K_F}^t < 0) \\ \mathcal{F}_h^{Out}(K_F) & \text{outflow boundaries of } K_F & (n_{K_F}^t > 0) \\ \mathcal{F}_h^{Vert}(K_F) & \text{vertical boundaries of } K_F & (n_{K_F}^t = 0) \end{array}$$

In particular, the family  $\mathcal{F}_h^{Vert}(K_F)$  of vertical boundaries includes external vertical edges  $\mathcal{F}_h^{Ext}(K_F)$  that correspond to the physical domain boundaries, and internal edges  $\mathcal{F}_h^{Int}(K_F)$  introduced to split heterogeneous macro-cells into homogeneous sub-cells. In the following, we omit the dependency on  $K_F$ , in order to simplify the notation.

Figure 6.6 illustrates the different tent types that, by the way, have been previously introduced in figure 6.1 when introducing the Tent Pitcher.

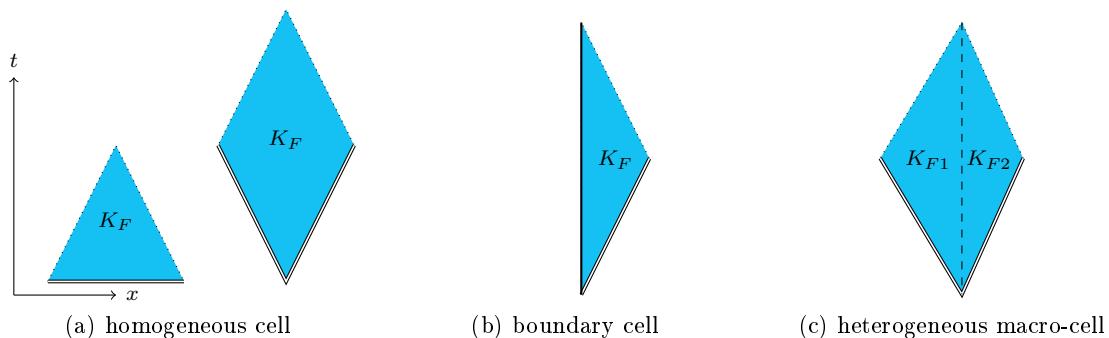


FIGURE 6.6: Three types of space-time tents.

The tent of homogeneous type 6.6(a) represents a regular homogeneous single cell  $K_F$  connected with the previously involved neighbour tents through the inflow edge  $\mathcal{F}_h^{In}$  (double line). The dotted boundary corresponds to the outflow edge  $\mathcal{F}_h^{Out}$  (figure 6.1(a),(d)).

The tent of boundary type 6.6(b) corresponds to the case of an element at the boundary (figure 6.1(c)). It is also a homogeneous single cell  $K_F$  connected with the previously computed neighbour tents through the inflow edge  $\mathcal{F}_h^{In}$  (double line), and bounded by the external vertical edge  $\mathcal{F}_h^{Ext}$  (thick line) on  $\partial\Omega_F \times I$ . The outflow edge  $\mathcal{F}_h^{Out}$  is pictured with a dotted line.

In the end, according to the examples (e) and (f) in figure 6.1, we consider the tent of heterogeneous type 6.6(c) representing the heterogeneous macro-cell, which is split thanks to internal vertical edges  $\mathcal{F}_h^{Int}$  (dashed line) into homogeneous sub-cells  $K_{F1}$  and  $K_{F2}$ . Once again, these sub-cells are connected to the previously involved neighbour tents through the inflow edge (double line). The dotted boundary corresponds to the outflow edge.

We introduce the local Trefftz space  $\mathbb{T}_F(K_F)$  of the test functions  $\boldsymbol{\omega}_F$  and  $q$  defined by:

$$\mathbb{T}_F(K_F) \equiv \left\{ (\boldsymbol{\omega}_F, q) \in V^h(K_F)^d \times V^h(K_F) \text{ such that, } \rho_F \frac{\partial \boldsymbol{\omega}_F}{\partial t} + \nabla q = 0 \text{ and } \frac{1}{c_F^2 \rho_F} \frac{\partial q}{\partial t} + \operatorname{div} \boldsymbol{\omega}_F = 0 \text{ in } K_F \in \mathcal{T}_{Fh}^{tp} \right\},$$

and the corresponding discrete Trefftz space  $\mathbb{T}_F^p(K_F)$  defined by:

$$\mathbb{T}_F^p(K_F) \equiv \left\{ (\boldsymbol{\omega}_F, q) \in \mathbb{T}_F(K_F), (\boldsymbol{\omega}_F, q) \in \mathbb{P}^p(K_F)^d \times \mathbb{P}^p(K_F) \right\}.$$

The local Trefftz-DG formulation for the acoustic system (3.1) in  $K_F$  reads as follows:

Seek  $(\mathbf{v}_{Fh}, p_h) \in \mathbb{T}_F^p(K_F)$  such that, for all  $K_F \in \mathcal{T}_{Fh}^{tp}$  and for all  $(\boldsymbol{\omega}_F, q) \in \mathbb{T}_F^p(K_F)$  it holds true:

$$a_{K_F}^{tp}((\mathbf{v}_{Fh}, p_h); (\boldsymbol{\omega}_F, q)) = l_{K_F}^{tp}(\boldsymbol{\omega}_F, q), \quad (6.1)$$

where the linear form  $l_{K_F}^{tp}(\cdot)$  is defined by:

$$\begin{aligned} l_{K_F}^{tp}(\boldsymbol{\omega}_F, q) \equiv & -\left(\frac{1}{2} + \beta_2\right) \int_{\mathcal{F}_h^{In}} \frac{1}{c_F^2 \rho_F} p_h^{in} q \mathbf{n}_{K_F}^t ds - \left(\frac{1}{2} + \alpha_2\right) \int_{\mathcal{F}_h^{In}} \rho_F \mathbf{v}_{Fh}^{in} \cdot \boldsymbol{\omega}_F \mathbf{n}_{K_F}^t ds \\ & - \frac{1}{2} \int_{\mathcal{F}_h^{In}} \left[ p_h^{in} \boldsymbol{\omega}_F \cdot \mathbf{n}_{K_F}^x + q \mathbf{v}_{Fh}^{in} \cdot \mathbf{n}_{K_F}^x \right] ds + \int_{\mathcal{F}_h^{Ext}} \left[ \alpha_1 g_{D_F} \boldsymbol{\omega}_F \cdot \mathbf{n}_{K_F}^x - q g_{D_F} \right] ds. \end{aligned}$$

and the bilinear form  $a_{K_F}^{tp}(\cdot; \cdot)$  is defined by:

$$\begin{aligned}
a_{K_F}^{tp}((\mathbf{v}_{Fh}, p_h); (\boldsymbol{\omega}_F, q)) \equiv & \\
& \int_{\mathcal{F}_h^{Out}} \left[ \frac{1}{c_F^2 \rho_F} p_h q n_{K_F}^t + \rho_F \mathbf{v}_{Fh} \cdot \boldsymbol{\omega}_F n_{K_F}^t + p_h \boldsymbol{\omega}_F \cdot \mathbf{n}_{K_F}^x + q \mathbf{v}_{Fh} \cdot \mathbf{n}_{K_F}^x \right] ds \\
& + \left( \frac{1}{2} - \beta_2 \right) \int_{\mathcal{F}_h^{In}} \frac{1}{c_F^2 \rho_F} p_h q n_{K_F}^t ds + \left( \frac{1}{2} - \alpha_2 \right) \int_{\mathcal{F}_h^{In}} \rho_F \mathbf{v}_{Fh} \cdot \boldsymbol{\omega}_F n_{K_F}^t ds \\
& + \frac{1}{2} \int_{\mathcal{F}_h^{In}} \left[ p_h \boldsymbol{\omega}_F \cdot \mathbf{n}_{K_F}^x + q \mathbf{v}_{Fh} \cdot \mathbf{n}_{K_F}^x \right] ds \\
& + \int_{\mathcal{F}_h^{Ext}} \left[ p_h \boldsymbol{\omega}_F \cdot \mathbf{n}_{K_F}^x + \alpha_1 (\mathbf{v}_{Fh} \cdot \mathbf{n}_{K_F}^x) (\boldsymbol{\omega}_F \cdot \mathbf{n}_{K_F}^x) \right] ds \\
& + \int_{\mathcal{F}_h^{Int}} \left[ \{p_h\} [\boldsymbol{\omega}_F]_x + \{\mathbf{v}_{Fh}\} \cdot [q]_x + \alpha_1 [\mathbf{v}_{Fh}]_x [\boldsymbol{\omega}_F]_x + \beta_1 [p_h]_x \cdot [q]_x \right] ds.
\end{aligned}$$

The superscript *in* corresponds to the inflow data previously computed on the neighbour tents.

It is worth mentioning that, by regrouping all the terms with respect to the factors  $n_{K_F}^t$  and  $\mathbf{n}_{K_F}^x$  respectively, we can rewrite the local bilinear form  $a_{K_F}^{tp}(\cdot; \cdot)$  in vector-matrix form as follows:

$$M_{K_F} = M_{K_F}^t n_{K_F}^t + \sum_{i=1}^d M_{K_F}^{x_i} n_{K_F}^{x_i}. \quad (6.2)$$

Equation (6.2) is restricted to polygonal cells where  $\mathbf{n}_{K_F}^x$  and  $n_{K_F}^t$  are constant on each edge. We get an expression of  $M_{K_F}$  that is similar to the one in [84], corresponding to the surface terms of the proposed space-time formulation of wave equations involving standard DG elements.

As in chapter 3, we restrict the problem to the homogeneous system with  $g_{D_F} \equiv 0$ , in order to simplify the presentation. Then, our approach does not lose generality since this term appears on the right-hand side of the formulation, and can be easily bounded above provided  $g_{D_F}$  is regular enough.

To establish the well-posedness of the local variational formulation (6.1) we proceed in similar way as in chapter 3. The analysis is carried out in the framework of [72] for acoustic wave equation.

We introduce the following quantities:

$$\begin{aligned} |||(\boldsymbol{\omega}_F, q)|||_{K_F}^{tp} &\equiv \left[ \frac{1-\theta_F}{2} \left\| \left( \frac{1}{c_F^2 \rho_F} \right)^{1/2} q (n_{K_F}^t)^{1/2} \right\|_{L^2(\mathcal{F}_h^{Out})}^2 + \frac{1-\theta_F}{2} \left\| \rho_F^{1/2} \boldsymbol{\omega}_F (n_{K_F}^t)^{1/2} \right\|_{L^2(\mathcal{F}_h^{Out})}^2 \right. \\ &\quad + \frac{\theta_F}{2} \left\| \left( \frac{1}{c_F^2 \rho_F} \right)^{1/2} q (n_{K_F}^t)^{1/2} + \rho_F^{1/2} \boldsymbol{\omega}_F (n_{K_F}^t)^{1/2} \right\|_{L^2(\mathcal{F}_h^{Out})}^2 \\ &\quad + \left\| \beta_2^{1/2} \left( \frac{1}{c_F^2 \rho_F} \right)^{1/2} q |n_{K_F}^t|^{1/2} \right\|_{L^2(\mathcal{F}_h^{In})}^2 + \left\| \alpha_2^{1/2} \rho_F^{1/2} \boldsymbol{\omega}_F |n_{K_F}^t|^{1/2} \right\|_{L^2(\mathcal{F}_h^{In})}^2 \\ &\quad \left. + \left\| \alpha_1^{1/2} (\boldsymbol{\omega}_F \cdot \mathbf{n}_{K_F}^x) \right\|_{L^2(\mathcal{F}_h^{Ext})}^2 + \left\| \alpha_1^{1/2} [\boldsymbol{\omega}_F]_x \right\|_{L^2(\mathcal{F}_h^{Int})}^2 + \left\| \beta_1^{1/2} [q]_x \right\|_{L^2(\mathcal{F}_h^{Int})}^2 \right]^{1/2}, \end{aligned}$$

$$\begin{aligned} |||(\boldsymbol{\omega}_F, q)|||_{K_F^*}^{tp} &\equiv \left[ |||(\boldsymbol{\omega}_F, q)|||_{K_F}^{tp2} \right. \\ &\quad + \frac{1}{1-\theta_F} \left\| \rho_F^{1/2} \boldsymbol{\omega}_F (n_{K_F}^t)^{1/2} \right\|_{L^2(\mathcal{F}_h^{Out})}^2 + \frac{1}{1-\theta_F} \left\| \left( \frac{1}{c_F^2 \rho_F} \right)^{1/2} q (n_{K_F}^t)^{1/2} \right\|_{L^2(\mathcal{F}_h^{Out})}^2 \\ &\quad + \left\| \left( \frac{1}{2\beta_2} + 1 \right)^{1/2} \left( \frac{1}{c_F^2 \rho_F} \right)^{1/2} q \right\|_{\mathcal{F}_h^{In}}^2 + \left\| \left( \frac{1}{2\alpha_2} + 1 \right)^{1/2} \rho_F^{1/2} \boldsymbol{\omega}_F \right\|_{\mathcal{F}_h^{In}}^2 \\ &\quad \left. + \left\| \alpha_1^{-1/2} q \right\|_{L^2(\mathcal{F}_h^{Ext})}^2 + \left\| \beta_1^{-1/2} \{\boldsymbol{\omega}_F\} \right\|_{L^2(\mathcal{F}_h^{Int})}^2 + \left\| \alpha_1^{-1/2} \{q\} \right\|_{L^2(\mathcal{F}_h^{Int})}^2 \right]^{1/2}. \end{aligned}$$

*Remark:* By definition,  $n_{K_F}^t$  is positive in  $\mathcal{F}_h^{Out}$ , while it is negative in  $\mathcal{F}_h^{In}$ .

The parameter  $\theta_F$  is assumed to be in  $[0, 1)$  so that, similarly to the theorem 3.1, we can prove that  $||| \cdot |||_{K_F}^{tp}$  and  $||| \cdot |||_{K_F^*}^{tp}$  define norms in  $\mathbb{T}_F(K_F)$ . We then have that:

$$\begin{aligned} a_{K_F}^{tp}((\boldsymbol{\omega}_F, q); (\boldsymbol{\omega}_F, q)) &\equiv \\ &\quad \int_{\mathcal{F}_h^{Out}} \left[ \frac{1}{c_F^2 \rho_F} q^2 n_{K_F}^t + \rho_F \boldsymbol{\omega}_F \cdot \boldsymbol{\omega}_F n_{K_F}^t + 2q \boldsymbol{\omega}_F \cdot \mathbf{n}_{K_F}^x \right] ds \\ &\quad + \frac{1}{2} \int_{\mathcal{F}_h^{In}} \left[ \frac{1}{c_F^2 \rho_F} q^2 n_{K_F}^t + \rho_F \boldsymbol{\omega}_F \cdot \boldsymbol{\omega}_F n_{K_F}^t + 2q \boldsymbol{\omega}_F \cdot \mathbf{n}_{K_F}^x \right] ds \\ &\quad - \beta_2 \int_{\mathcal{F}_h^{In}} \frac{1}{c_F^2 \rho_F} q^2 n_{K_F}^t ds - \alpha_2 \int_{\mathcal{F}_h^{In}} \rho_F \boldsymbol{\omega}_F \cdot \boldsymbol{\omega}_F n_{K_F}^t ds \\ &\quad + \int_{\mathcal{F}_h^{Ext}} \left[ q \boldsymbol{\omega}_F \cdot \mathbf{n}_{K_F}^x + \alpha_1 (\boldsymbol{\omega}_F \cdot \mathbf{n}_{K_F}^x) (\boldsymbol{\omega}_F \cdot \mathbf{n}_{K_F}^x) \right] ds \\ &\quad + \int_{\mathcal{F}_h^{Int}} \left[ \{q\} [\boldsymbol{\omega}_F]_x + \{\boldsymbol{\omega}_F\} \cdot [q]_x + \alpha_1 [\boldsymbol{\omega}_F]_x [\boldsymbol{\omega}_F]_x + \beta_1 [q]_x \cdot [q]_x \right] ds = \end{aligned}$$

$$\begin{aligned}
& \overbrace{\int_{\mathcal{F}_h^{Out}} \frac{1}{2n_{K_F}^t} \left[ \frac{1}{c_F^2 \rho_F} (qn_{K_F}^t)^2 + \rho_F (\boldsymbol{\omega}_F n_{K_F}^t) \cdot (\boldsymbol{\omega}_F n_{K_F}^t) + 2(qn_{K_F}^t) (\boldsymbol{\omega}_F \cdot \mathbf{n}_{K_F}^x) \right]}^{[6]} ds \\
& + \frac{1}{2} \overbrace{\int_{\mathcal{F}_h^{Out} \cup \mathcal{F}_h^{In}} \left[ \frac{1}{c_F^2 \rho_F} qq n_{K_F}^t + \rho_F \boldsymbol{\omega}_F \cdot \boldsymbol{\omega}_F n_{K_F}^t \right]}^{[4]} ds + \overbrace{\int_{\mathcal{F}_h^{Int}} \left[ \alpha_1 \llbracket \boldsymbol{\omega}_F \rrbracket_x \llbracket \boldsymbol{\omega}_F \rrbracket_x + \beta_1 \llbracket q \rrbracket_x \cdot \llbracket q \rrbracket_x \right]}^{[1]} ds \\
& + \overbrace{\int_{\mathcal{F}_h^{In}} \beta_2 \frac{1}{c_F^2 \rho_F} (q|n_{K_F}^t|^{1/2})^2 ds + \int_{\mathcal{F}_h^{In}} \alpha_2 \rho_F (\boldsymbol{\omega}_F |n_{K_F}^t|^{1/2}) \cdot (\boldsymbol{\omega}_F |n_{K_F}^t|^{1/2}) ds}^{[2]} \\
& + \overbrace{\int_{\mathcal{F}_h^{Out} \cup \mathcal{F}_h^{In} \cup \mathcal{F}_h^{Ext}} q \boldsymbol{\omega}_F \cdot \mathbf{n}_{K_F}^x ds + \int_{\mathcal{F}_h^{Int}} \left[ \{q\} \llbracket \boldsymbol{\omega}_F \rrbracket_x + \{ \boldsymbol{\omega}_F \} \cdot \llbracket q \rrbracket_x \right]}^{[5]} ds \\
& + \overbrace{\int_{\mathcal{F}_h^{Ext}} \alpha_1 (\boldsymbol{\omega}_F \cdot \mathbf{n}_{K_F}^x) (\boldsymbol{\omega}_F \cdot \mathbf{n}_{K_F}^x) ds}^{[3]}.
\end{aligned}$$

Each term of the above equality is estimated in mesh-dependent  $L^2$ -norms as follows:

$$[1] \equiv \int_{\mathcal{F}_h^{Int}} \left[ \alpha_1 \llbracket \boldsymbol{\omega}_F \rrbracket_x \llbracket \boldsymbol{\omega}_F \rrbracket_x + \beta_1 \llbracket q \rrbracket_x \cdot \llbracket q \rrbracket_x \right] ds = \left\| \alpha_1^{1/2} \llbracket \boldsymbol{\omega}_F \rrbracket_x \right\|_{L^2(\mathcal{F}_h^{Int})}^2 + \left\| \beta_1^{1/2} \llbracket q \rrbracket_x \right\|_{L^2(\mathcal{F}_h^{Int})}^2;$$

$$\begin{aligned}
[2] & \equiv \int_{\mathcal{F}_h^{In}} \beta_2 \frac{1}{c_F^2 \rho_F} (q|n_{K_F}^t|^{1/2})^2 ds + \int_{\mathcal{F}_h^{In}} \alpha_2 \rho_F (\boldsymbol{\omega}_F |n_{K_F}^t|^{1/2}) \cdot (\boldsymbol{\omega}_F |n_{K_F}^t|^{1/2}) ds = \\
& \left\| \beta_2^{1/2} \left( \frac{1}{c_F^2 \rho_F} \right)^{1/2} q |n_{K_F}^t|^{1/2} \right\|_{L^2(\mathcal{F}_h^{In})}^2 + \left\| \alpha_2^{1/2} \rho_F^{1/2} \boldsymbol{\omega}_F |n_{K_F}^t|^{1/2} \right\|_{L^2(\mathcal{F}_h^{In})}^2
\end{aligned}$$

$$[3] \equiv \int_{\mathcal{F}_h^{Ext}} \alpha_1 (\boldsymbol{\omega}_F \cdot \mathbf{n}_{K_F}^x) (\boldsymbol{\omega}_F \cdot \mathbf{n}_{K_F}^x) ds = \left\| \alpha_1^{1/2} (\boldsymbol{\omega}_F \cdot \mathbf{n}_{K_F}^x) \right\|_{L^2(\mathcal{F}_h^{Ext})}^2;$$

$$[4] \equiv \frac{1}{2} \int_{\mathcal{F}_h^{Out} \cup \mathcal{F}_h^{In}} \left[ \frac{1}{c_F^2 \rho_F} qq n_{K_F}^t + \rho_F \boldsymbol{\omega}_F \cdot \boldsymbol{\omega}_F n_{K_F}^t \right] ds = \int_{K_F} \left[ \frac{1}{c_F^2 \rho_F} q \frac{\partial q}{\partial t} + \rho_F \boldsymbol{\omega}_F \cdot \frac{\partial \boldsymbol{\omega}_F}{\partial t} \right] dv;$$

$$\begin{aligned}
[5] & \equiv \int_{\mathcal{F}_h^{Int}} \left[ \{q\} \llbracket \boldsymbol{\omega}_F \rrbracket_x + \{ \boldsymbol{\omega}_F \} \cdot \llbracket q \rrbracket_x \right] ds + \int_{\mathcal{F}_h^{Out} \cup \mathcal{F}_h^{In} \cup \mathcal{F}_h^{Ext}} q \boldsymbol{\omega}_F \cdot \mathbf{n}_{K_F}^x ds = \\
& \int_{\mathcal{F}_h^{Int}} \llbracket q \boldsymbol{\omega}_F \rrbracket_x ds + \int_{\mathcal{F}_h^{Out} \cup \mathcal{F}_h^{In} \cup \mathcal{F}_h^{Ext}} q \boldsymbol{\omega}_F \cdot \mathbf{n}_{K_F}^x ds = \int_{K_F} \left[ \boldsymbol{\omega}_F \cdot \nabla q + q \operatorname{div} \boldsymbol{\omega}_F \right] dv;
\end{aligned}$$

$$\begin{aligned}
[4] + [5] &\equiv \int_{K_F} \left[ \boldsymbol{\omega}_F \cdot \nabla q + q \operatorname{div} \boldsymbol{\omega}_F + \frac{1}{c_F^2 \rho_F} q \frac{\partial q}{\partial t} + \rho_F \boldsymbol{\omega}_F \cdot \frac{\partial \boldsymbol{\omega}_F}{\partial t} \right] dv = \\
&\int_{K_F} \underbrace{q \left( \frac{1}{c_F^2 \rho_F} \frac{\partial q}{\partial t} + \operatorname{div} \boldsymbol{\omega}_F \right)}_{=0 \text{ in } \mathbf{T}_F(K_F)} dv + \int_{K_F} \underbrace{\boldsymbol{\omega}_F \cdot \left( \rho_F \frac{\partial \boldsymbol{\omega}_F}{\partial t} + \nabla q \right)}_{=0 \text{ in } \mathbf{T}_F(K_F)} dv.
\end{aligned}$$

Thus, for the bilinear form  $a_{K_F}^{tp}(\cdot; \cdot)$  we obtain:

$$\begin{aligned}
a_{K_F}^{tp}((\boldsymbol{\omega}_F, q); (\boldsymbol{\omega}_F, q)) &= \\
&\left\| \alpha_1^{1/2} \llbracket \boldsymbol{\omega}_F \rrbracket_x \right\|_{L^2(\mathcal{F}_h^{Int})}^2 + \left\| \beta_1^{1/2} \llbracket q \rrbracket_x \right\|_{L^2(\mathcal{F}_h^{Int})}^2 + \left\| \alpha_1^{1/2} (\boldsymbol{\omega}_F \cdot \mathbf{n}_{K_F}^x) \right\|_{L^2(\mathcal{F}_h^{Ext})}^2 \\
&+ \left\| \beta_2^{1/2} \left( \frac{1}{c_F^2 \rho_F} \right)^{1/2} q |n_{K_F}^t|^{1/2} \right\|_{L^2(\mathcal{F}_h^{In})}^2 + \left\| \alpha_2^{1/2} \rho_F^{1/2} \boldsymbol{\omega}_F |n_{K_F}^t|^{1/2} \right\|_{L^2(\mathcal{F}_h^{In})}^2 \\
&+ \int_{\mathcal{F}_h^{Out}} \frac{1}{2n_{K_F}^t} \left[ \frac{1}{c_F^2 \rho_F} (qn_{K_F}^t)^2 + \rho_F (\boldsymbol{\omega}_F n_{K_F}^t) \cdot (\boldsymbol{\omega}_F n_{K_F}^t) + 2(qn_{K_F}^t) (\boldsymbol{\omega}_F \cdot \mathbf{n}_{K_F}^x) \right] ds.
\end{aligned}$$

It is worth noting that, by definition of the outflow edges,  $n_{K_F}^t$  is positive at  $\mathcal{F}_h^{Out}$ . Moreover, both values  $n_{K_F}^t$  and  $\mathbf{n}_{K_F}^x$  stay constant at any point of the edge  $\mathcal{F}_h^{Out}$  of the macro-cell  $K_F$  due to its polygonal shape.

If we consider  $\theta_F = \max_{\mathcal{F}_h^{Out}(K_F)} \frac{c_F |\mathbf{n}_{K_F}^x|}{|n_{K_F}^t|} \in [0, 1)$  the following coercivity estimate:

$$a_{K_F}^{tp}((\boldsymbol{\omega}_F, q); (\boldsymbol{\omega}_F, q)) \geq |||(\boldsymbol{\omega}_F, q)|||_{K_F}^{tp^2}, \quad \forall (\boldsymbol{\omega}_F, q) \in \mathbf{T}_F(K_F).$$

To establish the continuity property we bound above each term of the bilinear and linear forms using weighted Cauchy-Schwartz inequality. Summing the contribution of each term, we obtain the following continuity estimates:

$$\begin{aligned}
|a_{K_F}^{tp}((\mathbf{v}_F, p); (\boldsymbol{\omega}_F, q))| &\leq C_1^{tp} |||(\mathbf{v}_F, p)|||_{K_F^*}^{tp} |||(\boldsymbol{\omega}_F, q)|||_{K_F}^{tp}, \\
|l_{K_F}^{tp}(\boldsymbol{\omega}_F, q)| &\leq \\
&\left[ \left\| \left( \frac{1}{2\alpha_2} + 1 \right)^{1/2} \rho_F^{1/2} \mathbf{v}_F^{in} \right\|_{L^2(\mathcal{F}_h^{In})}^2 + \left\| \left( \frac{1}{2\beta_2} + 1 \right)^{1/2} \left( \frac{1}{c_F^2 \rho_F} \right)^{1/2} p^{in} \right\|_{L^2(\mathcal{F}_h^{In})}^2 \right]^{1/2} |||(\boldsymbol{\omega}_F, q)|||_{K_F}^{tp},
\end{aligned}$$

We retain from chapter 3 definitions of the global continuous Trefftz space  $\mathbf{T}_F(\mathcal{T}_{Fh}^{tp})$  and the corresponding discrete Trefftz space  $\mathbf{T}_F^p(\mathcal{T}_{Fh}^{tp})$ . The global tent-pitching Trefftz-DG formulation can be obtained by summing the local results (6.1) over all elements  $K_F$ :

Seek  $(\mathbf{v}_{Fh}, p_h) \in \mathbf{T}_F^p(\mathcal{T}_{Fh}^{tp})$  such that, for all  $(\boldsymbol{\omega}_F, q) \in \mathbf{T}_F^p(\mathcal{T}_{Fh}^{tp})$ , it holds true:

$$\mathcal{A}_{TDG_F}^{tp}((\mathbf{v}_{Fh}, p_h); (\boldsymbol{\omega}_F, q)) = \ell_{TDG_F}^{tp}(\boldsymbol{\omega}_F, q), \quad (6.3)$$

where

$$\begin{aligned} \mathcal{A}_{TDG_F}^{tp}((\mathbf{v}_{Fh}, p_h); (\boldsymbol{\omega}_F, q)) &= \sum_{K_F \in \mathcal{T}_{Fh}^{tp}} a_{K_F}^{tp}((\mathbf{v}_{Fh}|_{K_F}, p_h|_{K_F}); (\boldsymbol{\omega}_F|_{K_F}, q|_{K_F})), \\ \ell_{TDG_F}^{tp}(\boldsymbol{\omega}_F, q) &= \sum_{K_F \in \mathcal{T}_{Fh}^{tp}} l_{K_F}^{tp}(\boldsymbol{\omega}_F|_{K_F}, q|_{K_F}). \end{aligned}$$

The norms  $||| \cdot |||_{TDG_F}^{tp}$  and  $||| \cdot |||_{TDG_F^*}^{tp}$  in  $\mathbf{T}_F(\mathcal{T}_{Fh}^{tp})$  can be defined by summing the corresponding local norms  $||| \cdot |||_{K_F}^{tp}$  and  $||| \cdot |||_{K_F^*}^{tp}$  over all elements  $K_F$ .

The coercivity and continuity properties of the global bilinear and linear forms (6.3), as well as the consistency of  $\mathcal{A}_{TDG_F}^{tp}(\cdot; \cdot)$  follows from the ones for each local bilinear and linear forms.

**Theorem 6.1.** Let  $\theta_F = \max_{\mathcal{F}_h^{Out}(K_F)} \frac{c_F |\mathbf{n}_{K_F}^x|}{|\mathbf{n}_{K_F}^t|}$ . Then if  $\theta_F \in [0, 1)$ , the global variational problem (6.3) admits a unique weak solution  $(\mathbf{v}_{Fh}, p_h) \in \mathbf{T}_F^p(\mathcal{T}_{Fh}^{tp})$ . Moreover, the following estimate holds true:

$$|||(\mathbf{v}_F - \mathbf{v}_{Fh}, p - p_h)|||_{TDG_F}^{tp} \leq (1 + C_1^{tp}) \inf_{(\boldsymbol{\omega}_F, q) \in \mathbf{T}_F^p(\mathcal{T}_{Fh}^{tp})} |||(\mathbf{v}_F - \boldsymbol{\omega}_F, p - q)|||_{TDG_F^*}^{tp}.$$

*Proof.* The well-posedness of the global problem (6.3) follows straightforwardly from the coercivity and continuity estimations, the consistency of the global bilinear form, and from the fact that  $\mathbf{T}_F^p(\mathcal{T}_{Fh}^{tp})$  is a finite dimensional space.  $\square$

With respect to the different cell types (see figure 6.6), the local linear system (6.1) can be rewritten in vector-matrix form.

**Tent of a homogeneous type:**

$$M_{K_F} U_{K_F} = B_{K_F}^{In_1} U_{K_F}^{In_1} + B_{K_F}^{In_2} U_{K_F}^{In_2}. \quad (6.4)$$

Here,  $M_{K_F}$  is the matrix that corresponds to the left-hand side bilinear operator  $a_{K_F}^{tp}(\cdot; \cdot)$ , computed inside the element  $K_F$ , and acting on the vector  $U_{K_F}$  of unknowns,  $B_{K_F}^{In_1}$  and  $B_{K_F}^{In_2}$  are the right-hand side linear form, computed inside the cell  $K_F$ , and acting on the vectors  $U_{K_F}^{In_1}$  and  $U_{K_F}^{In_2}$ , that correspond to the numerical solution set on the inflow edge of  $K_F$  and computed previously in the neighbour to  $K_F$  tents (double line in figure 6.6(a)).

**Tent of a regular boundary type:**

$$M_{K_F} U_{K_F} = B_{K_F}^{In} U_{K_F}^{In} + B_{K_F}^{Ext} U_{K_F}^{Ext}. \quad (6.5)$$

Compared to the previous case, this formulation involves the right-hand side linear operator  $B_{K_F}^{Ext}$  which corresponds to the integration at the external vertical edges (thick line in figure 6.6(b)).

**Tent of the regular and irregular heterogeneous type:**

$$M_{K_F} [U_{K_{F1}}, U_{K_{F2}}] = B_{K_{F1}}^{In} U_{K_{F1}}^{In} + B_{K_{F2}}^{In} U_{K_{F2}}^{In}. \quad (6.6)$$

This formulation couples two sub-cells  $K_{F1}$   $K_{F2}$  with different parameters through the internal vertical edge (dashed line in figure 6.6(c)). It is worth noting that in this case the matrix  $M_{K_F}$  represents the left-hand side bilinear form for the macro-cell composed of elementary sub-cells.

It is important to mention that the stability condition  $c_F |\mathbf{n}_{K_F}^x| \leq |n_{K_F}^t|$  can be considered as a CFL condition.

### 6.2.2 Tent-pitching Trefftz-DG formulation for the elastodynamic system

As in the acoustic case (section 6.2.1), we introduce a conforming space-time mesh  $\mathcal{T}_{Sh}^{tp}$  on  $Q_S \equiv \Omega_S \times I$  of non-overlapping arbitrarily-shaped space-time elements  $K_S \in \mathcal{T}_{Sh}^{tp}$ , whose edges belong to the classes:  $\mathcal{F}_h^{In}$ ,  $\mathcal{F}_h^{Out}$ ,  $\mathcal{F}_h^{Int}$  or  $\mathcal{F}_h^{Ext}$  (see section 6.2.1).

Similarly to the previous section, we introduce the the local Trefftz space  $T_S(K_S)$  is defined in each  $K_S$  by:

$$T_S(K_S) \equiv \left\{ (\boldsymbol{\omega}_S, \underline{\boldsymbol{\xi}}) \in V^h(K_S)^d \times V^h(K_S)^{d^2} \text{ such that, } \underline{\mathbf{A}} \frac{\partial \underline{\boldsymbol{\xi}}}{\partial t} - \underline{\boldsymbol{\varepsilon}}(\boldsymbol{\omega}_S) = 0 \text{ and } \rho_S \frac{\partial \boldsymbol{\omega}_S}{\partial t} - \mathbf{div} \underline{\boldsymbol{\xi}} = 0 \text{ in } K_S \in \mathcal{T}_{Sh}^{tp} \right\},$$

and the corresponding discrete Trefftz space  $T_S^p(\mathcal{T}_{Sh}^{tp})$  defined by:

$$T_S^p(K_S) \equiv \left\{ (\boldsymbol{\omega}_S, \underline{\boldsymbol{\xi}}) \in T_S(K_S), (\boldsymbol{\omega}_S, \underline{\boldsymbol{\xi}}) \in \mathbb{P}^p(K_S)^d \times \mathbb{P}^p(K_S)^{d^2} \right\}.$$

The local Trefftz-DG formulation for the first order ES (3.11) in the element  $K_S$  reads as follows:

Seek  $(\mathbf{v}_{Sh}, \underline{\boldsymbol{\sigma}}_h) \in \mathbb{T}_S^p(K_S)$  such that, for all  $K_S \in \mathcal{T}_{Sh}^{tp}$  and for all  $(\boldsymbol{\omega}_S, \underline{\boldsymbol{\xi}}) \in \mathbb{T}_S^p(K_S)$ , it holds true:

$$a_{K_S}^{tp}((\mathbf{v}_{Sh}, \underline{\boldsymbol{\sigma}}_h); (\boldsymbol{\omega}_S, \underline{\boldsymbol{\xi}})) = l_{K_S}^{tp}(\boldsymbol{\omega}_S, \underline{\boldsymbol{\xi}}). \quad (6.7)$$

The bilinear form  $a_{K_S}^{tp}(\cdot; \cdot)$  is defined by:

$$\begin{aligned} a_{K_S}^{tp}((\mathbf{v}_{Sh}, \underline{\boldsymbol{\sigma}}_h); (\boldsymbol{\omega}_S, \underline{\boldsymbol{\xi}})) \equiv & \int_{\mathcal{F}_h^{Out}} \left[ \underline{\mathbf{A}} \underline{\boldsymbol{\sigma}}_h : \underline{\boldsymbol{\xi}} \mathbf{n}_{K_S}^t + \rho_S \mathbf{v}_{Sh} \cdot \boldsymbol{\omega}_S \mathbf{n}_{K_S}^t - \underline{\boldsymbol{\sigma}}_h : (\boldsymbol{\omega}_S \otimes \mathbf{n}_{K_S}^x) - \underline{\boldsymbol{\xi}} \mathbf{v}_{Sh} \cdot \mathbf{n}_{K_S}^x \right] ds \\ & + \left(\frac{1}{2} - \delta_2\right) \int_{\mathcal{F}_h^{In}} \underline{\mathbf{A}} \underline{\boldsymbol{\sigma}}_h : \underline{\boldsymbol{\xi}} \mathbf{n}_{K_S}^t ds + \left(\frac{1}{2} - \gamma_2\right) \int_{\mathcal{F}_h^{In}} \rho_S \mathbf{v}_{Sh} \cdot \boldsymbol{\omega}_S \mathbf{n}_{K_S}^t ds \\ & - \frac{1}{2} \int_{\mathcal{F}_h^{In}} \left[ \underline{\boldsymbol{\sigma}}_h : (\boldsymbol{\omega}_S \otimes \mathbf{n}_{K_S}^x) - \underline{\boldsymbol{\xi}} \mathbf{v}_{Sh} \cdot \mathbf{n}_{K_S}^x \right] ds \\ & - \int_{\mathcal{F}_h^{Ext}} \left[ \underline{\boldsymbol{\xi}} \mathbf{v}_{Sh} \cdot \mathbf{n}_{K_S}^x - \delta_1 (\underline{\boldsymbol{\sigma}}_h \mathbf{n}_{K_S}^x) \cdot (\underline{\boldsymbol{\xi}} \mathbf{n}_{K_S}^x) \right] ds \\ & - \int_{\mathcal{F}_h^{Int}} \left[ \{\underline{\boldsymbol{\sigma}}_h\} : \llbracket \boldsymbol{\omega}_S \rrbracket_x + \{\mathbf{v}_{Sh}\} \cdot \llbracket \underline{\boldsymbol{\xi}} \rrbracket_x - \gamma_1 \llbracket \mathbf{v}_{Sh} \rrbracket_x : \llbracket \boldsymbol{\omega}_S \rrbracket_x - \delta_1 \llbracket \underline{\boldsymbol{\sigma}}_h \rrbracket_x \cdot \llbracket \underline{\boldsymbol{\xi}} \rrbracket_x \right] ds, \end{aligned}$$

and the linear form  $l_{K_S}^{tp}(\cdot)$  is defined by:

$$\begin{aligned} l_{K_S}^{tp}(\boldsymbol{\omega}_S, \underline{\boldsymbol{\xi}}) \equiv & -\left(\frac{1}{2} + \delta_2\right) \int_{\mathcal{F}_h^{In}} \underline{\mathbf{A}} \underline{\boldsymbol{\sigma}}_h^{in} : \underline{\boldsymbol{\xi}} \mathbf{n}_{K_S}^t ds - \left(\frac{1}{2} + \gamma_2\right) \int_{\mathcal{F}_h^{In}} \rho_S \mathbf{v}_{Sh}^{in} \cdot \boldsymbol{\omega}_S \mathbf{n}_{K_S}^t ds \\ & - \frac{1}{2} \int_{\mathcal{F}_h^{In}} \left[ \underline{\boldsymbol{\sigma}}_h^{in} : (\boldsymbol{\omega}_S \otimes \mathbf{n}_{K_S}^x) - \underline{\boldsymbol{\xi}} \mathbf{v}_{Sh}^{in} \cdot \mathbf{n}_{K_S}^x \right] ds + \int_{\mathcal{F}_h^{Ext}} \left[ \delta_1 \underline{\boldsymbol{\xi}} \mathbf{g}_{D_S} \cdot \mathbf{n}_{K_S}^x + \mathbf{g}_{D_S} \cdot \boldsymbol{\omega}_S \right] ds. \end{aligned}$$

Here again, we restrict the problem to the homogeneous system with  $\mathbf{g}_{D_S} \equiv 0$ , since this term appears in the right-hand side of formulation, and can always be bounded above, provided  $\mathbf{g}_{D_S}$  is regular enough.

The study of elastodynamic formulation requires exactly the same steps as the acoustic case. Hence, we only provide the results without detailing the calculations. We introduce parameter  $\theta_S \equiv \max_{\mathcal{F}_h^{Out}(K_S)} \frac{|\mathbf{n}_{K_S}^x|}{\sqrt{\rho_S |\underline{\mathbf{A}}| |\mathbf{n}_{K_S}^t|}}$ , and we define two quantities:

$$\begin{aligned}
|||(\boldsymbol{\omega}_S, \underline{\boldsymbol{\xi}})|||_{K_S}^{tp} &\equiv \left[ \frac{1-\theta_S}{2} \left\| |\underline{\boldsymbol{\xi}}|_{\underline{\mathbf{A}}} (n_{K_S}^t)^{1/2} \right\|_{L^2(\mathcal{F}_h^{Out})}^2 + \frac{1-\theta_S}{2} \left\| \rho_S^{1/2} \boldsymbol{\omega}_S (n_{K_S}^t)^{1/2} \right\|_{L^2(\mathcal{F}_h^{Out})}^2 \right. \\
&\quad + \frac{\theta_S}{2} \left\| |\underline{\boldsymbol{\xi}}|_{\underline{\mathbf{A}}} (n_{K_S}^t)^{1/2} + \rho_S^{1/2} \boldsymbol{\omega}_S (n_{K_S}^t)^{1/2} \right\|_{L^2(\mathcal{F}_h^{Out})}^2 \\
&\quad + \left\| \delta_2^{1/2} |\underline{\boldsymbol{\xi}}|_{\underline{\mathbf{A}}} |n_{K_S}^t|^{1/2} \right\|_{L^2(\mathcal{F}_h^{In})}^2 + \left\| \gamma_2^{1/2} \rho_S^{1/2} \boldsymbol{\omega}_S |n_{K_S}^t|^{1/2} \right\|_{L^2(\mathcal{F}_h^{In})}^2 \\
&\quad \left. + \left\| \delta_1^{1/2} (\underline{\boldsymbol{\xi}} \mathbf{n}_{K_S}^x) \right\|_{L^2(\mathcal{F}_h^{Ext})}^2 + \left\| \gamma_1^{1/2} \llbracket \boldsymbol{\omega}_S \rrbracket_x \right\|_{L^2(\mathcal{F}_h^{Int})}^2 + \left\| \delta_1^{1/2} \llbracket \underline{\boldsymbol{\xi}} \rrbracket_x \right\|_{L^2(\mathcal{F}_h^{Int})}^2 \right]^{1/2},
\end{aligned}$$

$$\begin{aligned}
|||(\boldsymbol{\omega}_S, \underline{\boldsymbol{\xi}})|||_{K_S^*}^{tp} &\equiv \left[ (|||(\boldsymbol{\omega}_S, \underline{\boldsymbol{\xi}})|||_{K_S}^{tp})^2 \right. \\
&\quad + \frac{1}{1-\theta_S} \left\| \rho_S^{1/2} \boldsymbol{\omega}_S (n_{K_S}^t)^{1/2} \right\|_{L^2(\mathcal{F}_h^{Out})}^2 + \frac{1}{1-\theta_S} \left\| |\underline{\boldsymbol{\xi}}|_{\underline{\mathbf{A}}} (n_{K_S}^t)^{1/2} \right\|_{L^2(\mathcal{F}_h^{Out})}^2 \\
&\quad + \left\| \left( \frac{1}{2\delta_2} + 1 \right)^{1/2} |\underline{\boldsymbol{\xi}}|_{\underline{\mathbf{A}}} \right\|_{\mathcal{F}_h^{In}}^2 + \left\| \left( \frac{1}{2\gamma_2} + 1 \right)^{1/2} \rho_S^{1/2} \boldsymbol{\omega}_S \right\|_{\mathcal{F}_h^{In}}^2 \\
&\quad \left. + \left\| \delta_1^{-1/2} \underline{\boldsymbol{\xi}} \right\|_{L^2(\mathcal{F}_h^{Ext})}^2 + \left\| \delta_1^{-1/2} \llbracket \boldsymbol{\omega}_S \rrbracket \right\|_{L^2(\mathcal{F}_h^{Int})}^2 + \left\| \gamma_1^{-1/2} \llbracket \underline{\boldsymbol{\xi}} \rrbracket \right\|_{L^2(\mathcal{F}_h^{Int})}^2 \right]^{1/2}.
\end{aligned}$$

If  $\theta_S \in [0, 1)$ ,  $||| \cdot |||_{K_S^*}^{tp}$  and  $||| \cdot |||_{K_S}^{tp}$  define two norms in  $\mathbf{T}_S(K_S)$ . Moreover, if  $\theta_S \in [0, 1)$  we have

$$a_{K_S}^{tp}((\boldsymbol{\omega}_S, \underline{\boldsymbol{\xi}}); (\boldsymbol{\omega}_S, \underline{\boldsymbol{\xi}})) \geq |||(\boldsymbol{\omega}_S, \underline{\boldsymbol{\xi}})|||_{K_S}^{tp^2},$$

and

$$|a_{K_S}^{tp}((\mathbf{v}_S, \underline{\boldsymbol{\sigma}}); (\boldsymbol{\omega}_S, \underline{\boldsymbol{\xi}}))| \leq C_2^{tp} |||(\mathbf{v}_S, \underline{\boldsymbol{\sigma}})|||_{K_S^*}^{tp} |||(\boldsymbol{\omega}_S, \underline{\boldsymbol{\xi}})|||_{K_S}^{tp},$$

$$\begin{aligned}
|l_{K_S}^{tp}(\boldsymbol{\omega}_S, \underline{\boldsymbol{\xi}})| &\leq \\
&\left[ \left\| \left( \frac{1}{\gamma_2} + 1 \right)^{1/2} \rho_S^{1/2} \mathbf{v}_S^{in} \right\|_{L^2(\mathcal{F}_h^{In})}^2 + \left\| \left( \frac{1}{\delta_2} + 1 \right)^{1/2} |\underline{\boldsymbol{\sigma}}|_{\underline{\mathbf{A}}} n_{K_S}^t \right\|_{L^2(\mathcal{F}_h^{In})}^2 \right]^{1/2} |||(\boldsymbol{\omega}_S, \underline{\boldsymbol{\xi}})|||_{K_S}^{tp},
\end{aligned}$$

which says that  $a_{K_S}^{tp}(\cdot; \cdot)$  is coercive and continuous, and  $l_{K_S}^{tp}(\cdot)$  is continuous.

Summing the local results (6.7) over all elements  $K_S$ , we obtain the global tent-pitching Trefftz-DG problem, defined in the global discrete Trefftz space  $\mathbf{T}_S^p(\mathcal{T}_{Sh}^{tp})$  by:

Seek  $(\mathbf{v}_{Sh}, \underline{\boldsymbol{\sigma}}_h) \in \mathbf{T}_S^p(\mathcal{T}_{Sh}^{tp})$  such that, for all  $(\boldsymbol{\omega}_S, \underline{\boldsymbol{\xi}}) \in \mathbf{T}_S^p(\mathcal{T}_{Sh}^{tp})$ , it holds true:

$$\mathcal{A}_{TDG_S}^{tp}((\mathbf{v}_{Sh}, \underline{\boldsymbol{\sigma}}_h); (\boldsymbol{\omega}_S, \underline{\boldsymbol{\xi}})) = \ell_{TDG_S}^{tp}(\boldsymbol{\omega}_S, \underline{\boldsymbol{\xi}}), \quad (6.8)$$

where

$$\begin{aligned} \mathcal{A}_{TDG_S}^{tp}((\mathbf{v}_{Sh}, \underline{\boldsymbol{\sigma}}_h); (\boldsymbol{\omega}_S, \underline{\boldsymbol{\xi}})) &\equiv \sum_{K_S \in \mathcal{T}_{Sh}^{tp}} a_{K_S}^{tp}((\mathbf{v}_{Sh}|_{K_S}, \underline{\boldsymbol{\sigma}}_h|_{K_S}); (\boldsymbol{\omega}_S|_{K_S}, \underline{\boldsymbol{\xi}}|_{K_S})), \\ \ell_{TDG_S}^{tp}(\boldsymbol{\omega}_S, \underline{\boldsymbol{\xi}}) &\equiv \sum_{K_S \in \mathcal{T}_{Sh}^{tp}} \ell_{K_S}^{tp}(\boldsymbol{\omega}_S|_{K_S}, \underline{\boldsymbol{\xi}}|_{K_S}). \end{aligned}$$

If  $\theta_S \in [0, 1)$ , the consistency of each  $a_{K_S}^{tp}(\cdot, \cdot)$ , the coercivity and continuity properties of the bilinear and linear forms of each local problem (6.7) provide the consistency of  $\mathcal{A}_{TDG_S}^{tp}(\cdot; \cdot)$ , as well as the coercivity and the continuity properties of the global bilinear and linear forms with respect to the norms defined by:

$$\begin{aligned} |||(\boldsymbol{\omega}_S, \underline{\boldsymbol{\xi}})|||_{TDG_S}^{tp} &\equiv \sum_{K_S \in \mathcal{T}_{Sh}^{tp}} |||(\boldsymbol{\omega}_S|_{K_S}, \underline{\boldsymbol{\xi}}|_{K_S})|||_{K_S}^{tp}, \\ |||(\boldsymbol{\omega}_S, \underline{\boldsymbol{\xi}})|||_{TDG_S^*}^{tp} &\equiv \sum_{K_S \in \mathcal{T}_{Sh}^{tp}} |||(\boldsymbol{\omega}_S|_{K_S}, \underline{\boldsymbol{\xi}}|_{K_S})|||_{K_S^*}^{tp}. \end{aligned}$$

**Theorem 6.2.** *If  $\theta_S \in [0, 1)$ , the global variational problem (6.8) admits a unique weak solution  $(\mathbf{v}_{Sh}, \underline{\boldsymbol{\sigma}}_h) \in \mathbf{T}_S^p(\mathcal{T}_{Sh}^{tp})$ . Moreover, the following estimate holds true:*

$$|||(\mathbf{v}_S - \mathbf{v}_{Sh}, \underline{\boldsymbol{\sigma}} - \underline{\boldsymbol{\sigma}}_h)|||_{TDG_S}^{tp} \leq (1 + C_2^{tp}) \inf_{(\boldsymbol{\omega}_S, \underline{\boldsymbol{\xi}}) \in \mathbf{T}_S^p(\mathcal{T}_{Sh}^{tp})} |||(\mathbf{v}_S - \boldsymbol{\omega}_S, \underline{\boldsymbol{\sigma}} - \underline{\boldsymbol{\xi}})|||_{TDG_S^*}^{tp}.$$

*Proof.* The well-posedness of the global problem (6.3) follows straightforwardly from the coercivity and continuity estimations, the consistency of the global bilinear form, and from the fact that  $\mathbf{T}_S^p(\mathcal{T}_{Sh}^{tp})$  is a finite dimensional space.  $\square$

We refer to section 6.2.1 for the vector-matrix formulations of the linear system (6.7) with respect to the different tent types. The same conclusions hold true.

### 6.2.3 Tent-pitching Trefftz-DG formulation for the elasto-acoustic system

We retain the definitions from the previous sections 6.2.1 and 6.2.2. We introduce a conforming space-time mesh  $\mathcal{T}_h^{tp}$  on  $Q \equiv Q_F \cup Q_S$  of non-overlapping arbitrarily-shaped space-time elements:

- $K_{FF}$  - element in fluid with no neighbours in solid
- $K_{SS}$  - element in solid with no neighbours in fluid
- $K_{FS}$  - element in fluid with a neighbour in solid
- $K_{SF}$  - element in solid with a neighbour in fluid

For any element  $K_{FS}$  and its neighbour in solid  $K_{SF}$ , we define the macro-element  $K = K_{FS} \cup K_{SF}$ . The elasto-acoustic coupling leads us to introduce a fourth type of tent, which corresponds to the numerical coupling of elementary sub-cells through the fluid-solid interface inside one macro-cell  $K = K_{FS} \cup K_{SF}$  (see figure 6.7).

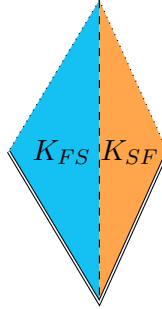


FIGURE 6.7: Fourth type of space-time tents (heterogeneous fluid-solid macro-cell).

The local Trefftz-DG formulation for the first order Elasto-Acoustic System (EAS) in macro-element  $K \in \mathcal{T}_h^{tp}$  reads as follows:

Seek  $(\mathbf{v}_{Fh}, p_h, \mathbf{v}_{Sh}, \underline{\boldsymbol{\sigma}}_h) \in \mathbb{T}_F^p(K_{FS}) \times \mathbb{T}_S^p(K_{SF}) \equiv \mathbb{T}^p(K)$  such that, for all  $(\boldsymbol{\omega}_F, q, \boldsymbol{\omega}_S, \underline{\boldsymbol{\xi}}) \in \mathbb{T}^p(K)$ , it holds true:

$$a_K^{tp}((\mathbf{v}_{Fh}, p_h, \mathbf{v}_{Sh}, \underline{\boldsymbol{\sigma}}_h); (\boldsymbol{\omega}_F, q, \boldsymbol{\omega}_S, \underline{\boldsymbol{\xi}})) = l_K^{tp}(\boldsymbol{\omega}_F, q, \boldsymbol{\omega}_S, \underline{\boldsymbol{\xi}}). \quad (6.9)$$

Herein, the linear form  $l_K^{tp}(\cdot)$  is defined in the terms of:  $l_{K_F}^{tp}(\cdot)$  and  $l_{K_S}^{tp}(\cdot)$  by:

$$l_K^{tp}(\boldsymbol{\omega}_F, q, \boldsymbol{\omega}_S, \underline{\boldsymbol{\xi}}) = l_{K_F}^{tp}(\boldsymbol{\omega}_F, q) + l_{K_S}^{tp}(\boldsymbol{\omega}_S, \underline{\boldsymbol{\xi}}),$$

and the bilinear form  $a_K^{tp}(\cdot; \cdot)$  is defined by:

$$\begin{aligned} a_K^{tp}((\mathbf{v}_{Fh}, p_h, \mathbf{v}_{Sh}, \underline{\boldsymbol{\sigma}}_h); (\boldsymbol{\omega}_F, q, \boldsymbol{\omega}_S, \underline{\boldsymbol{\xi}})) \equiv & \\ & \int_{\mathcal{F}_h^{Out}} \left[ \frac{1}{c_F^2 \rho_F} p_h q n_{K_F}^t + \rho_F \mathbf{v}_{Fh} \cdot \boldsymbol{\omega}_F n_{K_F}^t + p_h \boldsymbol{\omega}_F \cdot \mathbf{n}_{K_F}^x + q \mathbf{v}_{Fh} \cdot \mathbf{n}_{K_F}^x \right] ds \\ & \int_{\mathcal{F}_h^{Out}} \left[ \underline{\mathbf{A}} \underline{\boldsymbol{\sigma}}_h : \underline{\boldsymbol{\xi}} n_{K_S}^t + \rho_S \mathbf{v}_{Sh} \cdot \boldsymbol{\omega}_S n_{K_S}^t - \underline{\boldsymbol{\sigma}}_h : (\boldsymbol{\omega}_S \otimes \mathbf{n}_{K_S}^x) - \underline{\boldsymbol{\xi}} \mathbf{v}_{Sh} \cdot \mathbf{n}_{K_S}^x \right] ds \\ & + \frac{1}{2} \int_{\mathcal{F}_h^{In}} \left[ \frac{1}{c_F^2 \rho_F} p_h q n_{K_F}^t + \rho_F \mathbf{v}_{Fh} \cdot \boldsymbol{\omega}_F n_{K_F}^t + p_h \boldsymbol{\omega}_F \cdot \mathbf{n}_{K_F}^x + q \mathbf{v}_{Fh} \cdot \mathbf{n}_{K_F}^x \right] ds \\ & + \frac{1}{2} \int_{\mathcal{F}_h^{In}} \left[ \underline{\mathbf{A}} \underline{\boldsymbol{\sigma}}_h : \underline{\boldsymbol{\xi}} n_{K_S}^t + \rho_S \mathbf{v}_{Sh} \cdot \boldsymbol{\omega}_S n_{K_S}^t - \underline{\boldsymbol{\sigma}}_h : (\boldsymbol{\omega}_S \otimes \mathbf{n}_{K_S}^x) - \underline{\boldsymbol{\xi}} \mathbf{v}_{Sh} \cdot \mathbf{n}_{K_S}^x \right] ds \end{aligned}$$

$$\begin{aligned}
& + \beta_2 \int_{\mathcal{F}_h^{In}} \frac{1}{c_F^2 \rho_F} p_h q n_{K_F}^t ds + \alpha_2 \int_{\mathcal{F}_h^{In}} + \rho_F \mathbf{v}_{Fh} \cdot \boldsymbol{\omega}_F n_{K_F}^t ds \\
& + \delta_2 \int_{\mathcal{F}_h^{In}} \underline{\underline{\mathbf{A}}} \boldsymbol{\sigma}_h : \underline{\underline{\boldsymbol{\xi}}} n_{K_S}^t + ds + \gamma_2 \int_{\mathcal{F}_h^{In}} \rho_S \mathbf{v}_{Sh} \cdot \boldsymbol{\omega}_S n_{K_S}^t - ds \\
& + \int_{\mathcal{F}_h^{Ext}} \left[ p \boldsymbol{\omega}_F \cdot \mathbf{n}_{K_F}^x + \alpha_1 (\mathbf{v}_{Fh} \cdot \mathbf{n}_{K_F}^x) (\boldsymbol{\omega}_F \cdot \mathbf{n}_{K_F}^x) \right] ds \\
& - \int_{\mathcal{F}_h^{Ext}} \left[ \underline{\underline{\boldsymbol{\xi}}} \mathbf{v}_{Sh} \cdot \mathbf{n}_{K_S}^x - \delta_1 (\boldsymbol{\sigma}_h \mathbf{n}_{K_S}^x) \cdot (\underline{\underline{\boldsymbol{\xi}}} \mathbf{n}_{K_S}^x) \right] ds \\
& + \int_{\mathcal{F}_h^{Int}} \left[ q \mathbf{v}_{Sh} \cdot \mathbf{n}_{K_F}^x - p \boldsymbol{\omega}_S \cdot \mathbf{n}_{K_F}^x \right] ds \\
& + \int_{\mathcal{F}_h^{Int}} \left[ \alpha_1 (\mathbf{v}_{Fh} \cdot \mathbf{n}_{K_F}^x - \mathbf{v}_{Sh} \cdot \mathbf{n}_{K_F}^x) (\boldsymbol{\omega}_F \cdot \mathbf{n}_{K_F}^x - \boldsymbol{\omega}_S \cdot \mathbf{n}_{K_F}^x) \right] ds \\
& + \int_{\mathcal{F}_h^{Int}} \left[ \delta_1 (\boldsymbol{\sigma}_h \mathbf{n}_{K_S}^x + p_h \mathbf{n}_{K_S}^x) \cdot (\underline{\underline{\boldsymbol{\xi}}} \mathbf{n}_{K_S}^x + q \mathbf{n}_{K_S}^x) \right] ds,
\end{aligned}$$

Taking into account the definitions and notations given in the previous sections, we define the stability parameter  $\theta = \max\{\theta_F, \theta_S\}$  and, assuming that  $\theta \in [0, 1)$ , we equip the continuous Trefftz space  $\mathbb{T}(K) \equiv \mathbb{T}_F(K_{FS}) \times \mathbb{T}_S(K_{SF})$  with two norms defined as follows:

$$\begin{aligned}
|||(\boldsymbol{\omega}_F, q, \boldsymbol{\omega}_S, \underline{\underline{\boldsymbol{\xi}}})|||_K^{tp} & \equiv \left[ |||(\boldsymbol{\omega}_F, q)|||_{K_F}^{tp^2} + |||(\boldsymbol{\omega}_S, \underline{\underline{\boldsymbol{\xi}}})|||_{K_S}^{tp^2} \right. \\
& \quad + \left\| \alpha_1^{1/2} (\boldsymbol{\omega}_F \cdot \mathbf{n}_{K_F}^x - \boldsymbol{\omega}_S \cdot \mathbf{n}_{K_F}^x) \right\|_{L^2(\mathcal{F}_h^{Int})}^2 \\
& \quad \left. + \left\| \delta_1^{1/2} (\underline{\underline{\boldsymbol{\xi}}} \mathbf{n}_{K_S}^x + q \mathbf{n}_{K_S}^x) \right\|_{L^2(\mathcal{F}_h^{Int})}^2 \right]^{1/2},
\end{aligned}$$

$$|||(\boldsymbol{\omega}_F, q, \boldsymbol{\omega}_S, \underline{\underline{\boldsymbol{\xi}}})|||_{K^*}^{tp} \equiv \left[ (|||(\boldsymbol{\omega}_F, q)|||_{K_F^*}^{tp})^2 + (|||(\boldsymbol{\omega}_S, \underline{\underline{\boldsymbol{\xi}}})|||_{K_S^*}^{tp})^2 + \left\| q \right\|_{L^2(\mathcal{F}_h^{Int})}^2 + \left\| \boldsymbol{\omega}_S \right\|_{L^2(\mathcal{F}_h^{Int})}^2 \right]^{1/2}.$$

If  $\theta \in [0, 1)$ , we have

$$a_K^{tp}((\boldsymbol{\omega}_F, q, \boldsymbol{\omega}_S, \underline{\underline{\boldsymbol{\xi}}}); (\boldsymbol{\omega}_F, q, \boldsymbol{\omega}_S, \underline{\underline{\boldsymbol{\xi}}})) \geq |||(\boldsymbol{\omega}_F, q, \boldsymbol{\omega}_S, \underline{\underline{\boldsymbol{\xi}}})|||_K^{tp^2},$$

and

$$|a_K^{tp}((\mathbf{v}_F, p, \mathbf{v}_S, \boldsymbol{\sigma}); (\boldsymbol{\omega}_F, q, \boldsymbol{\omega}_S, \underline{\underline{\boldsymbol{\xi}}}))| \leq (C_1^{tp} + C_2^{tp}) |||(\mathbf{v}_F, p, \mathbf{v}_S, \boldsymbol{\sigma})|||_{K^*}^{tp} |||(\boldsymbol{\omega}_F, q, \boldsymbol{\omega}_S, \underline{\underline{\boldsymbol{\xi}}})|||_K^{tp},$$

$$|l_K^{tp}(\boldsymbol{\omega}_F, q, \boldsymbol{\omega}_S, \underline{\boldsymbol{\xi}})| \leq \left[ \left\| \left( \frac{1}{2\alpha_2} + 1 \right)^{1/2} \rho_F^{1/2} \mathbf{v}_F^{in} \right\|_{L^2(\mathcal{F}_h^{In})}^2 + \left\| \left( \frac{1}{2\beta_2} + 1 \right)^{1/2} \left( \frac{1}{c_F^2 \rho_F} \right)^{1/2} p^{in} \right\|_{L^2(\mathcal{F}_h^{In})}^2 \right. \\ \left. \left\| \left( \frac{1}{\gamma_2} + 1 \right)^{1/2} \rho_S^{1/2} \mathbf{v}_S^{in} \right\|_{L^2(\mathcal{F}_h^{In})}^2 + \left\| \left( \frac{1}{\delta_2} + 1 \right)^{1/2} \left| \underline{\boldsymbol{\sigma}}^{in} \right|_{\underline{\mathbf{A}}} n_{K_S}^t \right\|_{L^2(\mathcal{F}_h^{In})}^2 \right]^{1/2} \|\boldsymbol{\omega}_F, q, \boldsymbol{\omega}_S, \underline{\boldsymbol{\xi}}\|_K^{tp}.$$

The global tent-pitching Trefftz-DG problem can then be defined by summing the local formulations (6.1) over all elements  $K_{FF} \in \mathcal{T}_h^{tp}$ , the local formulations (6.7) over all elements  $K_{SS} \in \mathcal{T}_h^{tp}$ , and the local formulations (6.9) over all macro-elements  $K \in \mathcal{T}_h^{tp}$ . We obtain:

Seek  $(\mathbf{v}_{Fh}, p_h, \mathbf{v}_{Sh}, \underline{\boldsymbol{\sigma}}_h) \in \mathbf{T}^p(\mathcal{T}_h^{tp})$  such that, for all  $(\boldsymbol{\omega}_F, q, \boldsymbol{\omega}_S, \underline{\boldsymbol{\xi}}) \in \mathbf{T}^p(\mathcal{T}_h^{tp})$ , it holds true:

$$\mathcal{A}_{TDG}^{tp}((\mathbf{v}_{Fh}, p_h, \mathbf{v}_{Sh}, \underline{\boldsymbol{\sigma}}_h); (\boldsymbol{\omega}_F, q, \boldsymbol{\omega}_S, \underline{\boldsymbol{\xi}})) = \ell_{TDG}^{tp}(\boldsymbol{\omega}_F, q, \boldsymbol{\omega}_S, \underline{\boldsymbol{\xi}}), \quad (6.10)$$

where

$$\ell_{TDG}^{tp}(\boldsymbol{\omega}_F, q, \boldsymbol{\omega}_S, \underline{\boldsymbol{\xi}}) \equiv \sum_{K_{FF} \in \mathcal{T}_h^{tp}} l_{K_{FF}}^{tp}(\boldsymbol{\omega}_F|_{K_{FF}}, q|_{K_{FF}}) + \sum_{K_{SS} \in \mathcal{T}_h^{tp}} l_{K_{SS}}^{tp}(\boldsymbol{\omega}_S|_{K_{SS}}, \underline{\boldsymbol{\xi}}|_{K_{SS}}) \\ + \sum_{K \in \mathcal{T}_h^{tp}} l_K^{tp}(\boldsymbol{\omega}_F|_{K_{FS}}, q|_{K_{FS}}, \boldsymbol{\omega}_S|_{K_{SF}}, \underline{\boldsymbol{\xi}}|_{K_{SF}})$$

and

$$\mathcal{A}_{TDG}^{tp}((\mathbf{v}_{Fh}, p_h, \mathbf{v}_{Sh}, \underline{\boldsymbol{\sigma}}_h); (\boldsymbol{\omega}_F, q, \boldsymbol{\omega}_S, \underline{\boldsymbol{\xi}})) \equiv \\ \sum_{K_{FF} \in \mathcal{T}_h^{tp}} a_{K_{FF}}^{tp}((\mathbf{v}_{Fh}|_{K_{FF}}, p_h|_{K_{FF}}); (\boldsymbol{\omega}_F|_{K_{FF}}, q|_{K_{FF}})) \\ + \sum_{K_{SS} \in \mathcal{T}_h^{tp}} a_{K_{SS}}^{tp}((\mathbf{v}_{Sh}|_{K_{SS}}, \underline{\boldsymbol{\sigma}}_h|_{K_{SS}}); (\boldsymbol{\omega}_S|_{K_{SS}}, \underline{\boldsymbol{\xi}}|_{K_{SS}})) \\ + \sum_{K \in \mathcal{T}_h^{tp}} a_K^{tp}((\mathbf{v}_{Fh}|_{K_{FS}}, p_h|_{K_{FS}}, \mathbf{v}_{Sh}|_{K_{SF}}, \underline{\boldsymbol{\sigma}}_h|_{K_{SF}}); (\boldsymbol{\omega}_F|_{K_{FS}}, q|_{K_{FS}}, \boldsymbol{\omega}_S|_{K_{SF}}, \underline{\boldsymbol{\xi}}|_{K_{SF}})).$$

By the analogy with previous cases, if  $\theta \in [0, 1)$ , based on the coercivity and continuity estimates, and the consistency of the bilinear forms  $a_{K_F}^{tp}(\cdot, \cdot)$ ,  $a_{K_S}^{tp}(\cdot, \cdot)$ ,  $a_K^{tp}(\cdot, \cdot)$  we derive the same properties for the global bilinear form  $\mathcal{A}_{TDG}^{tp}(\cdot; \cdot)$  with respect to the norms  $\|\cdot\|_{TDG}^{tp}$  and  $\|\cdot\|_{TDG^*}^{tp}$  that are defined by summing the local norms  $\|\cdot\|_{K_F}^{tp}$  and  $\|\cdot\|_{K_F^*}^{tp}$  over all elements  $K_{FF}$ , the local norms  $\|\cdot\|_{K_S}^{tp}$  and  $\|\cdot\|_{K_S^*}^{tp}$  over all elements  $K_{SS}$ , and the local norms  $\|\cdot\|_K^{tp}$  and  $\|\cdot\|_{K^*}^{tp}$  over all macro-elements  $K$ .

**Theorem 6.3.** *If  $\theta \in [0, 1)$ , the global variational problem (6.10) admits a unique weak solution  $(\mathbf{v}_{Fh}, p_h, \mathbf{v}_{Sh}, \underline{\boldsymbol{\sigma}}_h) \in \mathbf{T}^p(\mathcal{T}_h^{tp})$ . Moreover, the following estimate holds true:*

$$\begin{aligned} & \|\|(\mathbf{v}_F - \mathbf{v}_{Fh}, p - p_h, \mathbf{v}_S - \mathbf{v}_{Sh}, \underline{\boldsymbol{\sigma}} - \underline{\boldsymbol{\sigma}}_h)\|\|_{TDG}^{tp} \leq \\ & (1 + C_1^{tp} + C_2^{tp}) \inf_{(\boldsymbol{\omega}_F, q, \boldsymbol{\omega}_S, \underline{\boldsymbol{\xi}}) \in \mathbf{T}^p(\mathcal{T}_h^{tp})} \|\|(\mathbf{v}_F - \boldsymbol{\omega}_F, p - q, \mathbf{v}_S - \boldsymbol{\omega}_S, \underline{\boldsymbol{\sigma}} - \underline{\boldsymbol{\xi}})\|\|_{TDG^*}^{tp}. \end{aligned}$$

*Proof.* The well-posedness of the global problem (6.10) follows straightforwardly from the coercivity and continuity estimations, the consistency of the global bilinear form, and from the fact that  $\mathbf{T}^p(\mathcal{T}_h^{tp})$  is a finite dimensional space.  $\square$

In a vector-matrix form, the local linear system (6.9) can be represented similarly to the vector-matrix formulation written for the tent of heterogeneous type (6.6).

### 6.3 Space-time tent mesh examples

In this section, we give some 1D+time and 2D+time examples of space-time tent mesh construction which will be used for further numerical tests (see section 6.4).

#### 6.3.1 1D+time homogeneous and heterogeneous tent meshes

We consider three examples of 1D+time tent meshes. Figures 6.8 describe the construction of a uniform tent (a) with  $\Delta x$  fixed and a non-uniform tent (b) with twice smaller  $\Delta x$  and  $\Delta t$  in the middle zone. The mesh 6.8(b) is typically what is needed to follow the geometrical properties of a heterogeneous medium. The special feature of these meshes is the special type of element connection: we must solve the formulation in the entire element for each new tent.

In figure 6.9, we consider a heterogeneous medium, which is composed of two layers, with twice smaller  $\Delta x$  in the right layer compared to the left one. Compared to the previous example, here the restriction on tent construction imposes the coupling of two formulations with different medium parameters in two neighbour elements at the interface between two medium layers.

#### 6.3.2 2D+time homogeneous tent mesh

The 2D+time example of space-time tent meshes is given in figure 6.10. Even though the mesh elements are now pyramids and tetrahedra, we can consider the same three types of element connections as in the 1D+time case.

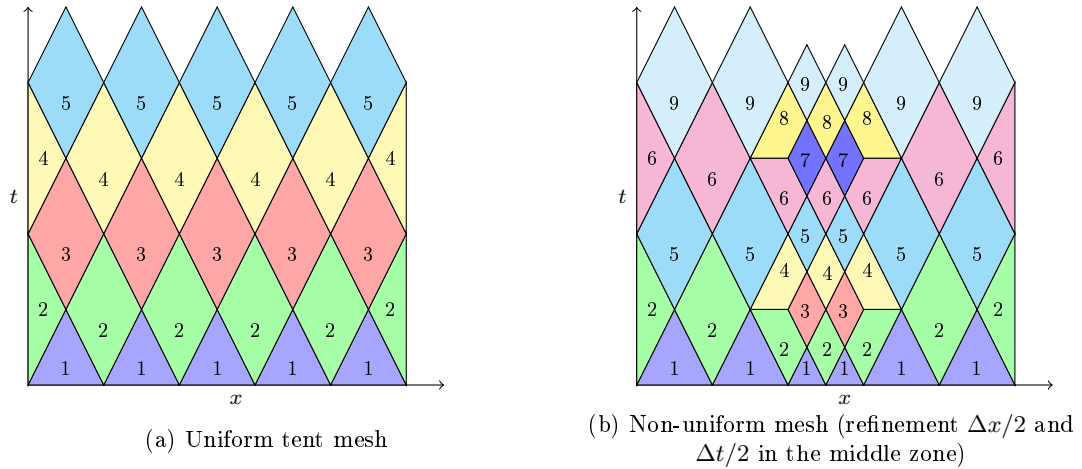


FIGURE 6.8: Space-time tent meshes for 1D+time homogeneous medium.

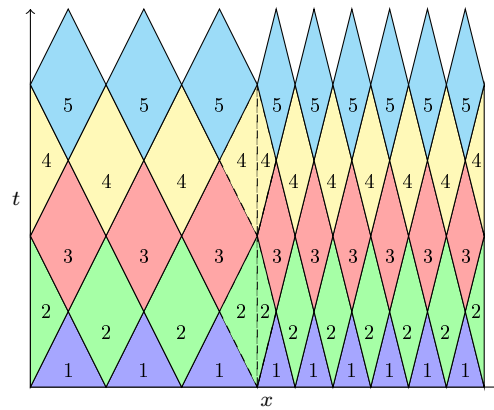


FIGURE 6.9: Space-time tent meshes for 1D+time heterogeneous medium (refinement  $\Delta x/2$  in the right zone)

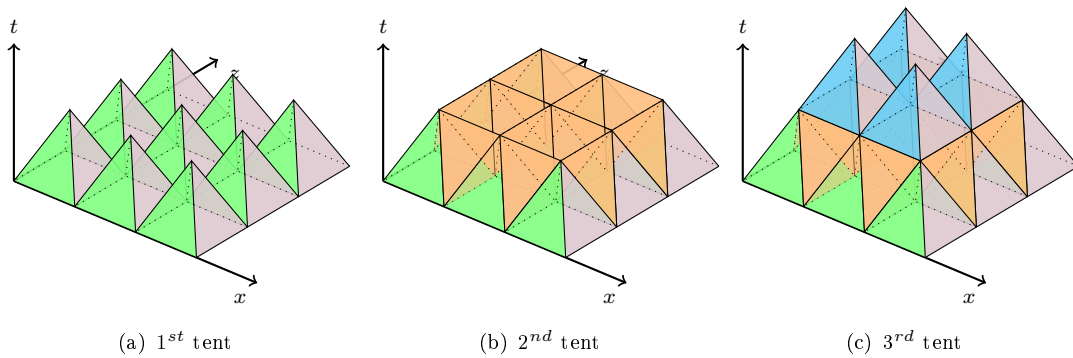


FIGURE 6.10: Space-time uniform tent meshes for 2D+time homogeneous medium.

## 6.4 Numerical results

In this section, we display some numerical results obtained from the implementation of the Tent Pitcher algorithm for solving Trefftz-DG acoustic and elastodynamic formulations in 1D+time and 2D+time dimensions. Here and further, the penalty parameters

are  $\alpha_1 = \beta_1 = 0.5$  for 1D and 2D acoustic tests, and  $\delta_1 = \gamma_1 = 0.5$  for 2D elastodynamic tests. All parameters are dimensionless.

### 6.4.1 1D Acoustics

We address the problem of solving the acoustic wave equation in a homogeneous and a heterogeneous domain. The objective is to validate the numerical method based on the tent strategy by comparison with the analytical solutions. The convergence profile is also considered.

#### 6.4.1.1 Homogeneous acoustic medium with periodical boundary conditions

We consider a 1D homogeneous acoustic medium  $\Omega_F \equiv [0, 1]$  with periodic boundary conditions and a time interval  $I \equiv [0, 0.5]$ . We set the medium parameters  $c_F = 1$ ,  $\rho_F = 1$  to be constant in  $\Omega_F \times I$ . We retain the uniform tent mesh example 6.8(a), and we reproduce the same tent construction by choosing  $2c_F\Delta t = \Delta x = 0.01$ . The approximation degree is  $p=3$ . Initial conditions are imposed on the velocity,  $v_{F0}(x) = 10(x - 0.2) \cdot \exp(-\pi^2(x - 0.2)^2/0.2^2)$ , and the pressure,  $p_0(x) = c_F v_{F0}$ .

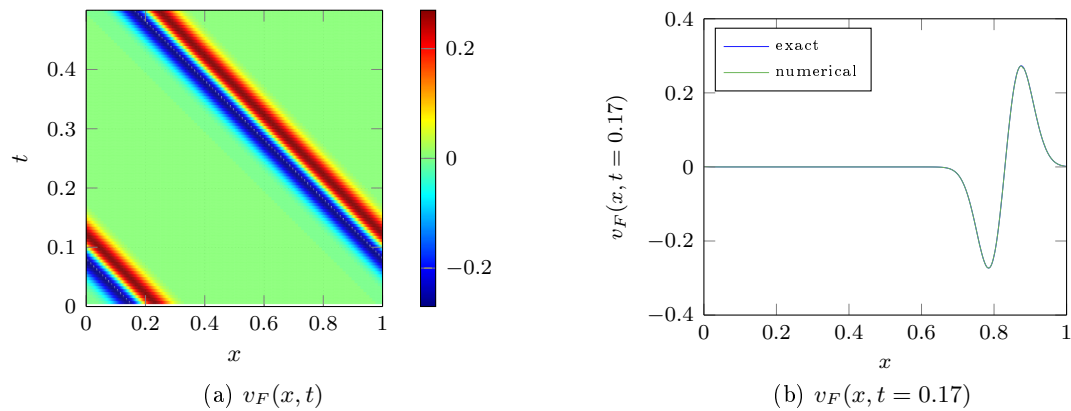


FIGURE 6.11: Propagation of the numerical velocity  $v_F(x, t)$  in a homogeneous 1D fluid domain.

Figure 6.11(a) shows the propagation of the numerical velocity  $v_F(x, t)$ . In figure 6.11(b), we compare the exact and numerical velocities at time  $t = 0.17$ . We can see that both signals match well, thus, validating the implementation.

The results of a convergence study for the numerical velocity  $v_F(x, t)$  are given in figure 6.12. It shows the  $L^2$ -norm in time and space of numerical error as a function of cell size  $\Delta x = 2c_F\Delta t$ . In all the cases, the convergence rate is of order  $p+1$  or higher. Here again, we observe a superconvergence phenomenon as for the 1D standard Trefftz-DG case.

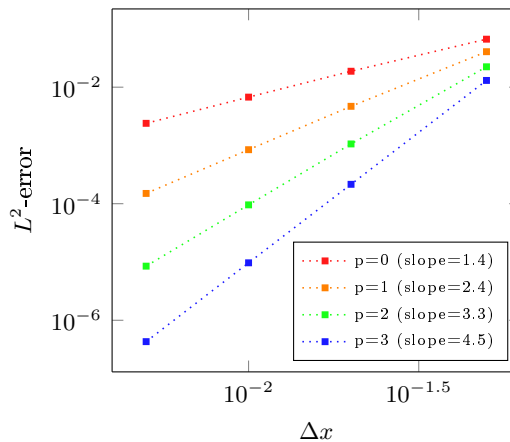


FIGURE 6.12: Convergence of the numerical velocity  $v_F$  as a function of cell size  $\Delta x = 2c_F\Delta t$ .

#### 6.4.1.2 Heterogeneous acoustic medium with periodic boundary conditions

We consider a 1D heterogeneous acoustic medium which is composed of three homogeneous layers  $\Omega_F \equiv [0, 0.4) \cup [0.4, 0.6) \cup [0.6, 1]$ , and the time interval is  $I \equiv [0, 0.5]$ . The medium parameters are  $c_F = 1$ ,  $\rho_F = 1$  in the left-hand side and right-hand side layers and  $c_F = 2$ ,  $\rho_F = 1$  in the middle one. We reproduce the same tent construction as in figure 6.9 by choosing  $2c_F\Delta t = \Delta x = 0.01$ . The approximation degree is  $p=3$ . To generate the wave, we take  $v_{F0}(x) = 10(x - 0.2) \cdot \exp(-\pi^2(x - 0.2)^2/0.2^2)$  as an initial condition for the velocity, and  $p_0(x) = -c_F v_{F0}$  for the pressure. Periodic boundary conditions are imposed at  $\partial\Omega_F$ .

Figure 6.13(a) pictures the propagation of the numerical velocity in the three-layered medium, while figure 6.13(b) displays the numerical solution at time  $t = 0.17$ .

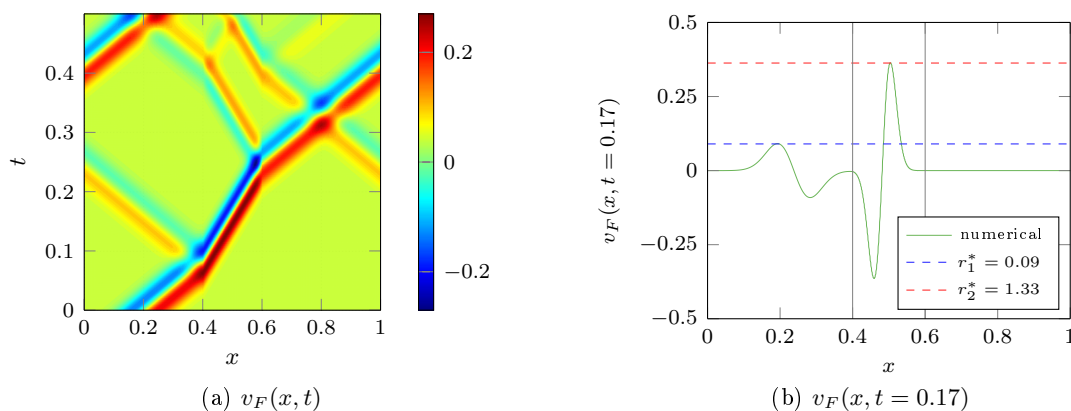


FIGURE 6.13: Propagation of the numerical velocity  $v_F(x, t)$  in a heterogeneous 1D fluid domain.

The propagation of the numerical solution through the interface  $x = 0.4$  between two layers properly reproduces the physics of the model, based on values of the reflection

coefficients  $r_1$  and  $r_2$ . They can be analytically computed using the medium parameters as follows:  $r_1 = (c_{F1} - c_{F2})(c_{F1} + c_{F2})^{-1} = 0.33$  and  $r_2 = (2c_{F1})(c_{F1} + c_{F2})^{-1} = 1.33$ , defining the amplitudes of the reflected  $r_1^* = r_1 \cdot \max_{x \in (0,1)} v_{F0} = 0.09$  and incident  $r_2^* = r_2 \cdot \max_{x \in (0,1)} v_{F0} = 0.36$  waves (blue and red dashed lines respectively in figure 6.13(b)).

### 6.4.2 Homogeneous 2D acoustics

In this section we test the tent Trefftz-DG formulation applied to the 2D+time acoustic model. We consider a 2D homogeneous acoustic medium  $\Omega_F \equiv [0, 1] \times [0, 1]$  with periodic boundary conditions and the time interval is  $I \equiv [0, 0.7]$ . The medium parameters  $c_F = 1$ ,  $\rho_F = 1$  are constant in  $\Omega_F \times I$ . We retain the uniform tent mesh example as in figure 6.10, and we reproduce the same tent construction by choosing  $\sqrt{2}c_F\Delta t = \Delta x = \Delta y = 0.01$ . The degree of approximation in space and time is  $p=3$ . We have a Gaussian

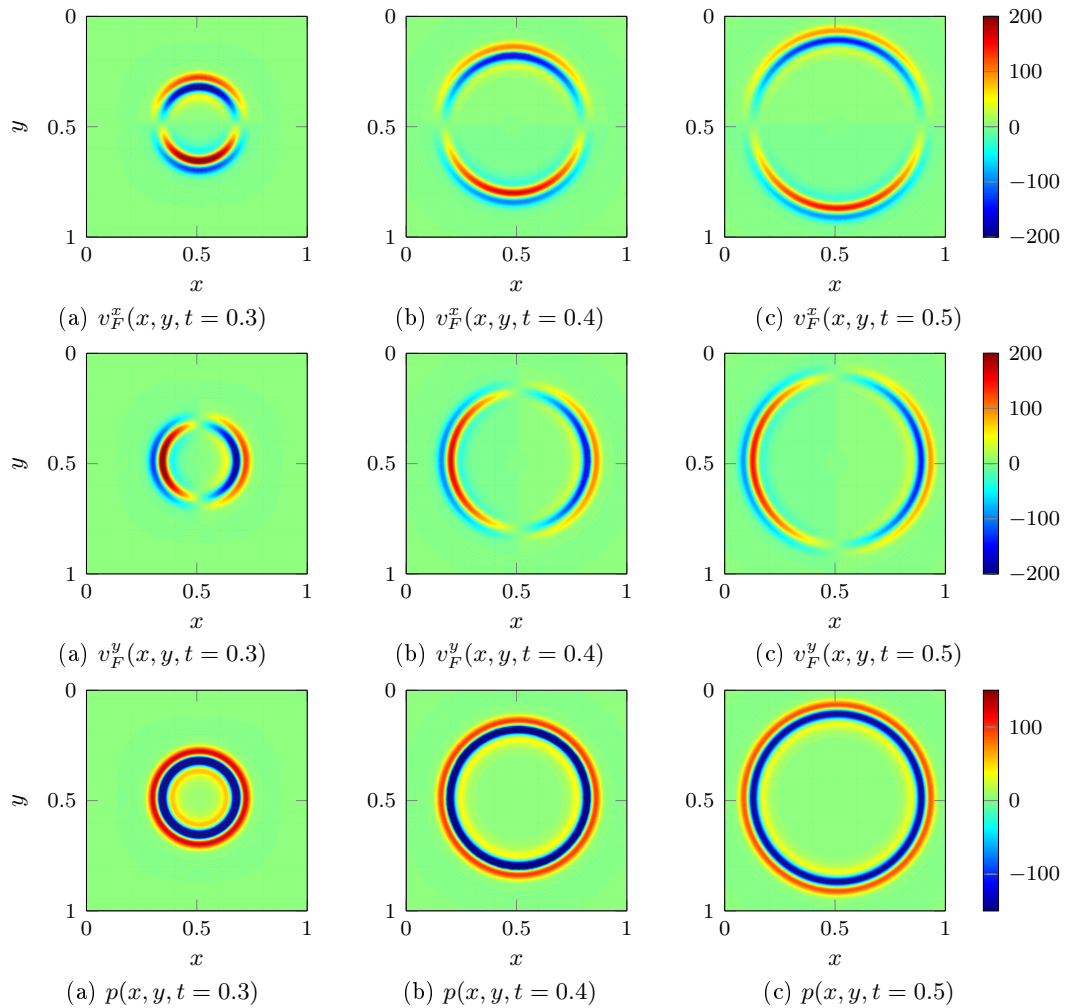


FIGURE 6.14: Propagation of the numerical velocity  $\mathbf{v}_F \equiv (v_F^x, v_F^y)$  and the pressure  $p$  in a homogeneous 2D fluid domain at time  $t = 0.3, 0.4, 0.5$ .

source term  $f(t) = -50\pi^2(t-0.2) \cdot \exp(-25\pi^2(t-0.2)^2)$  at the point  $(0.5, 0.5)$  and zero initial conditions.

Figure 6.14 shows the propagation of the components  $v_F^x, v_F^y$  of the numerical velocity  $\mathbf{v}_F \equiv (v_F^x, v_F^y)$ , and the pressure  $p$  as well.

In figure 6.15, we compare the seismograms of  $v_S^x$  and  $v_S^y$ , computed at the point  $(0.25, 0.25)$  with analytical solutions computed with *Gar6more2D* [1]. Both the curves match well, validating thus the numerical formulation.

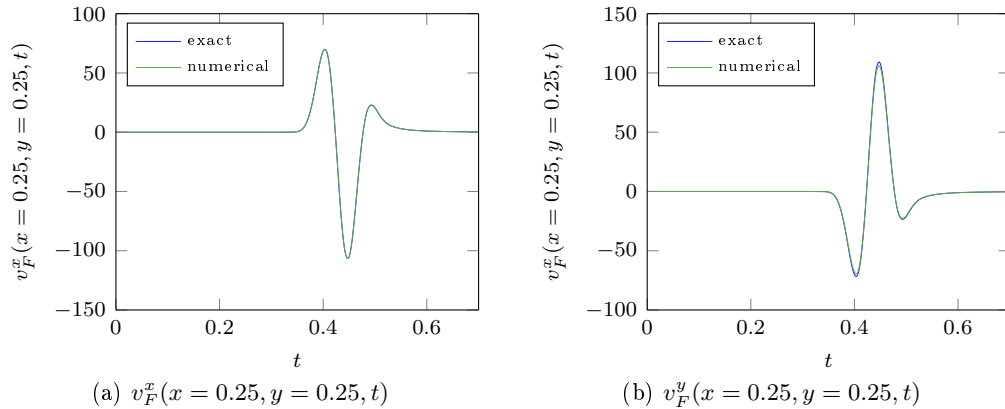


FIGURE 6.15: The seismograms for the exact and numerical velocities  $\mathbf{v}_F \equiv (v_F^x, v_F^y)$  in a homogeneous 2D fluid domain.

The convergence of the numerical velocity  $\mathbf{v}_F(x, t)$  for different approximation degrees  $p=0, 1, 2, 3$  is shown in figure 6.16. It represents the  $L^2$ -norm in space and time of numerical error as a function of cell size  $\Delta x = \Delta y = \sqrt{2}c_F\Delta t$ . In all the cases, the convergence is at least of order  $p$  and reaches  $p+1$  for  $p = 2, 3$ . Hence, the Tent Pitcher algorithm converges as well as standard Trefftz-DG methods, even with a source point.

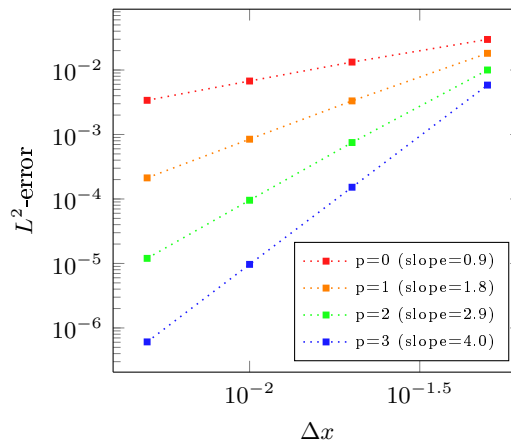


FIGURE 6.16: Convergence of the numerical velocity  $\mathbf{v}_F$  as a function of cell size  $\Delta x = \Delta y = \sqrt{2}c_F\Delta t$ .

### 6.4.3 Homogeneous 2D elastodynamics

We consider a 2D homogeneous elastic medium  $\Omega_S \equiv [0, 2] \times [0, 2]$  and a time interval  $I \equiv [0, 0.9]$ . We choose the following medium parameters:  $\lambda = \mu = 1$ ,  $\rho_S = 1$  in  $\Omega_S \times I$ . We use the same tent pitching mesh as in figure 6.10 by choosing  $\sqrt{2}V_P\Delta t = \Delta x = \Delta y = 0.01$ . The degree of approximation in space and time is  $p=3$ . At point  $(1, 1)$ , we impose a Gaussian source term  $f(t) = -50\pi^2(t - 0.2) \cdot \exp(-25\pi^2(t - 0.2)^2)$  and we have zero initial conditions.

Figures 6.17 and 6.18 show the propagation of the numerical velocity  $\mathbf{v}_S$  and the stress tensor  $\underline{\sigma}$  at times  $t = 0.3, 0.4, 0.5$ . Even if we observe the same numerical artifacts caused by the source point emitted in the elastic medium in the case of the stress propagation (see chapter 5), we can clearly see that the  $P$ - and  $S$ - wave propagation is well reproduced. The numerical results are validated through comparisons with analytical solutions computed with *Gar6more2D* [1] as depicted in figure 6.19.

The convergence of the numerical velocity  $\mathbf{v}_S(x, t)$  for different approximation degrees  $p=0, 1, 2, 3$  is shown in figure 6.20. It represents the  $L^2$ -norm in space and time of numerical error as a function of cell size  $\Delta x = \Delta y = \sqrt{2}V_P\Delta t$ . We can see that the convergence is at least of order  $p$  and reaches approximately  $p+1$  for  $p = 2, 3$ . Once again, the Tent Pitcher algorithm converges as well as standard Trefftz-DG methods, even with a source point.

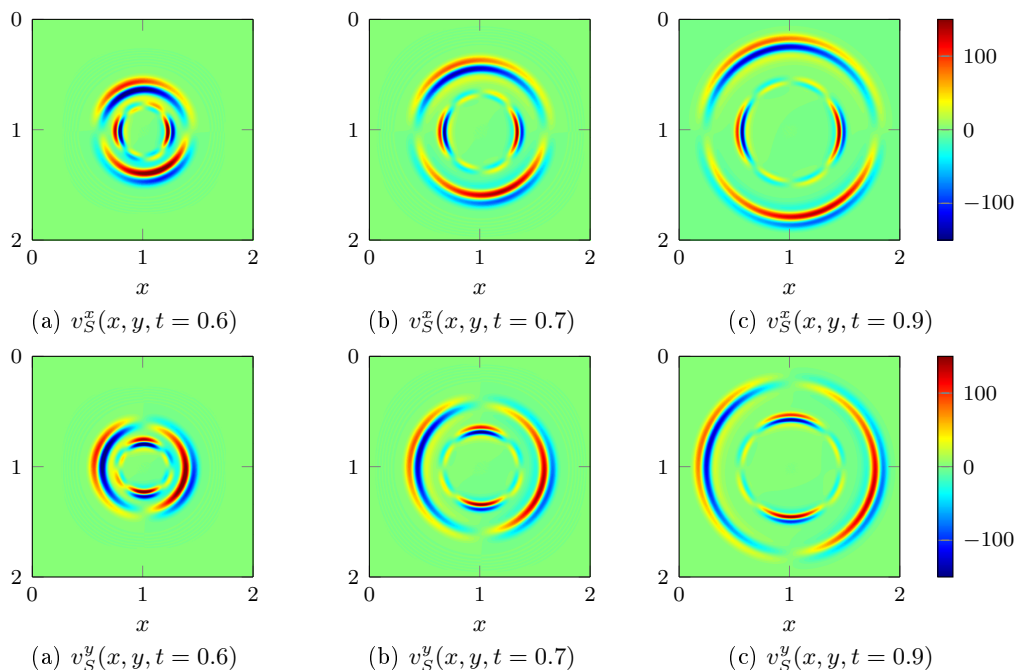


FIGURE 6.17: Propagation of the numerical velocity  $\mathbf{v}_S \equiv (v_S^x, v_S^y)$  in a homogeneous 2D solid domain at time  $t = 0.6, 0.7, 0.9$ .

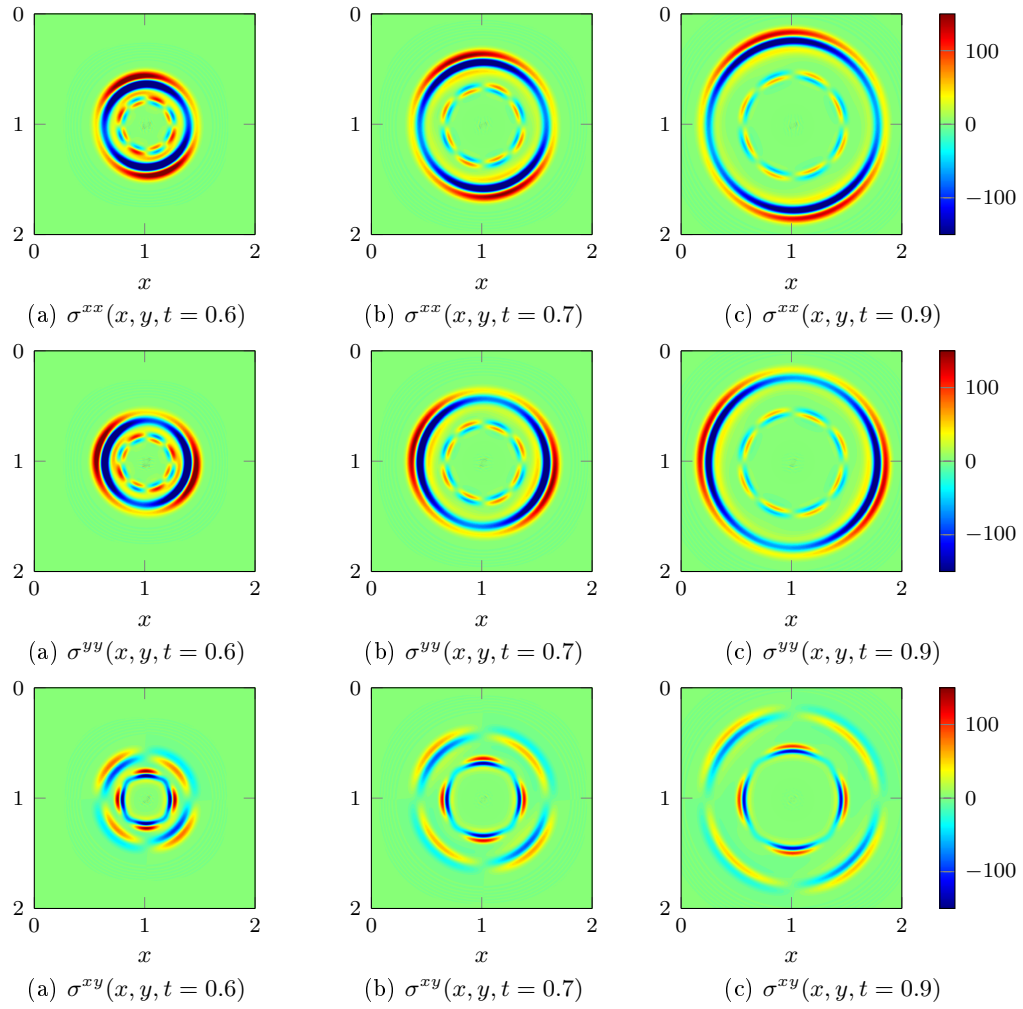


FIGURE 6.18: Propagation of the numerical stress tensor in a homogeneous 2D solid domain.

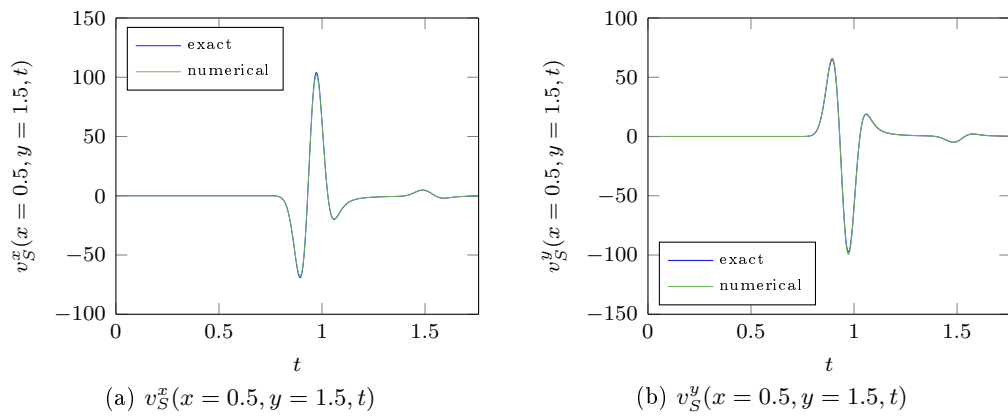


FIGURE 6.19: The seismograms for the exact and numerical velocities  $\mathbf{v}_S \equiv (v_S^x, v_S^y)$  in a homogeneous 2D solid domain at time  $t = 0.3, 0.4, 0.5$ .

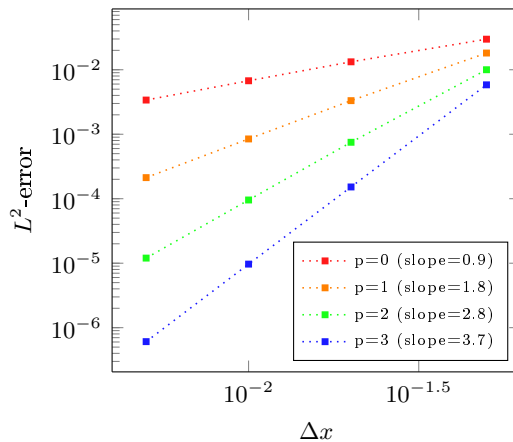


FIGURE 6.20: Convergence of the numerical velocity  $\mathbf{v}_S$  as a function of cell size  $\Delta x = \Delta y = \sqrt{2}V_P\Delta t$ .

#### 6.4.4 2D Elasto-acoustics

In this section, we illustrate the tent Trefftz-DG formulation of the 2D+time elasto-acoustic problem.

We consider a 2D elasto-acoustic medium composed of two homogeneous layers: the acoustic one  $\Omega_F \equiv [0, 2] \times [0, 1]$  and the elastic one  $\Omega_S \equiv [0, 2] \times [1, 2]$ . The time interval is  $I \equiv [0, 0.8]$ . The medium parameters  $\lambda = \mu = 1$ ,  $\rho_S = 1$  are constant in  $\Omega_S \times I$ . The approximation degree in space and time is  $p=3$ . We retain the uniform 2D+time tent

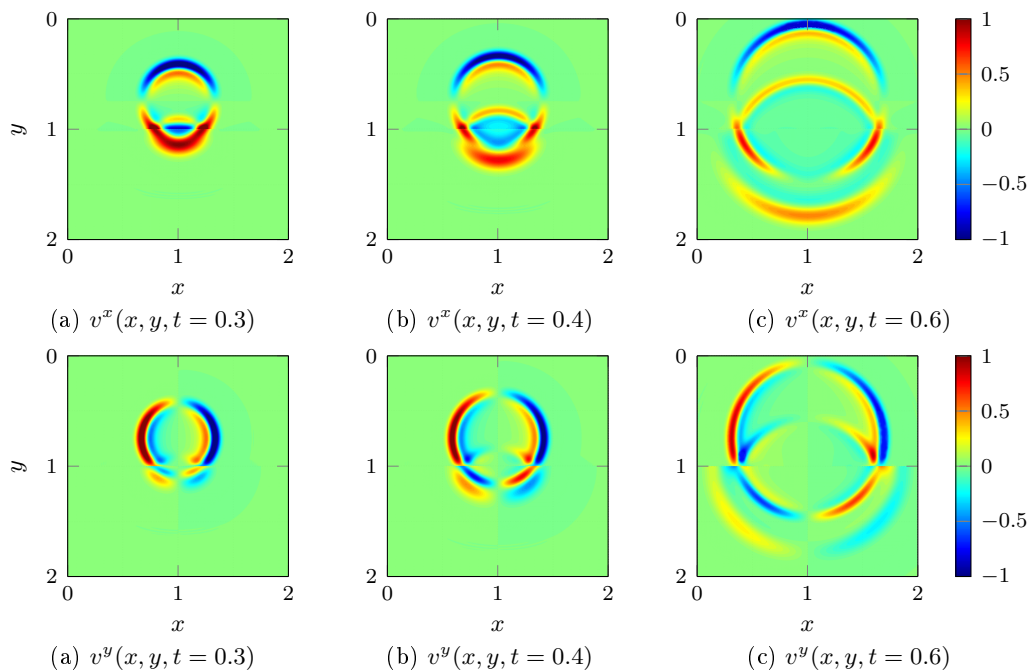


FIGURE 6.21: Propagation of the numerical velocity  $\mathbf{v} \equiv (v^x, v^y)$  in a 2D fluid-solid domain at time  $t = 0.3, 0.4, 0.6$ .

mesh example as in figure 6.10 and we reproduce the same tent construction by choosing  $\min\{V_P, c_F\}\Delta t = \Delta x/\sqrt{2} = \Delta y/\sqrt{2} = 0.007$ . The source term is a Gaussian function  $f(t) = 10\exp(-40\pi^2(t - 0.2)^2)$  emitted at point  $(1, 0.75)$  in the acoustic layer, and we have zero initial conditions.

Figure 6.21 shows the propagation of the numerical velocity  $\mathbf{v} \equiv (v^x, v^y)$  at times  $t = 0.3, 0.4, 0.6$ . We can clearly observe all the types of waves (incident, reflected  $P$ -,  $S$ -waves).

The numerical solutions are validated thanks to analytical seismograms at the point  $(1.5, 1.5)$  and computed with *Gar6more2D* [1] as displayed in figure 6.22.

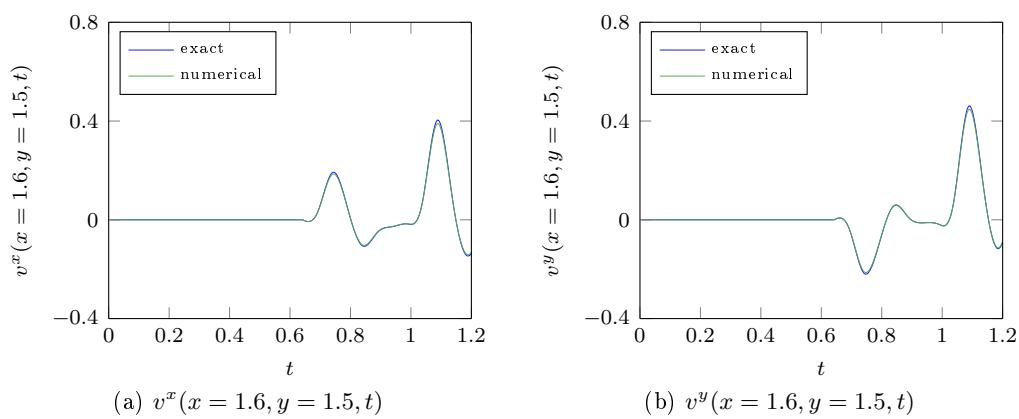


FIGURE 6.22: The seismograms for the exact and numerical velocities  $\mathbf{v} \equiv (v^x, v^y)$  in a 2D fluid-solid domain.

### 6.4.5 Test of performance

In the previous sections, we have checked that the Tent Pitcher coupled with the Trefftz-DG approach delivers accurate wave solutions. Here, we compare the three Trefftz-DG solution methodologies that are proposed in this manuscript. These tests of performance are obviously preliminary and will require a deeper study after the codes are parallelized. Nevertheless these tests are informative for the future which consists in applying the Trefftz-DG method to industrial problems.

In figure 6.23, we depict the computational times as a function of the cell number used for the space discretization. We compare the two first Trefftz-DG algorithms involving an exact inversion ( $TDG2D_{ei}$ ) or an approximate (iterative) one ( $TDG2D_{ai}$ ) of the global space-time discrete matrix with the Trefftz-DG solution obtained on the tent pitching mesh ( $TDG2D_{tp}$ ). The histogram clearly indicates that the Tent Pitcher largely improves the capabilities of the Trefftz-DG algorithm. It is worth noting that the initial approach, involving the exact inversion of the global matrix, is not even able to deliver a solution

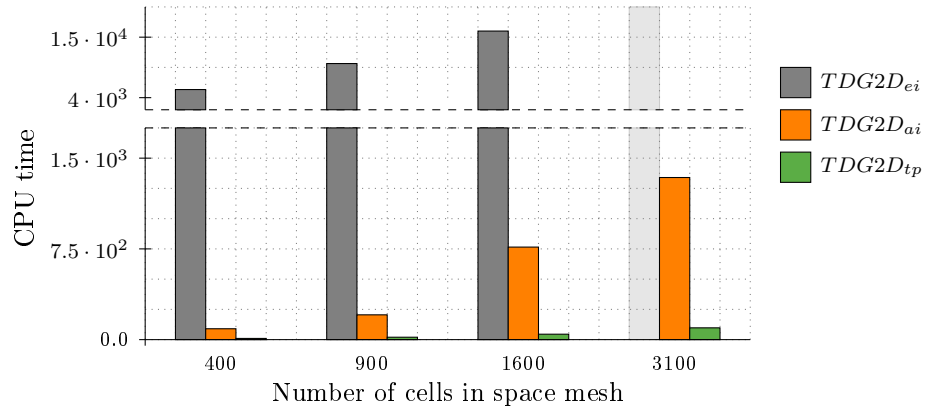


FIGURE 6.23: Speedup of using three algorithms for different model sizes

when the number of cells exceeds 3000. It means that this solution methodology, we proposed at first, should not be used for tackling large problems and even more so in industry.

## 6.5 Conclusion

We have implemented the Trefftz-DG method in a tent pitching mesh which contributes to accelerate the computations by avoiding the (exact or approximate) inversion of the global matrix. We have seen that the convergence properties of the Trefftz-DG algorithm are kept. The Tent Pitcher is adapted to the parallelization and it accounts for local-time steps easily. This is a very promising algorithm which encourages us to carry on in this way for solving realistic problems suggested by the geophysical industry.



## Chapter 7

# Conclusion

This PhD thesis has been prepared in the framework of an industrial research program gathering researchers of Inria and research engineers of Total. Our joint objective is the development of advanced numerical methods for solving wave problems in very large domains with numerous source terms. The propagation domain is the subsurface of the Earth including heterogeneities and topography effects. It is thus a challenging problem, in particular because it requires a huge computational power which needs a proper utilization to avoid reaching the limits of the computing capacities. Regarding this domain of research, some key words arise quite naturally: high-order approximation and *hp*-adaptivity for accuracy and efficiency, discontinuous finite elements for parallelization, fast time integration for limiting the computational duration, optimal sparsity for reducing the memory storage and also making the computations faster. In this PhD thesis, we have addressed all these features by proposing to develop a Trefftz approximation of transient wave problems involving discontinuous basis functions. Trefftz-DG solution methodologies are now popular and their implementation has mainly been done in the time-harmonic domain. Very few papers have been devoted to the case of transient wave problems and, to the best of our knowledge, they only deal with the case of acoustic and electromagnetic waves with some numerical experiments in 1D+time dimensions. Hence this thesis provides some contributions to the implementation of new algorithms for solving wave problems in geophysics.

This thesis aimed at assessing the potential of Trefftz-DG formulations in an industrial framework provided by Total and based on DG technologies for solving wave problems. We have thus developed a space-time Trefftz-DG formulation of the elastic wave equations and later on of the elasto-acoustic problem using space-time polynomial Trefftz basis. We have constructed a polynomial basis of discontinuous functions that are solution to the elastic and elasto-acoustic wave equations from the approximation of space-time plane

waves. They are displayed in the appendix of this manuscript. Thanks to former work by A. Moiola and his co-authors, we have proven that the proposed formulation is well posed and we have validated the corresponding numerical method for toy problems allowing the computing of analytical solutions. We have also performed a numerical convergence analysis which shows that the order of the method is optimal. At this stage in the thesis work, it is worth noting that we have implemented a prototype code which highlighted some difficulties for a use in an industrial environment according to the different constraints regarding the size of the problems to be solved and the time of execution. In particular, we have implemented a slab-by-slab change-over in time procedure and propose to invert the global space-time matrix thanks to an explicit representation of the wavefield providing a stability condition. The corresponding computational costs have been considerably reduced, but the method did not exploit fully the physical properties of the wavefields. This led us to investigate Tent Pitcher algorithm which consists in constructing the numerical solution by following the wave fronts. It results in covering the space-time domain by tent-like elements respecting the propagation cone inherited from the finite propagation speed principle. We have obtained preliminary results showing very promising directions for investigation. But the optimization and the parallelization of the code is still on-going, general boundary conditions must also be implemented to provide software adapted to geophysical exploration involving regional computations. We would like to analyze the influence of the penalty terms on the performance of the code. It would be interesting to compare different basis functions to possibly define an optimal set. This work is the first step of the development of a branch of DIP DG technologies coupling DG with Trefftz methodology. It will be followed by further studies including the parallelization in time of our numerical methods and their extension to 3D problems which is far from being obvious. In this regard, the report [106] deserves a particular attention providing a parallel mesh generator in 4D. As far as the parallelization is concerned, we would like to consider the ideas recently developed in [47] where the parallelization is based on the diagonalization of the time stepping matrix proposed in [80]. We also have to consider the implementation of more complex boundary conditions. Indeed, in this work, we have restricted ourselves to the case of Dirichlet boundary conditions, which do not involve any differential operator. This kind of conditions are thus well-suited to Trefftz formulations, where the variational formulation do not contain differential operators. We now wish to adress the case of high-order absorbing boundary conditions requiring the introduction of high-order differential operators in the formulation.

The literature on Trefftz-DG approach shows that, even if the principal ideas and the algorithms have been known since the beginning of the 20<sup>th</sup> century, their practical application has been delayed because of a lack of computer performance. Thus, even in the

beginning of the 21<sup>st</sup>, discontinuous discretizations were deemed to be less competitive or even impossible to employ for solving industrial problems, because of unaffordable numerical overcosts, when compared to the popular finite difference method, for example. Even if the growth of performance of computers resulted in a tendency to prefer more accurate and stable numerical methods instead of the cheaper, but less robust ones, in practice, the choice of a numerical method is still dictated by the balance between numerical cost and accuracy.

The initial formulation of Trefftz-DG method provides a highly accurate and unconditionally stable algorithm, but it requires inverting a sparse matrix which increases significantly the computational burden. Now the implementation of Trefftz-DG in a tent pitching mesh opens new possibilities for this DG technology. Nevertheless, we are aware of the role of the computer capabilities which is still crucial, even if the numerical method is optimized. Computer scientists will surely have to consider new technologies and among them, the quantum computing could have an important influence.

According to the Moore's law, the performance of computers doubles every one and a half year. It suggests that the problem of optimization of the existing variational algorithms will stay actual for the next few years. However, Moore's law has a natural limit: the size of the modern transistors is already comparable to the size of viruses, and the more we decrease it, the less it is possible to maintain classical physics principles, because the particles start to behave as waves, revealing quantum properties.

Quantum computing uses the principles of quantum mechanics to perform the calculations, following the ideas of Richard Feynman displayed in the lecture of 1959 "There's Plenty of Room at the Bottom". Later this idea was explored by Paul Benioff [19] and Yuri Manin in 1980 [81], Richard Feynman in 1982 [44], and David Deutsch in 1985 [35].

A digital computer uses bits as a binary form of information as either a 1 or a 0 while a quantum computer uses quantum bits or  $q$ -bits which can utilize data in a variety of states due to the quantum mechanical principles of superposition and entanglement.

These principles allow multiple states to exist at the same time which helps the  $q$ -bit to operate with the utmost efficiency. Quantum computing opens thus the route for large scale computations by providing a way for accelerating significantly the computations.

Currently, the field of quantum computing is a new-born discipline of scientific computing but a proof of concept is already available using a very small number of  $q$ -bits. For example, a small 20  $q$ -bit quantum computer exists and is available for experiments via the IBM quantum experience project. Furthermore, in 2017-2018 the IBM, Intel and Google companies reported about tests of quantum processors containing 50, 49, and 72  $q$ -bits, respectively, all realized using superconducting circuits.

Even though, the use of quantum computers for solving physical problems stays globally unavailable from the engineering point of view, there already exist many analytical algorithms, whose concept and theory have already been proved. One of them is the quantum algorithm for linear systems of equations or "HHL algorithm" [55], developed by Harrow, Hassidim and Lloyd in 2009. The algorithm estimates the result of a scalar measurement on the solution to a given linear system of equations. From a numerical point of view, linear equations play an important role in all the fields of science and engineering. In particular, the Trefftz-DG formulation of a wave problem described in this thesis also reduces to solving a linear system with a global sparse matrix. Moreover, when applied to real models, the data sets as well as the matrix size grow rapidly over the time. The HHL algorithm is expected to provide a speedup over the classical ones, when applied to sparse linear systems of  $N$  variables with a low condition number  $\kappa$  (which is the case for the Trefftz-DG problem). The algorithm has a run time of  $O(\log(N)\kappa^2)$ , which is exponentially faster than the best classical ones ( $O(N\kappa)$  or  $O(N\sqrt{\kappa})$  for positive semi-defined matrices)[55]. An implementation of the quantum algorithm for linear systems of equations was demonstrated later on by Cai et al. [26], Braz et al. [16]. and Pan et al. [87] in 2013 - 2014.

To conclude and according to the discussion in [20], the upcoming years will be exciting since the practical testing of quantum algorithms will become more and more feasible. Thus, the great hope of modern numerical analysis, is that the development of the quantum computing will create the possibility of using algorithms advanced enough to tackle realistic physical problems, but still computationally intensive in the existing computing environment.

## Appendix A

# Some useful identities for the standard DG terms

The demonstration of coercivity and continuity properties proposed in chapter 3 is based on definitions and properties of the average and space and time normal jump notations for scalar  $q$ , vector  $\boldsymbol{\omega}$  and tensor  $\boldsymbol{\xi}$  fields. Herein, we consider some useful identities for the standard DG terms, including the formulas of space and time elementwise integration by parts.



## A.1 Jump and average identities

Based on the definitions and properties of the space and time normal jumps and average between elements (see chapter 3), we consider the following proposition:

**Proposition A.1.** *For scalar  $q$ , vector  $\boldsymbol{\omega}$  and tensor  $\underline{\boldsymbol{\xi}}$  fields the following identities hold true:*

$$\{\{q\}\}[q]_t = \frac{1}{2} \llbracket q^2 \rrbracket_t; \quad (\text{A.1})$$

$$\{\{\boldsymbol{\omega}\}\} \cdot \llbracket \boldsymbol{\omega} \rrbracket_t = \frac{1}{2} \llbracket \boldsymbol{\omega} \cdot \boldsymbol{\omega} \rrbracket_t; \quad (\text{A.2})$$

$$\{\{\underline{\boldsymbol{A}}\underline{\boldsymbol{\xi}}\}\} : \llbracket \underline{\boldsymbol{\xi}} \rrbracket_t = \frac{1}{2} \llbracket \underline{\boldsymbol{A}}\underline{\boldsymbol{\xi}} : \underline{\boldsymbol{\xi}} \rrbracket_t; \quad (\text{A.3})$$

$$\{\{q\}\}[\boldsymbol{\omega}]_x + \{\{\boldsymbol{\omega}\}\} \cdot [q]_x = \llbracket q\boldsymbol{\omega} \rrbracket_x; \quad (\text{A.4})$$

$$\{\{\underline{\boldsymbol{\xi}}\}\} : \llbracket \boldsymbol{\omega} \rrbracket_x + \{\{\boldsymbol{\omega}\}\} \cdot \llbracket \underline{\boldsymbol{\xi}} \rrbracket_x = \llbracket \underline{\boldsymbol{\xi}}\boldsymbol{\omega} \rrbracket_x. \quad (\text{A.5})$$

*Proof.*

(A.1) :

$$\{\{q\}\}[q]_t = \frac{1}{2} (q_{|K_F^-} + q_{|K_F^+}) (q_{|K_F^-} n_{K_F^-}^t + q_{|K_F^+} n_{K_F^+}^t) = \frac{1}{2} (q_{|K_F^-}^2 n_{K_F^-}^t + q_{|K_F^+}^2 n_{K_F^+}^t) = \frac{1}{2} \llbracket q^2 \rrbracket_t;$$

(A.2) :

$$\begin{aligned} \{\{\boldsymbol{\omega}\}\} \cdot \llbracket \boldsymbol{\omega} \rrbracket_t &= \frac{1}{2} ((\boldsymbol{\omega} \cdot \boldsymbol{\omega})_{|K_F^-} + (\boldsymbol{\omega} \cdot \boldsymbol{\omega})_{|K_F^+}) ((\boldsymbol{\omega} \cdot \boldsymbol{\omega})_{|K_F^-} n_{K_F^-}^t + (\boldsymbol{\omega} \cdot \boldsymbol{\omega})_{|K_F^+} n_{K_F^+}^t) = \\ &= \frac{1}{2} ((\boldsymbol{\omega} \cdot \boldsymbol{\omega})_{|K_F^-} n_{K_F^-}^t + (\boldsymbol{\omega} \cdot \boldsymbol{\omega})_{|K_F^+} n_{K_F^+}^t) = \frac{1}{2} \llbracket \boldsymbol{\omega} \cdot \boldsymbol{\omega} \rrbracket_t; \end{aligned}$$

(A.3) :

$$\begin{aligned} \{\{\underline{\boldsymbol{A}}\underline{\boldsymbol{\xi}}\}\} : \llbracket \underline{\boldsymbol{\xi}} \rrbracket_t &= \frac{1}{2} ((\underline{\boldsymbol{A}}\underline{\boldsymbol{\xi}} : \underline{\boldsymbol{\xi}})_{|K_F^-} + (\underline{\boldsymbol{A}}\underline{\boldsymbol{\xi}} : \underline{\boldsymbol{\xi}})_{|K_F^+}) ((\underline{\boldsymbol{A}}\underline{\boldsymbol{\xi}} : \underline{\boldsymbol{\xi}})_{|K_F^-} n_{K_F^-}^t + (\underline{\boldsymbol{A}}\underline{\boldsymbol{\xi}} : \underline{\boldsymbol{\xi}})_{|K_F^+} n_{K_F^+}^t) = \\ &= \frac{1}{2} ((\underline{\boldsymbol{A}}\underline{\boldsymbol{\xi}} : \underline{\boldsymbol{\xi}})_{|K_F^-} n_{K_F^-}^t + (\underline{\boldsymbol{A}}\underline{\boldsymbol{\xi}} : \underline{\boldsymbol{\xi}})_{|K_F^+} n_{K_F^+}^t) = \frac{1}{2} \llbracket \underline{\boldsymbol{A}}\underline{\boldsymbol{\xi}} : \underline{\boldsymbol{\xi}} \rrbracket_t; \end{aligned}$$

(A.4) :

$$\begin{aligned} \{\{q\}\}[\boldsymbol{\omega}]_x + \{\{\boldsymbol{\omega}\}\} \cdot [q]_x &= ((q\boldsymbol{\omega})_{|K_F^-} \cdot n_{K_F^-}^x + (q\boldsymbol{\omega})_{|K_F^+} \cdot n_{K_F^+}^x) \\ &+ \frac{1}{2} (q_{|K_F^-} \boldsymbol{\omega}_{|K_F^+} \cdot n_{K_F^+}^x + q_{|K_F^+} \boldsymbol{\omega}_{|K_F^-} \cdot n_{K_F^-}^x + q_{|K_F^-} \boldsymbol{\omega}_{|K_F^+} \cdot n_{K_F^-}^x + q_{|K_F^+} \boldsymbol{\omega}_{|K_F^-} \cdot n_{K_F^+}^x) = \\ &\llbracket q\boldsymbol{\omega} \rrbracket_x; \end{aligned}$$

(A.5) :

$$\begin{aligned} \{\underline{\xi}\} : \llbracket \underline{\omega} \rrbracket_x + \{\underline{\omega}\} \cdot \llbracket \underline{\xi} \rrbracket_x &= ((\underline{\xi}\underline{\omega})|_{K_F^-} \cdot n_{K_F^-}^x + (\underline{\xi}\underline{\omega})|_{K_F^+} \cdot n_{K_F^+}^x) \\ &+ \frac{1}{2}((\underline{\xi}|_{K_F^-} \underline{\omega}|_{K_F^+}) \cdot n_{K_F^+}^x + (\underline{\xi}|_{K_F^+} \underline{\omega}|_{K_F^-}) \cdot n_{K_F^-}^x + (\underline{\xi}|_{K_F^-} \underline{\omega}|_{K_F^+}) \cdot n_{K_F^-}^x + (\underline{\xi}|_{K_F^+} \underline{\omega}|_{K_F^-}) \cdot n_{K_F^+}^x) = \\ &\llbracket \underline{\xi}\underline{\omega} \rrbracket_x. \end{aligned}$$

□

## A.2 Space and time elementwise integration by parts

Some formulas of the space and time elementwise integration by parts are given below:

**Proposition A.2.** *For scalar  $q$ , vector  $\underline{\omega}$  and tensor  $\underline{\xi}$  fields the following integral identities hold true:*

$$\sum_{K_F \in \mathcal{T}_h} 2 \int_{K_F} q \frac{\partial q}{\partial t} dv = \int_{\mathcal{F}_h^{\Omega_F}} \llbracket q^2 \rrbracket_t ds + \int_{\mathcal{F}_h^{T_F}} q^2 ds - \int_{\mathcal{F}_h^{0_F}} q^2 ds; \quad (\text{A.6})$$

$$\sum_{K_F \in \mathcal{T}_h} 2 \int_{K_F} \underline{\omega} \cdot \frac{\partial \underline{\omega}}{\partial t} dv = \int_{\mathcal{F}_h^{\Omega_F}} \llbracket \underline{\omega} \cdot \underline{\omega} \rrbracket_t ds + \int_{\mathcal{F}_h^{T_F}} \underline{\omega} \cdot \underline{\omega} ds - \int_{\mathcal{F}_h^{0_F}} \underline{\omega} \cdot \underline{\omega} ds; \quad (\text{A.7})$$

$$\sum_{K_S \in \mathcal{T}_h} 2 \int_{K_S} \underline{\xi} : \frac{\partial \underline{\underline{A}} \underline{\xi}}{\partial t} dv = \int_{\mathcal{F}_h^{\Omega_S}} \llbracket \underline{\underline{A}} \underline{\xi} : \underline{\xi} \rrbracket_t ds + \int_{\mathcal{F}_h^{T_S}} \underline{\underline{A}} \underline{\xi} : \underline{\xi} ds - \int_{\mathcal{F}_h^{0_S}} \underline{\underline{A}} \underline{\xi} : \underline{\xi} ds; \quad (\text{A.8})$$

$$\sum_{K_F \in \mathcal{T}_h} \int_{K_F} (\underline{\omega} \cdot \nabla q + q \operatorname{div} \underline{\omega}) dv = \int_{\mathcal{F}_h^{Q_F}} \llbracket q \underline{\omega} \rrbracket_x ds + \int_{\mathcal{F}_h^{D_F} \cup \mathcal{F}_h^{F_S}} q \underline{\omega} \cdot n_K^x ds; \quad (\text{A.9})$$

$$\sum_{K_S \in \mathcal{T}_h} \int_{K_S} (\underline{\omega} \cdot \operatorname{div} \underline{\xi} + \underline{\xi} : \underline{\varepsilon}(\underline{\omega})) dv = \int_{\mathcal{F}_h^{Q_S}} \llbracket \underline{\xi} \underline{\omega} \rrbracket_x ds + \int_{\mathcal{F}_h^{D_S} \cup \mathcal{F}_h^{F_S}} \underline{\xi} \underline{\omega} \cdot n_K^x ds. \quad (\text{A.10})$$

*Proof.* The above identities follows straightforwardly from the Green's formulas of integration by parts [7], and the symmetry and positiveness of the considered tensor fields.

□

## Appendix B

# Trefftz-DG polynomial basis

We provide the examples of 2D+time Trefftz-DG polynomial bases for acoustic B.1 and elastodynamic B.2 problems. They represent the couples of polynomial functions  $(\phi_v, \phi_p)$  for velocity and pressure respectively in the acoustic case, and  $(\phi_v, \phi_\sigma)$  for velocity and stress respectively in the elastodynamic case. The considered approximation degrees are  $p = 0, 1, 2, 3$ .



## B.1 2D Acoustic system

<b>p=0</b>	$N_{dof}=3$	
$\phi_1^{vx} = 0$ $\phi_2^{vx} = 1$ $\phi_3^{vx} = 0$	$\phi_1^{vy} = 0$ $\phi_2^{vy} = 0$ $\phi_3^{vy} = 1$	$\phi_1^p = -c_F$ $\phi_2^p = 0$ $\phi_3^p = 0$
<b>p=1</b>	$N_{dof}=9$	
$\phi_4^{vx} = -t$ $\phi_5^{vx} = x$ $\phi_6^{vx} = 0$ $\phi_7^{vx} = 0$ $\phi_8^{vx} = y$ $\phi_9^{vx} = 0$	$\phi_4^{vy} = 0$ $\phi_5^{vy} = 0$ $\phi_6^{vy} = x$ $\phi_7^{vy} = -t$ $\phi_8^{vy} = 0$ $\phi_9^{vy} = y$	$\phi_4^p = x$ $\phi_5^p = -c_F^2 t$ $\phi_6^p = 0$ $\phi_7^p = y$ $\phi_8^p = 0$ $\phi_9^p = -c_F^2 t$
<b>p=2</b>	$N_{dof}=18$	
$\phi_{10}^{vx} = -2xt$ $\phi_{11}^{vx} = 0$ $\phi_{12}^{vx} = -yt$ $\phi_{13}^{vx} = -\frac{xy}{c_F^2}$ $\phi_{14}^{vx} = -\frac{t^2}{2}$ $\phi_{15}^{vx} = x^2$ $\phi_{16}^{vx} = y^2$ $\phi_{17}^{vx} = 0$ $\phi_{18}^{vx} = -2xy$	$\phi_{10}^{vy} = 0$ $\phi_{11}^{vy} = -2yt$ $\phi_{12}^{vy} = -xt$ $\phi_{13}^{vy} = -\frac{t^2}{2}$ $\phi_{14}^{vy} = -\frac{xy}{c_F^2}$ $\phi_{15}^{vy} = -2xy$ $\phi_{16}^{vy} = 0$ $\phi_{17}^{vy} = x^2$ $\phi_{18}^{vy} = y^2$	$\phi_{10}^p = x^2 + c_F^2 t^2$ $\phi_{11}^p = y^2 + c_F^2 t^2$ $\phi_{12}^p = xy$ $\phi_{13}^p = yt$ $\phi_{14}^p = xt$ $\phi_{15}^p = 0$ $\phi_{16}^p = 0$ $\phi_{17}^p = 0$ $\phi_{18}^p = 0$
<b>p=3</b>	$N_{dof}=30$	
$\phi_{19}^{vx} = -c_F^2 t^3 - 3x^2 t$ $\phi_{20}^{vx} = 0$ $\phi_{21}^{vx} = -2xyt$ $\phi_{22}^{vx} = -xt^2$ $\phi_{23}^{vx} = -\frac{c_F^2 t^3}{3} - y^2 t$ $\phi_{24}^{vx} = 0$ $\phi_{25}^{vx} = -\frac{yt^2}{2}$ $\phi_{26}^{vx} = x^3$ $\phi_{27}^{vx} = y^3$ $\phi_{28}^{vx} = x^2 y$ $\phi_{29}^{vx} = xy^2$ $\phi_{30}^{vx} = 0$	$\phi_{19}^{vy} = 0$ $\phi_{20}^{vy} = -c_F^2 t^3 - 3y^2 t$ $\phi_{21}^{vy} = -\frac{c_F^2 t^3}{3} - x^2 t$ $\phi_{22}^{vy} = -\frac{x^2 y}{c_F^2}$ $\phi_{23}^{vy} = -2xyt$ $\phi_{24}^{vy} = -\frac{y^3}{3c_F^2} - y^2 t$ $\phi_{25}^{vy} = -\frac{xy^2}{2c_F^2} - \frac{xt^2}{2}$ $\phi_{26}^{vy} = -3x^2 y$ $\phi_{27}^{vy} = 0$ $\phi_{28}^{vy} = -xy^2$ $\phi_{29}^{vy} = -\frac{y^3}{3}$ $\phi_{30}^{vy} = x^3$	$\phi_{19}^p = x^3 + 3c_F^2 xt^2$ $\phi_{20}^p = y^3 + 3c_F^2 yt^2$ $\phi_{21}^p = x^2 y + c_F^2 yt^2$ $\phi_{22}^p = \frac{c_F^2 t^3}{3} + x^2 t$ $\phi_{23}^p = y^2 x + c_F^2 xt^2$ $\phi_{24}^p = \frac{c_F^2 t^3}{3} + y^2 t$ $\phi_{25}^p = xyt$ $\phi_{26}^p = 0$ $\phi_{27}^p = 0$ $\phi_{28}^p = 0$ $\phi_{29}^p = 0$ $\phi_{30}^p = 0$

TABLE B.1: Trefftz-DG polynomial basis for velocity  $v_F = (v_F^x(x, y, t); v_F^y(x, y, t))^T$  and pressure  $p = p(x, y, t)$  fields (degree p=0,1,2,3).

## B.2 2D Elastodynamic system

<b>p=0</b>	$N_{dof}=5$			
$\phi_1^{v_x} = 1$	$\phi_1^{v_y} = 0$	$\phi_1^{\sigma_{xx}} = 0$	$\phi_1^{\sigma_{yy}} = 0$	$\phi_1^{\sigma_{xy}} = 0$
$\phi_2^{v_x} = 0$	$\phi_2^{v_y} = 1$	$\phi_2^{\sigma_{xx}} = 0$	$\phi_2^{\sigma_{yy}} = 0$	$\phi_2^{\sigma_{xy}} = 0$
$\phi_3^{v_x} = 0$	$\phi_3^{v_y} = 0$	$\phi_3^{\sigma_{xx}} = 1$	$\phi_3^{\sigma_{yy}} = 0$	$\phi_3^{\sigma_{xy}} = 0$
$\phi_4^{v_x} = 0$	$\phi_4^{v_y} = 0$	$\phi_4^{\sigma_{xx}} = 0$	$\phi_4^{\sigma_{yy}} = 1$	$\phi_4^{\sigma_{xy}} = 0$
$\phi_5^{v_x} = 0$	$\phi_5^{v_y} = 0$	$\phi_5^{\sigma_{xx}} = 0$	$\phi_5^{\sigma_{yy}} = 0$	$\phi_5^{\sigma_{xy}} = 0$
<b>p=1</b>	$N_{dof}=15$			
$\phi_6^{v_x} = -y$	$\phi_6^{v_y} = x$	$\phi_6^{\sigma_{xx}} = 0$	$\phi_6^{\sigma_{yy}} = 0$	$\phi_6^{\sigma_{xy}} = 0$
$\phi_7^{v_x} = t$	$\phi_7^{v_y} = 0$	$\phi_7^{\sigma_{xx}} = x$	$\phi_7^{\sigma_{yy}} = 0$	$\phi_7^{\sigma_{xy}} = 0$
$\phi_8^{v_x} = 0$	$\phi_8^{v_y} = 0$	$\phi_8^{\sigma_{xx}} = y$	$\phi_8^{\sigma_{yy}} = 0$	$\phi_8^{\sigma_{xy}} = 0$
$\phi_9^{v_x} = a_{11}x + 2a_{13}y$	$\phi_9^{v_y} = a_{12}y$	$\phi_9^{\sigma_{xx}} = t$	$\phi_9^{\sigma_{yy}} = 0$	$\phi_9^{\sigma_{xy}} = 0$
$\phi_{10}^{v_x} = 0$	$\phi_{10}^{v_y} = 0$	$\phi_{10}^{\sigma_{xx}} = 0$	$\phi_{10}^{\sigma_{yy}} = x$	$\phi_{10}^{\sigma_{xy}} = 0$
$\phi_{11}^{v_x} = 0$	$\phi_{11}^{v_y} = t$	$\phi_{11}^{\sigma_{xx}} = 0$	$\phi_{11}^{\sigma_{yy}} = y$	$\phi_{11}^{\sigma_{xy}} = 0$
$\phi_{12}^{v_x} = a_{12}x + 2a_{23}y$	$\phi_{12}^{v_y} = a_{22}y$	$\phi_{12}^{\sigma_{xx}} = 0$	$\phi_{12}^{\sigma_{yy}} = t$	$\phi_{12}^{\sigma_{xy}} = 0$
$\phi_{13}^{v_x} = 0$	$\phi_{13}^{v_y} = 0$	$\phi_{13}^{\sigma_{xx}} = 0$	$\phi_{13}^{\sigma_{yy}} = 0$	$\phi_{13}^{\sigma_{xy}} = x$
$\phi_{14}^{v_x} = t$	$\phi_{14}^{v_y} = 0$	$\phi_{14}^{\sigma_{xx}} = 0$	$\phi_{14}^{\sigma_{yy}} = 0$	$\phi_{14}^{\sigma_{xy}} = y$
$\phi_{15}^{v_x} = a_{13}x + 2a_{33}y$	$\phi_{15}^{v_y} = a_{23}y$	$\phi_{15}^{\sigma_{xx}} = 0$	$\phi_{15}^{\sigma_{yy}} = 0$	$\phi_{15}^{\sigma_{xy}} = t$

TABLE B.2: Trefftz-DG polynomial basis for velocity  $v_S = (v_S^x(x, y, t); v_S^y(x, y, t))^T$  and stress  $\sigma = (\sigma_{xx}(x, y, t), \sigma_{yy}(x, y, t), \sigma_{xy}(x, y, t))$  fields (degree p=0,1).

<b>p=2</b>	$N_{\text{dof}}=30$			
$\phi_{16}^{vx} = 0$	$\phi_{16}^{vy} = 0$	$\phi_{16}^{\sigma_{xx}} = y^2$	$\phi_{16}^{\sigma_{yy}} = 0$	$\phi_{16}^{\sigma_{xy}} = 0$
$\phi_{17}^{vx} = 2a_{11}xt$	$\phi_{17}^{vy} = 4a_{13}xt + 2a_{12}yt$	$\phi_{17}^{\sigma_{xx}} = a_{11}x^2 + t^2$	$\phi_{17}^{\sigma_{yy}} = a_{12}y^2$	$\phi_{17}^{\sigma_{xy}} = 2a_{13}x^2$
$\phi_{18}^{vx} = yt$	$\phi_{18}^{vy} = -xt$	$\phi_{18}^{\sigma_{xx}} = xy$	$\phi_{18}^{\sigma_{yy}} = -xy$	$\phi_{18}^{\sigma_{xy}} = 0$
$\phi_{19}^{vx} = \frac{a_{11}x^2}{2} - \frac{a_{12}y^2}{2} + \frac{t^2}{2}$	$\phi_{19}^{vy} = a_{13}x^2 + a_{12}y^2$	$\phi_{19}^{\sigma_{xx}} = xt$	$\phi_{19}^{\sigma_{yy}} = 0$	$\phi_{19}^{\sigma_{xy}} = 0$
$\phi_{20}^{vx} = a_{13}y^2 + a_{11}xy$	$\phi_{20}^{vy} = -\frac{a_{11}x^2}{2} + \frac{a_{12}y^2}{2}$	$\phi_{20}^{\sigma_{xx}} = yt$	$\phi_{20}^{\sigma_{yy}} = 0$	$\phi_{20}^{\sigma_{xy}} = 0$
$\phi_{21}^{vx} = 0$	$\phi_{21}^{vy} = 0$	$\phi_{21}^{\sigma_{xx}} = 0$	$\phi_{21}^{\sigma_{yy}} = x^2$	$\phi_{21}^{\sigma_{xy}} = 0$
$\phi_{22}^{vx} = 2a_{12}xt$	$\phi_{22}^{vy} = 4a_{23}xt + 2a_{22}yt$	$\phi_{22}^{\sigma_{xx}} = a_{12}x^2$	$\phi_{22}^{\sigma_{yy}} = a_{22}y^2 + t^2$	$\phi_{22}^{\sigma_{xy}} = 2a_{23}x^2$
$\phi_{23}^{vx} = 0$	$\phi_{23}^{vy} = 0$	$\phi_{23}^{\sigma_{xx}} = 0$	$\phi_{23}^{\sigma_{yy}} = xy$	$\phi_{23}^{\sigma_{xy}} = -\frac{x^2}{2}$
$\phi_{24}^{vx} = \frac{a_{12}x^2}{2} - \frac{a_{22}y^2}{2}$	$\phi_{24}^{vy} = a_{23}x^2 + a_{22}xy$	$\phi_{24}^{\sigma_{xx}} = 0$	$\phi_{24}^{\sigma_{yy}} = xt$	$\phi_{24}^{\sigma_{xy}} = 0$
$\phi_{25}^{vx} = a_{23}y^2 + a_{12}xy$	$\phi_{25}^{vy} = -\frac{a_{12}x^2}{2} + \frac{a_{22}y^2}{2} + \frac{t^2}{2}$	$\phi_{25}^{\sigma_{xx}} = 0$	$\phi_{25}^{\sigma_{yy}} = yt$	$\phi_{25}^{\sigma_{xy}} = 0$
$\phi_{26}^{vx} = 2yt$	$\phi_{26}^{vy} = -2xt$	$\phi_{26}^{\sigma_{xx}} = 0$	$\phi_{26}^{\sigma_{yy}} = 0$	$\phi_{26}^{\sigma_{xy}} = -x^2 + y^2$
$\phi_{27}^{vx} = 2a_{13}xt$	$\phi_{27}^{vy} = 4a_{33}xt + 2a_{23}yt$	$\phi_{27}^{\sigma_{xx}} = a_{13}x^2$	$\phi_{27}^{\sigma_{yy}} = a_{23}y^2$	$\phi_{27}^{\sigma_{xy}} = 2a_{33}x^2 + t^2$
$\phi_{28}^{vx} = 0$	$\phi_{28}^{vy} = 0$	$\phi_{28}^{\sigma_{xx}} = -\frac{x^2}{2}$	$\phi_{28}^{\sigma_{yy}} = -\frac{y^2}{2}$	$\phi_{28}^{\sigma_{xy}} = xy$
$\phi_{29}^{vx} = \frac{a_{13}x^2}{2} - \frac{a_{23}y^2}{2}$	$\phi_{29}^{vy} = a_{33}x^2 + a_{23}xy + \frac{t^2}{2}$	$\phi_{29}^{\sigma_{xx}} = 0$	$\phi_{29}^{\sigma_{yy}} = 0$	$\phi_{29}^{\sigma_{xy}} = xt$
$\phi_{30}^{vx} = a_{33}y^2 + a_{13}xy + \frac{t^2}{2}$	$\phi_{30}^{vy} = -\frac{a_{13}x^2}{2} + \frac{a_{23}y^2}{2}$	$\phi_{30}^{\sigma_{xx}} = 0$	$\phi_{30}^{\sigma_{yy}} = 0$	$\phi_{30}^{\sigma_{xy}} = yt$

TABLE B.3: Trefftz-DG polynomial basis for velocity  $v_S = (v_S^x(x, y, t); v_S^y(x, y, t))^T$  and stress  $\sigma = (\sigma_{xx}(x, y, t), \sigma_{yy}(x, y, t), \sigma_{xy}(x, y, t))$  fields (degree p=2).

$p=3$	$N_{\text{dof}}=50$			
$\phi_{31}^{vx} = x^3 + 3(\lambda + 2\mu)t^2x$	$\phi_{31}^{vy} = 0$	$\phi_{31}^{\sigma_{xx}} = (\lambda + 2\mu)^2t^3 + 3(\lambda + 2\mu)x^2t$	$\phi_{31}^{\sigma_{yy}} = \lambda(\lambda + 2\mu)t^3 + 3\lambda x^2t$	$\phi_{31}^{\sigma_{xy}} = 0$
$\phi_{32}^{vx} = y^3 + 3\mu t^2y$	$\phi_{32}^{vy} = 0$	$\phi_{32}^{\sigma_{xx}} = 0$	$\phi_{32}^{\sigma_{yy}} = 0$	$\phi_{32}^{\sigma_{xy}} = \mu t^3 + 3\mu y^2t$
$\phi_{33}^{vx} = x^2y + (\lambda + 2\mu)t^2y$	$\phi_{33}^{vy} = (\lambda + \mu)t^2x$	$\phi_{33}^{\sigma_{xx}} = 2(\lambda + 2\mu)xyt$	$\phi_{33}^{\sigma_{yy}} = 2\lambda xyt$	$\phi_{33}^{\sigma_{xy}} = \frac{\mu(2\lambda+3\mu)t^3}{3} + \mu x^2t$
$\phi_{34}^{vx} = \frac{(\lambda+2\mu)t^3}{3} + x^2t$	$\phi_{34}^{vy} = 0$	$\phi_{34}^{\sigma_{xx}} = (\lambda + 2\mu)t^2x$	$\phi_{34}^{\sigma_{yy}} = -y^2x + \lambda t^2x$	$\phi_{34}^{\sigma_{xy}} = x^2y$
$\phi_{35}^{vx} = y^2x + \mu t^2x$	$\phi_{35}^{vy} = (\lambda + \mu)t^2y$	$\phi_{35}^{\sigma_{xx}} = \frac{(\mu(\lambda+2\mu)+\lambda(\lambda+\mu))t^3}{3} + (\lambda + 2\mu)y^2t$	$\phi_{35}^{\sigma_{yy}} = \frac{((\lambda+\mu)(\lambda+2\mu)+\lambda\mu)t^3}{3} + \lambda y^2t$	$\phi_{35}^{\sigma_{xy}} = 2\mu xyt$
$\phi_{36}^{vx} = \frac{\mu t^3}{3} + y^2t$	$\phi_{36}^{vy} = 0$	$\phi_{36}^{\sigma_{xx}} = y^2x$	$\phi_{36}^{\sigma_{yy}} = 0$	$\phi_{36}^{\sigma_{xy}} = \mu t^2y$
$\phi_{37}^{vx} = xyt$	$\phi_{37}^{vy} = \frac{(\lambda+\mu)t^3}{6}$	$\phi_{37}^{\sigma_{xx}} = \frac{x^2y}{2} + \frac{(\lambda+2\mu)t^2y}{2}$	$\phi_{37}^{\sigma_{yy}} = \frac{t^2y}{2}$	$\phi_{37}^{\sigma_{xy}} = \frac{\mu t^2x}{2}$
$\phi_{38}^{vx} = 0$	$\phi_{38}^{vy} = x^3 + 3\mu t^2x$	$\phi_{38}^{\sigma_{xx}} = 0$	$\phi_{38}^{\sigma_{yy}} = 0$	$\phi_{38}^{\sigma_{xy}} = \mu^2t^3 + 3\mu x^2t$
$\phi_{39}^{vx} = 0$	$\phi_{39}^{vy} = y^3 + 3(\lambda + 2\mu)t^2y$	$\phi_{39}^{\sigma_{xx}} = l(\lambda + 2\mu)t^3 + 3\lambda y^2t$	$\phi_{39}^{\sigma_{yy}} = (\lambda + 2\mu)^2t^3 + 3(\lambda + 2\mu)y^2t$	$\phi_{39}^{\sigma_{xy}} = 0$
$\phi_{40}^{vx} = (\lambda + \mu)t^2x$	$\phi_{40}^{vy} = x^2y + \mu t^2y$	$\phi_{40}^{\sigma_{xx}} = \frac{((\lambda+\mu)(\lambda+2\mu)+\lambda\mu)t^3}{3} + \lambda x^2t$	$\phi_{40}^{\sigma_{yy}} = \frac{(\mu(\lambda+2\mu)+\lambda(\lambda+\mu))t^3}{3} + (\lambda + 2\mu)x^2t$	$\phi_{40}^{\sigma_{xy}} = 2\mu xyt$
$\phi_{41}^{vx} = 0$	$\phi_{41}^{vy} = \frac{\mu t^3}{3} + x^2t$	$\phi_{41}^{\sigma_{xx}} = 0$	$\phi_{41}^{\sigma_{yy}} = x^2y$	$\phi_{41}^{\sigma_{xy}} = \mu t^2x$
$\phi_{42}^{vx} = (\lambda + \mu)t^2y$	$\phi_{42}^{vy} = y^2x + (\lambda + 2\mu)t^2x$	$\phi_{42}^{\sigma_{xx}} = 2\lambda xyt$	$\phi_{42}^{\sigma_{yy}} = 2(\lambda + 2\mu)xyt$	$\phi_{42}^{\sigma_{xy}} = \frac{\mu(2\lambda+3\mu)t^3}{3} + \mu y^2t$
$\phi_{43}^{vx} = 0$	$\phi_{43}^{vy} = \frac{(\lambda+2\mu)t^3}{3} + y^2t$	$\phi_{43}^{\sigma_{xx}} = -x^2y + \lambda t^2y$	$\phi_{43}^{\sigma_{yy}} = (\lambda + 2\mu)t^2y$	$\phi_{43}^{\sigma_{xy}} = y^2x$
$\phi_{44}^{vx} = \frac{(\lambda+\mu)t^3}{6}$	$\phi_{44}^{vy} = xyt$	$\phi_{44}^{\sigma_{xx}} = \frac{\lambda t^2x}{2}$	$\phi_{44}^{\sigma_{yy}} = \frac{y^2x}{2} + \frac{(\lambda+2\mu)t^2x}{2}$	$\phi_{44}^{\sigma_{xy}} = \frac{\mu t^2y}{2}$
$\phi_{45}^{vx} = 0$	$\phi_{45}^{vy} = 0$	$\phi_{45}^{\sigma_{xx}} = x^3$	$\phi_{45}^{\sigma_{yy}} = 3y^2x$	$\phi_{45}^{\sigma_{xy}} = 3x^2y$
$\phi_{46}^{vx} = 0$	$\phi_{46}^{vy} = 0$	$\phi_{46}^{\sigma_{xx}} = y^3$	$\phi_{46}^{\sigma_{yy}} = 0$	$\phi_{46}^{\sigma_{xy}} = 0$
$\phi_{47}^{vx} = 0$	$\phi_{47}^{vy} = 0$	$\phi_{47}^{\sigma_{xx}} = 0$	$\phi_{47}^{\sigma_{yy}} = x^3$	$\phi_{47}^{\sigma_{xy}} = 0$
$\phi_{48}^{vx} = 0$	$\phi_{48}^{vy} = 0$	$\phi_{48}^{\sigma_{xx}} = 3x^2y$	$\phi_{48}^{\sigma_{yy}} = y^3$	$\phi_{48}^{\sigma_{xy}} = -3y^2x$
$\phi_{49}^{vx} = 0$	$\phi_{49}^{vy} = 0$	$\phi_{49}^{\sigma_{xx}} = 0$	$\phi_{49}^{\sigma_{yy}} = -3x^2y$	$\phi_{49}^{\sigma_{xy}} = x^3$
$\phi_{50}^{vx} = 0$	$\phi_{50}^{vy} = 0$	$\phi_{50}^{\sigma_{xx}} = -3xy^2$	$\phi_{50}^{\sigma_{yy}} = 0$	$\phi_{50}^{\sigma_{xy}} = y^3$

TABLE B.4: Trefftz-DG polynomial basis for velocity  $v_S = (v_S^x(x, y, t); v_S^y(x, y, t))^T$  and stress  $\sigma = (\sigma_{xx}(x, y, t), \sigma_{yy}(x, y, t), \sigma_{xy}(x, y, t))$  fields (degree  $p=3$ ).

## Appendix C

# Gaussian quadrature

Mathematicians and scientists are sometime confronted with definite integrals which are not easily evaluated analytically, even a function  $f(x)$  is known completely. To overcome this difficulty numerical methods are used. Numerical integration involves replacing an integral by a sum. The term quadrature is used as a synonym for numerical integration in one dimension. Let  $f(x)$  be a function which is defined on some interval  $[a, b]$  and on the set of distinct points  $x_0, x_1, \dots, x_n$  Then the numerical integration for approximation can be defined as

$$\int_a^b f(x)dx \simeq \sum_{l=1}^n f(x_l^G)w_l^G,$$

where  $w_i$  are the quadrature weights, and  $x_i$  are the quadrature points.

There are a number of numerical integration methods for evaluation of definite integrals. The most commonly used methods are the Newton-Cotes formulas and Gaussian quadrature rules. The numerical integration methods that are derived by integrating the Newton interpolation formulas are termed as Newton-Cotes integration formulas. The Trapezoidal rule and Simpson's rule are members of this family.

The specific of these methods is in a simple choice of points to evaluate a function  $f(x)$  in a known interval  $[a, b]$ . These methods are based on equally space points.

When we have freedom of choice regarding evaluation points, then more accuracy can be achieved. Gaussian quadrature is a powerful tool for approximating integrals. The quadrature rules are all based on special values of weights and abscissas. Abscissas are commonly called evaluation points or "Gauss points", which are normally pre-computed and available in most standard mathematics tables. Algorithms and computer codes are also available to compute them.

For the numerical tests we have computed the surface integrals on the segments (1e+time simulations), and on the triangular and rectangular faces (2e+time simulations).

## C.1 Integration over the unit segment and square

For the approximate integration over the unit segment  $[0, 1]$ , we have computed the following Gaussian points and weights:

$n$	$w^G$	$x^G$
15	1.5376620998e-02	6.0037409897e-03
	3.5183023744e-02	3.1363303799e-02
	5.3579610233e-02	7.5896708294e-02
	6.9785338963e-02	1.3779113431e-01
	8.3134602908e-02	2.1451391369e-01
	9.3080500007e-02	3.0292432646e-01
	9.9215742663e-02	3.9940295300e-01
	1.0128912096e-01	5.e-1
	9.9215742663e-02	1-3.9940295300e-01
	9.3080500007e-02	1-3.0292432646e-01
	8.3134602908e-02	1-2.1451391369e-01
	6.9785338963e-02	1-1.3779113431e-01
	5.3579610233e-02	1-7.5896708294e-02
	3.5183023744e-02	1-3.1363303799e-02
	1.5376620998e-02	1-6.0037409897e-03

TABLE C.1: Computed weights  $w^G$  and corresponding Gauss points  $x^G$  for 15 point integration over the unit segment.

The 2D integration over the unit square can be represented as a successive 1D integration in each of both directions. Thus, we can recall the Gaussian nodes and weights for 1D integration over the unit segment.

## C.2 Integration over the unit triangle

The Gaussian points and weights for unit triangles computed by Hussain et al. in [63] are presented here. The authors develop different strategies, one of them is the Gaussian quadrature formula for unit triangles (GQUTS), and they provide the numerical experiments comparing the accuracy. In the tables C.2 and C.3 we give the computed Gauss points  $(x^G, y^G)$  and weights  $w^G$  for  $n \times n$  point method CQUTS ( $n = 2, 3, 7$ ).

$n$	$w^G$	$x^G$	$y^G$
2	0.5283121635e-01	0.1666666667e+00	0.7886751346e+00
	0.1971687836e+00	0.6220084679e+00	0.2113248654e+00
	0.5283121635e-01	0.4465819874e-01	0.7886751346e+00
	0.1971687836e+00	0.1666666667e+00	0.2113248654e+00
3	0.9876542474e-01	0.2500000000e+00	0.5000000000e+00
	0.1391378575e-01	0.5635083269e-01	0.8872983346e+00
	0.1095430035e+00	0.4436491673e+00	0.1127016654e+00
	0.6172839460e-01	0.4436491673e+00	0.5000000000e+00
	0.8696116674e-02	0.1000000000e+00	0.8872983346e+00
	0.6846438175e-01	0.7872983346e+00	0.1127016654e+00
	0.6172839460e-01	0.5635083269e-01	0.5000000000e+00
	0.8696116674e-02	0.1270166538e-01	0.8872983346e+00
0.6846438175e-01	0.1000000000e+00	0.1127016654e+00	

TABLE C.2: Computed weights  $w^G$  and corresponding Gauss points  $(x^G, y^G)$  for  $n \times n$  point GQUTS ( $n = 2, 3$ ) [63].

$n$	$w^G$	$x^G$	$y^G$
7	0.2183621219e-01	0.2500000000e+00	0.5000000000e+00
	0.1185259869e-01	0.1485387122e+00	0.7029225757e+00
	0.2804474024e-01	0.3514612878e+00	0.2970774243e+00
	0.3777048400e-02	0.6461720360e-01	0.8707655928e+00
	0.2544928909e-01	0.4353827964e+00	0.1292344072e+00
	0.3442812316e-03	0.1272302191e-01	0.9745539562e+00
	0.1318557174e-01	0.4872769781e+00	0.2544604383e-01
	0.1994866947e-01	0.3514612878e+00	0.5000000000e+00
	0.1082804890e-01	0.2088224283e+00	0.7029225757e+00
	0.2562052651e-01	0.4941001474e+00	0.2970774243e+00
	0.3450556783e-02	0.9084178238e-01	0.8707655928e+00
	0.2324942860e-01	0.6120807933e+00	0.1292344072e+00
	0.3145212381e-03	0.1788659867e-01	0.9745539562e+00
	0.1204579851e-01	0.6850359770e+00	0.2544604383e-01
	0.1994866947e-01	0.1485387122e+00	0.5000000000e+00
	0.1082804890e-01	0.8825499604e-01	0.7029225757e+00
	0.2562052651e-01	0.2088224283e+00	0.2970774243e+00
	0.3450556783e-02	0.3839262482e-01	0.8707655928e+00
	0.2324942860e-01	0.2586847995e+00	0.1292344072e+00
	0.3145212381e-03	0.7559445160e-02	0.9745539562e+00
	0.1204579851e-01	0.2895179792e+00	0.2544604383e-01
	0.1461316874e-01	0.4353827964e+00	0.5000000000e+00
	0.7931962886e-02	0.2586847995e+00	0.7029225757e+00
	0.1876802249e-01	0.6120807933e+00	0.2970774243e+00
	0.2527665748e-02	0.1125328752e+00	0.8707655928e+00
	0.1703110194e-01	0.7582327176e+00	0.1292344072e+00
	0.2303989213e-03	0.2215753944e-01	0.9745539562e+00
	0.8824011376e-02	0.8486080534e+00	0.2544604383e-01
	0.1461316874e-01	0.6461720360e-01	0.5000000000e+00
	0.7931962886e-02	0.3839262482e-01	0.7029225757e+00
	0.1876802249e-01	0.9084178238e-01	0.2970774243e+00
	0.2527665748e-02	0.1670153200e-01	0.8707655928e+00
	0.1703110194e-01	0.1125328752e+00	0.1292344072e+00
	0.2303989213e-03	0.3288504390e-02	0.9745539562e+00
	0.8824011376e-02	0.1259459028e+00	0.2544604383e-01
	0.6764926484e-02	0.4872769781e+00	0.5000000000e+00
	0.3671971955e-02	0.2895179792e+00	0.7029225757e+00
	0.8688347794e-02	0.6850359770e+00	0.2970774243e+00
	0.1170141347e-02	0.1259459028e+00	0.8707655928e+00
	0.7884268950e-02	0.8486080534e+00	0.1292344072e+00
	0.1066593969e-03	0.2479854268e-01	0.9745539562e+00
	0.4084931154e-02	0.9497554135e+00	0.2544604383e-01
0.6764926484e-02	0.1272302191e-01	0.5000000000e+00	
0.3671971955e-02	0.7559445160e-02	0.7029225757e+00	
0.8688347794e-02	0.1788659867e-01	0.2970774243e+00	
0.1170141347e-02	0.3288504390e-02	0.8707655928e+00	
0.7884268950e-02	0.2215753944e-01	0.1292344072e+00	
0.1066593969e-03	0.6475011465e-03	0.9745539562e+00	
0.4084931154e-02	0.2479854268e-01	0.2544604383e-01	

TABLE C.3: Computed weights  $w^G$  and corresponding Gauss points  $(x^G, y^G)$  for  $n \times n$  point GQUTS ( $n = 7$ ) [63].



# Bibliography

- [1] Gar6more2D, 2013. URL <https://gforge.inria.fr/projects/gar6more2d/Magique-3D>.
- [2] R. Abedi, S.-H. Chung, J. Erickson, Y. Fan, M. Garland, D. Guoy, R. Haber, J. M. Sullivan, S. Thite, and Y. Zhou. Spacetime meshing with adaptive refinement and coarsening. In *Proceedings of the twentieth annual symposium on Computational geometry*, pages 300–309. ACM, 2004.
- [3] R. Abedi, R. B. Haber, S. Thite, and J. Erickson. An h-adaptive spacetime-discontinuous galerkin method for linear elastodynamics. *European Journal of Computational Mechanics/Revue Européenne de Mécanique Numérique*, 15(6):619–642, 2006.
- [4] R. Abedi, B. Petracovici, and R. B. Haber. A space-time discontinuous Galerkin method for linearized elastodynamics with element-wise momentum balance. *Computer Methods in Applied Mechanics and Engineering*, 195(25-28):3247–3273, 2006.
- [5] R. Abedi, S.-H. Chung, M. A. Hawker, J. Palaniappan, and R. B. Haber. Modeling evolving discontinuities with spacetime discontinuous Galerkin methods. In *IUTAM Symposium on Discretization Methods for Evolving Discontinuities*, pages 59–87. Springer, 2007.
- [6] K. Aki and P. G. Richards. Quantitative seismology. 2002.
- [7] G. Allaire. *Numerical analysis and optimization: an introduction to mathematical modelling and numerical simulation*. Oxford university press, 2007.
- [8] P. F. Antonietti, I. Mazzieri, N. Dal Santo, and A. Quarteroni. A high-order discontinuous Galerkin approximation to ordinary differential equations with applications to elastodynamics. *IMA Journal of Numerical Analysis*, 38(4):1709–1734, 2018.
- [9] I. Babuška and M. Zlámal. Nonconforming elements in the finite element method with penalty. *SIAM Journal on Numerical Analysis*, 10(5):863–875, 1973.

- [10] Z. Badics. Trefftz-discontinuous Galerkin and finite element multi-solver technique for modeling time-harmonic EM problems with high-conductivity regions. *IEEE Transactions on Magnetics*, 50(2):401–404, 2014.
- [11] C. Baldassari, H. Barucq, H. Calandra, B. Denel, and J. Diaz. Performance analysis of a high-order Discontinuous Galerkin method application to the reverse time migration. *Communications in Computational Physics*, 11(2):660–673, 2012.
- [12] L. Banjai, E. H. Georgoulis, and O. Lijoka. A Trefftz polynomial space-time discontinuous Galerkin method for the second order wave equation. *SIAM Journal on Numerical Analysis*, 55(1):63–86, 2017.
- [13] H. Barucq, A. Bendali, J. Diaz, and S. Tordeux. Trefftz methods based on shaped functions locally computed with discontinuous galerkin methods. application to the helmholtz equation. *Book of Abstracts ENUMATH 2017*, page 207.
- [14] H. Barucq, J. Diaz, R. Djellouli, and E. Estecahandy. High-order Discontinuous Galerkin approximations for elasto-acoustic scattering problems. In *XXIV Congress on Differential Equations and Applications/XIV Congress on Applied Mathematics (XXIV CEDYA/XIV CMA)*, 2015.
- [15] H. Barucq, A. Bendali, M. Fares, V. Mattesi, and S. Tordeux. A symmetric trefftz-dg formulation based on a local boundary element method for the solution of the helmholtz equation. *Journal of Computational Physics*, 330:1069–1092, 2017.
- [16] S. Barz, I. Kassal, M. Ringbauer, Y. O. Lipp, B. Dakić, A. Aspuru-Guzik, and P. Walther. A two-qubit photonic quantum processor and its application to solving systems of linear equations. *Scientific reports*, 4:6115, 2014.
- [17] F. Bassi and S. Rebay. A high-order accurate discontinuous finite element method for the numerical solution of the compressible Navier–Stokes equations. *Journal of computational physics*, 131(2):267–279, 1997.
- [18] F. Bassi, S. Rebay, G. Mariotti, S. Pedinotti, and M. Savini. A high-order accurate discontinuous finite element method for inviscid and viscous turbomachinery flows. In *Proceedings of the 2nd European Conference on Turbomachinery Fluid Dynamics and Thermodynamics*, pages 99–109. Technologisch Instituut, Antwerpen, Belgium, 1997.
- [19] P. Benioff. The computer as a physical system: A microscopic quantum mechanical Hamiltonian model of computers as represented by turing machines. *Journal of statistical physics*, 22(5):563–591, 1980.

- [20] R. Biswas, Z. Jiang, K. Kechezhi, S. Knysh, S. Mandra, B. O’Gorman, A. Perdomo-Ortiz, A. Petukhov, J. Realpe-Gómez, E. Rieffel, et al. A NASA perspective on quantum computing: Opportunities and challenges. *Parallel Computing*, 64:81–98, 2017.
- [21] E. Bossy. *Evaluation ultrasonore de l’os cortical par transmission axiale: modélisation et expérimentation in vitro et in vivo*. PhD thesis, Université Pierre et Marie Curie-Paris VI, 2003.
- [22] F. Brezzi and L. Marini. Virtual element and discontinuous Galerkin methods. In *Recent developments in discontinuous Galerkin finite element methods for partial differential equations*, pages 209–221. Springer, 2014.
- [23] I. Bubnov. Report on the works of Prof. Timoshenko which were awarded the Zhuranskii prize. Symposium of the Institute of Communication Engineers (Sborn. inta inzh. putei soobshch.). Technical report, Technical Report.
- [24] I. Bubnov. Structural Mechanics of Shipbuilding (in russian). 1914.
- [25] K. E. Bullen and B. A. Bolt. *An introduction to the theory of seismology*. Cambridge university press, 1985.
- [26] X.-D. Cai, C. Weedbrook, Z.-E. Su, M.-C. Chen, M. Gu, M.-J. Zhu, L. Li, N.-L. Liu, C.-Y. Lu, and J.-W. Pan. Experimental quantum computing to solve systems of linear equations. *Physical review letters*, 110(23):230501, 2013.
- [27] M. Ciałkowski and M. Jarosławski. The use of symbolic computation for generating of wave equations solution. *Zeszyty Naukowe Politechniki Poznańskiej, MR i T*, 56:115–140, 2003.
- [28] B. Cockburn. An introduction to the discontinuous Galerkin method for convection-dominated problems. In *Advanced numerical approximation of non-linear hyperbolic equations*, pages 150–268. Springer, 1998.
- [29] B. Cockburn and P.-A. Gremaud. Error estimates for finite element methods for scalar conservation laws. *SIAM Journal on Numerical Analysis*, 33(2):522–554, 1996.
- [30] B. Cockburn, F. Li, and C.-W. Shu. Locally divergence-free discontinuous Galerkin methods for the Maxwell equations. *Journal of Computational Physics*, 194(2): 588–610, 2004.
- [31] B. Cockburn, G. Kanschat, and D. Schötzau. A locally conservative ldg method for the incompressible navier-stokes equations. *Mathematics of Computation*, 74 (251):1067–1095, 2005.

- [32] G. Cohen, X. Ferrieres, and S. Pernet. A spatial high-order hexahedral discontinuous Galerkin method to solve Maxwell's equations in time domain. *Journal of Computational Physics*, 217(2):340–363, 2006.
- [33] C. Dawson and V. Aizinger. A discontinuous Galerkin method for three-dimensional shallow water equations. *Journal of Scientific Computing*, 22(1-3):245–267, 2005.
- [34] J. de la Puente, M. Käser, M. Dumbser, and H. Igel. An arbitrary high-order discontinuous Galerkin method for elastic waves on unstructured meshes-IV. Anisotropy. *Geophysical Journal International*, 169(3):1210–1228, 2007.
- [35] D. Deutsch. Quantum theory, the Church-Turing principle and the universal quantum computer. *Proc. R. Soc. Lond. A*, 400(1818):97–117, 1985.
- [36] J. Diaz. *Approches analytiques et numériques de problèmes de transmission en propagation d'ondes en régime transitoire. Application au couplage fluide-structure et aux méthodes de couches parfaitement adaptées*. PhD thesis, ENSTA ParisTech, 2005.
- [37] M. Dumbser and M. Käser. An arbitrary high-order discontinuous Galerkin method for elastic waves on unstructured meshes—II. The three-dimensional isotropic case. *Geophysical Journal International*, 167(1):319–336, 2006.
- [38] M. Dumbser, M. Kaser, and E. F. Toro. An arbitrary high-order discontinuous Galerkin method for elastic waves on unstructured meshes-V. Local time stepping and p-adaptivity. *Geophysical Journal International*, 171(2):695–717, 2007.
- [39] H. Egger, F. Kretschmar, S. M. Schnepf, and T. Weiland. A space-time discontinuous Galerkin Trefftz method for time dependent Maxwell's equations. *SIAM Journal on Scientific Computing*, 37(5):B689–B711, 2015.
- [40] J. Erickson, D. Guoy, J. M. Sullivan, and A. Üngör. Building spacetime meshes over arbitrary spatial domains. *Engineering with Computers*, 20(4):342–353, 2005.
- [41] C. Eskilsson and S. Sherwin. Discontinuous Galerkin spectral/hp element modelling of dispersive shallow water systems. *Journal of Scientific Computing*, 22(1-3):269–288, 2005.
- [42] L. C. Evans. *Partial differential equations*. 2010.
- [43] C. Farhat, I. Harari, and U. Hetmaniuk. A discontinuous Galerkin method with lagrange multipliers for the solution of Helmholtz problems in the mid-frequency regime. *Computer Methods in Applied Mechanics and Engineering*, 192(11-12):1389–1419, 2003.

- [44] R. P. Feynman. Simulating physics with computers. *International journal of theoretical physics*, 21(6-7):467–488, 1982.
- [45] G. Gabard. Discontinuous Galerkin methods with plane waves for time-harmonic problems. *Journal of Computational Physics*, 225(2):1961–1984, 2007.
- [46] B. G. Galerkin. Series solution of some problems of elastic equilibrium of rods and plates. *Vestn. Inzh. Tekh*, 19:897–908, 1915.
- [47] M. Gander, L. Halpern, J. Rannou, and J. Ryan. A direct time parallel solver by diagonalization for the wave equation. 2017.
- [48] M. J. Gander and G. Wanner. From Euler, Ritz, and Galerkin to modern computing. *Siam Review*, 54(4):627–666, 2012.
- [49] R. P. Gilbert. Function theoretic methods in partial differential equations. Technical report, INDIANA UNIV AT BLOOMINGTON DEPT OF MATHEMATICS, 1969.
- [50] F. X. Giraldo, J. S. Hesthaven, and T. Warburton. Nodal high-order discontinuous Galerkin methods for the spherical shallow water equations. *Journal of Computational Physics*, 181(2):499–525, 2002.
- [51] J. Gopalakrishnan, P. Monk, and P. Sepúlveda. A tent pitching scheme motivated by Friedrichs theory. *Computers & Mathematics with Applications*, 70(5):1114–1135, 2015.
- [52] J. Gopalakrishnan, J. Schöberl, and C. Wintersteiger. Mapped tent pitching schemes for hyperbolic systems. *SIAM Journal on Scientific Computing*, 39(6):B1043–B1063, 2017.
- [53] M. J. Grote, A. Schneebeli, and D. Schötzau. Interior penalty discontinuous Galerkin method for Maxwell’s equations: Energy norm error estimates. *Journal of Computational and Applied Mathematics*, 204(2):375–386, 2007.
- [54] K. Grysa and B. Maciejewska. Trefftz functions for the non-stationary problems. *Journal of Theoretical and Applied Mechanics*, 51(2):251–264, 2013.
- [55] A. W. Harrow, A. Hassidim, and S. Lloyd. Quantum algorithm for linear systems of equations. *Physical review letters*, 103(15):150502, 2009.
- [56] I. Herrera. Boundary methods: A criterion for completeness. *Proceedings of the National Academy of Sciences*, 77(8):4395–4398, 1980.
- [57] I. Herrera. Trefftz method: a general theory. *Numerical Methods for Partial Differential Equations: An International Journal*, 16(6):561–580, 2000.

- 
- [58] J. S. Hesthaven and T. Warburton. *Nodal discontinuous Galerkin methods: algorithms, analysis, and applications*. Springer Science & Business Media, 2007.
- [59] R. Hiptmair, A. Moiola, and I. Perugia. Plane wave discontinuous Galerkin methods for the 2D Helmholtz equation: analysis of the p-version. *SIAM Journal on Numerical Analysis*, 49(1):264–284, 2011.
- [60] R. Hiptmair, A. Moiola, and I. Perugia. Error analysis of Trefftz-discontinuous Galerkin methods for the time-harmonic Maxwell equations. *Mathematics of Computation*, 82(281):247–268, 2013.
- [61] R. Hiptmair, A. Moiola, and I. Perugia. A survey of Trefftz methods for the Helmholtz equation. In *Building bridges: connections and challenges in modern approaches to numerical partial differential equations*, pages 237–279. Springer, 2016.
- [62] T. J. Hughes and G. M. Hulbert. Space-time finite element methods for elastodynamics: formulations and error estimates. *Computer methods in applied mechanics and engineering*, 66(3):339–363, 1988.
- [63] F. Hussain, M. Karim, and R. Ahamad. Appropriate Gaussian quadrature formulas for triangles. *International Journal of Applied Mathematics and Computation*, 4(1):023–038, 2012.
- [64] J. Jirousek. Basis for development of large finite elements locally satisfying all field equations. *Computer Methods in Applied Mechanics and Engineering*, 14(1):65–92, 1978.
- [65] J. Jirousek and P. Teodorescu. Large finite elements method for the solution of problems in the theory of elasticity. *Computers & Structures*, 15(5):575–587, 1982.
- [66] J. Jirousek and L. Guex. The hybrid-Trefftz finite element model and its application to plate bending. *International Journal for Numerical Methods in Engineering*, 23(4):651–693, 1986.
- [67] M. Käser and M. Dumbser. An arbitrary high-order discontinuous Galerkin method for elastic waves on unstructured meshes—I. The two-dimensional isotropic case with external source terms. *Geophysical Journal International*, 166(2):855–877, 2006.
- [68] M. Käser and M. Dumbser. A highly accurate discontinuous Galerkin method for complex interfaces between solids and moving fluids. *Geophysics*, 73(3):T23–T35, 2008.

- [69] M. Käser, M. Dumbser, J. De La Puente, and H. Igel. An arbitrary high-order discontinuous Galerkin method for elastic waves on unstructured meshes—III. Viscoelastic attenuation. *Geophysical Journal International*, 168(1):224–242, 2007.
- [70] R. M. Kirby, S. J. Sherwin, and B. Cockburn. To CG or to HDG: a comparative study. *Journal of Scientific Computing*, 51(1):183–212, 2012.
- [71] F. Kretschmar, S. M. Schnepp, I. Tsukerman, and T. Weiland. Discontinuous Galerkin methods with Trefftz approximations. *Journal of computational and applied mathematics*, 270:211–222, 2014.
- [72] F. Kretschmar, A. Moiola, I. Perugia, and S. M. Schnepp. A priori error analysis of space–time Trefftz discontinuous Galerkin methods for wave problems. *IMA Journal of Numerical Analysis*, 36(4):1599–1635, 2015.
- [73] P. Le Tallec. *Modélisation et calcul des milieux continus*. Editions Ecole Polytechnique, 2009.
- [74] A. W. Leissa. The historical bases of the Rayleigh and Ritz methods. *Journal of Sound and Vibration*, 287(4-5):961–978, 2005.
- [75] G. Lin and G. E. Karniadakis. A discontinuous Galerkin method for two-temperature plasmas. *Computer methods in applied mechanics and engineering*, 195(25-28):3504–3527, 2006.
- [76] J. Loverich and U. Shumlak. A discontinuous Galerkin method for the full two-fluid plasma model. *Computer Physics Communications*, 169(1-3):251–255, 2005.
- [77] R. B. Lowrie, P. L. Roe, and B. Van Leer. Space-time methods for hyperbolic conservation laws. In *Barriers and Challenges in Computational Fluid Dynamics*, pages 79–98. Springer, 1998.
- [78] A. Maciag. Three-dimensional wave polynomials. *Mathematical Problems in Engineering*, 2005(5):583–598, 2005.
- [79] A. Maciag. The usage of wave polynomials in solving direct and inverse problems for two-dimensional wave equation. *International Journal for Numerical Methods in Biomedical Engineering*, 27(7):1107–1125, 2011.
- [80] Y. Maday and E. M. Rønquist. Parallelization in time through tensor-product space–time solvers. *Comptes Rendus Mathématique*, 346(1-2):113–118, 2008.
- [81] I. Manin Yu. Vychislimoe i Nevychislimoe.

- [82] A. Moiola and I. Perugia. A space–time Trefftz discontinuous Galerkin method for the acoustic wave equation in first-order formulation. *Numerische Mathematik*, 138(2):389–435, 2018.
- [83] A. Moiola, R. Hiptmair, and I. Perugia. Plane wave approximation of homogeneous Helmholtz solutions. *Zeitschrift für angewandte Mathematik und Physik*, 62(5):809, 2011.
- [84] P. Monk and G. R. Richter. A discontinuous Galerkin method for linear symmetric hyperbolic systems in inhomogeneous media. *Journal of Scientific Computing*, 22(1-3):443–477, 2005.
- [85] O. Omid, R. Abedi, S. Enayatpour, et al. An adaptive meshing approach to capture hydraulic fracturing. In *49th US Rock Mechanics/Geomechanics Symposium*. American Rock Mechanics Association, 2015.
- [86] J. Palaniappan, R. B. Haber, and R. L. Jerrard. A spacetime discontinuous Galerkin method for scalar conservation laws. *Computer Methods in Applied Mechanics and Engineering*, 193(33-35):3607–3631, 2004.
- [87] J. Pan, Y. Cao, X. Yao, Z. Li, C. Ju, H. Chen, X. Peng, S. Kais, and J. Du. Experimental realization of quantum algorithm for solving linear systems of equations. *Physical Review A*, 89(2):022313, 2014.
- [88] S. Petersen, C. Farhat, and R. Tezaur. A space–time discontinuous Galerkin method for the solution of the wave equation in the time domain. *International journal for numerical methods in engineering*, 78(3):275–295, 2009.
- [89] P. Quinlan. The torsion of an irregular polygon. *Proc. R. Soc. Lond. A*, 282(1389):208–227, 1964.
- [90] P. Quinlan. The edge function method in elastostatics. *Studies in numerical analysis*, 1974.
- [91] J. W. S. B. Rayleigh. *The theory of sound*, volume 2. Macmillan, 1896.
- [92] L. Rayleigh. On the calculation of Chladni’s figures for a square plate. *The London, Edinburgh, and Dublin Philosophical Magazine and Journal of Science*, 22(128):225–229, 1911.
- [93] W. H. Reed and T. Hill. Triangular mesh methods for the neutron transport equation. Technical report, Los Alamos Scientific Lab., N. Mex.(USA), 1973.
- [94] W. Ritz. Zur Theorie der Serienspektren. *Annalen der Physik*, 317(10):264–310, 1903.

- [95] W. Ritz. Über eine neue Methode zur Lösung gewisser Randwertaufgaben. *Nachrichten von der Gesellschaft der Wissenschaften zu Göttingen, Mathematisch-Physikalische Klasse*, 1908:236–248, 1908.
- [96] W. Ritz. Theorie der Transversalschwingungen einer quadratischen Platte mit freien Rändern. *Annalen der Physik*, 333(4):737–786, 1909.
- [97] K. Shahbazi, P. F. Fischer, and C. R. Ethier. A high-order discontinuous Galerkin method for the unsteady incompressible navier–stokes equations. *Journal of Computational Physics*, 222(1):391–407, 2007.
- [98] R. Tezaur and C. Farhat. Three-dimensional discontinuous Galerkin elements with plane waves and Lagrange multipliers for the solution of mid-frequency Helmholtz problems. *International journal for numerical methods in engineering*, 66(5):796–815, 2006.
- [99] S. Thite. Adaptive spacetime meshing for discontinuous Galerkin methods. *Computational Geometry: Theory and Applications*, 42(1):20–44, 2009.
- [100] L. L. Thompson. Design and analysis of space-time and Galerkin/least-squares finite element methods for fluid-structure interaction in exterior domains. *The Journal of the Acoustical Society of America*, 96(6):3813–3813, 1994.
- [101] S. Timoshenko. Sur la stabilité des systèmes élastiques — application d’une nouvelle méthode à la recherche de la stabilité de certaines parties constitutives des ponts. In *Annales des Ponts et Chaussées*, volume 39, pages 73–134, 1913.
- [102] S. Timoshenko. *Strength of materials Part 1*. D. Van Nostrand Co., Inc, 1940.
- [103] E. Trefftz. Ein Gegenstück zum Ritzschen Verfahren. In *Proc. 2nd Int. Cong. Appl. Mech. Zurich*, pages 131–137, 1926.
- [104] A. Üngör and A. Sheffer. Tent-Pitcher: A meshing algorithm for space-time discontinuous Galerkin methods. In *In proc. 9th int’l. meshing roundtable*. Citeseer, 2000.
- [105] A. Üngör and A. Sheffer. Pitching tents in space-time: Mesh generation for discontinuous Galerkin method. *International Journal of Foundations of Computer Science*, 13(02):201–221, 2002.
- [106] K. Voronin. A parallel mesh generator in 3D/4D [pre-print]. 2018.
- [107] D. Wang, R. Tezaur, and C. Farhat. A hybrid discontinuous in space and time Galerkin method for wave propagation problems. *International Journal for Numerical Methods in Engineering*, 99(4):263–289, 2014.

- 
- [108] L. C. Wilcox, G. Stadler, C. Burstedde, and O. Ghattas. A high-order discontinuous Galerkin method for wave propagation through coupled elastic-acoustic media. *Journal of Computational Physics*, 229(24):9373–9396, 2010.
- [109] L. Yin. *A Space-time Discontinuous Galerkin Finite-Element Method for Elastodynamic Analysis*. PhD thesis, University of Illinois at Urbana-Champaign, 2002.
- [110] L. Yin, A. Acharya, N. Sobh, R. B. Haber, and D. A. Tortorelli. A space-time discontinuous Galerkin method for elastodynamic analysis. In *Discontinuous Galerkin Methods*, pages 459–464. Springer, 2000.
- [111] A. Zieliński. On trial functions applied in the generalized Trefftz method. *Advances in Engineering Software*, 24(1-3):147–155, 1995.
- [112] O. Zienkiewicz. Trefftz type approximation and the generalized finite element method — history and development. *Computer Assisted Mechanics and Engineering Sciences*, 4:305–316, 1997.
- [113] O. Zienkiewicz, D. Kelly, and P. Bettess. The coupling of the finite element method and boundary solution procedures. *International journal for numerical methods in engineering*, 11(2):355–375, 1977.